Investigations into the cellular function of C9orf72

Christopher Paul Webster BSc (Hons)

Thesis submitted for the degree of Doctor of Philosophy,

The University of Sheffield

Sheffield

March 2016

ABSTRACT

Amyotrophic lateral sclerosis (ALS) is a fatal neurodegenerative disease characterised by degeneration of the upper and lower motor neurons. Cognitive impairment in ALS is common and as such ALS and frontotemporal dementia (FTD) now constitute a spectrum of disorders ranging from pure ALS through to pure FTD. The hallmark of these diseases is the presence of neuronal cytoplasmic inclusions immunoreactive for a range of cellular proteins, suggesting defective protein clearance may contribute to disease. Indeed, damage to the cellular degradation pathway of autophagy, and disrupted protein clearance, is a potential causative mechanism in many familial inherited cases of ALS.

The most common genetic cause of ALS and FTD is a hexanucleotide repeat expansion of GGGGCC within the first intron of *C9orf72*. How this repeat expansion causes disease is unknown but it has been shown to correlate with reduced expression of *C9orf72.* Thus, loss of functional C9orf72 protein could contribute to disease pathogenesis. As *C9orf72* codes for two conserved, but uncharacterised, protein isoforms this thesis set out to investigate the cellular function of C9orf72. C9orf72 was found to interact with FIP200, ULK1 and ATG13, all of which are members of the autophagy initiation complex. In line with this, C9orf72 protein levels were found to modulate autophagy initiation by regulating Rab1a dependent trafficking of the ULK1 autophagy initiation complex. Knockdown of C9orf72 by targeted siRNA resulted in defective autophagy initiation, which led to the accumulation of p62, similar to the inclusion pathology specifically associated with C9orf72 ALS/FTD. Furthermore, iNeurons derived from C9orf72 ALS/FTD patient induced neural progenitor cells were shown to have a basal autophagy deficit, which correlated with reduced expression of *C9orf72*.

Thus haploinsufficiency of *C9orf72,* leading to reduced C9orf72 protein levels and defective autophagy, could lead to the accumulation of protein aggregates, such as p62, and the development of ALS/FTD. This thesis has therefore identified a possible cellular mechanism by which reduced levels of C9orf72 may contribute to disease pathogenesis.

ACKNOWLEDGEMENTS

I am indebted to a number of people who have helped me throughout the preparation of this thesis. Firstly I would like to thank my parents and family for all their support and encouragement, especially my elder brothers, whose appreciation and experience of the lab and research process has been priceless.

I would like to send a huge thank you to my supervisors Dr Alexander Whitworth and Dr Kurt De Vos for their continual guidance and support throughout my project. I would like to thank Alex for giving me the opportunity to work in his lab prior to starting my PhD and all his help since that time. I thank Kurt for his unfailing optimism, encouragement and enthusiasm, which have kept me motivated and focussed over the past four years. I wish to extend a special thank you to Miss Emma Smith for her truly invaluable help with many sections of this thesis, and Dr Annekathrin Möller for her advice and open ear. A big thank you also goes to all other members of the De Vos and Grierson groups, as well as everyone within B10, past and present, who are too numerous to mention by name, for scientific discussion, friendship and support. I thank Dr Mathew Walsh and Dr Guillaume Hautbergue for their help and advice with *in-vitro* binding assays, and Miss Monika Myszczynska and Dr Laura Ferraiuolo for their help with the preparation of the iNeurons. My thanks also extend beyond the walls of SITraN to all the friends who have given advice and support whenever needed.

I wish to thank the Moody Endowment who funded my project and made this research possible, as well as Professor Dame Pamela Shaw for making this funding available. This thesis was also supported, in part, by funding from The Thierry Latran Foundation and the MRC.

Finally, and last but by no means least, I thank my fiancée Emma, whose tolerance and understanding of late nights and weekends, as well as her reassurance and support, has made the whole experience so much more manageable. I assure you it's all been worthwhile.

ABSTRACT ii

ACKNOWLEDGEMENTS iii

List of Figures ix

List of Tables xi

Abbreviations xii

1 Introduction 1

1.1 Motor Neuron Disease and Amyotrophic Lateral Sclerosis 1

1.2 Clinical and pathological feature of ALS 2

1.3 Genetics of ALS 4

1.4 Mechanisms of Disease in ALS 7

1.4.1 Oxidative Stress 7

1.4.2 Mitochondrial dysfunction 8

1.4.3 Glutamate Excitotoxicity 9

1.4.4 Axonal Transport Defects 10

1.4.5 RNA dysregulation 13

1.4.6 ER stress 14

1.4.7 Protein Aggregation 18

1.5 Protein Degradation 20

1.5.1 The Ubiquitin Proteasome System 20

1.5.2 Autophagy 21

1.5.2.1 Initiation 25

1.5.2.1.1 mTOR dependent autophagy 25

1.5.2.1.2 mTOR independent autophagy 26

1.5.2.2 Vesicle formation and elongation 29

1.5.2.3 Defining the cargo 30

1.5.2.4 Maturation, Transport and Fusion 30

1.5.2.5 Rab GTPases and autophagy 31

1.6 Dysfunctional autophagy in ALS 34

1.6.1 Alsin 36

1.6.2 FIG4 36

1.6.3 p62 36

1.6.4 Optineurin 37

1.6.5 VCP 37

1.6.6 Ubiquilin-2 38

1.6.7 CHMP2B 38
1.6.8 Dynactin 39
1.6.9 TBK1 39
1.6.10 SigR1 40
1.6.11 Spatacsin 40
1.7 C9ORF72 and ALS 41
1.7.1 Clinical and pathological features of the *C9orf72* repeat expansion 41
1.7.2 Pathogenic Mechanisms in C9orf72 ALS/FTD 43
1.7.2.1 RNA toxicity 43
1.7.2.2 Dipeptide repeat protein toxicity 44
1.7.2.3 Haploinsufficiency 46
1.7.3 C9orf72 protein 47
1.8 Hypothesis and aims 51
2 Materials and Methods 52
2.1 Materials 52
2.1.1 Stock Solutions 52
2.1.2 Microbiology reagents 53
2.1.2.1 Plasmids and vectors 53
2.1.2.2 *Escherichia coli* growth media 55
2.1.2.3 Reagents for preparation and purification of plasmid DNA 55
2.1.2.4 Reagents for cloning of FIP200 fragments, C9orf72S, C9orf72L and C9orf72L K14R 56
2.1.2.4.1 Primers for PCR generation of FIP200 fragments, C9orf72S, C9orf72L and C9orf72L K14R 56
2.1.2.4.2 PCR amplification 57
2.1.2.4.3 Reagents for cloning into pCR™-Blunt II-TOPO vector 58
2.1.2.4.4 Reagents for Transformation of XL10-Gold ultracompetent cells 58
2.1.2.4.5 Reagents for restriction digest of DNA 58
2.1.2.4.6 Reagents for agarose gel electrophoresis 58
2.1.2.4.7 Reagents for gel extraction of restriction digested DNA 59
2.1.2.4.8 Reagents for de-phosphorylation of linearized DNA vectors 59
2.1.2.4.9 Reagents for ligation of DNA vectors and inserts 59
2.1.2.4.10 Reagents for the transformation of Rosetta pLysS competent cells 59
2.1.2.4.11 Reagents for bacterial production of GST-tagged proteins 60
2.1.3 Mammalian cell culture and transfection 60
2.1.3.1 HeLa and Human embryonic kidney (HEK) 293 cell culture reagents 60
2.1.3.2 Lipofectamine 2000 transfection reagents 60
2.1.3.3 Lipofectamine RNAiMax siRNA transfection reagent 60

2.1.4 General biochemical reagents 61
2.1.4.1 Cell lysis buffer 61
2.1.4.2 Bradford reagents 61
2.1.4.3 Immunoprecipitation 61
2.1.4.4 *In vitro* binding assays 61
2.1.4.5 SDS-PAGE and Immunoblotting 62
2.1.4.5.1 SDS-polyacrylamide gel electrophoresis (SDS-PAGE) 62
2.1.4.5.2 Immunoblotting of proteins onto nitrocellulose membranes 63
2.1.4.5.3 Probing of nitrocellulose membranes with antibodies 63
2.1.4.6 RNA extraction and reverse-transcription quantitative PCR (RT-qPCR) . 65
2.1.4.6.1 RNA extraction 65
2.1.4.6.2 cDNA preparation and RT-qPCR 65
2.1.5 Microscopy 65
2.1.5.1 Immunofluorescence 65
2.1.5.2 Proximity Ligation Assay (PLA) 66
2.1.6 Drug treatments 66
2.1.6.1 Autophagy induction 66
2.1.6.2 Autophagy inhibition 66
2.1.6.3 Proteasome inhibition 66
2.1.6.4 Inhibition of protein translation 67
2.2 Methods 67
2.2.1 General molecular biology methods 67
2.2.1.1 Growth and storage of *E.coli* for plasmid DNA preparation 67
2.2.1.2 Plasmid DNA purification 67
2.2.1.3 Quantification of plasmid DNA 67
2.2.1.4 Restriction enzyme digest of DNA 68
2.2.1.5 Agarose gel electrophoresis of DNA 68
2.2.1.6 Cloning of FIP200 fragments, C9orf72 and C9orf72 K14R 68
2.2.1.6.1 PCR generation of FIP200 fragments, C9orf72S, C9orf72L and C9orf72L K14R 68
2.2.1.6.2 Sub cloning into pCR™-Blunt II TOPO vector 69
2.2.1.6.3 Transformation of XL10-Gold® ultracompetent cells 70
2.2.1.6.4 Screening of bacterial colonies 70
2.2.1.6.5 Restriction digest and agarose gel extraction of inserts and vector . 70
2.2.1.6.6 De-phosphorylation of linearized vectors 72
2.2.1.6.7 Ligation of purified inserts and linearized vectors 72
2.2.1.6.8 Transformation of Rosetta pLysS cells with 73
2.2.1.6.9 Bacterial production of GST-tagged proteins 73
2.2.2 Mammalian cell culture and transfection 74

2.2.2.1 HeLa and HEK293 cell culture ... 74
2.2.2.2 Induced Neural Progenitor Cell (iNPC) production and neuronal differentiation ... 74
2.2.2.3 Transient transfection of HeLa and HEK293 cells with plasmid DNA ... 75
2.2.2.4 siRNA transfection of HeLa and HEK293 cells ... 76
2.2.3 General Biochemical methods ... 77
2.2.3.1 Cell lysis ... 77
2.2.3.2 Bradford Assay ... 77
2.2.3.3 Immunoprecipitation ... 78
2.2.3.4 *In vitro* binding assays ... 78
2.2.3.5 SDS-PAGE and Immunoblot ... 79
2.2.3.5.1 SDS-PAGE ... 79
2.2.3.5.2 Coomassie staining of polyacrylamide gels ... 80
2.2.3.5.3 Transfer of proteins to nitrocellulose membranes ... 80
2.2.3.5.4 Antibody probing of nitrocellulose membranes ... 80
2.2.3.5.5 Densitometry of bands ... 81
2.2.3.6 Modulation of autophagy ... 81
2.2.3.7 Inhibition of protein translation ... 81
2.2.3.8 RNA extraction and RT-qPCR ... 82
2.2.3.8.1 RNA extraction ... 82
2.2.3.8.2 RT-qPCR ... 82
2.2.4 Microscopy ... 83
2.2.4.1 Immunofluorescence ... 83
2.2.4.2 Proximity Ligation Assay ... 83
2.2.4.3 Image Analysis ... 84
2.2.5 Statistical analysis ... 84
3 Identification of C9orf72 binding partners ... 85
3.1 Introduction ... 85
3.2 Results ... 86
3.2.1 Characterization of C9orf72 antibodies and siRNA ... 86
3.2.2 C9orf72 interacts FIP200 ... 96
3.2.3 C9orf72 interacts with ULK1 ... 103
3.2.4 C9orf72 interacts with ATG13 ... 108
3.2.5 Unbiased mass spec identification of C9orf72 binding partners ... 113
3.2.6 Unbiased Y2H screen ... 119
3.2.7 C9orf72 interacts with Cox6C ... 122
3.2.8 C9orf72 does not interact with OAT ... 126
3.2.9 C9orf72 interacts with Synapsin III ... 129

3.3 Discussion **133**

4 C9orf72 regulates the initiation of autophagy **137**

4.1 Introduction **137**

4.2 Results **137**

4.2.1 Loss of C9orf72 disrupts the initiation of autophagy 137

4.2.2 C9orf72 over expression induces autophagy 143

4.2.3 C9orf72 induces autophagy via the ULK1 initiation complex 147

4.2.4 Loss of C9orf72 does not affect ULK1 activation 150

4.2.5 C9orf72 regulates translocation of the ULK1 initiation complex to the phagophore via Rab1a 152

4.2.6 C9orf72 interacts with Rab1a 158

4.2.7 C9orf72 mediates the interaction between Rab1a and the ULK1 initiation complex 161

4.2.8 C9orf72 depletion induces p62 accumulation 167

4.2.9 C9orf72 ALS/FTD patient derived iNeurons show defective autophagy 169

4.3 Discussion **172**

5 C9orf72 turnover and stability **177**

5.1 Introduction **177**

5.2 Results **177**

5.2.1. Determination of the half-life of C9orf72 177

5.2.2. C9orf72 is a substrate of the proteasome 181

5.2.3. Mutation of Lysine 14 extends the half-life of C9orf72L 184

5.2.4. C9orf72 interacts with USP8 190

5.2.5. USP8 extends the half-life of C9orf72L 192

5.3. Discussion **197**

6 Discussion **200**

6.1 Summary **200**

6.2 Defective autophagy and ALS/FTD **201**

6.3 Consequences for the treatment of ALS/FTD **211**

6.4 C9orf72 as an effector of Rab biology **212**

6.5 C9orf72 and mitophagy **216**

6.6 Future directions **218**

7 References **222**

List of Figures

Figure 1.1	Axonal Transport……	11
Figure 1.2	The Unfolded Protein Response……..	15
Figure 1.3	Micro, Macro and Chaperone Mediated Autophagy.....	23
Figure 1.4	Macroautophagy……..	24
Figure 1.5	mTOR dependent and mTOR independent autophagy……	27
Figure 1.6	Autophagy and ALS……	35
Figure 1.7	C9orf72 transcriptional variants……	41
Figure 1.8	The predicted DENN-like domains of C9orf72…….	49
Figure 3.1	Commercial anti-C9orf72 antibodies detect transfected epitope tagged C9orf72 on immunoblot……..	88
Figure 3.2	Anti-C9orf72 HPA023873 is able to detect endogenous C9orf72…….	91
Figure 3.3	Commercial anti-C9orf72 antibodies detect transfected epitope tagged C9orf72 in immunofluorescence……	94
Figure 3.4	Commercial antibodies do not detect endogenous C9orf72 in immunofluorescence……..	95
Figure 3.5	C9orf72 interacts with FIP200……...	98
Figure 3.6	C9orf72 directly interacts with the N terminus of FIP200…..	101
Figure 3.7	C9orf72 interacts with ULK1……..	104
Figure 3.8	C9orf72 directly interacts with ULK1……	107
Figure 3.9	C9orf72 interacts with ATG13……...	109
Figure 3.10	C9orf72 directly interacts with ATG13……	112
Figure 3.11	A number of proteins specifically co-immunoprecipitate with C9orf72L……..	114
Figure 3.12	C9orf72 interacts with SMCR8……..	118
Figure 3.13	The Cox6C clones identified from the Y2H screen map across the transmembrane domain of Cox6C……	123
Figure 3.14	C9orf72L interacts with Cox6C……	125
Figure 3.15	Mapping of the OAT clones identified from the Y2H screen to the OAT amino acid sequence…….	127
Figure 3.16	C9orf72 does not interact with OAT……	128
Figure 3.17	The Synapsin III clones identified from the Y2H screen map across the conserved C domain of Synapsin III……	130
Figure 3.18	C9orf72 interacts with Synapsin III……...	132

Figure 4.1	Loss of C9orf72 inhibits autophagy induction…….	138
Figure 4.2	Loss of C9orf72 inhibits LC3-II formation……	141
Figure 4.3	C9orf72 induces EGFP-LC3-II formation…….	143
Figure 4.4	C9orf72 induces autophagy……...	145
Figure 4.5	C9orf72 induces autophagy via the ULK1 initiation complex…….	147
Figure 4.6	Loss of C9orf72 does not affect activation of ULK1…….....	150
Figure 4.7	C9orf72 regulates translocation of the ULK1 complex……..	152
Figure 4.8	C9orf72 regulates translocation of the ULK1 initiation complex via Rab1a……..……...	155
Figure 4.9	C9orf72 directly interacts with Rab1a……..	158
Figure 4.10	C9orf72 preferentially binds GTP-bound Rab1a……	161
Figure 4.11	C9orf72 regulates the interaction between Rab1a and ULK1…….	163
Figure 4.12	C9orf72 is required for the Rab1a dependent induction of autophagy…….	164
Figure 4.13	Loss of C9orf72 induces p62 accumulation……	167
Figure 4.14	C9ALS/FTD patient have reduced basal autophagy…….	169
Figure 5.1	Half-life of C9orf7…….	177
Figure 5.2	C9orf72S is a substrate of the proteasome…….....	180
Figure 5.3	C9orf72L is a substrate of the proteasome…….	181
Figure 5.4	UbPred predicted ubiquitination sites of C9orf72L…….	183
Figure 5.5	Mutation of lysine 14 extends the half-life of C9orf72L…….	186
Figure 5.6	C9orf72 interacts with USP8…….	189
Figure 5.7	USP8 extends the half-life of C9orf72L…….	191
Figure 5.8	USP8 extends the half-life of C9orf72S……...	193
Figure 6.1	The role of C9orf72 in autophagy initiation…….	201
Figure 6.2	Impact of ALS associated genes on the autophagy pathway…….	205
Figure 6.3	The Rab module……..	210

List of Tables

Table 1.1	Subtypes of motor neuron disease……	1
Table 1.2	FALS associated genes……..	6
Table 2.1	Vectors……...	53
Table 2.2	Plasmids……	54
Table 2.3	Primary antibodies……	63
Table 2.4	Secondary antibodies……..	64
Table 2.5	PCR cycling parameters of Phusion High Fidelity DNA polymerase……	69
Table 2.6	DNA transfection with Lipofectamine 2000……..	75
Table 2.7	siRNA transfection with Lipofectamine RNAiMax……...	76
Table 2.8	siRNA transfection with Lipofectamine 2000……...	77
Table 2.9	Plasmids and TnT quick-coupled transcription/translation kits…….	79
Table 3.1	Identities of the bands from C9orf72L pulldown……..	115
Table 3.2	Clones identified from the Y2H screen……	120
Table 5.1	C9orf72L lysine residues and UbPred prediction scores……...	184

Abbreviations

Units

°C	degree Celsius
Da	Dalton
g	gram
h	hour
l	litre
M	Molar
M	meter
min	minute
s	sec
V	Volt

Prefixes

c	centi
k	kilo
m	milli
µ	micro
n	nano

Other abbreviations

A	Adenine
AD	Autosomal dominant
ADP	Adenosine diphosphate
ALS	Amyotrophic lateral sclerosis
ALD-FTD	ALS with frontotemporal dementia
AMP	Adenosine monophosphate
AMPA	α-amin-3-hydroxy-5-methylisoxazole-4-propionic acid
AMPK	AMP-activated protein kinase
ANOVA	Analysis of variance
AR	Autosomal recessive
ATG	Autophagy related gene
ATP	Adenosine triphosphate
Bcl-2	B-cell lymphoma-2

bp	Base pair
BSA	Bovine Serum Albumin
C	Cytosine
cAMP	Cyclic AMP
C.elegans	*Caenorhabditis elegans*
C9orf72	*Chromosome 9 open reading frame 72* gene
C9orf72L	C9orf72 Long isoform (481 aa)
C9orf72S	C9orf72 Short isoform (222)
C9orf72 K14R	Lysine to arginine substitution at position 14 in C9orf72
Ca^{2+}	Calcium ion
Cox6C	Cytochrome C oxidase subunit 6C
C-terminal	Carboxyl terminal
Ctrl	Control
dDENN	Down-stream DENN
DMEM	Dulbecco's modified Eagle's medium
DMSO	Dimethyl sulphoxide
DNA	Deoxyribonucleic acid
DNase	Deoxyribonuclease
dNTP	Deoxyribonucleotide triphosphate
DPR	Dipeptide repeat
DTT	Dithiothreitol
DUB	Deubiquitinating enzyme
E.coli	*Escherichia coli*
EAAT	Excitatory amino acid transporter
ECL	Enhanced chemiluminescence
EDTA	Ethylenediaminetetraacetic acid
EGFP	Enhanced Green Fluorescent Protein
EGTA	Ethylene glycol-bis (β-aminoethylether) N,N,N',N'-tetraacetic acid
ER	Endoplasmic reticulum
ERAD	ER associated degradation
ev	Empty vector
FALS	Familial ALS
FIP200	Focal adhesion kinase family kinase interacting protein of 200 kDa
FUS	Fused in sarcoma

G	Guanine
GAP	GTPase activating enzyme
GAPDH	Glyceraldehyde 3-phosphate dehydrogenase
GDP	Guanosine diphosphate
GEF	Gaunosine nucleotide exchange factor
GluR2	Glutamate receptor 2
GMP-PNP	5'-Guanylyl imidodiphosphate
GTP	Guanosine triphosphate
GWAS	Genome wide association study
HEK293	Human embryonic kidney 293
HEPES	4-(2-hydroxyethyl)piperazine-1-ethansulphonic acid
HSP	Hereditary spastic paraplegia
IF	Immunofluorescence
IgG	Immunoglobulin G
IMS	Intermitochondrial space
iNPC	Induced Neural progenitor cell
IP_3	Inositol 1,4,5-triphosphate
IP3R	Inositol 1,4,5-triphosphate receptor
IP	Immunoprecipitation
iPSC	Induced pluripotent stem cells
IPTG	Isopropyl-1-thio-β-D-galactopyranoside
IRE1	Inositol requiring enzyme 1
K	Potassium
K-PIPES	PIPES buffered with KOH
LB	Luria Bertani
LC3	Microtubule-associated protein 1 light chain 3
MAM	Mitochondrial associated membranes
MND	Motor Neuron Disease
mRNA	Messenger RNA
mTOR	Mammalian target of rapamycin
MVB	Multivesicular body
NADPH	Nicotinamide adenine dinucleotide phosphate
NEK1	*NIMA-related kinase 1* gene
N-terminal	Amino terminal
OD	Optical density
OAT	Ornithine amino transferase

OMM	Outer mitochondrial membrane
PAS	Preautophagosomal structure
PBS	Phosphate buffered saline
PCR	Polymerase chain reaction
PDI	Protein Disulphide Isomerase
pH	Power of hydrogen
PI3K	Phosphatidylinositol 3-kinase
PINK1	Phosphatase and tensin homologue (PTEN)-induced kinase 1 protein
PTPIP51	Protein tyrosine phosphatase-interacting protein 51
Rac1	Ras-related C3 botulinum toxin substrate 1
RAN	Repeat associated non-ATG
Ras	Rat sarcoma
RB1CC1	*Retinoblastoma1-induced coiled coil 1* gene
RING	Really interesting new gene
RNA	Ribonucleic acid
RNase	Ribonuclease
ROS	Reactive oxygen species
Rcf	Relative centrifugal force
SALS	Sporadic ALS
SDS	Sodium dodecyl sulphate
SDS-PAGE	SDS polyacrylamide gel electrophoresis
SEM	Standard error of mean
SigR1	Sigma-1 receptor
SMA	Spinal muscular atrophy
SMCR8	Smith-Magenis Syndrome Chromosome Region, Candidate 8
SNARE	Soluble N-ethylmaleimide-sensitive factor-attached protein receptor
SNP	Single nucleotide polymorphism
SOD1	Cu/Zn superoxide dismutase 1
SynIII	Synapsin III
T	Thymine
TAE	Tris-acetate EDTA
TARDPB	*Trans-activation response DNA binding protein* gene
TBS	Tris-buffered saline

TDP-43	Trans-activation response DNA binding protein 43
TEMED	N,N,N',N'-tetramethylethylenediamine
Tris	Tris(hydroxymethyl)aminomethane
Ub	Ubiquitin
UBA	Ubiquitin-associated
uDENN	Up-stream DENN
ULK1	Un-coordinated (Unc) 51-like kinase 1
UPR	Unfolded Protein Response
UPS	Ubiquitin proteasome system
USP	Ubiquitin specific protease
v/v	Volume/volume
VAMP	Vesicle associated membrane protein
VAPB	Vesicle associated membrane protein-associated protein B
VCP	Valosin containing protein
VDAC	Voltage dependent anion channel
w/v	Weight/volume
XBP1	X-box-binding protein 1

1 Introduction

1.1 Motor Neuron Disease and Amyotrophic Lateral Sclerosis

Motor Neuron Disease (MND) is a collective term for a group of neurological disorders characterised by degeneration and loss of the motor neurons. The subtypes of MND are classified based on the involvement of the upper motor neurons or lower motor neurons in disease pathogenesis. Upper motor neurons originate in the cortex or brain stem and feed information down to the lower motor neurons of the spinal cord, which innervate into the muscle to bring about contraction and movement. The different subtypes of MND are detailed in Table 1.1

Table 1.1 Subtypes of motor neuron disease

Disease	Upper motor neurons	Lower motor neurons
Amyotrophic lateral sclerosis (AL)	Yes	Yes
Progressive bulbar palsy (PBP)	Yes	Yes
Progressive muscular atrophy (PMA)	No	Yes
Spinal muscular atrophy (SMA)	No	Yes
Kennedy's disease	No	Yes
Monomelic amyotrophy	No	Yes
Brachial amyotrophic diplagia	No	Yes
Primary lateral sclerosis	Yes	No
Hereditary spastic paraplegia (HSP)	Yes	No

Amyotrophic Lateral Sclerosis (ALS) is the most common form of MND. ALS is a progressive adult onset disease characterised by selective degeneration of upper and lower motor neurones, leading to muscle wasting and eventual premature death due to respiratory failure and paralysis. The median survival for ALS is less than 3 years from diagnosis, but a range of factors appears to impact on disease duration. For example, bulbar onset, older age at diagnosis, poor motor function at diagnosis and increased weight loss over time are all related to a shorter survival (Gordon et al., 2012).

The incidence of ALS is approximately 2 per 100,000 people per year (Alonso et al., 2009; Logroscino et al., 2010), with incidence rates peaking in the 7th and 8th decades of life (Alonso et al., 2009). Around 90% of cases are sporadic (SALS) with approximately 10% showing a genetic component and familial inheritance, termed familial ALS (FALS). The genetic loci associated with FALS are listed in Table 1.2, and will be discussed in more detail later.

1.2 Clinical and pathological feature of ALS

Sporadic and familial ALS cases are clinically indistinguishable suggesting a common disease mechanism. The majority of ALS cases present with upper or lower limb onset with aspects of upper and lower motor neuron degeneration, including muscle wasting and weakness (Kiernan et al., 2011). Death due to respiratory failure usually occurs within 2 to 5 years from diagnosis (Kiernan et al., 2011). Cognitive decline has also been linked to ALS, with up to 50% of sufferers presenting with cognitive impairment, and the most severe developing features of frontotemporal dementia (FTD) (Lomen-Hoerth et al., 2003; Ringholz et al., 2005). Indeed, some of the most common genetic causes of ALS, such as C9orf72 repeat expansions, which is the topic of this thesis and will be discussed in section 1.7, are now known to lead to FTD (Ferrari et al., 2011), and up to 25% of ALS patients are clinically diagnosed with FTD (Rippon et al., 2006). This places ALS and FTD on a spectrum of disorders ranging from pure ALS, through ALS with behavioural impairment, ALS with FTD, FTD with motor neuron involvement, to finally pure FTD at the other end of the spectrum (Swinnen and Robberecht, 2014).

In addition to motor neuron loss, the aggregation and accumulation of proteinaceous intraneuronal inclusions are considered a hallmark of ALS pathology (Wood et al., 2003). These intraneuronal inclusions are classified into three types: 1) ubiquitinated inclusions, 2) Bunina bodies and 3) hyaline conglomerate inclusions (Wood et al., 2003).

Nearly all inclusions observed in ALS are positive for ubiquitinated TAR-DNA-binding protein 43 (TDP-43), as are the accumulations found in FTD, thus suggesting a common mechanism for these clinically similar diseases (Neumann et al., 2006). These ubiquitinated inclusions (UBIs) are negative for proteins found in aggregates of other neurodegenerative disorders, such as tau

and α-synuclein, but are the most common inclusions found in both SALS and FALS (Wood et al., 2003). The accumulation of these aggregates is the first evidence suggesting that defective protein clearance and turnover may play a role in the pathogenesis of ALS. Aside from ubiquitin and TDP-43, the components of these inclusions have been shown to contain proteins known to be involved in the development of other rare cases of FALS, including Optineurin, Ubiquilin-2, Ataxin, p62 and FUS (Deng et al., 2011; Elden et al., 2010; Maruyama et al., 2010; Teyssou et al., 2013; Vance et al., 2009). Although mutations to these genes are known to cause FALS, the proteins themselves are found as inclusion components in SALS cases, suggesting a possible common mechanism of disease. p62 appears to be a relatively common component of these intraneuronal UBIs (Arai et al., 2003; Mizuno et al., 2006a), and is also found in inclusions of other neurodegenerative diseases besides ALS, including Alzheimer's disease and tauopathies (Kuusisto et al., 2001; Kuusisto et al., 2002). UBIs can also be categorised based on their morphology. They can be described as skein-like inclusions, which are filamentous in structure, or rounded Lewy body-like inclusions (Kato et al., 1989; Leigh et al., 1988; Lowe et al., 1988).

Bunina bodies, originally described by Bunina in 1962 (Bunina, 1962), are specific to ALS and are not found in other neurodegenerative disease. They are eosinophilic inclusions that are negative for ubiquitin but positive for cystatin-C, transferrin and potentially peripherin (Mizuno et al., 2006b; Mizuno et al., 2011; Okamoto et al., 1993). The actual origin of Bunina bodies is unclear but they may originate from the endoplasmic reticulum or Golgi apparatus (Okamoto et al., 1993; Okamoto et al., 2008; Takahashi et al., 1991). The relevance to the pathogenesis of ALS is unclear but they may be a cellular response to proteinaceous aggregates (Okamoto et al., 2008).

Hyaline conglomerate inclusions are found almost exclusively in FALS cases (Murayama et al., 1989). They are comprised of phosphorylated and non-phosphorylated neurofilaments (Hays et al., 2006; Hirano et al., 1984; Munoz et al., 1988). Defective neurofilament transport has been reported in mouse models of ALS (Collard et al., 1995). Phosphorylation of neurofilament side arms slows their axonal transport, thus potentially leading to accumulations of phosphorylated neurofilament and subsequent incorporation into hyaline

conglomerate inclusions (Ackerley et al., 2000; Ackerley et al., 2003; Munoz et al., 1988).

1.3 Genetics of ALS

The majority of cases of ALS are sporadic (SALS), but approximately 5-10% of cases are familial (FALS) (Byrne et al., 2011). The aetiology of SALS is unknown and no single gene has been associated with its development (Schymick et al., 2007). Twin studies of SALS cases, where at least one twin has been diagnosed with ALS, have shown that the chance of the other developing ALS is approximately 61%, suggesting a genetic role in many cases of SALS (Al-Chalabi et al., 2010). The clinical presentation is identical between SALS and FALS, suggesting the possibility of common pathways leading to disease.

A number of gene mutations have been shown to cause FALS, as detailed in table 1.2. The majority of FALS is autosomal dominant in inheritance but X-linked and autosomal recessive forms have been reported (Hadano et al. 2001; Deng et al. 2011). The first genetic locus identified was that on chromosome 21 (Siddique et al., 1991; Siddique et al., 1989), which was later identified as the *SOD1* gene (Rosen et al., 1993). Over 150 mutations in *SOD1* now account for approximately 20% of FALS cases (Abel et al., 2012), but mutations have also been identified in a minority of SALS cases (Jones et al., 1994).

To date, the most common genetic defect associated with ALS is the GGGGCC hexanucleotide repeat expansion within *chromosome 9 open reading frame 72* (*C9orf72*) (DeJesus-Hernandez et al., 2011; Renton et al., 2011). Prior to 2011, a number of genome wide association studies (GWAS) had identified a genetic locus on chromosome 9p21 as being associated with familial ALS or FTD (Boxer et al., 2011; Gijselinck et al., 2010; Le Ber et al., 2009; Morita et al., 2006; van Es et al., 2009; Vance et al., 2006). The repeat expansion accounts for approximately 40% of FALS cases from white European populations, but is less prevalent in Hispanic and Asian populations (DeJesus-Hernandez et al., 2011; Majounie et al., 2012; Renton et al., 2011). In a Finnish population the C9orf72 repeat expansion is causative for 46% of FALS (Renton et al., 2011). *C9orf72* repeat expansions also account for approximately 5% of total SALS cases (DeJesus-Hernandez et al., 2011; Majounie et al., 2012; Renton et al.,

2011). As *C9orf72* is the main topic of this thesis, *C9orf72* will be discussed in more detail in section 1.7.

Along with *C9orf72* and *SOD1*, mutations to *FUS* (Kwiatkowski et al., 2009; Vance et al., 2009) and *TARDPB* (Kabashi et al., 2008; Sreedharan et al., 2008) are the most common genetic defects associated with ALS. Mutations to *FUS* account for approximately 4% of FALS (Kwiatkowski et al., 2009; Vance et al., 2009), while mutations to *TARDBP* account for approximately 4.3% of FALS (Millecamps et al., 2010). Tar DNA binding protein of 43 kDa (TDP-43) encoded by *TARDBP* is a nuclear RNA and DNA binding protein involved in several aspects of RNA metabolism, including transcriptional repression and splicing (Ou et al., 1995; Wang et al., 2004). *FUS* encodes the FUS protein, which, similar to TDP-43, is involved in RNA metabolism (Lagier-Tourenne et al., 2010). Both mutated proteins are found in abnormal cytoplasmic inclusions, which may contribute to disease pathogenesis (Arai et al., 2006; Kwiatkowski et al., 2009; Vance et al., 2009). Potential mechanisms of disease associated with these genetic mutations will be discussed in section 1.4.

The role of other genetic factors in the development of sporadic ALS is uncertain. Multiple genetic screens as well as GWAS have revealed a number of susceptibility genes and genetic variants that may contribute to the development of ALS (Chio et al., 2009; Gijselinck et al., 2010; Takahashi et al., 2013; van Es et al., 2009). However, the majority are yet to be confirmed as definitive disease genes.

Association studies of sporadic ALS patients has identified loci on chromosome 9p21, corresponding to *C9orf72,* as well as 9p13.3, corresponding to a region within *UNC13A,* as being associated with increased risk of developing ALS (Shatunov et al., 2010; van Es et al., 2009). Indeed, *C9orf72* and *UNC13A* are considered shared risk loci for ALS and FTD, and thus *UNC13A* is considered a susceptibility gene for these diseases (Diekstra et al., 2014). UNC13A functions to prime presynaptic vesicles to bring about correct neurotransmitter release (Varoqueaux et al., 2002). Thus, defective neurotransmitter release may be implicated in the development of ALS and FTD (Diekstra et al., 2014).

In the same study that identified *TANK-binding kinase 1* (*TBK1*) as a definitive ALS gene (Cirulli et al., 2015), a number of other susceptibility genes were

identified. Loss of function variants within the *NIMA-related kinase 1* (*NEK1*) gene was identified in a number of cases (Cirulli et al., 2015). NEK1 was shown to interact with other known FALS associated proteins Alsin (ALS2), a Rab5 GTPase guanine nucleotide exchange factor, and VAPB. The role of Alsin in the development of ALS will be discussed in further detail in section 1.6.1, but the interaction of NEK1 with Alsin suggests a common pathway may be involved in these ALS cases.

Table 1.2 FALS associated genes

FALS type	Inheritance	Locus	Gene	Reference
ALS1	AD	21q22.1	SOD1	(Rosen et al., 1993)
ALS2	AR	2q33.2	ALS2	(Hadano et al., 2001a)
ALS3	AD	18q21	Unknown	(Hand et al., 2002)
ALS4	AD	9p34	SETX	(Chen et al., 2004)
ALS5	AR	15q21.1	SPG11	(Orlacchio et al., 2010)
ALS6	AD	16p11.2	FUS	(Kwiatkowski et al., 2009; Vance et al., 2009)
ALS7	AD	20p13	Unkown	(Sapp et al., 2003)
ALS8	AD	20q13.33	VAPB	(Nishimura et al., 2004)
ALS9	AD	14q11.1	ANG	(Greenway et al., 2006)
ALS10	AD	1p36.22	TARDBP	(Kabashi et al., 2008; Sreedharan et al., 2008)
ALS11	AD	6p21	FIG4	(Chow et al., 2009)
ALS12	AR/AD	10p13	OPTN	(Maruyama et al., 2010)
ALS13	AD	12q23-q24.1	ATXN2	(Elden et al., 2010)
ALS14	AD	9p13	VCP	(Johnson et al., 2010)
ALS15	X-linked	Xp11.21	UBQLN2	(Deng et al., 2011)
ALS16	AR/AD	9p13	SIGMAR1	(Al-Saif et al., 2011)
ALS17	AD	3p12.1	CHMP2B	(Parkinson et al., 2006)
ALS18	AD	17p13.3	PFN1	(Wu et al., 2012)
ALS19	AD	2q33.3-q34	ERBB4	(Takahashi et al., 2013)
ALS20	unknown	12q13.1	HNRNPA1	(Kim et al., 2013)
ALS21	AD	5q31.2	MATR3	(Johnson et al., 2014)
ALS/FTD1	AD	9p21	C9ORF72	(DeJesus-Hernandez et al., 2011; Renton et al., 2011)
ALS	AD	2p13.1	DCTN1	(Münch et al., 2004)
ALS	unknown	5q35	SQSTM1	(Fecto et al., 2011)
ALS	AD	12q14.2	TBK1	(Freischmidt et al., 2015)

AR – autosomal recessive: AD – autosomal dominant: Data were obtained from ALSoD (Abel et al., 2012)

1.4 Mechanisms of Disease in ALS

A number of mechanisms have been implicated in the pathogenesis of ALS. However, the underlying pathogenic process is incompletely understood in the majority of ALS cases. It is possible that a number of the proposed mechanisms described could contribute to disease, and unlikely that each mechanism is mutually exclusive. There is also evidence that the development of ALS likely involves other cell types aside from the motor neurons, such as astrocytes and microglia.

1.4.1 Oxidative Stress

The main form of oxidative stress in cells arises from the production of reactive oxygen species (ROS) during normal cellular metabolism. ROS are mainly produced by electron leakage across the electron transport chain leading to the reduction of molecular oxygen and production of hydrogen peroxide (H_2O_2) and the superoxide oxygen free radical ($O_2^{\cdot}$) (Cadenas et al., 1977).

Several pieces of evidence suggest oxidative stress may be involved in the development of ALS. Firstly, oxidative damage to protein has been found to be greater in post mortem spinal cord tissue of sporadic ALS patients compared to controls, as has the oxidation to lipids and nuclear DNA (Ferrante et al., 1997; Shaw et al., 1995; Shibata et al., 2001). Markers of oxidative stress are also elevated in urine, sera and cerebrospinal fluid (CSF) of sporadic ALS patients (Mitsumoto et al., 2008; Simpson et al., 2004; Smith et al., 1998). Secondly, mutant TDP-43, a known cause of FALS, has also been shown to cause oxidative stress when overexpressed in neuronal cell lines (Duan et al., 2010). TDP-43 pathology is a hallmark of ALS and it is therefore possible that oxidative stress plays a role in many forms of familial, as well as sporadic, ALS. Finally, the mouse model of SOD1 ALS shows enhanced oxygen free radical production, accompanied by Ca^{2+} dysregulation and mitochondrial dysfunction (Kruman et al., 1999).

The case for the role of oxidative stress as a pathogenic mechanism is further strengthened by evidence suggesting that the nuclear erythroid 2-related factor 2 (Nrf2) pathway may be dysregulated in ALS (Sarlette et al., 2008). Nrf2 is a transcription factor regulating the anti-oxidant response (Ma, 2013). In ALS spinal cord post mortem tissue, Nrf2 mRNA and protein levels were found to be

reduced compared to controls suggesting a dysregulation of the antioxidant response (Sarlette et al., 2008).

Activated microglia may also be involved in ROS production in ALS. SOD1 in microglia has been shown to bind the GTPase Rac1, inhibiting its GTPase activity (Harraz et al., 2008). SOD1 normally dissociates from Rac1 in response to increased NADPH oxidase-dependent (Nox-dependent) $O_2^{\cdot -}$ production, leading to Nox complex inactivation. However, mutant SOD1 in microglia does not release Rac1 in response to increased local ROS production and so Nox activity is sustained, thereby increasing ROS production (Harraz et al., 2008). NADPH oxidase activity has been found to be upregulated in ALS patients and mouse models of ALS (Marden et al., 2007; Wu et al., 2006).

1.4.2 Mitochondrial dysfunction

There are multiple evidences for the involvement of mitochondrial dysfunction in the development of ALS, much of which comes from the study of mouse and cellular models of mutant SOD1 ALS. Firstly, mitochondrial morphology defects, such as mitochondrial swelling and fragmentation, are seen in both FALS and SALS (Menzies et al., 2002; Sasaki and Iwata, 2007; Song et al., 2013). This morphology defect is also seen at a pre-symptomatic stage is some mouse models of SOD1 ALS, suggesting an early event in the pathogenesis of disease (Wong et al., 1995).

Secondly, while mutant SOD1 has been shown to increase oxidative stress, the mutant protein has also been shown to accumulate on the outer-mitochondrial membrane (OMM) and also in the intermembrane space (IMS) of neuronal mitochondria, disrupting mitochondrial biology and function by blocking protein import and export from these organelles (Higgins et al., 2002; Liu et al., 2004; Pasinelli et al., 2004; Vande Velde et al., 2008).

Thirdly, perturbed energy production, as assessed by the activity of the respiratory chain proteins, has been reported in the spinal cord of ALS patients as well as SOD1 mouse models (Mattiazzi et al., 2002; Wiedemann et al., 2002). The effects seen by the expression of mutant SOD1 may be linked to its interaction with the voltage-dependent anion channel 1 (VDAC1) on the OMM, resulting in reduced ADP import and ATP synthesis (Israelson et al., 2010). This could also account for disturbed calcium buffering and homeostasis in models of

SOD1 ALS (Damiano et al., 2006; Nguyen et al., 2009), as VDAC1 is involved in Ca^{2+} exchange between mitochondria and the ER (De Stefani et al., 2012). Disrupted calcium uptake by mitochondria has also been reported in VAPB associated ALS, suggesting a mechanism that may be involved in a wide range of ALS cases (De Vos et al., 2012).

Finally, mutant SOD1 has been shown to aggregate the anti-apoptotic protein Bcl-2, thereby reducing functional Bcl-2 in neuronal cells, leading to disruption of the anti-apoptotic machinery (Pasinelli et al., 2004). This potential disruption to the anti-apoptotic machinery may be the cause of increased caspase activation and apoptosis in models of SOD1 ALS (Sathasivam et al., 2005)

1.4.3 Glutamate Excitotoxicity

Glutamate is the main neurotransmitter involved in signal transduction within the central nervous system. The excitatory signal from glutamate is reversed by efficient removal of glutamate from the synaptic cleft by a family of glutamate re-uptake transporters, the most common of which is excitatory amino acid transporter 2 (EAAT2) (Danbolt, 2001). Prolonged or excessive neurotransmitter excitation has been implicated in neuronal injury in a process called excitotoxicity. Excitotoxicity can be caused by reduced removal of glutamate or by increased release from the pre-synaptic neuron (Fray et al., 1998; Milanese et al., 2011; Rothstein et al., 1992). Several observations indicate glutamate excitotoxicity is involved in the pathogenesis of ALS.

Firstly, excitotoxicity is observed at an early and even pre-symptomatic stage of disease, with patients showing increased cortical hyperexcitability prior to the development of clinical features in *SOD1* patients (Vucic et al., 2008). Excitotoxicity could therefore be one of the initiating factors for the development of ALS. In support of this, FALS patient derived induced pluripotent stem cells (iPSCs) are shown to have intrinsic hyperexcitability, which could account for the neuronal vulnerability in ALS (Wainger et al., 2014).

Secondly, glutamate levels have been shown to be elevated in the cerebral spino fluid (CSF) of ALS patients (Fiszman et al., 2010; Spreux-Varoquaux et al., 2002; Yáñez et al., 2011). This may be related to the fact that EAAT2 expression is down regulated in the spinal cord and motor cortex of ALS patients (Fray et al., 1998; Rothstein et al., 1992; Rothstein et al., 1995). This is

supported by the mouse models of SOD1 ALS, which exhibit decreased EAAT2 expression as well as increased glutamate release into the synaptic cleft (Boston-Howes et al., 2006; Milanese et al., 2011).

α-amin-3-hydroxy-5-methylisoxazole-4-propionic acid (AMPA) receptors are a class of postsynaptic ionotropic glutamate receptors (Dingledine et al., 1999). Motor neurons appear to be particularly susceptible to AMPA receptor mediated excitotoxicity, possibly due to their role in calcium uptake into the postsynaptic neuron (Carriedo et al., 1996; King et al., 2007). The GluR2 subunit of AMPA receptors is the main determinant of calcium permeability of these receptors (Hollmann et al., 1991). GluR2 mRNA can be post-transcriptionally edited at Gln 607 site to produce Arg 607 (the Gln/Arg site) (Melcher et al., 1996) rendering the receptor calcium impermeable (Hume et al., 1991). Reduced Gln/Arg editing of GluR2 has been reported in ALS patients (Kawahara et al., 2004; Kwak et al., 2010; Takuma et al., 1999), which may lead to increased calcium influx in ALS patients and neuronal vulnerability (Takuma et al., 1999). This calcium influx may overload the mitochondrial calcium buffering capacity of the neurons, leading increased ROS production (Carriedo et al., 2000).

Finally, the involvement of excitotoxicity in the development of disease is strengthened by the fact that the only drug proven to affect disease progression and increase patient lifespan is riluzole (Lacomblez et al., 1996), which has shown to have anti-excitotoxic effects (Bensimon et al., 1994). However, it is worth noting that the actual action of riluzole may extend beyond the ability to modulate the glutamate neurotransmitter (Cheah et al., 2010).

1.4.4 Axonal Transport Defects

Axonal transport involves the transport and delivery of cellular cargos from the cell body to the distal axon and visa versa. Transport from the cell body to the distal axon is termed anterograde transport and is mediated by kinesin motor proteins. Transport from the distal axon back towards the cell body is termed retrograde transport and is mediated by the motor protein cytoplasmic dynein-1. These motor proteins move along microtubules, with kinesins moving towards the plus end (the “growing” end) and cytoplasmic dynein-1 moving towards the minus end (Figure 1.1). Several lines of evidence implicate axonal transport defects in the pathogenesis of ALS.

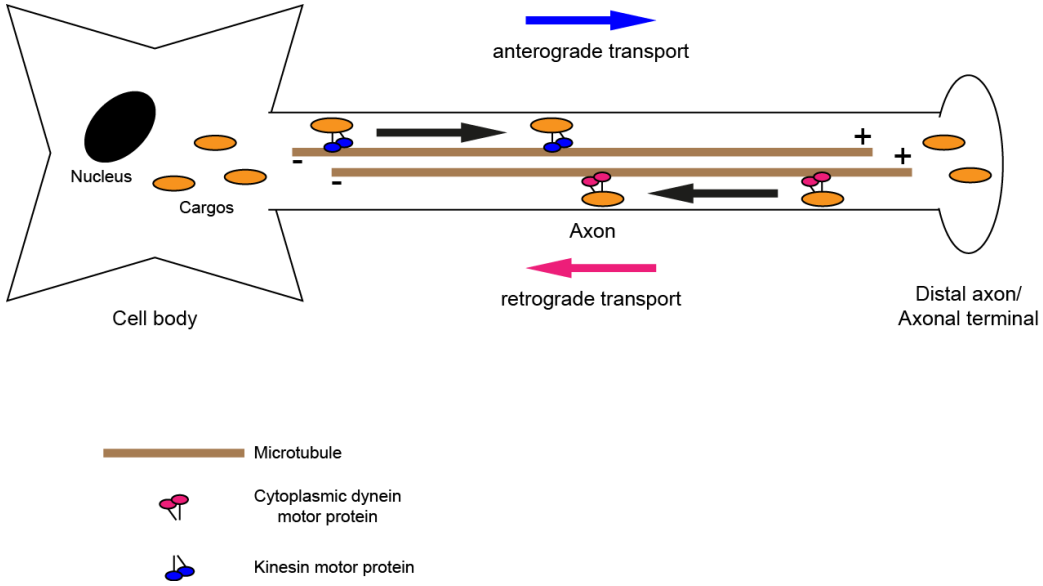

Figure 1.1. Axonal Transport. Microtubules are polarised structures with the growing, plus end located at the synapse and the minus end located at the cell body. Kinesin motor proteins transport cargo along the microtubules in an anterograde fashion from the cell body to the synapse. Cytoplasmic dynein transports cargo in a retrograde fashion from the synapse to the cell body.

Firstly, mutations to the p150 subunit of dynactin are linked to ALS and FTD (Münch et al., 2005; Münch et al., 2004; Puls et al., 2003). Dynactin is a large protein complex and also a component of the cytoplasmic dynein motor protein (Gill et al., 1991). Mutant dynactin may disrupt the dynein/dynactin complex leading to reduced transport and protein aggregation (Levy et al., 2006). The *Legs at odd angles* (LOA) mutant mouse carries a missense point mutation in the dynein heavy chain, leading to motor neuron loss and inclusion body formation (Hafezparast et al., 2003), supporting the idea that disruption to axonal transport can lead to neurodegeneration.

Secondly, neurofilaments, which are transported via slow axonal transport, accumulate in ALS suggesting disrupted axonal transport may promote this aggregate associated pathology (Ackerley et al., 2000; Ackerley et al., 2003).

Evidence from the SOD1 (G93A) mouse model also implicates disruption to the axonal transport pathway in the pathogenesis of ALS, as anterograde movement of mitochondria is particularly affected in these animals (Bilsland et al., 2010; De Vos et al., 2007; Kieran et al., 2005; Williamson and Cleveland, 1999). Reduced numbers of mitochondria in the distal axon could lead to a localised energy deficiency and degeneration (De Vos et al., 2007). However, others have demonstrated that axonal degeneration can occur independently of axonal transport defects. For example, Marinkovic et al demonstrated that the SOD1 (G85R) mouse model of ALS develops axonal degeneration without an apparent effect on transport, while over expression of wild type SOD1 in a mice leads to chronic transport defects but ultimately no degeneration (Marinković et al., 2012). These data support the idea that multiple mechanisms may contribute to disease, and it is unlikely that each mechanism is mutually exclusive.

Disruption to axonal transport has been documented in other neurological diseases including hereditary spastic paraplagia (HSP) and SMA (Fallini et al., 2011; Kasher et al., 2009; Xu et al., 2016). Mutations in spastin are the most common cause of HSP and have been shown to lead to reduced anterograde transport of mitochondria as well as amyloid precursor protein (APP) containing cargos (Kasher et al., 2009). In the case of SMA, reduced transport of mRNA as well as mitochondria has been reported as potentially pathogenic mechanisms (Fallini et al., 2011; Xu et al., 2016). The survival of motor neuron (SMN) protein appears to be involved in axonal transport of mRNA via its interactions with

other RNA binding proteins, linking two potential mechanisms of neurodegeneration: axonal transport defects and RNA dysregulation (Fallini et al., 2011; Saal et al., 2014)

1.4.5 RNA dysregulation

Mutations in several RNA homeostasis related proteins, such as senataxin, FUS, TDP-43 and Matrin 3, are causative for some forms of FALS, suggesting RNA dysregulation is involved in disease pathogenesis (Chen et al., 2004; Johnson et al., 2014; Kwiatkowski et al., 2009; Sreedharan et al., 2008; Vance et al., 2009).

TDP-43 is a nuclear DNA and RNA binding protein involved in a variety of cellular processes including transcriptional repression and exon skipping (Ou et al., 1995; Wang et al., 2004). Mutations to TDP-43 lead to its aberrant cytoplasmic accumulation and inclusion into ubiquitinated aggregates (Arai et al., 2006; Kabashi et al., 2008; Neumann et al., 2006). The loss of nuclear TDP-43 and redistribution to the cytoplasm is seen as an early event in the pathogenesis of ALS (Giordana et al., 2010). This mislocalisation has been shown to result in dysfunctional splicing in motor neurons (Highley et al., 2014). Whether the loss of TDP-43 function, or a gain of toxic function related to the cytoplasmic aggregates, is the underlying causes of ALS is unknown.

Crosslinking and immunoprecipitation (iCLIP) has revealed some of the RNA binding targets of TDP-43, which comprise a number of ALS related genes, including FUS and TDP-43 itself (Sephton et al., 2011; Tollervey et al., 2011). TDP-43 also interacts with the other FALS related protein Matrin 3 (Johnson et al., 2014; Salton et al., 2011). Thus loss of nuclear TDP-43 may therefore impact on other ALS associated genes, supporting a loss of function mechanism.

FUS related ALS is characterised by ubiquitinated inclusions of FUS, which are negative for TDP-43 (Kwiatkowski et al., 2009; Vance et al., 2009). FUS is normally localised to the nucleus and is involved in a range of RNA processing activities including transcriptional regulation, splicing and RNA translocation (Belly et al., 2005; Fujii et al., 2005; Meissner et al., 2003; Uranishi et al., 2001; Wang et al., 2008; Zinszner et al., 1997). ALS associated *FUS* mutations lead to

global alterations to splicing, similar to the effect *FUS* depletion (Sun et al., 2015). Thus, FUS loss of function may contribute to ALS pathogenesis.

TDP-43 and FUS may also be involved in RNA stress granule formation (Andersson et al., 2008; Colombrita et al., 2009; Dormann et al., 2010). Stress granules are cytoplasmic sites of stalled mRNA translation in response to stress, leading to the accumulation of mRNA, RNA binding proteins and translational initiation components (Buchan and Parker, 2009). Mutant TDP-43 and FUS readily accumulate in stress granules (Baron et al., 2013; Walker et al., 2013), thus supporting a toxic gain of function of both mutant proteins.

1.4.6 ER stress

To maintain cellular homeostasis, cells monitor stress levels through a range of sensors and respond via a number of inducible pathways that rectify the imbalance. Accumulation of mis or unfolded protein in the ER lumen induces ER stress and the unfolded protein response (UPR) detailed in Figure 1.2 (for review see (Hetz, 2012)). The UPR seeks to rebalance protein homeostasis in a number of ways. Firstly, further protein translation is inhibited helping to reduce the burden on the ER, while an upregulation of molecular chaperones helps to aid correct folding of the already translated proteins. Secondly, the main cellular degradation pathways of ER associated degradation (ERAD) are upregulated to further remove the burden of the unfolded proteins. Finally, chronic ER stress signals that the cell has failed to adapt and thus apoptosis is induced.

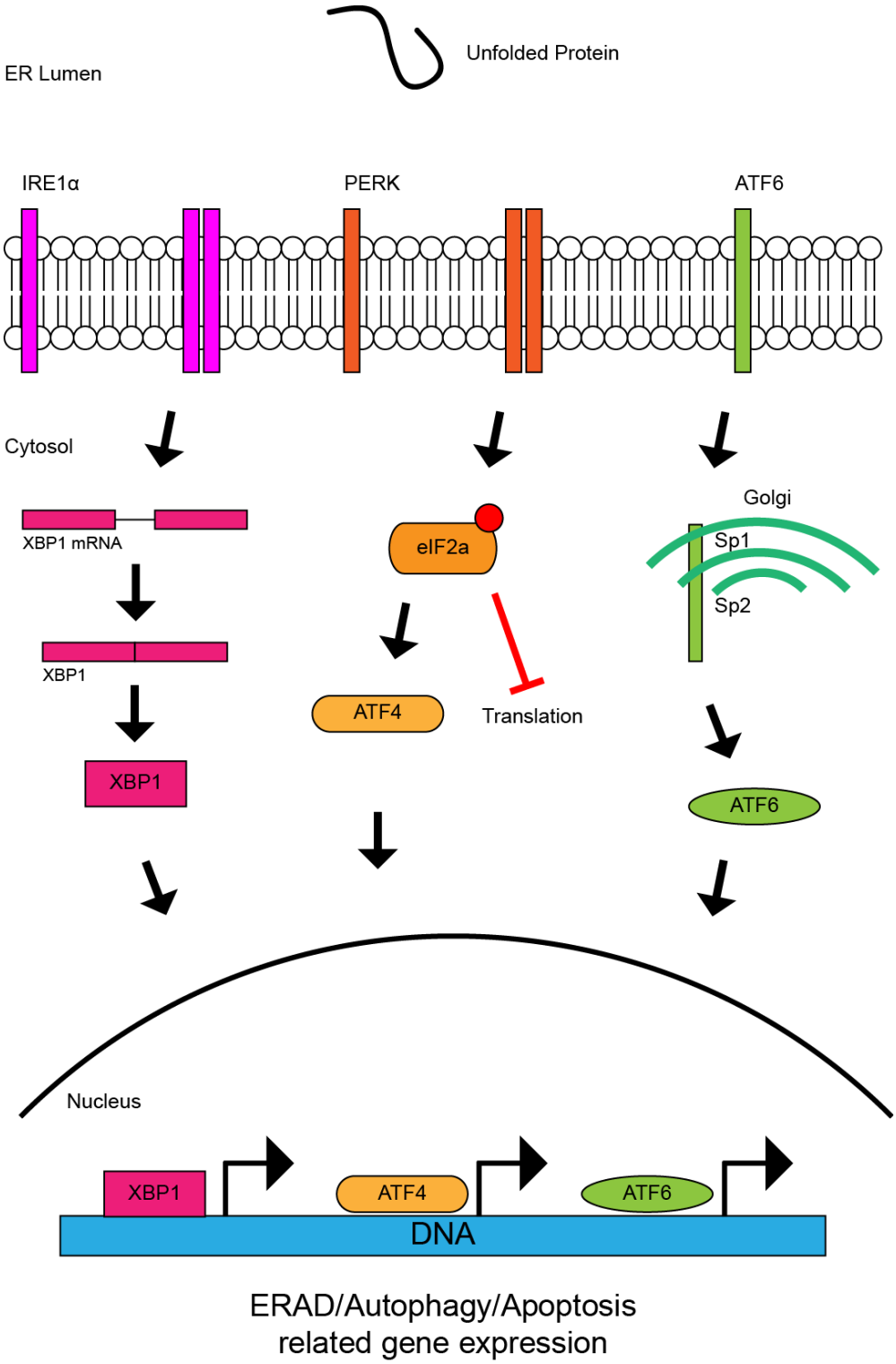

Figure 1.2. The Unfolded Protein Response (UPR). ER stress causes Inositol-requiring protein 1α (IRE1α) dimerization. Dimerization activates its intrinsic RNAse activity, which allows splicing of the XBP1 mRNA to produce a function XBP1 transcription factor. XBP1 increase expression of genes related to protein folding and ERAD. Protein kinase RNA-like ER kinase (PERK) dimerization

leads to phosphorylation of the eukaryotic initiation factor eIF2α, inhibiting general protein synthesis. Inhibition of general translation allows the translation of the ATF4 transcription factor. ATF4 increases expression of genes related to autophagy and apoptosis. Upon ER stress ATF6 translocates from the ER to the Golgi where it is processed by two proteases, Site 1 protease (S1P) and Site 2 protease (S2P). Proteolytic cleavage produces a cytosolic fragment of ATF6, which is a functional transcription factor. ATF6 leads to expression of genes related to ERAD but also XBP1, thus promoting the UPR.

Evidence for ER stress in ALS is firstly supported by the fact that all three sensors of UPR (IRE1, PERK and ATF6) are elevated in the CSF and spinal cord of SALS patients (Atkin et al., 2008). Similarly, increased levels of UPR related chaperone proteins, such as the protein disulphide isomerase (PDI) family, are up-regulated in SALS patients and the G93A SOD1 mouse model (Atkin et al., 2006; Atkin et al., 2008). UPR activation is evident as early as postnatal day 5 in the G93A SOD1 mouse model, indicating an early event in pathogenesis (Saxena et al., 2009). Elevated levels of activated caspase-12 have also been reported in the SOD1 mouse model, suggesting prolonged UPR activation and apoptosis is a possible cause of motor neurodegeneration in these mice (Atkin et al., 2006; Wootz et al., 2004).

Secondly, mutations in VAPB are causative for ALS (Nishimura et al., 2004). VAPB is an integral ER protein and has been implicated in UPR activation (Gkogkas et al., 2008; Kanekura et al., 2006). Several investigations have reported that the P56S mutation in VAPB, which leads to ALS, induces ER stress by hampering efficient UPR activation (Chen et al., 2010; Gkogkas et al., 2008; Kanekura et al., 2006; Suzuki et al., 2009). This is potentially due to the P56S mutant recruiting wild type VAPB into cytoplasmic aggregates, leading to its loss of function in UPR activation (Suzuki et al., 2009). VAPB also interacts with the outer mitochondrial membrane (OMM) protein PTPIP51 at mitochondrial associated membrane (MAM) sites (De Vos et al., 2012; Stoica et al., 2014). ER-mitochondrial contacts at MAM are essential to maintain calcium homeostasis. The P56S mutant has been shown to enhance the interaction with PTPIP51 leading to disrupted calcium homeostasis and elevated calcium levels, in turn disrupting anterograde axonal transport of mitochondria (De Vos et al., 2012; Morotz et al., 2012). Thus, mutations in VAPB provide evidence of links between multiple pathogenic mechanisms associated with ALS, namely mitochondrial dysfunction, disrupted axonal transport and ER stress.

Finally, TDP-43 also appears to be linked to ER stress. The hyperphosphorylated ubiquitinated TDP-43 aggregates are generated from cleavage of the full-length protein to leave possibly pathogenic C-terminal fragments (Arai et al., 2006; Neumann et al., 2006). In a motor neuron like cell line, chemical induction of ER stress led to increased TDP-43 cleavage and C-terminal fragment production (Suzuki et al., 2011). Also ALS associated

mutations in TDP-43 were shown to trigger a number of ER stress responses including XBP-1 and ATF6 activation (Walker et al., 2013).

1.4.7 Protein Aggregation

Maintaining protein homeostasis is essential for cell survival. The occurrence of protein aggregates therefore indicates that protein aggregation is a potential pathogenic mechanism in ALS and FTD. Protein homeostasis or proteostasis refers to the equilibrium between protein biosynthesis and clearance. A complex regulatory network exists within cells to maintain the equilibrium between production and degradation, promoting cellular health and survival. Eukaryotic cells have two major pathways of protein degradation, the proteasome and the lysosome. The proteasome selectively recognises ubiquitinated protein substrates, while autophagy denotes delivery of cytoplasmic components, including whole organelles, to the lysosome, see sections 1.5.1 and 1.5.2.

Ubiquitinated and hyperphosphorylated TDP-43 is a prominent feature of the aggregates associated with ALS and FTD (Arai et al., 2006; Neumann et al., 2006). The presence of these TDP-43 aggregates in both SALS and FALS provides strong evidence that aberrant aggregation of TDP-43 plays an important role in the development of disease (Sreedharan et al., 2008). While the loss of nuclear TDP-43 may contribute to disease, the cytoplasmic aggregation of this protein may also be toxic (Fang et al., 2014).

Aside from TPD-43, other protein species are found in these ALS associated inclusions. Hyaline conglomerate inclusions are comprised of hyperphosphorylated neurofilament protein, which can lead to their reduced transport and subsequent aggregation (Ackerley et al., 2003; Hirano et al., 1984; Manetto et al., 1988), while Bunina bodies consist of cystatin C (Okamoto et al., 1993). Cystatin C has been shown to upregulate the cellular recycling pathway of autophagy as a neuroprotective mechanism (Tizon et al., 2010; Watanabe et al., 2014). Aberrant accumulation of cystatin C may therefore impede its normal function, leading to a reduced ability of the cell to induce this cellular clearance pathway. Similarly to TDP-43, cytoplasmic aggregates of mutated FUS protein are found in FUS-related FALS (Kwiatkowski et al., 2009; Vance et al., 2009), while accumulations of misfolded SOD1 have been reported in sporadic ALS in Lewy Body like inclusions and also familial ALS, particularly FALS cases that are caused by SOD1 mutations (Shibata et al., 1994). Using epitope specific

antibodies for SOD1, researchers have shown that these accumulations are specifically made from misfolded mutant SOD1, which are found prior to onset of symptoms in SOD1 mouse models of ALS, suggesting misfolding and the accumulations of SOD1 are an early pathogenic event in the development of ALS (Rakhit et al., 2007). There also appears to be a propensity of wild type SOD1 to misfold and aggregate suggesting a role in SALS (Rakhit et al., 2004; Rakhit et al., 2002).

The presence of these protein aggregates therefore suggests defective protein degradation and clearance is a factor in their formation.

1.5 Protein Degradation

Degradation in eukaryotic cells is mediated by two systems: the ubiquitin proteasome system (UPS) and the autophagy pathway. These will be discussed in more detail below.

1.5.1 The Ubiquitin Proteasome System

The ubiquitin proteasome system (UPS) involves the specific clearance of ubiquitinated proteins by the proteasome, a multimeric ATP-dependent protease complex (Voges et al., 1999). Ubiquitin is a small 8.5 kDa heat stable regulatory protein responsible for the targeting of protein substrates to the proteasome (Ciechanover et al., 1978). The functional 26S proteasome comprises of the core 20S protease, capped with two 19S regulatory units (Driscoll and Goldberg, 1990; Eytan et al., 1989; Hoffman et al., 1992; Voges et al., 1999).

There are three enzymes required for ubiquitin conjugation to a target substrate: the E1 ubiquitin-activating enzyme, the E2 ubiquitin conjugating enzyme and the E3 ubiquitin ligase. The E1 ubiquitin-activating enzyme activates ubiquitin in an ATP dependent manner, forming a thiolester link between the E1 enzyme and the ubiquitin molecule (Ciechanover et al., 1982; Ciechanover et al., 1981). The ubiquitin molecule is then transferred from the E1 enzyme to the active site of the E2 ubiquitin-conjugating enzyme, allowing for the transfer of ubiquitin from the E2 enzyme to the target protein by the action of the E3 ubiquitin ligase (Ciechanover et al., 1982; Hershko et al., 1983). By binding specifically to the substrate target and the E2 ubiquitin-conjugate, the E3 ubiquitin ligase adds specificity to the cascade by ensuring that only the correct E2 enzyme is brought into contact with the specific substrate (Berndsen and Wolberger, 2014).

The conjugation of ubiquitin to a target protein occurs via the amino side chain of an internal lysine of the substrate and the carboxyl group of the C-terminal glycine of ubiquitin, forming an isopeptide bond (Goldknopf and Busch, 1977). Consequently, further ubiquitin moieties can be ligated to the initial ubiquitin by the use of one of the seven internal lysine residues of ubiquitin: lysine 6, lysine 11, lysine 27, lysine 29, lysine 33, lysine 48 and lysine 63. This allows for poly-ubiquitination of a substrate and complex ubiquitin chain formation (Chau et al., 1989; Hershko and Heller, 1985). Depending on the ubiquitin lysine residue used, the fate of the protein can vary, ranging from degradation (Chau et al., 1989; Thrower et al., 2000), to enhanced enzymatic activity (Al-Hakim et al.,

2008), to even increased protein stability (Nishikawa et al., 2004). However, polyubiquitination through lysine 48 is typically the main signal for degradation via the proteasome (Chau et al., 1989; Thrower et al., 2000).

There are more than 600 E3 ligases encoded in the human genome (Li et al., 2008). Eukaryotic E3 ligases are classified into 3 distinct families based on conserved domain structure and how the ubiquitin moiety is transferred from the E2 conjugating enzyme onto the internal lysine of target protein substrates (Berndsen and Wolberger, 2014; Metzger et al., 2012). The really interesting new gene (RING) family of E3 ligases transfer ubiquitin from the E2 enzyme directly onto the protein substrate (Özkan et al., 2005; Zheng et al., 2002), while Homology to E6AP C terminus (HECT) and RING between RING (RBR) E3 families act in a two-step process, transferring ubiquitin from the E2 conjugate onto the E3 ligase and then onto the protein substrate (Huibregtse et al., 1995).

While E3 ligases promote poly-ubiquitin of protein substrates, the removal of ubiquitin is mediated by a class of proteins called the de-ubiquitinating enzymes (DUBs). There are approximately 79 DUBs encoded in the human genome (Nijman et al., 2005). Essentially a class of proteases, the DUBs can be divided into five sub-classes based on their catalytic protease domains. The Ubiquitin Specific Protease (USP) family is by far the largest group with over 50 known *USP* genes (Nijman et al., 2005). DUBs also display targeted specificity either to the type of ubiquitin chain, or to the target protein that has been ubiquitinated.

1.5.2 Autophagy

Autophagy, literally meaning “self eating’ involves the delivery of cytosolic components and organelles (dubbed mitophagy in case of mitochondria) to the lysosome for degradation.

Autophagy is classified into three types depending on how the substrates are delivered to the lysosome: chaperone mediated autophagy (CMA), microautophagy, and macroautophagy (Figure 1.3). CMA is the selective uptake and degradation of intracellular proteins which contain the consensus sequence Lys-Phe-Glu-Arg-Gln (KFERQ) (Dice, 1990). Proteins containing this sequence are bound by heat shock cognate protein of 70 kDa (Hsc70) and delivered to the lysosome via the lysosomal associated membrane protein 2A (LAMP-2A) (Cuervo and Dice, 1996). Microautophagy is the simplest form of autophagy as

no intermediates or adaptors are required, the lysosomal membrane simply invaginates and pinches off, internalising a portion of the cytoplasm plus the substrates to be degraded (Marzella et al., 1981; Mortimore et al., 1988). Macroautophagy, often seen as classical autophagy, is the bulk clearance of cytoplasmic components and requires a large number of essential adaptors and intermediates. Although initially identified in yeast, macroautophagy is highly conserved amongst eukaryotes (Mizushima et al., 1998). Macroautophagy, herein termed autophagy, acts as a quality control mechanism for the cell, turning over damaged organelles, such as mitochondria, as well as degrading long-lived and misfolded proteins (Knecht et al., 1988; Mortimore et al., 1988; Ravikumar et al., 2004; Webb et al., 2003).

The autophagic process can be separated into distinct steps: initiation, vesicle formation and elongation, cargo recruitment, maturation and fusion, and degradation, which are detailed in Figure 1.4. The proteins involved at different stages of mammalian autophagy are numerous and complex.

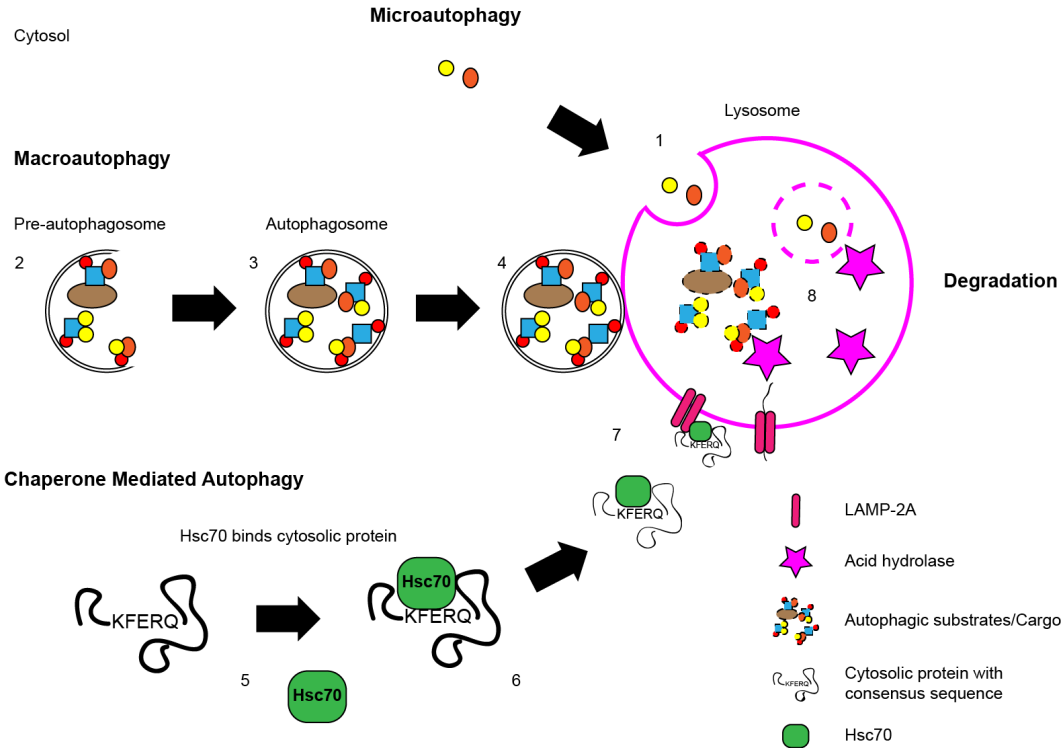

Figure 1.3. Micro, Macro and Chaperone Mediated Autophagy. **(1)** In Microautophagy the lysosomal membrane invaginates, engulfing a portion of the cytoplasm and any substrates to be degraded. **(2)** Macroautophagy involves the formation of a double membrane structure called the autophagosome. **(3)** Autophagic substrates, including misfolded proteins and organelles, are brought into contact with the preautophagosomal structure via the action of a number of autophagy receptors, such as p62 and optineurin. **(4)** The mature autophagosome fuses with the lysosome and the contents are degraded. **(5)** Chaperone mediated autophagy involves the recognition of cytosolic proteins containing the KFERQ motif by the Hsc70 chaperone **(6)**. **(7)** Hsc70 mediates the delivery of the cytosolic protein to the LAMP-2A receptor on the lysosome. The protein substrate unfolds and is translocated across the lysosomal membrane to de degraded. **(8)** Resident acid hydrolyses of the lysosome bring about effective degradation of all autophagic substrates.

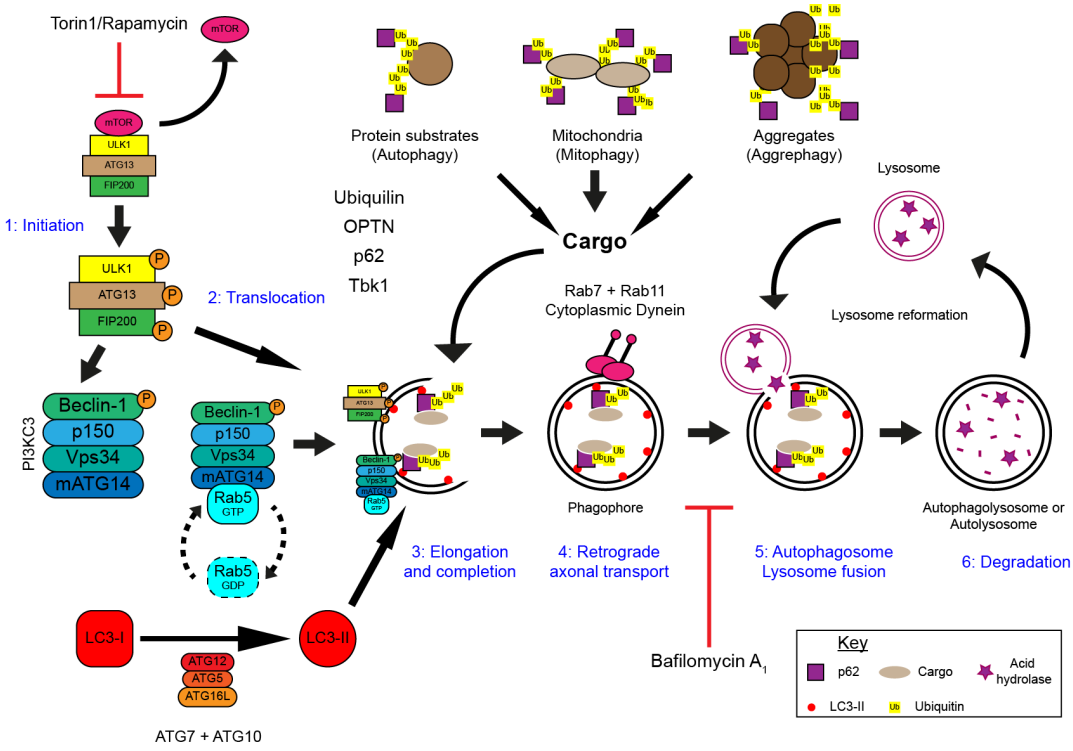

Figure 1.4. Macroautophagy. **1) Initiation.** Autophagy is induced as the inhibitory action of mTOR on the autophagy initiation complex is lost, leading to the activation of ULK1. The activated ULK1-FIP200-ATG13 complex initiates autophagy, by activating the Vps34 complex, leading to the formation of the phagophore. **2) Translocation.** The active ULK1 complex and the Vps34 complex translocate to the site of autophagosome formation. **3) Elongation and completion.** Recruited by the Vps34 complex, the Atg12-Atg5-16L conjugation complex brings about LC3-I lipidation forming LC3-II and promoting elongation of the autophagosome. The autophagy substrates, targeted for autophagy by poly-ubiquitination and/or bound autophagy receptors, such as p62 and optineurin, become nucleated by their interaction with essential autophagy proteins found on the newly formed membrane structure such as LC3-II, allowing for their efficient encapsulation into the autophagosome. **4) Retrograde transport.** Cytoplasmic dynein motor protein is recruited to autophagosomes by the action of Rab7 and Rab11, allowing for the retrograde transport of autophagosomes along microtubules. **5) Fusion.** Delivery of autophagosomes to the lysosome allows for their fusion, which is mediated by the SNAREs VAMP7 and VAMP8 as well as Rab7 and LAMP1 and 2. **6) Degradation.** The autophagolysosome cargo is degraded by components of the lysosome, such as the acid hydrolases. The sites of action of the autophagy inducers, rapamycin and Torin1, and the autophagy inhibitor, bafilomycin A1, are also indicated.

1.5.2.1 Initiation

Initiation involves the formation of a double membrane structure called the isolation membrane or pre-autophagosomal structure (PAS), and the accumulation of a number of essential autophagy proteins to the autophagic membrane (Suzuki et al., 2001). A hierarchical scaffold of autophagy related proteins is seen in both yeast and mammals, although mammalian initiation does not occur at a single phagophore site, as in yeast (Itakura and Mizushima, 2010). Initiation of autophagy is dependent upon a heterotetrameric protein complex, which translocates to the isolation membrane upon the induction of autophagy (Jung et al., 2009). The complex is comprised of Unc-51-like kinase (ULK1), focal-adhesion kinase family-interacting protein of 200 kDa (FIP200), ATG13 and ATG101 (Ganley et al., 2009; Hara et al., 2008; Hosokawa et al., 2009b; Jung et al., 2009; Mercer et al., 2009). Autophagy initiation is regulated in two ways, mTOR dependent and mTOR independent initiation.

1.5.2.1.1 mTOR dependent autophagy

Under basal conditions the mammalian target of rapamycin (mTOR) kinase keeps autophagy in check by phosphorylating and inactivating ULK1 at serine 757 (S757) (Kim et al., 2011). Inhibition of mTOR by starvation or with small molecule inhibitors, such as rapamycin or Torin1, leads to the dephosphorylation of ULK1 at S757, and the subsequent activating phosphorylations at serine 317 and 777 by autophosphorylation and AMP activated kinase (AMPK), a nutrient sensing kinase (Kim et al., 2011). ATG101 appears to stabilise both ATG13 and ULK1 and is essential for autophagy initiation (Hosokawa et al., 2009b; Mercer et al., 2009). The ULK-FIP200-ATG13-ATG101 essentially acts as a framework for the recruitment of other autophagy related proteins and the eventual formation of the autophagosome structure. The induction of autophagy is detailed in figure 1.5.

Upon autophagy initiation and ULK1 activation, ULK1 phosphorylates FIP200 and ATG13, as well as undergoing autophosphorylation (Ganley et al., 2009; Hosokawa et al., 2009b; Jung et al., 2009). The kinase activity of ULK is essential for autophagy induction, resulting in conformational changes within the C-terminal domain (CTD), allowing for membrane association and interaction with subsequent autophagy proteins (Chan et al., 2009). FIP200 appears to determine the localisation of ULK1 to the isolation membrane, and thus, is essential for initiation (Hara et al., 2008). The loss of ULK1, FIP200 or ATG13 is

sufficient to prevent the autophagic response (Chan et al., 2007; Hara et al., 2008; Hosokawa et al., 2009a; Young et al., 2006), suggesting that the complex as a whole is essential for mTOR dependent autophagy initiation (Ganley et al., 2009; Hosokawa et al., 2009a; Jung et al., 2009).

1.5.2.1.2 mTOR independent autophagy

Inositol 1,4,5-triphosphate (IP_3) and cyclic AMP (cAMP) levels control the mTOR independent induction of autophagy (Williams et al., 2008). Increased levels of IP_3 bind to IP_3 receptors (IP_3R) on the ER, releasing Ca^{2+} ions (Berridge, 1993). Increased cytosolic Ca^{2+} activates of the calpain family of cysteine proteases (Williams et al., 2008). Activation of these proteases is dependent upon their binding of two Ca^{2+} ions (Moldoveanu et al., 2002). Activated calpains inhibit autophagy by cleaving downstream autophagy proteins beclin1 and ATG5 (Norman et al., 2010). Calpain activation also leads to cleavage and activation of the G-stimulatory protein α ($G_s\alpha$) (Bamsey et al., 2000), which increases cAMP levels (Sato-Kusubata et al., 2000; Williams et al., 2008). Increased cAMP levels cause the Epac dependent activation of Rap2B and the subsequent activation of phospholipase C-ε (PLCε) (Kopperud et al., 2003; Williams et al., 2008). Activated PLCε promotes the formation of IP_3 from phosphatidylinositol 4,5-bisphosphate (PIP_2) completing the cycle and thus maintaining autophagy inhibition via calpain activation (Sarkar et al., 2005).

Reduced IP_3 levels decrease the release of ER calcium leading to calpain inactivation. Inactive caplains can neither inhibit autophagy nor cleave $G_s\alpha$. Decreased cytosolic Ca^{2+} also results in decreased mitochondrial activity resulting in decreased ATP output. Decreases in ATP production, and the associated increase in AMP, leads to activation of AMP-activated protein kinase (AMPK) (Cardenas et al., 2010). AMPK phosphorylates ULK1 directly, leading to activation of the ULK1 initiation complex and the activation of autophagy (Kim et al., 2011). The mTOR dependent and mTOR independent pathways are outlined in Figure 1.5.

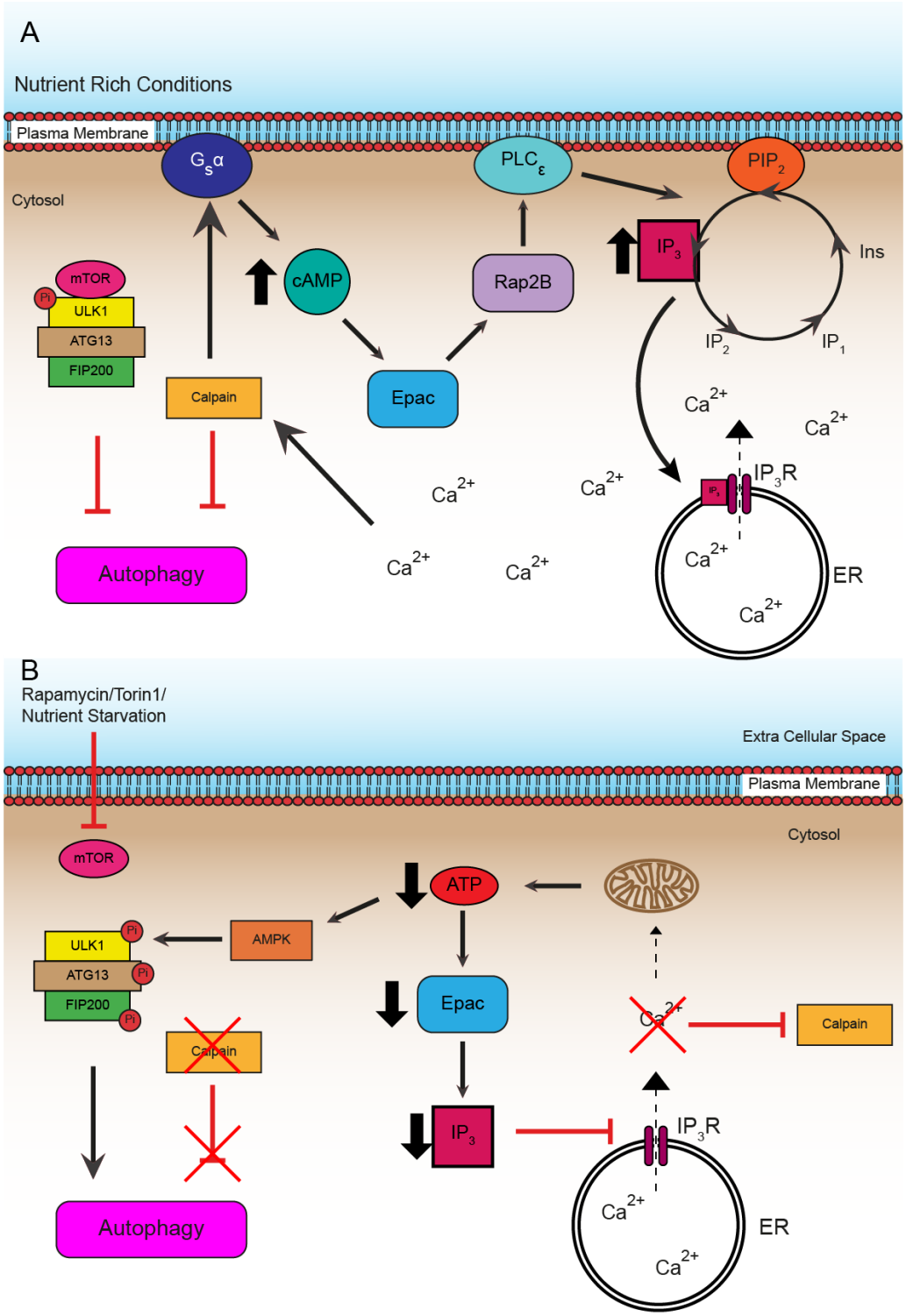

Figure 1.5. mTOR dependent and mTOR independent autophagy. In mTOR dependent autophagy, mTOR binds to the ULK1 initiation complex during nutrient rich conditions, phosphorylating and inactivating ULK1 (A). Upon mTOR inhibition, mTOR is release from this complex leading to the activation of ULK1. ULK1 phosphorylates itself as well as ATG13 and FIP200, leading to activation of the complex and the initiation of autophagy (B). mTOR independent

autophagy is cyclic. In A) High levels of cyclic AMP (cAMP) lead to activation of the Rap GEF Epac. Epac activates Rap2B leading to activation of phospholipase C-ε (PLCε). PLCε enhances the formation of Inositol 1,4,5-triphosphate (IP_3) from phosphatidylinositol 4,5-bisphosphate (PIP_2). IP_3 leads to inhibition of autophagy, but also binds the IP_3 receptors (IP_3R) on the ER, bringing about release of Ca^{2+}. Increased cytosolic calcium activates the calpain family of cysteine proteases. Calpains inhibit autophagy but also activate the G-stimulatory protein α ($G_s\alpha$), which in turn increases the cytosolic levels of cAMP thus propagating the inhibition of autophagy. During autophagy induction in B) IP_3 levels fall, leading to reduced Ca^{2+} release from the ER resulting in calpain inactivation. In addition, low cytosolic Ca^{2+} leads to reduced Ca^{2+} uptake by the mitochondria reducing the ATP output. Lower levels of ATP result in the activation of AMP-activated protein kinase (AMPK), which phosphorylates ULK1 leading to autophagy initiation. Reduced ATP production also results in reduced cAMP levels and so the Epac/Rap2B pathway is no longer induced.

1.5.2.2 Vesicle formation and elongation

As detailed in Figure1.4, after autophagy induction, activated ULK1 phosphorylates its downstream target, Beclin-1, leading to activation of the class III phosphatidylinositol 3-kinase (PI3K) complex (PI3KC3) (Russell et al., 2013). The PI3KC3 complex is comprised of the class III PI3K, vacuolar protein sorting 34 (Vps34), Beclin-1, p150 and mATG14/Barkor (Furuya et al., 2005; Itakura et al., 2008; Liang et al., 1999; Sun et al., 2008). The PI3K complex functions to synthesise phosphatidylinositol 3-phosphate (PtdIns3P), a signalling lipid that is essential for autophagosome formation and the recruitment of further components required for autophagosome extension and closure (Axe et al., 2008; Backer, 2008; Devereaux et al., 2013; Vergne et al., 2009).

Elongation of the double membrane structure is dependent on two protein conjugates as detailed in Figure 1.4, the ATG12-ATG5-ATG16L1 conjugate and the microtubule-associated protein 1 light chain 3 (LC3) lipid conjugate (Hanada et al., 2007). The ubiquitin-like protein (Ubl) ATG12 is covalently bound to ATG5 by the actions of ATG7 and ATG10 (Mizushima et al., 1998). The ATG12-ATG5 conjugate interacts with the multimeric protein ATG16L1, which directs this complex to the newly forming isolation membrane, possibly via its interaction with FIP200 (Fujita et al., 2008; Gammoh et al., 2013; Matsushita et al., 2007; Mizushima et al., 2003; Nishimura et al., 2013). ATG12-5-16L1 is then able to function as an E3 ubiquitin-ligase-like enzyme for the conjugation of phosphatidylethanolamine (PE) to the C-terminal of LC3-I, forming LC3-II (Hanada et al., 2007; Noda et al., 2013). LC3-II has been shown to be a component of the autophagosome membrane and is therefore often used as a marker of autophagosomes during the study of autophagy (Kabeya, 2000; Kabeya et al., 2004).

The actual origin of the autophagosomal membrane is unclear (Tooze and Yoshimori, 2010). Most evidence suggests that membrane lipids are recruited from multiple existing membrane sources such as the ER, Golgi, plasma membrane or mitochondria, due to the range of markers present within them (Axe et al., 2008; Hailey et al., 2010; Hayashi-Nishino et al., 2009; Ravikumar et al., 2010; Yen et al., 2010; Ylä-Anttila et al., 2009). There is also evidence that the PI3KC member ATG14/Barkor is able to bind the soluble N-ethylmaleimide-sensitive factor attachment protein receptor (SNARE), syntaxin-17, which is localised to ER-mitochondria contact sites, thus suggesting ER-mitochondrial

membranes may also play a role in autophagosome biogenesis (Hamasaki et al., 2013). In yeast, ATG9, a transmembrane protein required for autophagosome formation, forms vesicular and tubular structures during the early stages of autophagy induction, aiding in the formation of a PAS (Mari et al., 2010). The mammalian homologue of ATG9 (mATG9) is localised to the Golgi network, but redistributes to LC3 positive membranes during autophagy induction (Young et al., 2006), suggesting mATG9 may also function in membrane delivery for autophagosome formation.

The formation of mature autophagosomes is thought to require the fusion of multiple ATG16-positive precursor membranes, which is mediated by a number of SNAREs including vesicle associated membrane protein 7 (VAMP7), syntaxin-7 and syntaxin-8 (Moreau et al., 2011; Moreau and Rubinsztein, 2012).

1.5.2.3 Defining the cargo

The targeting of specific cargos for autophagic breakdown is dependent on substrate ubiquitination (Kim et al., 2008). Ubiquitinated substrates are recognised by autophagy receptor proteins such as p62/SQSTM1 (Sequestosome) and optineurin (Bjørkøy et al., 2005; Pankiv et al., 2007; Wild et al., 2011; Wong and Holzbaur, 2014). P62 binds ubiquitin on the substrate via its ubiquitin associated (UBA) domains and LC3 on the pre-autophagosome via its LC3-interacting region (LIR) (Lamark et al., 2009). Thus ubiquitinated substrates are targeted to autophagosomes, along with p62 itself (Kim et al., 2008; Komatsu et al., 2007; Pankiv et al., 2007). Loss or reduction of p62 expression has been shown to lead to increased cell death under stress conditions while inhibition of autophagy has been shown to increase the number of p62/LC3 positive inclusions within cells (Bjørkøy et al., 2005). Consequently, pathological accumulations of p62 are indicative of defective autophagy (Pankiv et al., 2007).

1.5.2.4 Maturation, Transport and Fusion

Autophagosome formation can occur at multiple positions within the cytosol, and thus autophagosomes are transported towards the centrosome to facilitate their final fusion with lysosomes (Kimura et al., 2008). The transport of autophagosomes to the centrosome is mediated by the molecular motor protein cytoplasmic dynein and its binding partner dynactin (Gill et al., 1991; Jahreiss et al., 2008; Kimura et al., 2008; Ravikumar et al., 2005). Transport of

autophagosomes is particularly important in neuronal cells, where autophagosomes can form at the very distal tip of the axon, and so must be transported over a considerable distance to allow fusion with the lysosomes, which are particularly enriched at the cell body (Lee et al., 2011; Maday et al., 2012). Several studies indicate that cytoplasmic dynein is required for retrograde transport of autophagosomes in neurons (Katsumata et al., 2010; Kimura et al., 2008; Ravikumar et al., 2005). Autophagosomes are thought to recruit cytoplasmic dynein via their fusion with late endosomes (Cheng et al., 2015).

The fusion of autophagosomes with other membrane vesicles, such as multivesicular bodies (MVBs) and late endosomes, forms amphisomes, prelysosomal hybrid organelles (Fader et al., 2008; Filimonenko et al., 2007; Razi et al., 2009). This fusion event is thought to be essential for degradation of aggregate prone autophagy substrates (Filimonenko et al., 2007). Autophagosome and MVB fusion is mediated by the SNARE VAMP3, as well as members of endosomal sorting complexes required for transport (ESCRT) machinery (Fader et al., 2009; Filimonenko et al., 2007; Rusten et al., 2007). The SNAREs, VAMP7 and VAMP8, mediate the final fusion event of the autophagosome with the lysosome (Fader et al., 2009; Furuta et al., 2010).

After fusion with the lysosome, active acid hydrolyses such as the cathepsin family members, degrade the autophagosome cargo, recycling nutrients and metabolites, namely amino acids, back to the cytosol for the maintenance of normal cellular function (Tanida et al., 2005). The syntaxin-5 SNARE complex is required for correct lysosome function by mediating the activity of lysosomal proteases (Renna et al., 2011). The recycling of autophagic cargo feeds back to the mTOR complex 1 (mTORC1) reactivating mTOR and re-inhibiting autophagy (Yu et al., 2010).

1.5.2.5 Rab GTPases and autophagy

GTPases act as molecular switches for a range of processes, switching from an inactive GDP bound state to an active GTP-bound state, a process that is mediated by the guanine nucleotide exchange factors (GEFs). The Rab family of GTPases regulate a wide range of membrane trafficking events, from vesicle formation to transport and fusion (Zerial and McBride, 2001). It is therefore not surprising that these molecular switches have been found to play important roles

throughout the autophagy pathway (Ao et al., 2014). For a review of the Rab involvement in autophagy see Ao et al. 2014 (Ao et al., 2014).

The monomeric GTPase Rab1 controls traffic from the ER to the Golgi, but is also required for autophagosome formation (Zoppino et al., 2010), while in yeast the Rab1 homologue, Ypt1 interacts with ATG9 and regulates trafficking of the ATG1 complex (the homologue of the ULK1 complex) to the PAS (Kakuta et al., 2012; Lipatova et al., 2012; Wang et al., 2013). Interestingly, knock down of Rab1a inhibits autophagosome formation and also results in reduced recruitment of mATG9, which resides in the Golgi, to LC3 positive structures (Winslow et al., 2010; Winslow and Rubinsztein, 2011; Young et al., 2006). Rab33B, another Golgi resident Rab, interacts with the ATG16L conjugate, again supporting the role of Golgi membrane in the formation of autophagosomes (Itoh et al., 2008).

Rab5 is known to activate Vps34 and also to interact with Beclin1 in a Vps34 dependent manner, suggesting Rab5 is a component of the PI3K complex (Ao et al., 2014; Ravikumar et al., 2008). The Rab5 GEF, Alsin, is also implicated in ALS, as will be discussed in section 1.6.

Like the Golgi and ATG9 vesicles, ER membranes have been implicated in autophagosome formation. Rab32 may aid in the recruitment of ER membranes to newly forming autophagosomes (Hirota and Tanaka, 2009). However, Rab32 is also mitochondrial associated and thus may be involved mitophagy as well as bulk autophagy (Alto et al., 2002).

Rab7 is important for the progression of autophagy, interacting indirectly with LC3 positive vesicles to mediate their transport and perinuclear accumulation (Gutierrez et al., 2004; Jäger et al., 2004; Pankiv et al., 2010). Indeed, Rab7 is required for the recruitment of dynactin and dynein to the late endosomes and autophagosomes to mediate their retrograde transport (Johansson et al., 2007). Rab7 also plays an important role in the final autophagosome-lysosome fusion event (Gutierrez et al., 2004; Jäger et al., 2004). The recruitment of Rab7 to the autophagosome-lysosome membranes is dependent on the lysosomal associated membrane proteins (LAMP) 1 and 2 (Jäger et al., 2004).

Rab11 localisation to MVBs may be important for their fusion with the autophagosomes (Fader et al., 2008), and thus Rab11 may also be involved in recruitment of late endosomes and dynein to autophagosomes.

1.6 Dysfunctional autophagy in ALS

The role of autophagy in neuronal health is well established. Neuronal-specific knock-out of a number of autophagy genes in mice, such as *Atg7*, *Atg5* and *RB1CC1* (*FIP200*), all lead to neurodegeneration, which is accompanied by reduced motor function and cytoplasmic inclusion body accumulation in neurons (Hara et al., 2006; Komatsu et al., 2006; Liang et al., 2010). Several ALS/FTD related genes show direct links to the autophagy pathway, and can be placed at distinct positions within the process. These examples will be discussed below. The FALS associated mutations and their links to the steps of autophagy are detailed in Figure 1.6.

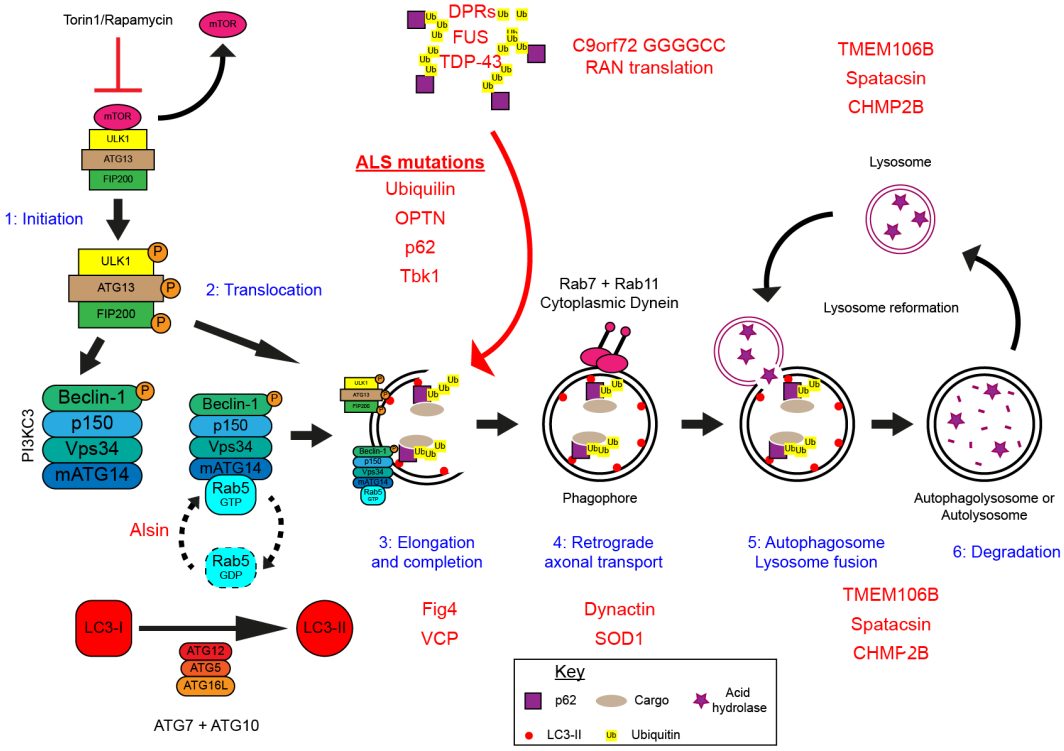

Figure 1.6. Autophagy and ALS. The steps of autophagy affected by single gene mutations in FALS. Alsin mutations affect Rab5 activation and thus activation of the PI3K complex. Mutation in proteins such as p62, Optineurin, UBQLIN2 and Tbk1 are thought to prevent sequestration of substrates to the autophagosome in cases of ALS. Mutations in VCP and FIG4 may lead to ALS due to a failure in maturation of the autophagosome leading to defective autophagy. Mutations in dynactin, which causes a subset of FALS, disrupts dynein-mediated transport, possibly resulting in damaged transport of autophagosomes. Mutated SOD1 has also been implicated in the disruption of cytoplasmic dynein-mediated transport. Damage to transport may lead to dysfunctional autophagy by preventing maturation of the autophagosomes and their subsequent fusion with the lysosome. Mutations that are thought to prevent fusion with the lysosome essentially block the final step of autophagy. Ubiquilins regulate autophagosome delivery to the lysosome. UBQLIN2 mutations, which cause FALS, possibly lead to disease due to impaired fusion with the lysosome. As part of the ESCRT-III complex, mutations to CHMP2B may inhibit the final fusion step and therefore the completion of autophagy. The C9orf72 associated dipeptide repeat proteins may increase pressure on the autophagy pathway. TMEM106B is involved in lysosomal biology and SNPs in TMEM106B modulate C9ALS/FTD.

1.6.1 Alsin

The protein product from the *ALS2* gene, Alsin, is a GEF for Rab5 (Topp et al., 2004). As described above, Rab5 interacts with the Vps34 complex to bring about activation of the complex and recruitment of the ATG12-ATG5 conjugation system (Ravikumar et al., 2008). Pathogenic missense mutation in *ALS2* lead to the loss of function of Alsin as a Rab5 GEF, thus leading to defective Vps34 activation and defective autophagosome formation and ultimately the development of ALS (Hadano et al., 2001a; Hadano et al., 2010; Otomo et al., 2011). Loss of Alsin in a SOD1 mouse model of ALS exacerbates disease due to reduced lysosomal degradation and increase pathogenic protein accumulation (Hadano et al., 2010).

1.6.2 FIG4

Mutations to the phosphoinositide 5-phosphatase *FIG4* gene cause approximately 1-2% of ALS, as well as another neurological disorder, Charcot-Marie-Tooth (CMT) 4J, a rare autosomal recessive, but severe form of CMT characterised by juvenile onset (Chow et al., 2009; Chow et al., 2007). FIG4 regulates the cellular levels of phosphatidylinositol-3,5-biphosphate ($PI(3,5)P_2$), a signalling lipid known to function in autophagy (Ferguson et al., 2009). $FIG4^{-/-}$ mice accumulate a number of proteins associated with autophagy, including p62 and LC3-II, suggesting defective clearance (Ferguson et al., 2009). Mutations in *FIG4* lead to loss of function and therefore reduced $PI(3,5)P_2$ signalling. This may result in defective autophagy by inhibiting vesicle fusion or reducing the activity of the lysosome (Ferguson et al., 2009).

1.6.3 p62

Mutations in p62 have been found in FALS and SALS (Fecto et al., 2011; Hirano et al., 2013; Rubino et al., 2012; Teyssou et al., 2013). As described, p62 is one of the main autophagy receptors, delivering ubiquitinated cargo to the autophagosome for degradation (Matsumoto et al., 2011; Pankiv et al., 2007). Accumulations of p62 are therefore indicative of dysfunctional autophagy, and these inclusions are seen in patients with these mutations (Teyssou et al., 2013). A missense mutation in exon 8 and a substitution in exon 7, which may affect splicing, are located in the UBA domain of p62 (Teyssou et al., 2013). This may disrupt the ability of p62 to bind its ubiquitinated substrates leading to a loss of function of p62 and the accumulation of protein aggregates.

1.6.4 Optineurin

Optineurin functions in a similar way to p62, acting as an autophagy receptor and bringing cargoes, such as protein aggregates and mitochondria, into contact with the autophagosome by its interaction with LC3-II (Wild et al., 2011; Wong and Holzbaur, 2014). Nonsense and missense mutations in *OPTN* causative for ALS have been described, all of which result in increased inclusion body accumulation, which contain optineurin (Ito et al., 2011; Korac et al., 2013; Maruyama et al., 2010; Weishaupt et al., 2013). The Q398X nonsense mutation and the E478G missense mutation result in premature stop codon formation, and the likelihood of nonsense mediated decay, suggesting a loss of function of optineurin, and reduced autophagic clearance of protein aggregates (Ito et al., 2011; Maruyama et al., 2010). Due to the involvement of optineurin in mitophagy (Wong and Holzbaur, 2014), loss of functional optineurin could also result in the accumulation of dysfunctional mitochondria, therefore combining the mechanisms of protein aggregation and mitochondrial dysfunction in the development of optineurin related ALS.

1.6.5 VCP

Valosin containing protein, VCP, is a multi ubiquitin chain binding protein, and is involved in delivery of substrates to the proteasome for degradation (Dai and Li, 2001). R191Q and R155H missense mutations in VCP are causative for a form of autosomal dominant ALS (Johnson et al., 2010). Loss of VCP leads to accumulations of autophagy substrates due to failure to clear the mature autophagosomes, reminiscent of the effect of FIG4 mutations (Ferguson et al., 2009; Ju et al., 2009; Tresse et al., 2010). In VCP mutant cells or VCP knock down cells, LC3 positive autophagosomes fail to fuse with the lysosomes, thus resulting in the accumulation of ubiquitin, p62 and LC3 positive structures (Ju et al., 2009; Tresse et al., 2010). How the mutations cause this autophagy defect is unclear, but other reports have implicated VCP in ubiquitinated substrate sorting through endosomal trafficking (Ritz et al., 2011), a process closely linked to the autophagy pathway (Razi et al., 2009). The defect in autophagy caused by these mutations leads to the redistribution of TDP-43 from the nucleus to the cytoplasm of cells, suggesting that TDP-43 may be a substrate of autophagy (Ju et al., 2009). Indeed, the induction of autophagy is able to enhance the clearance of TDP-43, reducing mislocalisation and aggregation (Barmada et al., 2014). Mutations to *VCP* are also associated with inclusion body myopathy, Paget's disease of bone and FTD (IBMPFD), which is characterised by

muscular accumulations and inclusions of ubiquitin, TDP-43 as well as p62 and LC3 (Johnson et al., 2010; Watts et al., 2004). Similar to p62 mutations, which are causative for Paget's disease of bone (Layfield et al., 2006), the role of VCP in IBMPFD may be due to defects in the ubiquitin binding ability of VCP (Watts et al., 2004).

1.6.6 Ubiquilin-2

Mutations to the ubiquitin-like protein ubiquilin-2 have been shown to cause dominantly inherited X-linked ALS and ALS/dementia (Deng et al., 2011). Ubiquilin-2 mutants develop protein inclusions, the hallmark of ALS, with ubiquilin-2 protein being a component of these inclusions (Deng et al., 2011). The C terminus of ubiquilin-2 is able to bind poly-ubiquitin chains and aid in delivery of substrates to the proteasome (Ko et al., 2004). However, ubiquilin-2 has also been implicated in the autophagy pathway, binding both ubiquitinated substrates and LC3 in a similar fashion to p62 (N'Diaye et al., 2009a; N'Diaye et al., 2009b; Rothenberg et al., 2010). Loss of ubiquilin-2 inhibits autophagy induction and autophagosome formation leading to increased susceptibility to starvation-induced stress (N'Diaye et al., 2009a; N'Diaye et al., 2009b). It has been proposed that the ubiquilin-2 mutants are defective in the delivery of poly-Ub substrates (Chang and Monteiro, 2015). Ubiquilin-2 also co-localises with optineurin on Rab11, p62 and ULK1 positive vesicles (Osaka et al., 2015). ALS associated ubiquilin-2 mutations result in loss of ubiquilin-2 from these vesicles suggesting a loss of function mechanism (Osaka et al., 2015).

1.6.7 CHMP2B

The charged multivesicular body protein 2B (CHMP2B) is involved in the endosomal ESCRT-III complex, with mutations known to cause FTD (Skibinski et al., 2005), as well as predominantly lower motor neuron ALS (Cox et al., 2010; Parkinson et al., 2006). The ESCRT-III complex functions to sort ubiquitinated integral membrane proteins into intraluminal vesicles and MVBs. The formation of these MVBs has been shown to be required for efficient autophagic degradation, with loss of ESCRT members or expression of mutant CHMP2B leading to the accumulation of autophagic markers such as p62 and LC3-II (Filimonenko et al., 2007). Expression of mutant CHMP2B in cells leads to accumulations of LC3-II and disrupted lysosomal localisation, supporting a role of CHMP2B in autophagy (Cox et al., 2010; Lee et al., 2007). This accumulation is potentially due to failure of the final fusion step required for

degradation of ubiquitinated substrates (Filimonenko et al., 2007; Urwin et al., 2010).

1.6.8 Dynactin

Dynactin interacts with cytoplasmic dynein to bring about retrograde transport of cargos (Fig 1.1) (Waterman-Storer et al., 1997). Missense mutation in the p150 subunit of dynactin (*DCTN1*) was initially found in one kindred suffering from a form of lower motor neuron disease (Puls et al., 2003). Since this time, multiple point mutations have been discovered within *DCTN1*, leading to a variety of phenotypes and neurodegenerative diseases, including Parkinson's and ALS (Münch et al., 2005; Münch et al., 2004; Vilariño-Güell et al., 2009). This suggests that dynactin is important for neuronal health and is indeed involved in neurodegeneration. The mutations within *DCTN1* appear to act as risk or susceptibility factors for the development of ALS (Münch et al., 2005). The ALS associated mutations of dynactin appear to disrupt dynein-dynactin function leading to aggregation of mutant dynactin and other proteins (Levy et al., 2006). As autophagosomes are transported in a retrograde manner in neurons by the dynein-dynactin complex (Maday et al., 2012), mutation in the p150 subunit of dynactin may lead to disease due to failed transport and accumulation of autophagosomes.

1.6.9 TBK1

A number of loss of function mutations within the *TANK-binding kinase 1* (*TBK1*) gene are associated with FALS/FTD by a mechanism of haploinsufficiency (Freischmidt et al., 2015). TBK1 regulates autophagy by directly phosphorylating optineurin, which increases its interaction with LC3 and the autophagosomes (Weidberg and Elazar, 2011). As an autophagy receptor, increasing the interaction of optineurin with LC3-II increases the delivery of substrates to the autophagosomes (Weidberg and Elazar, 2011). TBK1 also phosphorylates p62 to efficiently regulate the autophagosomal clearance of mitochondria (Matsumoto et al., 2015). As optineurin and p62 are both adaptor proteins of TBK1 (Pilli et al., 2012; Wild et al., 2011), loss of function of TBK1 could result in reduced autophagosome maturation and defective autophagic clearance, suggesting defective autophagy could be contributing to disease in these patients.

1.6.10 SigR1

Mutation in Sigma-1 receptor (SigR1) has been reported to cause juvenile onset ALS and FTD (Al-Saif et al., 2011), which may be a result of loss of function of SigR1 (Prause et al., 2013). SigR1 is located at ER mitochondrial contact sites, and is involved in regulating calcium signalling and cell survival (Hayashi and Su, 2007). However, SigR1 activation has also been linked to autophagy induction (Schrock et al., 2013). Interestingly, loss of SigR1 leads to disrupted ER and mitochondrial morphology as well as defective autophagic degradation (Vollrath et al., 2014).

1.6.11 Spatacsin

Deletions within *SPG11* lead to frame shift mutations and premature stop codon formation, resulting in loss of function of the *SPG11* gene product, Spatacsin, leading to classical hereditary spastic paraplegia as well as juvenile recessive ALS (Orlacchio et al., 2010). Loss of Spatacsin results in autophagosome accumulation, which fail to clear, possibly as a result of defective lysosome biogenesis (Chang et al., 2014; Renvoisé et al., 2014). Evidence from patient derived neurons and mouse models suggests loss of Spatacsin leads to reduced anterograde vesicle transport and therefore defective axonal transport (Pérez-Brangulí et al., 2014). As neuronal biology relies heavily on the cells ability to efficiently transport cargos to and from the cell body, defective axonal transport can be catastrophic for the neuronal health. Both defective autophagy and decreased axonal transport could be at play to bring about motor neuron degeneration in these patients.

Thus, defective autophagy is a potentially common mechanism of disease in ALS and FTD.

1.7 C9ORF72 and ALS

In 2011 Renton et al. and DeJesus-Hernandez et al. discovered the genetic mutation that was associated with chromosome 9p21-linked ALS (DeJesus-Hernandez et al., 2011; Renton et al., 2011). This section will discuss the current understanding of C9orf72 related ALS.

1.7.1 Clinical and pathological features of the *C9orf72* repeat expansion

Previous linkage analysis studies had identified a locus on chromosome 9p21 that appeared to be involved in the development of ALS, FTD and ALS with FTD (Boxer et al., 2011; Morita et al., 2006; Vance et al., 2006). In 2011 this locus was identified as a large hexanucleotide repeat expansion of GGGGCC within the first intron of the *C9orf72* gene (DeJesus-Hernandez et al., 2011; Renton et al., 2011) (Figure 1.7).

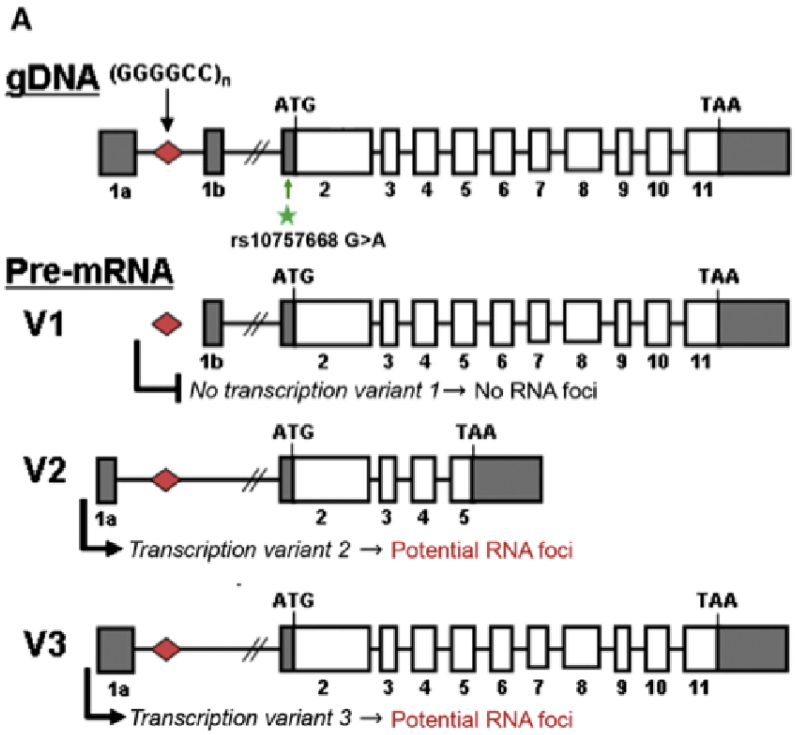

Figure 1.7. C9orf72 transcriptional variants. **A)** Overview of the genomic structure of the *C9ORF72* locus (top panel) and the *C9ORF72* transcripts produced by alternative pre-mRNA splicing (bottom panels). Boxes represent coding (white) and non-coding (grey) exons and the positions of the start codon (ATG) and stop codon (TAA) are indicated. The GGGGCC repeat is indicated

with a red diamond. The position of rs10757668 is indicated with a green star. Reused with permission from DeJesus-Hernandez et al. 2011 (DeJesus-Hernandez et al., 2011).

This defect has been shown to be the most common genetic cause of ALS and FTD, with frequencies varying within different populations. For example, the repeat expansion accounted for 46% of FALS and 29.3% of FTD cases in a Finnish population (Renton et al., 2011), 43% of FALS and 35% of familial FTD in a cohort from northern England (Cooper-Knock et al., 2012), but only 3.4% of FALS in a Japanese population (Konno et al., 2013b). Giving rise to such relatively high proportions of FALS and FTD cases, as well as a proportion of sporadic cases, led to the name, C9ALS/FTD (Cooper-Knock et al., 2012; Majounie et al., 2012). The pathology and clinical phenotypes typical of ALS are observed in C9ALS/FTD, however there are also a number of differences. Aside from the higher than expected incidence of FTD amongst C9orf72 related ALS patients, there is also an increase in bulbar onset (approximately 20% more than non C9orf72 carriers) as well as a shorter disease progression compared to non-C9orf72 carriers, both of which suggest a more severe and aggressive disease progression (Chiò et al., 2012; Cooper-Knock et al., 2012).

A repeat size of greater than 30 is generally considered pathogenic, but repeats of greater than 2000 have been reported in some patients (Buchman et al., 2013; DeJesus-Hernandez et al., 2011; Renton et al., 2011; van Blitterswijk et al., 2013), and relatively small repeats of 20-30 have been correlated with increased risk of ALS and FTD (Byrne et al., 2013; Gómez-Tortosa et al., 2013). A definite link between repeat length and severity of disease is yet to be established with reports of no correlation between repeat length and age of onset in ALS (Dols-Icardo et al., 2014; van Blitterswijk et al., 2013). However, repeat length in FTD does appear to correlate with age of onset (van Blitterswijk et al., 2013).

Anticipation in genetics describes the tendency for a disease to present at an earlier age of onset in subsequent generations. While there is little evidence for a link between disease severity and repeat length in ALS, there does appear to be a level of anticipation, with an earlier age of onset identified in the youngest generations (Benussi et al., 2014; Chiò et al., 2012).

The pathology of C9orf72 patients is consistent with other forms of ALS, and includes the hallmark phosphorylated TDP-43-positive neuronal cytoplasmic inclusions (Cooper-Knock et al., 2012). However, C9ALS/FTD cases can be distinguished from other ALS and FTD cases by the presence of specific ubiquitin and p62 positive, TDP-43 negative, neuronal cytoplasmic inclusions and intranuclear inclusions in the cerebellum, hippocampus and the neocortex (Al-Sarraj et al., 2011; Arai et al., 2006; Cooper-Knock et al., 2012; Stewart et al., 2012). There is also pathology associated with the repeat itself, namely nuclear RNA foci and dipeptide repeat proteins. Both these inclusions may relate directly to the mechanism of disease as detailed in section 1.7.2.

1.7.2 Pathogenic Mechanisms in C9orf72 ALS/FTD

To date there are 3 main disease mechanisms associated with the repeat expansion: 1) RNA toxicity of the repeat expansion, 2) protein toxicity from aberrantly transcribed dipeptide repeat proteins from the repeat expansion and 3) haploinsufficiency of *C9orf72*. All 3 mechanisms have been previously described in other repeat expansion disorders associated with neurodegeneration (Taneja et al., 1995; Zu et al., 2011).

1.7.2.1 RNA toxicity

Nuclear RNA foci transcribed from the repeat expansion were found in the original studies detailing the C9orf72 repeat expansion patients (DeJesus-Hernandez et al., 2011). The repeat expansion is transcribed in a bidirectional manner, giving rise to sense and antisense transcripts (Gendron et al., 2013; Lagier-Tourenne et al., 2013; Mizielinska et al., 2013). These repeat expansions are thought to cause disease due to the sequestration of RNA binding proteins to the large RNA expansion, perturbing normal cellular function. A number of groups have identified a range of RNA binding proteins (RBPs) that interact with the repeat expansion, including heterogeneous nuclear ribonucleoproteins (hnRNPs) A1 (hnRNP A1) and H1/F (hnRNP H1/F) and serine/arginine-rich splicing factor 2 (SRSF2) (Cooper-Knock et al., 2014; Lee et al., 2013; Mori et al., 2013a; Sareen et al., 2013; Xu et al., 2013). All these proteins are involved in RNA metabolism and so their increased recruitment to this aberrant expansion may lead to their dysfunction, and the development of disease.

RNA-editing deaminase RNA-specific B2 (ADARB2) was also shown to bind specifically to the repeat expansion in induced-pluripotent stem cells (iPSC)

derived neurons from C9ALS patients. Loss of ADARB2 leads to an increase in iPSC neuron susceptibility to glutamate (Donnelly et al., 2013). Therefore, recruitment of ADARB2 to these transcribed repeats may lead to its loss of function, increased excitotoxicty and the development of ALS (Donnelly et al., 2013).

The guanine and cytosine rich nature of the repeat expansion lends itself to the formation of DNA and RNA secondary structures, including hairpin loops and G-quadruplex structures, which are tetrameric planar stacks of four G bases (Haeusler et al., 2014; Su et al., 2014). These G-quadruplex structures lead to abortive transcription, an increase in truncated transcripts as well as recruitment of nucleolin (Haeusler et al., 2014). Redistribution of nucleolin from the nucleolus to these G-quadruplex repeat expansions-associated structures may result in decreased ribosomal RNA maturation, leading to nucleolar stress and cell death (Haeusler et al., 2014).

Mouse models of the C9orf72 repeat expansion have been shown to recapitulate aspects of C9ALS/FTD. Mice virally transduced with a vector harbouring 66 G_4C_2 repeats exhibited pathology similar to C9ALS/FTD, namely the phosphorylated TDP-43 neuronal inclusions as well as RNA foci (Chew et al., 2015). While these mice did exhibit cortical neuron loss they did not show motor neuron loss or indeed the ubiquitin/p62 positive, TDP-43 negative inclusions, which are specific to C9ALS/FTD (Chew et al., 2015). Transgenic mice carrying a bacterial artificial chromosome (BAC) containing the human *C9orf72* gene with 100-1000 G_4C_2 repeats (O'Rourke et al., 2015) or approximately 500 repeats (Peters et al., 2015) showed RNA foci formation and nucleolin redistribution. However, expression of these repeats did not lead to neurodegeneration or behavioural phenotypes (O'Rourke et al., 2015; Peters et al., 2015).

1.7.2.2 Dipeptide repeat protein toxicity

Evidence from other repeat expansion disorders has shown that repeat expansions can be translated in a non-ATG dependent manner, termed repeat-associated non-ATG (RAN) translation (Zu et al., 2011). While this leads to repeating units of individual amino acids in trinucleotide repeat expansion disorders (e.g. polyglutamine proteins in myotonic dystrophy), the hexanucleotide repeat expansion in C9orf72 gives rise to dipeptide repeat

(DPR) proteins (Mori et al., 2013b). Similar to the CAG expansion in the *ataxin8* gene in spinocereballar ataxia 8 (Zu et al., 2011), this hexanucleotide stretch within *C9orf72* can be translated in all 3 reading frames, as well as the sense and antisense direction (Mori et al., 2013a). This leads to the production of 5 DPR species: poly-(Glycine-Alanine) (poly-GA), poly-(Glycine-Arginine) (poly-GR), poly-(Glycine-Proline) (poly-GP), poly-(Proline-Arginine) (poly-PR) and poly-(Alanine-Proline) (poly-AP) (Mori et al., 2013a; Mori et al., 2013b). All 5 of these DPR species are found to aggregate in p62 positive, TDP-43 negative, ubiquitinated cytoplasmic inclusions in patients (May et al., 2014; Mori et al., 2013a). However, poly-GA proteins appear to be the most prevalent component of these inclusions (Mori et al., 2013a; Mori et al., 2013b), while poly-GR and poly-PR proteins have the most nuclear localisation out of all the species (Mori et al., 2013b). The differences in abundance and distribution could indicate different modes of disease for the different DPRs.

Evidence for a possible role of DPR protein toxicity in the development of C9ALS/FTD comes from the study of *Drosophila* models of *C9orf72* repeat expansion related DPR proteins. Expression of 36 and 100 repeats of poly-GR and poly-PR DPR proteins in the *Drosophila* eye caused degeneration of the eye, indicating neuronal toxicity (Mizielinska et al., 2014). This study also employed an RNA only model where interruption of the repeat expansion with stop codons prevented the formation of DPR proteins. In this case, the expansion alone was not sufficient to cause toxicity and did not cause neurodegeneration (Mizielinska et al., 2014), suggesting RNA toxicity alone is not sufficient to cause disease. DPR protein production has also been reported in the BAC mouse models of *C9orf72* repeat expansions, but as discussed above, there was no evidence of related neurotoxicity (O'Rourke et al., 2015; Peters et al., 2015).

Evidence from cell models also indicates poly-GR and poly-PR DPR proteins are particularly toxic. Both were capable of inducing nucleolar stress by binding irreversibly to the nucleolus leading to dysregulated RNA biogenesis and eventually cell death (Kwon et al., 2014). The toxicity of these species may be attributed to their effects on RNA processing and ribosome synthesis (Kwon et al., 2014). The ability of poly-GR and poly-PR proteins to interact with the nucleolus may be, in part, linked to the variation in distribution of the different DPR species.

The cytoplasmic aggregation of these ubiquitinated DPR species suggests their ineffective clearance. Their inclusion in p62 positive aggregates in C9ALS/FTD patients (May et al., 2014; Mori et al., 2013a) therefore suggests a failure or blockage of the autophagy pathway. However, the accumulation of such aggregates, labelled with both ubiquitin and p62, also suggests the formation of the so called aggresome, a structure of multiple misfolded and aggregating proteins that are cleared by a type of specialised autophagy, termed aggrephagy (Hyttinen et al., 2014) (see Fig. 1.4). Although potentially functioning as a protective mechanism, the formation of protein aggregates has been shown to be cytotoxic (Bucciantini et al., 2002).

The DPR species have also been reported to interact with a range of other cellular proteins, potentially perturbing their normal cellular function, thus leading to disease. Firstly, expression of 149 repeats of poly-GA in cortical neurons has identified a number of ubiquitin proteasome related binding partners, including p62, ubiquilin-1 and 2, as well as subunits of the proteasome machinery (May et al., 2014). GA rich repeats within the Epstein-Barr Virus (EBV) nuclear antigen (EBNA) 1 protein have previously been shown to disrupt and inhibit the ubiquitin proteasome system (Levitskaya et al., 1997), raising the possibility that the poly-GA DPR proteins have the same effect.

Secondly, Unc119 was identified as an interacting partner of poly-GA DPR proteins. Unc119 has been reported to function in axon development in *C.elegans,* and is conserved in humans (Knobel et al., 2001; Maduro et al., 2000). Unc119 also appears important for cellular trafficking in neurons, regulating transport of G proteins to their correct cellular compartment (Constantine et al., 2012; Zhang et al., 2011). Sequestration of Unc119 into cytoplasmic aggregates of poly-GA DPR proteins could therefore reduce the cellular pool of available Unc119, disrupting normal trafficking in neurons and possibly contributing to disease (May et al., 2014).

1.7.2.3 Haploinsufficiency

Several groups have reported reduced expression of *C9orf72* in patients (Belzil et al., 2013; Cooper-Knock et al., 2012; DeJesus-Hernandez et al., 2011; Donnelly et al., 2013; Gijselinck et al., 2012; Xi et al., 2013). Reduced C9orf72 has also been reported at the protein level in a number of disease relevant

tissues, such as the cerebellum, hippocampus and frontal cortex consistent with the idea that the repeat expansion leads to reduced C9orf72 transcription, and therefore less protein (Waite et al., 2014; Xiao et al., 2015). Thus loss of function of C9orf72 by haploinsufficiency could contribute to disease.

How the repeat expansion results in reduced *C9orf72* expression is unclear. The repeat expansion has been shown to lead to hypermethylation of a CpG island 5' of the C9orf72 gene (Xi et al., 2014; Xi et al., 2013) and it is well established that hypermethylation of CpG islands functions as a gene silencing mechanism (Al-Mahdawi et al., 2008; Greger et al., 1989; Herman et al., 1995; Jones and Baylin, 2002; Sephton et al., 2011; Sutcliffe et al., 1992). If the repeat expansion somehow promotes CpG methylation, then this could lead to the observed decrease in expression of *C9orf72*. Higher levels of methylation were reported to correlate with a shorter disease progression, suggesting increased methylation leads to a more severe phenotype (Xi et al., 2013). The precedent for this effect of non-coding repeat expansions on CpG island hypermethylation in other disorders such as Friedreich ataxia and fragile X mental retardation syndrome, strengthens the argument for the role in C9ALS/FTD (Al-Mahdawi et al., 2008; Sutcliffe et al., 1992).

Morpholino knockdown of C9orf72 in a zebrafish model led to decreased axonal length and reduced swimming ability associated with motor defects (Ciura et al., 2013). These defects were effectively rescued upon overexpression of human C9orf72 mRNA (Ciura et al., 2013). On the other hand neural specific ablation of C9orf72 in conditional C9orf72 knockout mice does not cause motor neuron degeneration or reduced survival but does result in reduced body weight (Koppers et al., 2015). This suggests that haploinsufficiency alone, is also not the sole cause of disease in C9ALS/FTD. However, these mice were not tested for the characteristic p62 positive pathology that is associated with C9ALS/FTD. It may be that loss of C9orf72 is able to replicate the disease associated pathology, suggesting that haploinsufficiency of C9orf72 does contribute towards disease pathogenesis.

1.7.3 C9orf72 protein

Three alternatively spliced C9orf72 mRNA transcripts give rise to two C9orf72 protein isoforms (Figure 1.7). Transcripts 1 and 3 encode a protein of 481 amino acids (C9orf72 Long, C9orf72L), while transcript 2 encodes a shorter protein of

222 amino acids lacking the last 6 exons, which encode 259 C-terminal amino acids (C9orf72 Short, C9orf72S) (DeJesus-Hernandez et al., 2011; Renton et al., 2011). Expression of these two isoforms has been reported in a range of tissues from liver to testis, but also across a range of brain regions including cerebellum, frontal cortex and hippocampus (DeJesus-Hernandez et al., 2011). C9orf72 appears to be particularly enriched in the cerebellum (Waite et al., 2014). The expression of C9orf72 has also been shown to be enriched in mouse neuronal cells, suggesting the functional C9orf72 protein is important to these cellular populations (Suzuki et al., 2013).

The C9orf72 protein is highly conserved across species, with up to 98% identity between mice and humans and 73% identity between zebrafish and humans, suggesting an important cellular role. While *Drosophila melanogaster* lack a C9orf72 homologue, the *Caenorhabditis elegans* homologue shares 26% identity with the human form (Therrien et al., 2013).

Although there are no obvious domains, C9orf72 does share secondary structural homology with the Differentially Expressed in Normal and Neoplasia (DENN) family of proteins (Levine et al., 2013; Zhang et al., 2012). DENN domain containing proteins are guanine nucleotide exchange factors (GEFs) for the Rab family of GTPases, exchanging guanine diphosphate (GDP) for guanine triphosphate (GTP), and thus regulating Rab activation (Marat et al., 2011). The functional DENN domain is made up of 3 distinct modules termed the upstream DENN (uDENN) or Longin domain, the central DENN domain and the downstream (dDENN) domain (Levivier et al., 2001). The position of these potential domains in relation to the C9orf72 protein isoforms is detailed in Figure 1.8. The structural homology with DENN proteins suggests that C9orf72 might function as a regulator of the Rab GTPases, which are involved in a variety of cellular membrane trafficking and transport events (Stenmark, 2009; Stenmark and Olkkonen, 2001; Zerial and McBride, 2001), as detailed in section 1.5.2.5. In agreement with this, C9orf72 has been shown to co-localise with a number of Rab proteins (Farg et al., 2014).

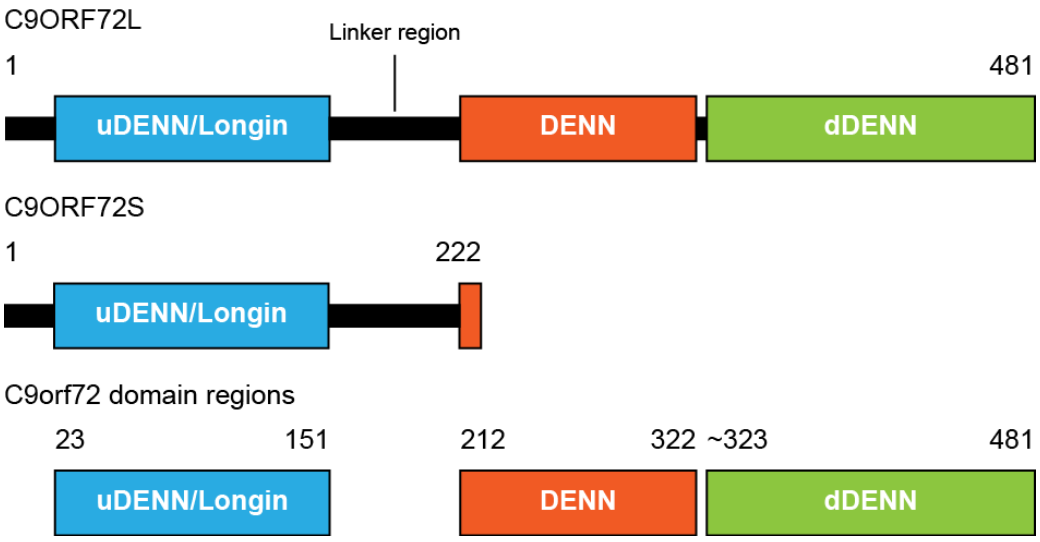

Figure 1.8 The predicted DENN-like domains of C9orf72. Coloured boxes indicate the different DENN modules with predicted secondary structure similar to that of known DENN proteins. The uDENN (or Longin) module (blue box) spans from amino acids 23 to 151. The central DENN domain (green box) spans from amino acids 212 to 322, while the dDENN module (orange box) spans from amino acid 323 to 481. The location of these DENN modules in relation to the full-length C9orf72L protein and C9orf72S are shown. C9orf72S is mainly comprised of the uDENN domain with a short section of the DENN domain. Black lines indicate linker regions with no predicted homology. Numbers indicate corresponding amino acids of C9orf72.

Isoform specific antibodies have been developed to investigate the difference in subcellular localisation of C9orf72S and C9orf72L (Xiao et al., 2015). C9orf72L was shown to have a diffuse cytoplasmic distribution, while C9orf72S displayed a more specific localisation to the nuclear membrane, which was observed to be more cytoplasmic in C9ALS patient motor neurons (Xiao et al., 2015). The antibody was also used to demonstrate the interaction of C9orf72S with members of the nuclear pore complex, including Importin β1 and Ran-GTPase, suggesting a possible role in nuclear import and export (Xiao et al., 2015). RNA foci formed from the repeat expansion, were also shown to disrupt nucleocytoplasmic transport by interacting with the Ran-GTPase activating protein (RanGAP) (Zhang et al., 2015), suggesting a common or shared mechanism of disease.

Further clues as to the function of the C9orf72 protein come from a GWAS that identifies single nucleotide polymorphisms (SNPs) in transmembrane protein 106 B (TMEM106B) as a modifier of disease risk (Van Deerlin et al., 2010). The major risk SNP (rs 1990622 T/C) is particularly associated with FTLD in patients with the GGGGCC C9orf72 repeat expansion (Gallagher et al., 2014; Van Blitterswijk et al., 2014; Vass et al., 2011). The TMEM106B protein has been shown to localise to the endo-lysosome compartment and is involved in various aspects of lysosomal biology, including size and trafficking (Brady et al., 2013; Schwenk et al., 2014; Stagi et al., 2014). The major risk allele for FTD in C9orf72 expansion patients is associated with a later age of onset of ALS as well as later age of death, while the minor allele appears to be protective for the development of FTD in C9orf72 expansion carriers (Van Blitterswijk et al., 2014). As variants of this endo-lysosomal associated protein are able to modify risk of FTLD-TDP in C9orf72 expansion carriers, it suggests lysosomal biology, and thus autophagy, may be involved in the pathogenesis of C9ALS/FTD. However, currently the exact function of the C9orf72 protein remains elusive.

1.8 Hypothesis and aims

As loss of function caused by haploinsufficiency of *C9orf72* is a possible cause of C9ALS/FTD, it is important to understand the cellular function of C9orf72. Substantial evidence points towards a role of defective autophagy in many cases of ALS. While the presence of TDP-43 positive inclusions is considered a hallmark of ALS, unlike other ALS cases C9orf72 patients also display specific p62-positive, TDP-43 negative, inclusions in the cerebellum and hippocampus. Accumulations of p62 are indicative of defective autophagy and as such defective autophagy may be involved in C9ALS/FTD.

C9orf72 codes for two protein isoforms of unknown function that are structurally related to the DENN family of Rab GEFs. Rabs are involved in a range of membrane trafficking events, including many aspects of autophagy. A previous study into the network organisation of the autophagy pathway identified C9orf72 as a possible interacting partner of FIP200 (Behrends et al., 2010). Thus, due to the potential role in Rab biology, the p62 positive accumulations in patients and the link with FIP200, this lead to the hypothesis that C9orf72 is involved in the autophagy pathway.

The aim of this thesis was to understand the function of the C9orf72, in particular, to test whether C9orf72 was involved in the autophagy pathway and whether loss of C9orf72 would disrupt this pathway. The aim was to initially identify a range of C9orf72 interacting proteins to provide clues as to the function of this uncharacterised protein, before investigating what effect modulating C9orf72 protein levels would have on cellular biology.

2 Materials and Methods

Unless otherwise stated all chemicals were purchased from Sigma. All solutions were prepared using distilled H_2O and sterilised by autoclaving or filtration through a 0.2 µm filter.

2.1 Materials

2.1.1 Stock Solutions

Acrylamide-bis-acrylamide (30%)
Ammonium Persulphate (APS; 10%)
Ampicillin (100 mg/ml)
Bafilomycin A_1 (100 µM)
B-mercaptoethanol
Bovine serum albumin (BSA)
Bradford reagent (5x stock)
Cycloheximide (10 mg/ml)
Dimethyl sulphoxide (DMSO; 100%)
Ethanol (100%)
Ethidium Bromide (10 mg/ml)
Ethylenediaminetetraacetic acid (EDTA; 0.5 M)
Ethylene glycol-bis (β-aminoethylether) N,N,N',N'-tetraacetic acid (EGTA; 0.25 M)
Foetal bovine serum (100%)
Formaldehyde (37% (w/v))
Glacial acetic acid (100%)
Glycerol (100% (v/v))
Hydrochloric acid (HCl)
Isopropyl β-D-1-thiogalactopyranoside (IPTG; 1 M)
Kanamycin (100 mg/ml)
K-Piperazine-N,N'-bis (2-ethanesulphonic acid) buffered with potassium hydroxide to pH 6.8 (K-PIPES; 400 mM)
Magnesium chloride ($MgCl_2$; 1 M)
Methanol (100%)
MG132 (N-(Benzyloxycarbonyl)leucinylleucinylleucinyl; 10 mM)
NP40 (Nonidet P-40 or octylphenoxypolyethoxyethanol or IGEPAL CA-630; 100%)

Phosphate buffered saline (PBS; 137 mM NaCl, 2.7 mM KCl, 0.7 mM KH_2PO_4, 4 mM Na_2HPO_4)

Potassium chloride

Rapamycin (1 mM)

Sodium dodecyl sulphate (SDS; 10% (w/v))

Sodium chloride (NaCl; 5 M)

Sodium pyruvate (100 mM)

TEMED (N,N,N',N'-tetramethylethylenediamine; 100%)

Torin1 (1 mM)

Trypsin-EDTA

Tris-buffered saline (TBS; 20 mM Tris (tris(hydroxymethyl)aminomethane); 137 mM NaCl buffered with HCl to pH 7.6

Tris-HCl (1.5 M Tris buffered with HCl to pH 8.8)

Tris-HCl (0.5 M Tris buffered with HCl to pH 6.8)

Triton X-100 (100%)

Tween-20 (100%)

2.1.2 Microbiology reagents

2.1.2.1 Plasmids and vectors

Vectors used for in-house cloning and other expression plasmids are detailed in Table 2.1 and 2.2.

Table 2.1 Vectors

Vector	Expression	Supplier
pCI-neo	Mammalian	Promega
pCI-neo-Myc	Mammalian	Promega – modified in house
pRK5	Mammalian	BD Biosciences
pGEX6p1	Bacterial	GE Healthcare Life Sciences

Table 2.2 Expression plasmids

Protein	Vector backbone	Reference/scource
Cox6C-Myc-DDK	pCMV6entry-myc/DDK	Origene
EGFP	pEGFP-C2	Clontech
EGFP-LC3	pEGFP-C1	Prof Chris Miller (Basic and Clinical Neuroscience, Kings Collage London, UK)
EGFP-USP8	EGFP-C1	Prof Sylvie Urbe (Institute of Translational Medicine, University of Liverpool, UK) (Row et al., 2006)
FIP200-6xHis 1-638	pCI-neo	In house: See 2.2.1.6
FIP200-6xHis 639-1373	pCI-neo	In house: See 2.2.1.6
FIP200-6xHis 1374-1591	pCI-neo	In house: See 2.2.1.6
FLAG-C9orf72L	3xFLAG-CMV	In house: Dr. Mathew Walsh and Dr. Adrian Higginbottom
FLAG-C9orf72S	3xFLAG-CMV	In house: Dr. Mathew Walsh and Dr. Adrian Higginbottom
FLAG-FIP200	3xFLAG-CMV10	Addgene #24300 (Hara et al., 2008)
GST	pGEX6p1	GE Healthcare Life Sciences
GST-C9orf72L	pGEX6p1	In house: See 2.2.1.6
GST-C9orf72S	pGEX6p1	In house: See 2.2.1.6
HA-ULK	pRK5	Addgene #31963 (Jung et al., 2009)
mCherry-EGFP-LC3	pmCherry-C1-pEGFP	Dr. Xuejun Jiang (Memorial Sloan-Kettering Cancer Centre, NYC, USA) (Ganley et al., 2009)
mCherry-FIP200	pmCherry-C1-EGFP	Prof Terje Johansen

		(Institute for Medical Biology, University of Tromsø, Norway) (Pankiv et al., 2007)
mVenus	pCI-neo	In house: Dr Kurt De Vos from prSETB-mVenus
Myc-ATG13	pRK5	Addgene #3165 (Jung et al., 2009)
Myc-C9orf72L	pRK5	In house: Dr. Mathew Walsh and Dr. Adrian Higginbottom
Myc-C9orf72L	pCI-neo-Myc	In house: See 2.2.1.6
Myc-C9orf72L K14R	pCI-neo-Myc	In house: See 2.2.1.6
Myc-C9orf72S	pRK5	In house: Dr. Mathew Walsh and Dr. Adrian Higginbottom
Myc-Rab1a	pCMV-intron myc	Addgene #46776 (Dupre et al., 2006)
Myc-Rab1a Q70L	pCMV-intron myc	In-house from Myc-Rab1a: Miss Emma Smith
OAT-Myc-DDK	pCMV6entry-myc/DDK	Origene
SMCR8-Myc-DDK	pCMV6entry-myc/DDK	Origene
Synapsin III-Myc-DDK	pCMV6entry-myc/DDK	Origene

2.1.2.2 *Escherichia coli* growth media

Luria Bertani agar (LB agar; 32 g/l)

LB-ampicillin agar (LB agar supplemented with 100 µg/ml ampicillin)

LB-kanamycin agar (LB agar supplemented with 100 µg/ml kanamycin)

LB broth (20 g/l)

LB-ampicillin broth (LB broth supplemented with 100 µg/ml ampicillin)

LB-kanamycin broth (LB broth supplemented with 100 µg/ml kanamycin)

2.1.2.3 Reagents for preparation and purification of plasmid DNA

Plasmids were isolated from bacterial culture using a Nucleospin® plasmid purification kit. The reagents used were provided with the kit:

Resuspension buffer A1 supplemented with RNase A

Lysis buffer A2
Neutralisation buffer A3
Wash buffer AW
Wash buffer A4 supplemented with ethanol (80% (v/v) final ethanol concentration)
Elution buffer AE

2.1.2.4 Reagents for cloning of FIP200 fragments, C9orf72S, C9orf72L and C9orf72L K14R

2.1.2.4.1 Primers for PCR generation of FIP200 fragments, C9orf72S, C9orf72L and C9orf72L K14R

FIP200 fragments were generated with Xho1 restriction sites at the 5' end and 6xHis repeats followed by Not1 restriction site at the 3' end using the following primers, in preparation for cloning into the pCI-neo expression vector.

Xho1-FIP200 Fw:
5'-CTCGAGGCCACCATGAAGTTATATGTATTTCTGGTTA-3'

Xho1-FIP200 639 Fw:
5'-CTGGAGGCCACCATGCAAAAGGCATCTGTGAGTCAG-3'

Xho1-FIP200 1374 Fw:
5'-CTCGAGGCCACCATGGATCGAGCTCGTTTGCTTGAG-3'

FIP200-6xHis-Not1 Rev:
5'-
GCGGCCGCTCAATGGTGGTGGTGATGATGTTATACTTTCTTATTCCATGAT
ACG-3'

FIP200 638-6xHis-Not1 Rev:
5'-
GCGGCCGCTCAATGGTGGTGGTGATGATGTTCACTCAGTAGATCTGTAATG
-3'

FIP200 1373-6xHis-Not1 Rev:

5’-
GCGGCCGCTCAATGGTGGTGGTGATGATGTTCAGAAAGTGACTCTATCAAA
T-3’

The lysine residue at position 14 in C9orf72 was mutated using missense bp mutation in the PCR primer. Primers contained a 5’ Xho1 restriction site and a 3’ Not1 restriction site in preparation for cloning into the pCI-neo-Myc expression vector. The primer sequences are detailed below:

Xho1-C9orf72 K14R Fw:
5’-
CTCGAGGCCACCATGTCGACTCTTTGCCCACCGCCATCTCCAGCTGTTGC
CAGGACAGAGAT-3’

C9orf72L-Not1 Rev:
5’-GCGGCCGCTTAAAAAGTCATTAGAACATC-3’

C9orf72S and C9orf72L sequences were amplified by PCR with Xho1 and Not1 restriction sites 5’ and 3’ in preparation for cloning into the pGEX6p1 GST expression vector. The primer sequences were as follows:

Xho1-C9orf72 Fw:
5’-CTCGAGGCCACCATGTCGACTCTTTGCCCACCG-3’

C9orf72S-Not1 Rev:
5’-GCGGCCGCTTACTTGAGAAGAAAGCCTTC-3’

C9orf72-Not1 Rev:
5’-GCGGCCGCTTAAAAAGTCATTAGAACATC-3’

2.1.2.4.2 PCR amplification

PCR was conducted using the Phusion High-Fidelity DNA polymerase kit (New England BioLabs). The manufacturer supplied the following reagents:

5x Phusion HF Buffer
10 mM dNTP’s
Phusion High Fidelity DNA polymerase

2.1.2.4.3 Reagents for cloning into pCR™-Blunt II-TOPO vector

The Zero Blunt® TOPO® PCR cloning kit (Invitrogen) was used for blunt ended cloning. The following reagents were supplied with the kit:

10 ng/µl pCR™-Blunt II TOPO plasmid DNA in:
50% glycerol
50 mM Tris-HCl pH 7.4
1 mM EDTA
2 mM DTT
0.1% Triton X-100
100 µg/ml BSA
30 µM bromophenol blue

Salt solution:
1.2 M NaCl
0.06 M $MgCl_2$

Nuclease Free water

2.1.2.4.4 Reagents for Transformation of XL10-Gold ultracompetent cells

The following reagents were supplied by the manufacturer (Stratagene: An Agilent Technologies Division):

XL10-Gold® ultracompetent cells
XL10-Gold® β-mercaptoethanol mix

2.1.2.4.5 Reagents for restriction digest of DNA

Plasmid DNA was digested using the FastDigest™ enzyme system (Thermo Fisher Scientific).
Nuclease free water
10x FastDigest® Green Buffer
FastDigest® enzymes (*Xho1* and *Not1*)
Plasmid DNA

2.1.2.4.6 Reagents for agarose gel electrophoresis

Tris-Acetate EDTA (TAE) buffer:
40 mM Tris

0.11% (v/v) glacial acetic acid
1 mM EDTA
buffered to pH 8.0 with NaOH

Agarose

2.1.2.4.7 Reagents for gel extraction of restriction digested DNA

The GenElute™ Gel Extraction Kit (Sigma) was used for gel extraction and purification of restriction digested plasmid DNA after agarose gel electrophoresis.

The reagents supplied by the manufacturer were:
Column Preparation Solution
Gel Solubilisation Solution
Wash Solution Concentrate (to be diluted with 48 ml 100% ethanol)
GenElute Binding Column G
Collection Tubes, 2 ml

Other reagents required were:
100% ethanol for dilution of wash solution concentrate
100% isopropanol

2.1.2.4.8 Reagents for de-phosphorylation of linearized DNA vectors

10x Antarctic Phosphatase Reaction Buffer
Antarctic Phosphatase
Linearized vector DNA

2.1.2.4.9 Reagents for ligation of DNA vectors and inserts

1:3 molar ratio of linearized vector to insert
Nuclease free water
2x Quick Ligation Buffer
Quick T4 DNA Ligase

2.1.2.4.10 Reagents for the transformation of Rosetta pLysS competent cells

Rosetta pLysS cells (Novagen)

LB-chloramphenicol-ampicillin agar (LB agar supplemented with 34 µg/ml chloramphenicol and 100 µg/ml ampicillin)
Terrific Broth (TB; 1.2% (w/v) Tryptone, 2.4% (w/v) Yeast Extract, 17 M Monopotassium phosphate (KH_2PO_4) and 72 M Dipotassium phosphate (K_2HPO_4) and 0.4% glycerol)
TB-Chloramphenicol-Ampicillin (TB supplemented with 34 µg/ml chloramphenicol and 100 µg/ml ampicillin)

2.1.2.4.11 Reagents for bacterial production of GST-tagged proteins

Rosetta pLysS competent cells with pGEX6p1 plasmid of interest
TB-Ampicillin (TB supplemented with 100 µg/ml ampicillin)
0.5 mM IPTG (working concentration; 1 M stock)

2.1.3 Mammalian cell culture and transfection

2.1.3.1 HeLa and Human embryonic kidney (HEK) 293 cell culture reagents

HeLa and HEK293 cells were cultured in Dulbecco's modified Eagle's medium (DMEM) with 4.5 g/l glucose supplemented with 10% (v/v) FBS and 1 mM sodium pyruvate. Cells were washed with phosphate buffered saline and detected with Trypsin-EDTA solution.

2.1.3.2 Lipofectamine 2000 transfection reagents

OptiMEM reduced serum media
Lipofectamine 2000 transfection reagent

2.1.3.3 Lipofectamine RNAiMax siRNA transfection reagent

OptiMEM reduced serum media
Lipofectamine RNAiMax transfection reagent
Non targeting control siRNA
C9orf72 siRNA #2: gugcuauagauguaaaguu
C9orf72 siRNA #D: gaucagggucagaguauua
FIP200 siRNA #1 caaguuagagguugaacuu
FIP200 siRNA #2 gaucuuaugugaucgucca
Rab1a siRNA #1 gaacaaucaccuccaguua
Rab1a siRNA #2 cagaucaggaguccuucaa

2.1.4 General biochemical reagents

2.1.4.1 Cell lysis buffer

Radioimmunoprecipitation assay (RIPA) buffer:

50 mM Tris HCl pH 6.8

150 mM NaCl

1 mM EDTA

1 mM EGTA

0.1% (w/v) SDS

0.5% (w/v) deoxycholic acid

1% (v/v) Triton X-100

Complete protease inhibitor cocktail

5x Laemmli buffer

250 mM Tris-HCl pH 6.8

10% (w/v) SDS

0.5% (w/v) Bromophenol blue

50% (v/v) glycerol

25% (v/v) β-mercaptoethanol

2.1.4.2 Bradford reagents

Distilled H_2O

5x BioRad Protein Assay Dye reagent concentrate (Bradford reagent)

2.1.4.3 Immunoprecipitation

BRB80 lysis buffer:

80 mM K-PIPES pH 6.8

150 mM NaCl

1 mM EDTA

1% (v/v) NP40

Protease inhibitor cocktail

50% protein G bead slurry

2.1.4.4 *In vitro* binding assays

Bacterial lysis and binding:

RB100 lysis buffer:

25 mM HEPES (pH 7.5)

100 mM KOAc
10 mM $MgCl_2$
1 mM DTT
0.05% (v/v) Triton X-100
10% (v/v) glycerol

GST protein binding:
50% glutathione-agarose (GSH) bead slurry
RB100 buffer

in vitro protein translation
TnT Quick-coupled Transcription/Translation Kit (Promega):
Reticulocyte lysate
$^{[35]}$S-radiolabelled methionine

GSH elution buffer
50 mM Tris-HCl (pH 7.5)
100 mM NaCl
40 mM reduced glutathione

2.1.4.5 SDS-PAGE and Immunoblotting

2.1.4.5.1 SDS-polyacrylamide gel electrophoresis (SDS-PAGE)

Resolving gel:
375 mM Tris-HCl pH 8.8
10, 12 or 15% (v/v) acrylamide
0.1% (w/v) SDS
0.1% (w/v) APS
0.1% (v/v) TEMED

Stacking gel:
117 mM Tris-HCl pH 6.8
5.6% (v/v) acrylamide
0.1% (w/v) SDS
0.05% (w/v) APS
0.3% (v/v) TEMED

Running buffer:
25 mM Tris
192 mM glycine
0.1% (w/v) SDS

2.1.4.5.2 Immunoblotting of proteins onto nitrocellulose membranes

Nitrocellulose membrane

Transfer buffer:
25 mM Tris
192 mM glycine
20% (v/v) methanol

Ponceau S:
5% (v/v) glacial acetic acid
0.1% (w/v) Ponceau S

2.1.4.5.3 Probing of nitrocellulose membranes with antibodies

TBS-Tween
0.1% (v/v) Tween-20 in TBS

Blocking buffer
0.1% (v/v) Tween-20 in TBS
5% (w/v) dried milk powder

Enhanced Chemiluminescence (ECL) reagent kit (ThermoFisher Scientific):
Solution A (luminol solution)
Solution B (peroxide solution)
Reagents mixed 1:1
Autoradiography film (GE Healthcare)

The primary and secondary antibodies and their dilutions are detailed in Table 2.3 and 2.4

Table 2.3 Primary antibodies

Antibody	Supplier	Species	Dilution
α-tubulin (DM1A)	Sigma	Mouse	WB: 1:10,000
FLAG tag (M2)	Sigma	Mouse	WB: 1:2000, IF: 1:1000
GFP (JL8)	Clontech	Mouse	WB: 1:5000
Myc tag (9B11)	Cell Signalling	Mouse	WB: 1:2000, IF: 1:2000
p62 (610833)	BD Biosciences	Mouse	IF: 1:1000
ATG13 (#6940)	Cell Signalling	Rabbit	WB 1:1000
C9orf72 (HPA023873)	Sigma - Atlas	Rabbit	WB: 1:250, IF: 1:100
C9orf72 (22637-1-AP)	ProteinTech	Rabbit	WB: 1:250, IF 1:100
C9orf72 (sc-138763)	Santa Cruz	Rabbit	WB: 1:500, IF: 1:100
FIP200 (SAB4200135)	Sigma	Rabbit	WB: 1:500
GAPDH (14C10)	Signalling	Rabbit	WB 1:1000
HA	Sigma	Rabbit	WB: 1:2000, IF: 1:1000
LC3 (NB100-2220)	Novus Biological	Rabbit	WB: 1:1000
Myc tag (#9106)	Abcam	Rabbit	WB: 1:2000, IF: 1:1000
Phopho-ULK1 S757 (#6888)	Cell Signalling	Rabbit	WB: 1:1000
ULK1	Cell Signalling	Rabbit	WB: 1:1000

Table 2.4 Secondary antibodies

Antibody	Supplier	Species	Dilution
Anti-mouse IgG conjugated to horseradish peroxidase	Abcam	Goat	WB: 1:5000
Anti-rabbit IgG conjugated to horseradish peroxidase	Dako	Goat	WB: 1:5000
Anti-mouse IgG coupled to Alexa Fluor 488	Invitrogen	Goat	IF: 1:500
Anti-mouse IgG coupled to Alexa Fluor 568	Invitrogen	Donkey	IF: 1:500
Anti-rabbit IgG coupled to Alexa Fluor 488	Invitrogen	Goat	IF: 1:500
Ant-rabbit IgG coupled to Alexa Fluor 568	Invitrogen	Goat	IF: 1:500

2.1.4.6 RNA extraction and reverse-transcription quantitative PCR (RT-qPCR)

2.1.4.6.1 RNA extraction

Trizol reagent (Invitrogen)

Chloroform

Isopropanol

75% ethanol

RNase free water

2.1.4.6.2 cDNA preparation and RT-qPCR

cDNA preparation:

NEB DNase

10x DNase buffer

25 mM EDTA

Reverse transcription:

Oligo(dT)

25 mM dNTP mix

5x reverse transcriptase buffer

100 mM DTT

Superscript III Reverse Transcriptase

qPCR:

2x SYBR Green

Primer sequences:

C9orf72 (S and L), FW: gttgatagattaacacatataatccgg

C9orf72 (S and L) REV: cagtaagcattggaataatactctga

Rab1a FW: tgtccagcatgaatcccgaa

Rab1a REV: ggcaagactttccaacccct

GAPDH FW: gggtggggctcatttgcaggg

GAPDH REV: tgggggcatcagcagagggg

2.1.5 Microscopy

2.1.5.1 Immunofluorescence

Fixing solution:

3.7% (v/v) formaldehyde in PBS

Quenching solution:

50 mM NH_4Cl in PBS

Permeabilisation solution:

0.2% (v/v) Triton X-100 in PBS

Blocking solution:

0.2% (v/v) cold water fish gelatin in PBS

Mounting medium:

Dako fluorescent mounting medium

2.1.5.2 Proximity Ligation Assay (PLA)

Blocking solution

Antibody diluent

PLA probe MINUS (5x stock)

PLA probe PLUS (5 x stock)

Wash buffer A

Wash buffer B

Detection reagent Orange (excitation 554 nm: emission 579 nm)

2.1.6 Drug treatments

2.1.6.1 Autophagy induction

Rapamcyin induction:

500 nM rapamycin in DMEM cell culture medium

Torin1 induction:

250 nM Torin1 in DMEM cell culture medium

2.1.6.2 Autophagy inhibition

Bafliomycin treatment:

100 nM Bafilomycin A_1 in DMEM cell culture medium

2.1.6.3 Proteasome inhibition

MG132 treatment:

10 µM MG132 in DMEM cell culture medium

2.1.6.4 Inhibition of protein translation

Cycloheximide treatment:

30 µg/ml cycloheximide in DMEM cell culture medium

2.2 Methods

2.2.1 General molecular biology methods

2.2.1.1 Growth and storage of *E.coli* for plasmid DNA preparation

E.coli transformed with plasmids of interest were stored at -80 ^{o}C in sterile 25% (v/v) glycerol in LB broth containing the correct antibiotic for the plasmid.

When culturing bacteria for plasmid purification, *E.coli* containing the desired plasmid were spread onto LB agar plates containing the appropriate antibiotic. *E.coli* were grown for 16 h at 37 ^{o}C. Single colonies were picked and grown in a 1 ml starter culture of LB broth containing the correct antibiotic at 37 ^{o}C with shaking for 6 h. 100 µl of starter culture was added to 5 ml of LB broth with correct antibiotic and incubated at 37 ^{o}C for 16 h while shaking at 220 rpm.

2.2.1.2 Plasmid DNA purification

Plasmid DNA was purified using a Nucleospin Plasmid purification kit. *E.coli* from a 5 ml overnight bacterial culture were pelleted at 4,000 rpm. The bacterial pellet was then resuspended in 250 µl of Resuspension buffer A1. Cells were lysed at room temperature for 5 min using 250 µl of Lysis buffer A2. The lysis buffer was then neutralised by adding 300 µl of Neutralisation buffer A3. Lysates were washed over the silica membrane of the spin column by centrifugation. Plasmid DNA binds to the silica membrane. The membranes were washed with 500 µl Wash buffer AW and then 600 µl Wash buffer A4. Purified plasmid DNA was eluted from the silica membrane in 50 µl Elution buffer AE.

2.2.1.3 Quantification of plasmid DNA

Spectrophotometric quantitation of plasmid DNA was performed using a NanoDrop 1000 (Thermo Scientific) spectrophotometer. The absorbance of DNA samples at 260 nm and 280 nm was recorded. An optical density (OD) of 1 at 260 nm corresponds to a DNA concentration of 50 µg/ml. Protein contaminants absorb at 280 and so the ratio of OD readings at 260 nm and 280 nm indicates purity of the sample ($OD_{260/280}$). Pure DNA has an $OD_{260/280}$ value of

1.8. 1 µl of elution buffer was used as a blank reading before 1 µl of experimental samples were analysed.

2.2.1.4 Restriction enzyme digest of DNA

Plasmid DNA was digested with the appropriate FastDigest restriction enzyme and corresponding FastDigest buffer according to the manufacturers instructions (ThermoFisher Scientific). 1 µl of FastDigest enzyme is sufficient to cut 1 µg of DNA in 5 - 15 min at 37 ^{o}C. Although no star activity is reported at with such short incubation times the volume of enzyme never exceeded 10% v/v of the final volume. Reactions were set up in the order as follows:

15.5 µl H_2O
2 µl 10x FastDigest® Green Buffer
2 µl DNA (up to 1 µg)
0.5 µl FastDigest® Enzyme

2.2.1.5 Agarose gel electrophoresis of DNA

Agarose was dissolved in boiling TAE buffer at a final concentration of 0.5-1.5% (w/v) with 1 µl ethidium bromide added per 100 ml and cast on a horizontal gel bed with suitable comb. After setting gels were placed in an electrophoresis gel tank, submerged in TAE buffer and run at 100 V. Nucleic acid markers were used to determine DNA band size (Hyperladder, Bioline).

2.2.1.6 Cloning of FIP200 fragments, C9orf72 and C9orf72 K14R

2.2.1.6.1 PCR generation of FIP200 fragments, C9orf72S, C9orf72L and C9orf72L K14R

FIP200 fragments were generated using Phusion High Fidelity DNA polymerase (New England BioLabs), 3xFLAG-CMV10-hFIP200 as template and the primers indicated in 2.1.2.4.1. C9orf72L, C9orf72L K14R for cloning into pCI-neo-Myc were generated using Phusion High Fidelity DNA polymerase (New England BioLabs), pRK5-Myc-C9orf72L as template and the primers indicated in 2.1.2.4.1. C9orf72S and C9orf72L for cloning into pGEX6p1 vectors were generated using Phusion High Fidelity DNA polymerase (New England BioLabs), pRK5-Myc-C9orf72L as template and the primers indicated in 2.1.2.4.1.

The individual reaction mix was as follows:

12.4 µl nuclease free H_2O

4 µl 5 x High Fidelity Phusion Buffer

0.4 µl 10 mM dNTP's

1 µl template DNA (5 ng/µl stock)

1 µl 10 µM Fw Primer

1 µl 10 µM Rev Primer

0.2 µl Phusion High Fidelity DNA polymerase

The PCR reaction cycle are detailed in table 2.5

Table 2.5 PCR cycling parameters of Phusion High Fidelity PCR

Step	Number of Cycles	Temperature (°C)	Time
Initiation	1	98	2 min
Denaturation	35	98 Melt	10 s
		65 Anneal	20 s
		72 Extension	10 s
Extension	1	72 Final extension	10 min
Cooling	1	4	Hold

2.2.1.6.2 Sub cloning into pCR™-Blunt II TOPO vector

Phusion High Fidelity DNA polymerase produces blunt ended products. The blunt ended FIP200 fragments, C9orf72L, C9orf72L K14R and C9orf72S were cloned into the pCR™-Blunt II-TOPO vector using the Zero Blunt TOPO PCR Cloning Kit (ThermoFisher Scientific) according to the manufacturers instructions. The pCR™-Blunt II-TOPO vector is supplied linearized with viral topoisomerase covalently bound to the 3' end of the DNA. The topoisomerase cleaves the DNA backbone at 5'-CCCTT forming a phosphor-tyrosyl bond between the DNA backbone and the enzyme (Shuman, 1994). This bond is then attacked by the 5'OH group of the blunt PCR product, releasing the topoisomerase form the DNA backbone.

Ligation of the FIP200 fragments, C9orf72L, C9orf72L K14R and C9orf72S into the pCR™-Blunt II-TOPO was conducted as follows:

4 µl fresh blunt PCR product

0.5 µl sterile H_2O
1 µl salt solution
0.5 µl pCR™-Blunt II-TOPO vector

Reactions were mixed and incubated at room temperature for 10 min before transformation into *E.coli.*

2.2.1.6.3 Transformation of XL10-Gold® ultracompetent cells

1 µl of β-mercaptoethanol (supplied with XL10-Gold® ultracompetent cells) was added to 25 µl thawed XL10-Gold® ultracompetent and the cells mixed by swirling before incubation on ice for 10 min. 4 µl of the pCR™-Blunt II-TOPO vector with new insert was added to the cells and incubated on ice for 30 min. Cells were then heat shocked at 42 °C for 30 s before placing back on ice for 2 min. Following heat shock, 500 µl pre-warmed LB broth (without antibiotic) was added to the cells. Cells were incubated at 37 °C for 1 h while shaking at 220 rpm. After incubation cells were pulsed down at 500 x g and resuspended in 50 µl LB broth before plating onto LB-kanamycin agar plates for growth and selection. The pCR™-Blunt II-TOPO vector confers kanamycin resistance. Plates were incubated at 37 °C for 16 h.

2.2.1.6.4 Screening of bacterial colonies

After overnight incubation at 37 °C, bacterial colonies were picked using sterile inoculation loops. Plasmid DNA was prepped from these colonies following the protocol detailed in section 2.2.1.2. To screen for the correct insert, pCR™-Blunt II-TOPO plasmid DNA was subjected to restriction digest with Xho1 and Not1 restriction enzymes as detailed in section 2.2.1.4 and analysed by agarose gel electrophoresis detailed in 2.2.1.5.

2.2.1.6.5 Restriction digest and agarose gel extraction of inserts and vector

After screening of positive pCR™-Blunt II-TOPO clones, inserts were excised by double restriction digest with Xho1 and Not1 FastDigest restriction enzymes (Thermo Fisher Scientific). To allow ligation of these inserts into the appropriate expression vectors, pCI-neo, pCI-Neo-Myc and pGEX6p1 vectors were subjected to restriction digest with the same restriction enzymes. Thus complementary sticky ends were produced to allow ligation. The restriction digests were set up as follows:

FIP200 fragment, C9orf72L K14R, C9orf72S and C9orf72L pCR™-Blunt II-TOPO digest:

2 µg pCR™-Blunt II-TOPO vector with insert
4 µl FastDigest® Green Buffer
up to 38 µl with H_2O
1 µl Xho1 FD enzyme
1 µl Not1 FD enzyme

pCI-neo, pCI-neo-Myc and pGEX6p1 digest:

3 µg vector
4 µl FastDigest® Green Buffer
up to 38 µl with H_2O
1 µl Xho1 FD enzyme
1 µl Not1 FD enzyme

Restriction digests were incubated at 37 °C for 1h to allow complete digestion. Restriction digests were run on 1% agarose gels as detailed in section 2.2.1.5 to allow separation of insert and linearized vectors. Bands were visualized on transilluminator and excised using a scalpel blade.

Inserts and linearized plasmids were purified using a GenElute™ Gel Extraction Kit according to the manufacturers protocol. Excised bands were weighed and 300 µl Gel Solubilization Buffer added per 100 mg of gel (or 3 gel volumes) and incubated at 60 °C for 10 min or until the gel was completely dissolved. The GenElute Binding Column G was prepared by adding 500 µl Column Preparation Solution to maximise DNA binding to the membrane. The column and collection tube was centrifuged at 17,000 x g for 1 min and the flow-through discarded. After solubilisation of the gel, 1 gel volume of 100% isopropanol was added to Solubilization Buffer and mixed. DNA was bound to the column by loading this solution to the GenElute Binding Column G and centrifuging at 17,000 x g for 1 min. The flow through discarded and 700 µl Wash Solution loaded and centrifuged at 17,000 x g for 1 min. The flow through was discarded and the column centrifuged again at 17,000 x g for 1 min to remove excess ethanol from the Wash Solution. To elute the DNA, 30 µl Elution Solution (pre-heated to 65 °C) was added to the centre of the GenElute Binding Column G membrane and incubated for 1 min, before centrifuging at 17,000 x g for 1 min.

The purified inserts and linearized vectors were quantified as detailed in section 2.2.1.3.

2.2.1.6.6 De-phosphorylation of linearized vectors

To prevent re-ligation of the linearized vectors, vectors were dephosphorylated with Antarctic Phosphatase (New England BioLabs) to remove the 5' phosphate. The de-phosphorylation reaction was set up as follows:

27 µl eluted gel purified linearized vector
2.8 µl 10x Antarctic Phosphatase Reaction Buffer
0.2 µl Antarctic Phosphatase

The de-phosphorylation reaction was incubated at 37 ^{o}C for 20 min and then 75 ^{o}C for 10 min to inactivate the enzyme.

2.2.1.6.7 Ligation of purified inserts and linearized vectors

Ligation of purified inserts into linearized de-phosphorylated vectors was performed using Quick T4 DNA Ligase (New England BioLabs). For efficient ligation a 1:3 molar ratio of vector to insert was used. The ligation reaction was set up as follows:

50 ng of linearized vector with 3-fold molar excess of insert
up to 10 µl with H_2O
10 µl 2x Quick Ligation Buffer
1 µl Quick T4 DNA Ligase

Ligation reactions were mixed and incubated at room temperature for 5 min, before chilling on ice. The following ligations were performed:

Xho1-FIP200-6xHis 1-638-Not1 was ligated into pCI-neo
Xho1-FIP200-6xHis 639-1373-Not1 was ligated into pCI-neo
Xho1-FIP200-6xHis 1374-1591-Not1 was ligated into pCI-neo
Xho1-C9orf72L K14R-Not1 was ligated into pCI-neo-Myc
Xho1-C9orf72L-Not1 was ligated into pCI-neo-Myc
Xho1-C9orf72L-Not1 was ligated into pGEX6p1
Xho1-C9orf72S-Not1 was ligated into pGEX6p1

pCI-neo based vectors were transformed into XL10-Gold® *ultracompetent* cells as detailed in 2.2.1.6.3. pGEX6p1 based vectors were transformed into Rosetta pLysS cells for bacterial expression, as detailed in 2.2.1.6.7 below.

2.2.1.6.8 Transformation of Rosetta pLysS cells with

Rosetta pLysS cells are derivatives of BL-21 *E.coli* cells. 80 µl of Rosetta pLysS cells were thawed on ice and 500 ng of pGEX6p1 control, pGEX6p1-C9orf72S or pGEX6p1-C9orf7L vector added. Cells were incubated on ice for 10 min before heat shock at 42 ^{o}C for 30 s and then placed back on ice for 2 min. Following heat shock, 500 µl pre-warmed LB broth (without antibiotic) was added to the cells. Cells were incubated at 37 ^{o}C for 1 h while shaking at 220 rpm. After incubation cells were pulsed down at 500 x g and resuspended in 50 µl LB broth before plating onto LB-ampacillin/chloramphenicol agar plates for growth and selection. The pLysS cells carry a chloramphenicol resistant plasmid encoding a T7 lysozyme, while the pGEX6p1 vector confers ampicillin resistance. Plates were incubated at 37 ^{o}C for 16 h.

2.2.1.6.9 Bacterial production of GST-tagged proteins

After overnight incubation, multiple colonies were picked from the plates with a single sterile inoculation loop and cultured in 50 ml TB-chloramphenicol-ampicillin overnight at 37 ^{o}C while shaking at 220 rpm. After overnight incubation, 10 ml of this culture was used to inoculate 750 ml TB with ampicillin in baffled 1 l Erlenmeyer flasks to aid oxygenation while shaking, and mixed thoroughly. Chloramphenicol was absent from this TB as it can inhibit protein translation during the induction. The optical density of this solution was then measured using a WPA Spectrawave S1200 Visible Spectrophotometer (Biochrom Ltd) at 600 nm. Flasks were incubated at 37 ^{o}C while shaking at 220 rpm and the OD recorded every 30 min. When bacteria were in the exponential phase, i.e. doubling every 30 min, and an OD of 0.7 at 600 nm was reached, the Rosetta pLysS cells were induced to express the protein of interest from the pGEX6p1 vector by the addition of 0.5 mM IPTG for 3 h. After induction for 3 h at 37 ^{o}C while shaking at 220 rpm the culture was centrifuged at 4,000 rpm in an Avanti J-26 XP centrifuge (Beckman Coulter) using a JA-10 rotor, to pellet the bacteria. These induced bacterial pellets were then used in the *in vitro* binding assays as detailed in 2.2.3.3.

2.2.2 Mammalian cell culture and transfection

2.2.2.1 HeLa and HEK293 cell culture

HeLa and HEK293 cell cultures were maintained in a monolayer in DMEM at 37 ^{o}C in a 5% CO_2 atmosphere. Cells were passaged when then reached approximately 90% confluency. Growth media was removed and cells washed in PBS to remove excess serum. Cells were detached from the culture surface using Trypsin-EDTA solution at a sufficient volume to cover the surface of the culture vessel (e.g. 1 ml of Trypsin-EDTA to a 25 cm^2 culture flask). Cells were then incubated at 37 ^{o}C for 2 min. Trypsin-EDTA was quenched with the addition of DMEM cell culture medium (e.g. 4ml to 25 cm^2 culture flask). Cells were pipetted up and down to triturate them and the suspension split to new flasks and vessels for further culture or experimentation.

2.2.2.2 Induced Neural Progenitor Cell (iNPC) production and neuronal differentiation

iNPC production, and neuronal progenitor differentiation was performed by Dr. Laura Ferraiuolo and Miss Monika Myszczynska. Induced neural progenitor cells (iNPCs) were derived from human skin fibroblasts as previously described (Meyer et al., 2014). Briefly, 10,000 fibroblasts were transduced with lentiviral vectors for OCT3, Sox2, KLF4, and C-MYC for 12h. 48h after transduction, the cells were washed with PBS and fibroblast medium was replaced with NPC medium (DMEM/F-12 with Glutamax supplemented with 1 %N2, 1% B27, 20 ng/ml FGF-b, 20 ng/ml EGF and 5 µg/ml Heparin. As the cells started changing shape and form neurospheres they were expanded as neural rosettes. When the iNPC culture was confluent (~3 weeks) EGF and Heparin were withdrawn and the FGF-b concentration increased to 40 ng/ml. The iNPCs can be maintained for ~30 passages. iNPCs are not expanded by clone and therefore do not display clonal variability.

For differentiation, 30,000 iNPCs were plated in a 6-well plate coated with fibronectin (Millipore) and expanded to 70-80% confluence after which iNPC medium was replaced with neuron differentiation medium (DMEM/F-12 with Glutamax supplemented with 1% N2, and 2% B27). On day one of differentiation the cells were treated with 2.5 µM DAPT

(Tocris) to determine differentiation towards neuronal lineage. On day three the neuron differentiation medium was supplemented with 1 mM retinoic acid (Sigma), 0.5 mM Smoothened Agonist (SAG) (Millipore) and 2.5 mM Forskolin (Sigma) for 7 days. This protocol leads to typical yields of 70% ß-III tubulin (Tuj1) positive cells.

iNeuron experiments were repeated at least 3 times for each sample starting from iNPCs at different passages, typically between passage 10 and 20 to ensure that the results observed are not determined by batch effects or passage number.

2.2.2.3 Transient transfection of HeLa and HEK293 cells with plasmid DNA

HeLa and HEK293 cells were transiently transfected using Lipofectamine 2000 transfection reagent according to the manufacturers instructions. Cells were plated to 12 mm diameter cover slips in 24 well plates, 12 well plates, 6 well plates or 10 cm diameter plates the day before transfection to ensure approximately 70% confluency on the day of transfection. The volumes of each reagent are detailed in table 2.6.

Table 2.6 DNA transfection with Lipofectamine 2000

Plate	Lipofectamine 2000 per well (µl)	Lipofectamine 2000 OptiMEM vol (µl)	DNA per well (µg)	DNA OptiMEM Vol (µl)
24 well plate	1 µl	25 µl	0.5 µg	25 µl
12 well plate	2 µl	50 µl	1 µg	50 µl
6 well plate	4 µl	100 µl	2 µg	100 µl
10 mm plate	20 µl	250 µl	10 µg	250 µl

The correct volume of Lipofectamine 2000 transfection reagent was diluted in OptiMEM to give Mix A. Mix B contained the correct amount of plasmid DNA diluted in OptiMEM. Mix A was incubated for 5 min at room temperature and then combined with Mix B. The transfection solution was then incubated at room temperature for 15-20 min before being added drop-wise to the cells. Media was replaced on the cells after 6 h. Cells were incubated at 37 ^{o}C in a 5% CO_2

atmosphere for 24 h post transfection before cells were used for experimentation.

2.2.2.4 siRNA transfection of HeLa and HEK293 cells

HeLa cells were transfected with siRNA using the Lipofectamine RNAiMax transfection reagent according to the manufacturers instructions. Cells were seeded on 13 mm diameter cover slips the day before transfection. Cells were seeded such that they would reach 70-80% confluency 4 days post transfection. siRNA was reconstituted in 100 µl RNase free water to give 10 µM stocks of each siRNA. For RNAiMax siRNA transfection this stock solution was then diluted 1:10 in RNase free water. The volumes of each reagent are detailed in Table 2.7.

Table 2.7 siRNA transfection with Lipofectamine RNAiMax

Plate	RNAiMax vol per well (µl)	RNAiMax OptiMEM vol per well (µl)	Diluted siRNA vol per well (µl)	siRNA OptiMEM vol per well (µl)
24 well plate	0.6 µl	25 µl	0.6 µl	25 µl

Lipofectamine RNAiMax was diluted in OptiMEM to give Mix A and the correct volume of siRNA diluted separately in OptiMEM to give Mix B. Mix A was incubated for 5 min at room temperature before being combined with Mix B. The combined transfection solution was incubated at room temperature for 15-20 min before being added drop wise to the cells. The media on the cells was replaced after 6 h. Cells were incubated at 37 ^{o}C in a 5% CO_2 atmosphere for 4 days. Cells were either fixed for immunofluorescence on day 4 or transiently transfected with DNA constructs using Lipofectamine 2000 reagent on day 3 and then fixed for immunofluorescence on day 4.

HEK293 cells were transfected with siRNA using Lipofectamine 2000 transfection reagent according to the manufacturers protocol. Cells were seeded to 12 well or 6 well plates the day before transfection. Cells were seeded such that they should reach 70-80% confluency 4 days post transfection. siRNA was used from the 10 µM stock and not diluted further for use with Lipofectamine 2000 transfection. The volumes of each reagent are detailed in Table 2.8. The same protocol used for RNAiMax siRNA transfection was used for Lipofectamine 2000 siRNA transfection.

Table 2.8 siRNA transfection with Lipofectamine 2000

Plate	Lipofectamine 2000 vol per well (µ)	Lipofectamine 2000 OptiMEM vol per well (µl)	siRNA vol per well (µ)	siRNA OptiMEM vol per well (µl)
12 well plate	2 µl	50 µl	1 µl	50 µl
6 well plate	4 µl	100 µl	2 µl	100 µl

2.2.3 General Biochemical methods

2.2.3.1 Cell lysis

Cells were harvested in Trypsin-EDTA solution and resuspended in fresh DMEM cell culture medium to quench the trypsin. Cells were pelleted at 400 x g for 4 min and pellets washed in PBS. Cell pellets were lysed on ice for 30 min in ice-cold RIPA buffer. Lysates were clarified at 17,000 x g for 20 min at 4 ^{o}C.

2.2.3.2 Bradford Assay

The colorimetric Bradford assay was used to determine the protein concentration of cell lysates (Bradford, 1976). The assay is based on the principle that the Bradford reagent is able to bind protein, which results in a colour change of the reagent. This change in absorbance can be easily measured to quantify the amount of protein present in a sample. Bradford reagent was diluted 1:5 to give a working solution. Using a 96 well plate, the top row was reserved for Bradford reagent alone for background reads. The second row was reserved for the standard curve. 200 µg of BSA was added to 200 µl of Bradford reagent and added to the first well of the second row. A serial dilution of 1:2 was then conducted across this row to allow the construction of a standard curve. To measure protein concentration of the samples, 2 µl of sample was added to 200 µl of Bradford reagent, and a 1:2 serial dilution of each sample was conducted. The plate was read in a Pherastar plate reader (BMG LABTECH) at an absorption wavelength 595 nm. The Bradford-only average was subtracted from all readings and a standard curve constructed by plotting OD against protein concentration. Using the gradient of the standard curve the concentration of each sample was calculated using the equation: concentration = (OD x gradient x dilution factor).

2.2.3.3 Immunoprecipitation

Cells were harvested in Trypsin-EDTA solution and resuspended in fresh DMEM cell culture medium to quench the trypsin. Cells were pelleted at 400 x g for 4 min and pellets washed in PBS. Cells were lysed at 4 ^{o}C for 1 h with rolling in BRB80 buffer. Lysates were clarified at 17,000 x g for 20 min at 4 ^{o}C and the protein concentration measured via the Bradford assay (section 2.2.3.2). 50 µg of protein was kept as an Input sample. For the immunoprecipitation, 1 mg or protein was incubated with 1 µg of primary antibody for 16 h at 4 ^{o}C while rolling. 20 µl of 50% protein G sepharose bead slurry was added to each sample for 2 h at 4 ^{o}C while rolling to capture the antibody. Samples were centrifuged for 3 min at 3,000 x g at 4 ^{o}C to pellet the beads. Slow speeds were used to prevent the beads from crushing and collapsing. Immune pellets were washed 5 x in ice cold BRB80 immunoprecipitation lysis buffer. After the final wash, the remaining BRB80 buffer was removed and the proteins eluted from the protein G beads in 2 x laemmli buffer ready for analysis by SDS-PAGE and immunoblot. FLAG-tagged proteins were eluted by competition rather than 2 x laemmli by incubating the immune pellets in excess of the FLAG-peptide at 4 ^{o}C for 1 h while rolling. Beads were spun down at 3,000 x g and the eluate removed and prepared for SDS-PAGE and immunoblot. In all cases half the immunoprecipitation sample was analysed by SDS-PAGE and immunoblot, excluding endogenous immunoprecipitations. In these experiments the whole immune pellet was analysed.

2.2.3.4 *In vitro* binding assays

[^{35}S]-methionine labelled FLAG-FIP200 1-638, 639-1373, 1374-1591, HA-ULK, Myc-ATG13 or Myc-Rab1a proteins were produced from their corresponding vectors using the Sp6 or T7 TnT Quick Coupled Transcription/Translation kit (Promega) as detailed in Table 2.9. *In vitro* translated protein was produced according to the manufacturers instructions. Individual reactions were mixed as follows:

0.5 µg plasmid DNA in 1.5 µl H_2O
0.5 µl [^{35}S]-methionine
8 µl corresponding Reticulocyte lysate

Reactions were incubated at 37 ^{o}C for 90 min, and then placed on ice ready for use.

Table 2.9 Plasmids and TnT quick-coupled transcription/translation kits

Construct	Vector	Promoter/TnT Kit
6xHis-FIP200 1-638	pCI-neo	T7
6xHis-FIP200 639-1373	pCI-neo	T7
6xHis-FIP200 1374-1591	pCI-neo	T7
Myc-Rab1a	pCMV-intron	T7
Myc-ATG13	pRK5	Sp6
HA-ULK1	pRK5	Sp6

GST, GST-C9orf72S and GST-C9orf72L were expressed from the pGEX6p1 vector in Rosetta PLysS cells as detailed in section 2.2.1.6.9. 0.1 g GST cell pellet and 0.25 g GST-C9orf72 cell pellets were lysed by sonication in 1 ml of buffer RB100 and GST tagged proteins bound to 30 µl of glutathione-agarose (GSH) bead slurry. Binding reactions were carried out in 400 µl buffer RB100 containing the 30 µl GSH beads and bound proteins along with 8 µl of radiolabelled protein. In the case of myc-Rab1a 1 mM GDP or 1 mM GMP-PNP (Guanosine 5'-[β,γ-imido]triphosphate trisodium salt hydrate) was added to the binding assays as indicated. Proteins were eluted from GSH beads using glutathione elution buffer and analysed by SDS-PAGE. 1 µl reticulocyte lysate was loaded as input. The gel was stained with Coomassie to show GST-tagged proteins and radioactivity detected using a BioRad phosphorimager and phosphorplate.

2.2.3.5 SDS-PAGE and Immunoblot

2.2.3.5.1 SDS-PAGE

Protein samples were boiled in laemmli sample buffer at 95 ^{o}C for 5 min.

Depending on protein size, proteins were separated on 10, 12 and 15% polyacrylamide gels by electrophoresis at 100 V for 2 h (or until the dye front reached the bottom of the gel) using the Mini-PROTEAN Tetra Cell gel electrophoresis system (Bio-Rad) in 1 x running buffer. Depending on the number of samples 10 or 15 well combs were used. A Precision Plus Protein™ All Blue Prestained Protein Ladder (Bio-Rad) comprising of prestained proteins of 250, 150, 100, 75, 50, 37, 25, 20, 15 and 10 kDa was used to determine molecular weights of proteins of interest.

2.2.3.5.2 Coomassie staining of polyacrylamide gels

After separation of radiolabelled *in vitro* binding assay samples via SDS-PAGE, gels were stained with Coomassie G-250 to allow visualisation of purified proteins prior to exposure to a phophoplate. Gels were stained in Coomassie for 30 min at room temperature while shaking. After staining, gels were placed in destain for 30 min at room temperature while shaking. Destain was replaced every 30 min until background staining of the gel was removed and only the protein bands remained. Gels were washed thoroughly in H_2O before mounting and drying onto Whatmann paper. Destained, mounted and dried gels were exposed to a phosphoplate in a phophoplate cassette for 3 to 7 days.

2.2.3.5.3 Transfer of proteins to nitrocellulose membranes

After SDS-PAGE, proteins were transferred to Protran nitrocellulose membranes with a pore size of 0.45 µm. The transfer was set up as follows:

Cathode – Sponge / 2 x cellulose blot paper (Whatman) / SDS-PAGE gel / nitrocellulose membrane / 2 x cellulose blot paper / sponge – Anode

The sandwich was assembled submerged in transfer buffer, fixed into cassettes and placed in a Mini-Transblot cell (Bio-Rad). The transfer was run at 100 V for 1 h or 30 V for 16 h. After transfer membranes were stained in Ponceau S solution for 1 min to determine transfer efficiency of proteins and allow membranes to be cut accurately as necessary. Membranes were rinsed for 1 min in ultrapure H_2O to remove excess Ponceau S solution.

2.2.3.5.4 Antibody probing of nitrocellulose membranes

Membranes were blocked in 5% milk TBST for 1 h at room temperature while shaking. Membranes were then incubated with primary antibodies at the appropriate concentration (Table 2.3) in blocking buffer for 1 h at room temperature or for 16 h at 4 ^{o}C. After incubation with primary antibodies, membranes were washed 3 x for 10 min TBST while shaking. Blots were then probed with an appropriate dilution of secondary antibody (Table 2.4) coupled to horseradish peroxidasee in TBST for 1 h at room temperature. After final washing of membranes for 3 x 10 min in TBST, bound secondary antibody was detected using enhanced chemiluminescence (ECL) detection reagents (ThermoFisher Scientific). Chemiluminescence was visualised on autoradiography film (GE Healthcare) or the Syngene G:Box Chemi system (Syngene). Oxidation of the luminol substrate in the presence of hydrogen peroxide by horseradish peroxidase-coupled secondary antibodies increases

the energy state of luminol, which emits energy as light as it returns to its ground state. ECL substrates enhance the light output of this reaction. ELC solutions were mixed in a 1:1 ratio (luminol solution A: peroxide solution B) and incubated on the nitrocellulose membrane for 5 min at room temperature while shaking. Membranes were placed in a clear plastic wallet before being placed in an X-ray cassette or the Syngene G:Box. When exposing to film, autoradiograph films were placed on top of the membrane in a dark room for 5 s to 1 h. Films were developed using developer and fixer.

2.2.3.5.5 Densitometry of bands

Bands detected on immunoblots were quantified using ImageJ (Abràmoff M. D, 2004). A region of interest was drawn around the bands of interest and a histogram constructed using the plot lanes tool. Background signal was subtracted from the histogram and the area under the histogram used to represent the level of the protein. In all cases the level of the protein of interest was normalised to that of a loading control.

2.2.3.6 Modulation of autophagy

Autophagy was induced in HeLa and HEK293 cells by incubation with 500 nM rapamycin for 6 h or 250 nM Torin1 for 3 h in DMEM cell culture medium at 37 ^{o}C in a 5% CO_2 atmosphere. Autophagy was inhibited by the addition of 100 nM Bafilomycin A_1 to the cell culture medium for 6 h at 37 ^{o}C in a 5% CO_2 atmosphere. To measure specifically autophagy initiation, autophagy was induced with rapamycin or Torin1 in the presence of Bafilomycin A_1. Cells were then lysed as above and the levels of LC3 analysed by SDS-PAGE and immunoblot. Where Torin1 was added along with Bafliomycin A_1, 250 nM Torin1 was added after the first 3 h of 100 nM Bafilomycin A_1 treatment.

2.2.3.7 Inhibition of protein translation

Protein translation was inhibited in HEK293 cells by the addition of 33 µg/ml of cycloheximide to the DMEM cell culture medium. Samples were harvested after different time points and the levels of the protein of interested analysed by SDS-PAGE and immunoblot.

To determine which system was responsible for degradation of C9orf72, HEK293 cells transfected with Myc-tagged C9orf72S and L were either untreated, treated with 100 nM Bafilomycin A_1, to inhibit autophagy, or 10 µM MG132, to inhibit the proteasome, in the presence of 33 µg/ml cycloheximide for

the indicated times. Levels of C9orf72 were analysed by SDS-PAGE and immunoblot to determine levels of C9orf72 protein.

2.2.3.8 RNA extraction and RT-qPCR

2.2.3.8.1 RNA extraction

RNA was extracted from HeLa, HEK293 and iNeuron cells using Trizol reagent (Invitrogen) according to the manufacturers instructions. 1 ml of Trizol was added per 10 cm^2 of cell monolayer and incubated at room temperature for 5 min. Cell lysate was transferred to 1.5 ml eppendorf and 200 µl chloroform added. Samples were shaken vigorously by hand for 15 s and then incubated at room temperature for 3 min. Samples were centrifuged at 12,000 x g for 15 min at 4 ^oC to separate the sample into three distinct phases. RNA remained exclusively in the upper aqueous phase. RNA was precipitated from the upper aqueous phase by mixing with 500 µl of isopropanol per 1 ml of Trizol used initially. Samples were incubated at room temperature for 10 min and then centrifuged at 12,000 for 10 min at 4 ^oC to pellet the RNA. The supernatant was removed and the RNA pellet washed once with 1 ml 75% ethanol per 1 ml of Trizol reagent used initially. Samples were mixed by vortex and centrifuged at 7,500 x g for 5 min at 4 ^oC. The supernatant was removed and the RNA pellet was allowed to air dry for 3 min. RNA was dissolved in 20 µl RNase free water and incubated at 55 ^oC for 10 min.

2.2.3.8.2 RT-qPCR

RNA from whole cell extraction was reverse transcribed into cDNA using Superscript III reverse transcriptase (Invitrogen) as follows:

2 µg RNA was transcribed in a final volume of 10 µl
2 µl 25 mM dNTP mix (NEB)
2 µl 5 x reverse transcriptase buffer (Invitrogen)
2 µl 0.1 M DTT
1 µl of Superscript III
1 µl of Oligo(dT) (Thermo Scientific).

RT-qPCR was performed using the Stratagene Mx3000P and MxPro v4.10 software. Samples were amplified in triplicate in 10 µl volumes using SYBR-Green master mix and 250 nM of each optimized forward

and reverse primer. Cycling conditions for RT-qPCR were as follows: 95˚C for 10 min to denature followed by 35 cycles of 95˚C for 30 s, 60˚C for 1 min. Levels of mRNA were quantified relative to GAPDH mRNA levels according to the ΔΔCt method.

2.2.4 Microscopy

2.2.4.1 Immunofluorescence

Immunostaining was performed as described previously (De Vos et al., 2005). HeLa or HEK293 cells on glass coverslips were fixed with 3.7 % formaldehyde in phosphate buffered saline (PBS) for 20 min at room temperature. After washing with PBS, residual formaldehyde was quenched by incubation with 50 mM NH_4Cl in PBS for 10 min at room temperature, followed by a second round of washing with PBS. Subsequently, the cells were permeabilized by incubation with 0.2% Triton-X100 in PBS for 3 min. Triton-X100 was removed by washing with PBS. After fixing, the cells were incubated with PBS containing 0.2% fish gelatine (PBS/F) for 30 min at room temperature and then with the primary antibody in PBS/F for 1 h. After washing with PBS/F, the cells were incubated with secondary antibody in PBS/F for 45 min at room temperature. After a final wash, the samples were mounted in fluorescence mounting medium (Dako). Images were recorded using MicroManager 1.4 software (Edelstein et al., 2014) on a Zeiss Axioplan 2 microscope fitted with a Hamamatsu C4880-80 multi-format CCD camera and a 63x, Plan Apochromate 1.4NA objective.

2.2.4.2 Proximity Ligation Assay

In-situ proximity ligation assays were performed using rabbit anti-HA (Sigma, 1:1000) and mouse anti-Myc (9B11, Cell Signaling, 1:2000) antibodies with the Duolink In-Situ Kit following the manufacturer's protocol (Olink Bioscience). HeLa cells seeded on glass cover slips and treated with control (Ctrl) or C9orf72 siRNA for 72 h were transfected with HA-ULK1, Myc-Rab1a or HA-ULK1+Myc-Rab1a along with mVenus to indicate co-transfection. 24 h post transfection, cells were fixed, quenched and permeabilized as described in 2.2.4.1. Samples were blocked according to the manufacturer's instructions using the blocking solution provided. Samples were then probed with anti-HA and anti-myc antibodies for 1 h at room temperature. After washing in Wash Buffer A, cells were incubated with mouse-minus and rabbit-plus PLA probes according to the manufactures instructions for 1 h at 37^{o}C in antibody diluent. After further

washes in Wash Buffer A, the PLA probes were ligated for 30 min at 37°C before the amplification step was performed for 100 min at 37°C using the Duolink Orange detection reagents. After final washes in Wash Buffer B the samples were mounted in fluorescence mounting medium (Dako).

2.2.4.3 Image Analysis

All image analysis was performed using ImageJ (Abràmoff M. D, 2004). mCherry-FIP200, EGFP-LC3 and mCherry-EGFP-LC3 puncta, and PLA proximity signals were counted in single cells using the Particle Analysis facility of ImageJ. Where possible the cells for analysis were selected based on fluorescence in the other channel, else the samples were blinded to the operator. Images were filtered using a Hat filter (7x7 kernel) (De Vos and Sheetz, 2007) to extract puncta and proximity signals and thresholded such that the visible puncta within the cell were highlighted, but no background was included. The result of thresholding was further checked against the original image to ensure no background signal was identified as puncta or signals. In case of mCherry-EGFP-LC3, puncta in the red and green channels were counted separately. Red only puncta were determined by subtracting the green puncta from the red puncta.

2.2.5 Statistical analysis

Calculations and statistical analysis were performed using Excel (Microsoft Corporation, Redmond, WA), and Prism 6 software (GraphPad Software Inc., San Diego, CA).

3 Identification of C9orf72 binding partners

3.1 Introduction

A hexanucleotide repeat expansion of GGGGCC in *C9orf72* is the most common genetic defect associated with ALS and FTD. *C9orf72* encodes two uncharacterised proteins that are highly conserved in vertebrates. As detailed in section 1.7.2, there are multiple mechanisms by which the expansion may cause disease, including *C9orf72* haploinsufficiency (Belzil et al., 2013; Cooper-Knock et al., 2012; DeJesus-Hernandez et al., 2011; Xi et al., 2013). Protein-protein interaction networks have been suggested as a possible method to predict protein function (Schwikowski et al., 2000; Vazquez et al., 2003). Thus by identifying binding partners of C9orf72, the aim was to characterize the cellular function of this protein.

The specific p62 positive, TDP-43 negative, pathology associated with C9ALS/FTD suggested that C9ALS/FTD patients might be deficient in autophagy (Al-Sarraj et al., 2011; Cooper-Knock et al., 2012; Stewart et al., 2012). A screening study investigating the autophagy network had previously identified C9orf72 as a potential interacting partner of FIP200 (Behrends et al., 2010). Interestingly, neural specific conditional knockout of FIP200 in mice leads to neurodegeneration, and cerebellar accumulations of p62, similar to C9ALS/FTD (Liang et al., 2010), suggesting loss of FIP200 and haploinsufficiency of C9orf72 may share a common pathology. Thus, in a hypothesis driven approach, the first set of protein interaction studies were focused around FIP200 and the autophagy pathway. To investigate the interaction of C9orf72 and members of the autophagy pathway co-immunoprecipitation experiments were conducted along with *in vitro* binding assays.

Secondly, two unbiased approaches were conducted to identify interacting partners: a mass spec screen, conducted by Dr. Mathew Walsh, Dr. Guillaume Hautbergue and Professor Pamela Shaw, and a yeast two hybrid (Y2H) screen. Positive hits received from these screens were then confirmed in the laboratory by co-immunoprecipitation experiments.

Firstly, a characterization of the C9orf72 protein was conducted using the commercially available antibodies in an attempt to detect endogenous C9orf72 via immunoblot and immunofluorescence.

3.2 Results

3.2.1 Characterization of C9orf72 antibodies and siRNA

Several commercial antibodies against C9orf72 are available, but their specificity for endogenous C9orf72 protein has been questioned (DeJesus-Hernandez et al., 2011). Recently, one group has developed isoform specific antibodies for C9orf72, which appear to detect endogenous C9orf72S and C9orf72L (Xiao et al., 2015). Unfortunately, these antibodies were unavailable during preparation of this thesis. Three commercial rabbit polyclonal anti-C9orf72 antibodies were tested: anti-C9orf72 from Santa Cruz Biotechnology (sc-138763), anti-C9orf72 from Atlas Antibodies (HPA023873) and anti-C9orf72 from ProteinTech (22637-1-AP). Santa Cruz anti-C9orf72 sc-138763 and ProteinTech anti-C9orf72 22637-1-AP were raised against peptides corresponding to unspecified internal regions of the C9orf72 protein, Atlas anti-C9orf72 HPA023873 was raised against amino acids 110 to 200 of C9orf72 protein. While Atlas anti-C9orf72 HPA023873 should recognise both isoforms of C9orf72, whether the other antibodies would have this ability was unknown. To determine the specificity of these antibodies, they were initially used in western blot analysis of HEK293 cell lysates. As a positive control HEK293 cells were transfected with either Myc-tagged C9orf72S or Myc-tagged C9orf72L. Both these constructs were produced in-house. HEK293 cells were transfected with empty vector, Myc-C9orf72S or Myc-C9orf72L. 24 h post transfection lysates were subjected to SDS-PAGE and immunoblot. Blots were probed with anti-Myc 9B11 antibody to show the positions of Myc-C9orf72S and Myc-C9orf72L (Fig. 3.1D) or one of the three commercial C9orf72 antibodies as indicated (Figs 3.1A-C). As shown in Figure 3.1 all three commercial antibodies were able to detect transfected Myc-tagged C9orf72S and L. However, at short exposures no commercially available antibodies produce a banding pattern that could correspond to endogenous C9orf72. The Santa Cruz anti-C9orf72 sc-138763 antibody detected a range of other bands with the longer exposure, but only in samples that had been transfected with Myc-C9orf72, suggesting these were some sort of aggregates or degradation products (Fig. 3.1A). There were faint bands in the empty vector transfected control lane at around 25 kDa and 50

kDa, possibly corresponding to endogenous C9orf72S and L (Fig 3.1A). A longer exposure with the anti-C9orf72 antibody from ProteinTech (22637-1-AP), revealed only a band that ran at a higher molecular weight than Myc-C9orf72L suggesting this antibody was unable to detected endogenous C9orf72 (Fig. 3.1B). A longer exposure with the Atlas anti-C9orf72 HPA023873 antibody revealed a slightly lighter band at approximately 50 kDA in all samples below that of Myc-C9orf72L, which could correspond to endogenous C9orf72L, but no band corresponding to endogenous C9orf72S was detected (Fig. 3.1C). It appeared that in all cases the strength of the Myc-C9orf72 signal was masking the normal banding pattern produced by the antibodies.

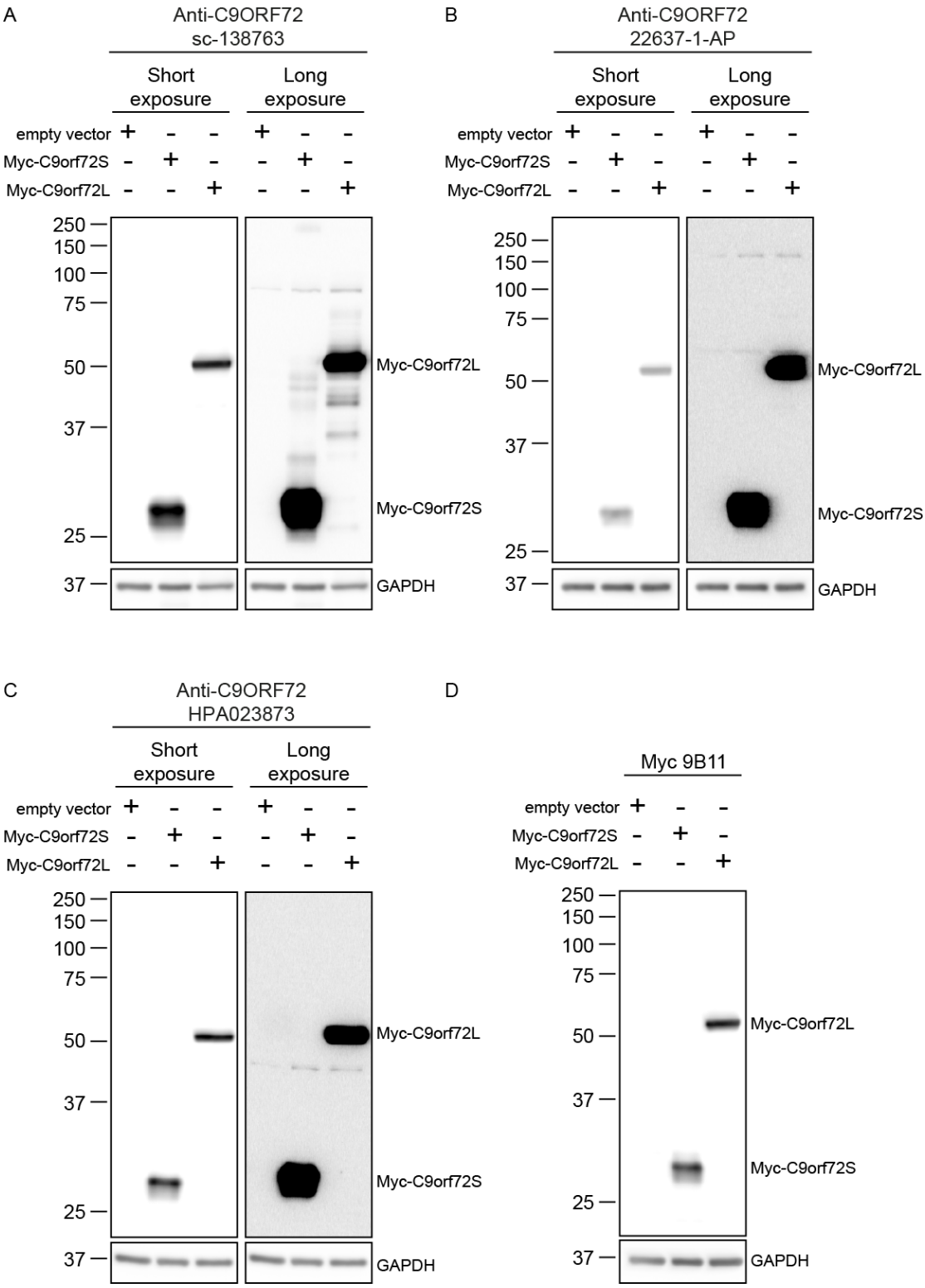

Figure 3.1 Commercial anti-C9orf72 antibodies detect transfected epitope tagged C9orf72 on immunoblot. HEK293 cells transfected with empty vector (Ctrl), Myc-tagged C9orf72S or Myc-tagged C9orf72L were lysed 24 h post

transfection and subjected to SDS-PAGE and immunoblot. Myc-tagged proteins were detected with anti-Myc antibodies (D). Blots were probed with three commercial anti-C9orf72 antibodies: anti-C9orf72 from Santa Cruz Biotechnology (sc-138763) (A), anti-C9orf72 from ProteinTech (22637-1-AP) (B) and anti-C9orf72 from Atlas Antibodies (HPA023873) (C).

To confirm whether the bands detected by the endogenous antibodies at longer exposures related to endogenous C9orf72, the antibodies were tested on cell samples that had been treated with targeted siRNA to ablate C9orf72 expression. HEK293 cells were treated with control (Ctrl) siRNA or C9orf72 targeted siRNA. After 4 days of treatment cells were harvested, lysed and samples analysed by SDS-PAGE and immunoblot. Samples were probed with anti-C9orf72 sc-138763, anti-C9orf72 22637-1-AP and anti-C9orf72 HPA023873. GAPDH was used as a loading control. The banding pattern detected by the Santa Cruz sc-138763 antibody was unaffected by C9orf72 siRNA suggesting that the bands at 25 kDa and 50 kDa (indicated by * in Fig. 3.2A) were non-specific and not endogenous C9orf72 (Fig. 3.2A). Similarly, the bands detected by the ProteinTech 22637-1-AP antibody at approximately 150 kDa and 60 kDa (indicated by * in Fig. 3.2B) were unaffected by C9orf72 siRNA, suggesting these were not related to endogenous C9orf72. However, the banding pattern detected by the Atlas HPA023873 antibody was altered after C9orf72 knock down (Fig. 3.2C). Three bands around 50 kDa (one at 50 kDa, one above and one below) were all reduced by C9orf72 siRNA (indicated by <), suggesting that these bands may relate to the endogenous C9orf72L signal (Fig. 3.2C). There was also a band at 75 kDa that was reduced, although how this related to the C9orf72L and S isoforms is unclear (Fig. 3.2C). There was no band corresponding to C9orf72S and also there was at least one high molecular weight band that was unaffected by siRNA knock down at approximately 150 kDa (*) (Fig. 3.2C). To detect this banding pattern, these commercial antibodies were used a relatively high concentrations of 1:250. This suggested that this antibody also had low specificity to endogenous C9orf72. The level of C9orf72 knock down was confirmed by quantitative PCR, which showed approximately 50% knockdown of C9orf72 mRNA after targeted siRNA (Fig. 3.2D). This led to the conclusion that it was unfeasible to conduct further experiments using these antibodies, even the Atlas HPA023873 antibody, as it was not possible to reliably detect the endogenous C9orf72 isoforms.

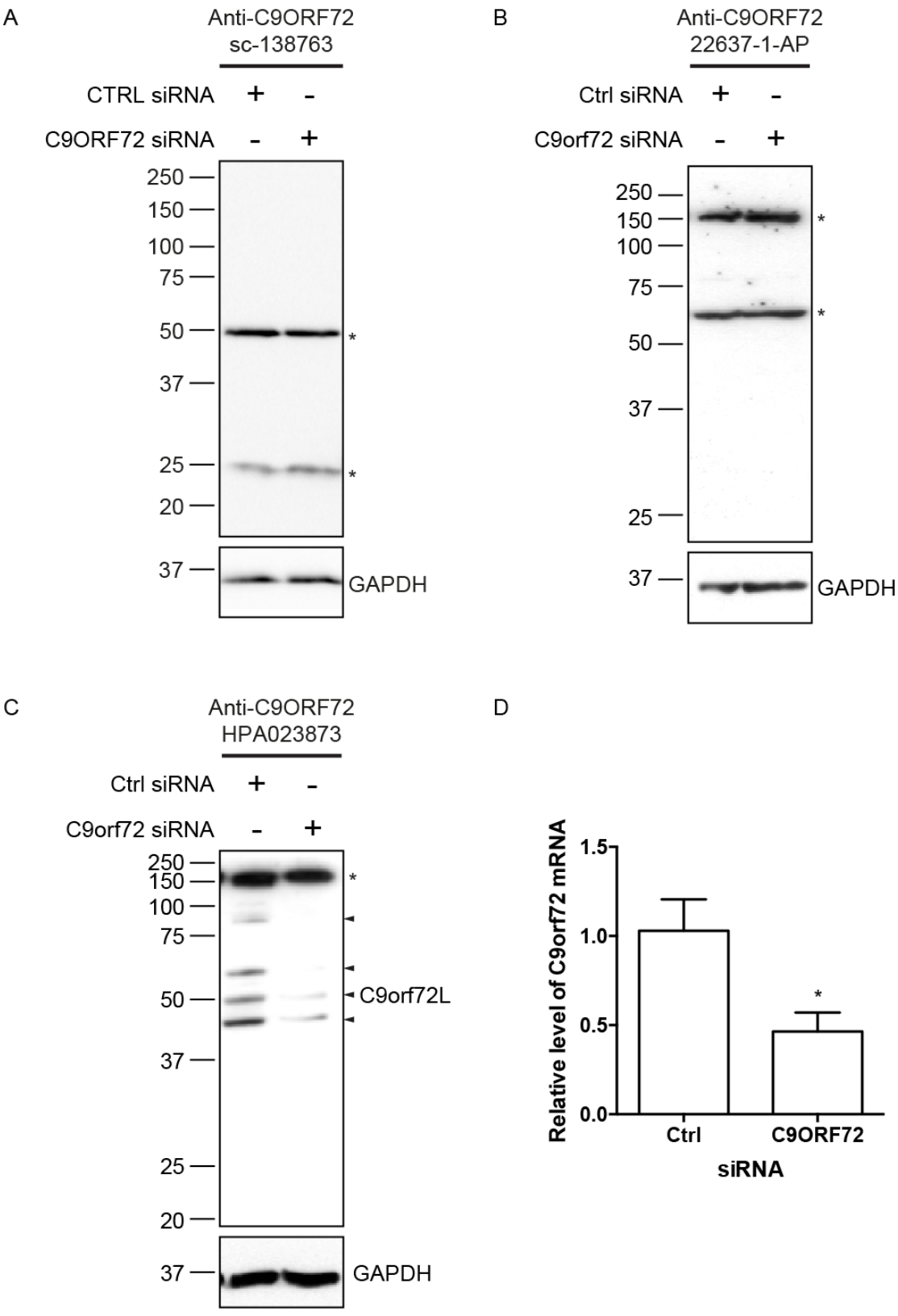

Figure 3.2 Anti-C9orf72 HPA023873 is able to detect endogenous C9orf72. HEK293 cells were transfected with non-targeting (Ctrl) siRNA or a pool of C9orf72 targeted siRNA. 4 days post transfection cells were lysed and samples analysed by SDS-PAGE and immunoblot. Immunoblots were probed for

endogenous C9orf72 with anti-C9orf72 from Santa Cruz Biotechnology (sc-138763) (A), anti-C9orf72 from ProteinTech (22637-1-AP) (B), and anti-C9orf72 from Atlas Antibodies (HPA023873) (C - < indicate possible C9orf72 bands, * indicate non-specific bands). (D) Level of C9orf72 mRNA was quantified by real time quantitative PCR (RT-qPCR). Graph represents mean relative level of C9orf72 mRNA after siRNA transfection (Mean±SEM; *t*-test; * $p \leq 0.05$; n = 3 experiments).

These antibodies were next tested on immunofluorescence experiments, to investigate the localisation of C9orf72. HeLa cells were fixed and stained with each of the commercial antibodies. As a positive control HeLa cells were transfected with Myc-C9orf72S or Myc-C9orf72L. Again, all three antibodies were able to detect transiently transfected C9orf72 as shown by the co-localisation of the Myc antibody signal and the corresponding C9orf72 antibody signal (Fig. 3.3A-C). Neither Myc-C9orf72S nor Myc-C9orf72L showed any specific sub cellular localisation, with all three anti-C9orf72 antibodies, as well as the Myc antibody, showing a diffuse distribution throughout the cytoplasm and nucleus. Both Myc-C9orf72S and Myc-C9orf72L showed a distinct absence from the nucleolar type structures of the nucleus (Fig. 3.3A-C). All three commercial antibodies showed a diffuse speckled pattern of staining throughout the cytoplasm, but with the Atlas HPA023873 and Santa Cruz sc-138763 antibodies also showing a much more nuclear localised signal that did not correspond to the Myc-C9orf72 signal (Fig. 3.3A and B). In comparison, the ProteinTech 22637-1-AP antibody showed a diffuse cytoplasmic speckled stain that was not enriched in the nucleus (Fig. 3.3C). To determine whether the signal seen with these antibodies via immunofluorescence was specific, the same staining was conducted on HEK293 cells that had been treated with C9orf72 siRNA to ablate expression (Fig. 3.4A). Cells that were treated with siRNA in Figure 3.2 were fixed and stained with the commercial C9orf72 antibodies. None of the commercial antibodies showed any difference in staining after C9orf72 siRNA (Fig. 3.4A). It was concluded that the commercial antibodies that were available at this time were unable to detect endogenous C9orf72 protein. For this reason, the investigations into C9orf72 binding partners were conducted on over-expressed, transiently transfected tagged-C9orf72.

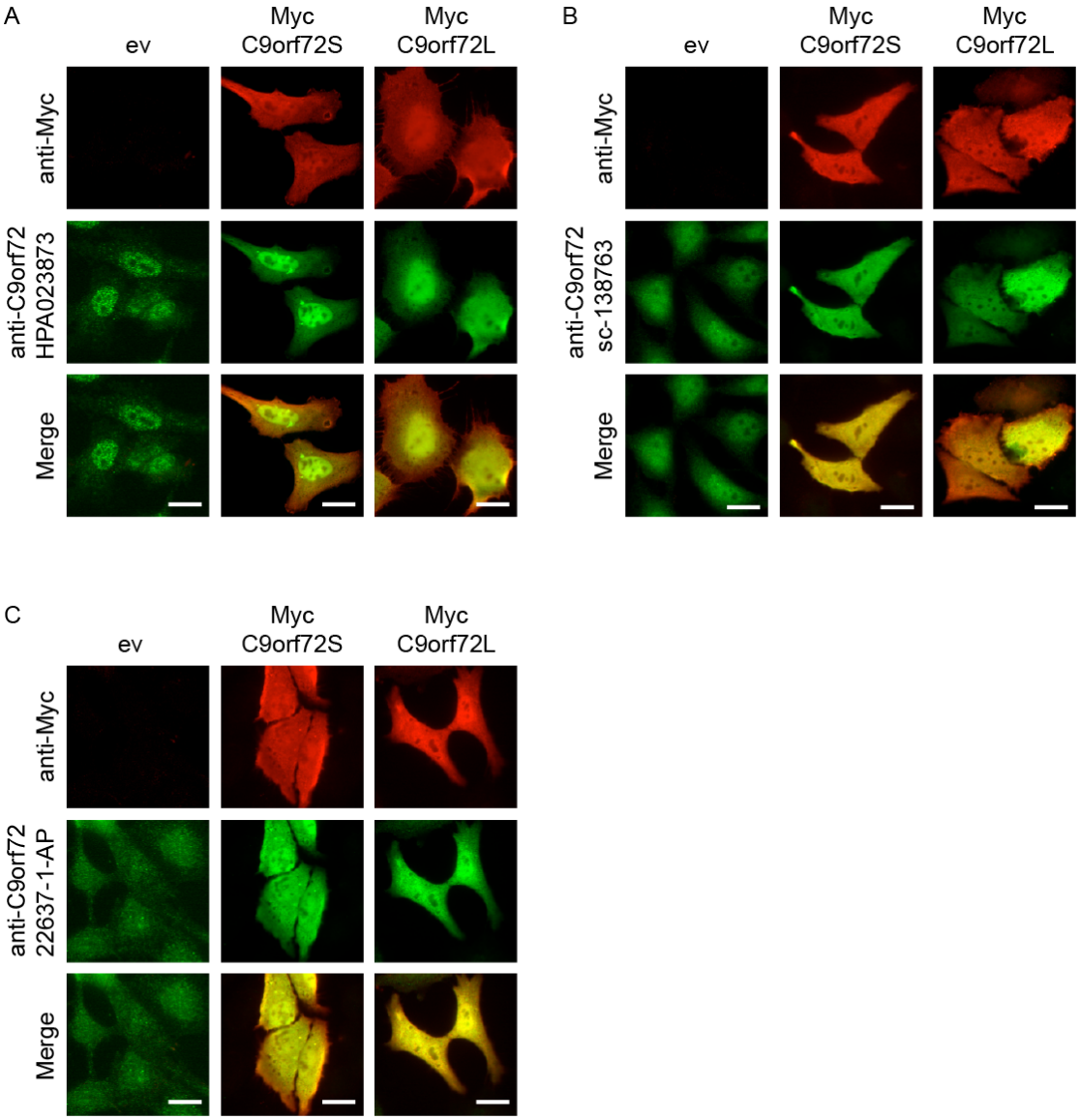

Figure 3.3 Commercial anti-C9orf72 antibodies detect transfected epitope tagged C9orf72 in immunofluorescence. HeLa cells were transfected with empty vector control (ev), Myc-C9orf72S or Myc-C9orf72L. Cells were fixed and co-stained with mouse anti-Myc (Alexa568) and either (A) rabbit anti-C9orf72 HPA023873 (Alexa488), (B) rabbit anti-C9orf72 sc-138763 or (C) rabbit-anti-C9orf72 22637-1-AP (Alexa488) (Alexa 488).

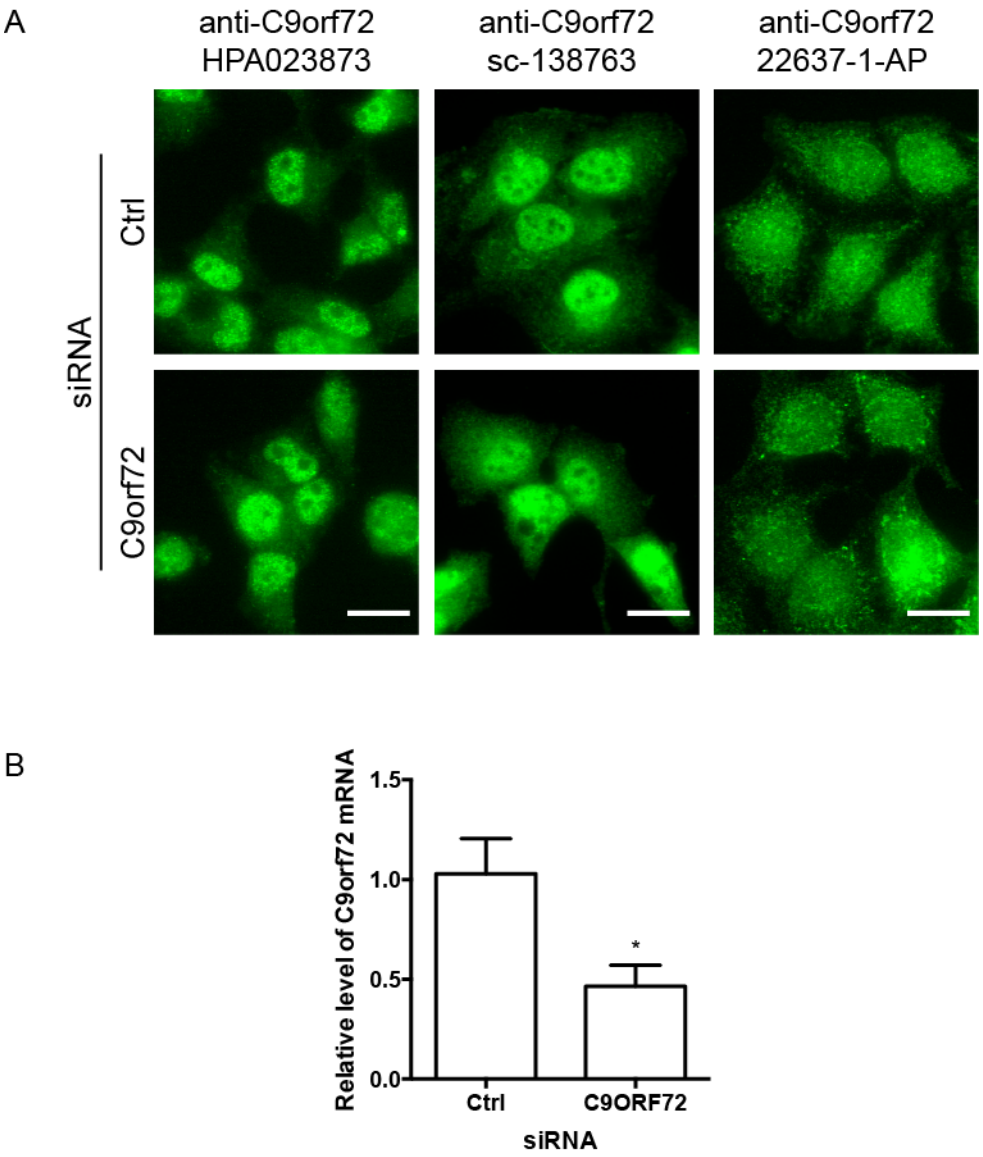

Figure 3.4 Commercial antibodies do not detect endogenous C9orf72 in immunofluorescence. (A) HEK293 cells were treated with non-targeting (Ctrl) siRNA or a pool of C9orf72 targeted siRNA for 4 days. Cells were then fixed and stained with rabbit anti-C9orf72 HPA023873 (Alexa 488), rabbit anti-C9orf72 sc-138763 (Alexa488), or rabbit-anti-C9orf72 22637-1-AP (Alexa488). (B) knockdown of C9orf72 was confirmed by RT-qPCR.

3.2.2 C9orf72 interacts with FIP200

Neuronal cytoplasmic inclusions are a hallmark of ALS (Wood et al., 2003). While C9ALS/FTD patients show TDP-43 positive accumulations that are typical of ALS, they also show characteristic p62 positive, TDP-43 negative pathology (Al-Sarraj et al., 2011; Cooper-Knock et al., 2012). P62 accumulations are indicative of dysfunctional autophagy (Pankiv et al., 2007), suggesting that C9orf72 patients may have a defective autophagy pathway and that the C9orf72 protein may function in this pathway. The p62 specific accumulations associated with C9ALS/FTD are primarily found within the hippocampus and the cerebellum (Al-Sarraj et al., 2011; Cooper-Knock et al., 2012). These cerebellar accumulations of p62 are also seen within a neural specific conditional FIP200 knock-out mouse model (Liang et al., 2010), suggesting that loss of FIP200 and haploinsufficiency of C9orf72 share a common pathology. Interestingly, a previous screen for proteins involved in the autophagy network highlighted C9orf72 as a potential binding partner of the essential autophagy protein FIP200 (Behrends et al., 2010). To further investigate this, the interaction of C9orf72 and FIP200 was investigated by co-immunoprecipitation and *in vitro* binding assays.

HEK293 cells were co-transfected with FLAG-tagged FIP200 and either empty vector, Myc-tagged C9orf72S or Myc-tagged C9orf72L. Cells were lysed 24 h post transfection. Myc-C9orf72 was immunoprecipitated from lysates using 9106 anti-Myc antibodies, and the immune pellets analysed by SDS-PAGE and immunoblot. FLAG-FIP200 was found to co-immunoprecipitate with both C9orf72S and C9orf7L (Fig. 3.5A).

As section 3.2.1 showed, the specificity of the commercial C9orf72 antibodies was questionable. It may be that there is little C9orf72 protein within HEK293 cells making the detection of endogenous protein difficult. Therefore, while it would be advantageous to show the interaction of FIP200 and C9orf72 at the endogenous level, there was no reliable way of immunoprecipitating endogenous C9orf72. As a compromise, the interaction of endogenous FIP200 and transfected C9orf72 was investigated. The specificity of the FIP200 antibody was first confirmed by western blot of FIP200 knockout mouse embryonic fibroblasts (MEFs). The antibody detected two bands in the wild-type control MEF, one under 150 kDa and one at approximately 250 kDa. The band at 250 kDa was absent in the FIP200 $^{-/-}$ MEFs showing this to be endogenous

FIP200 and that the antibody was able to detect the endogenous protein (Fig. 3.5B). Next, HEK293 cells were transiently transfected with empty vector, Myc-C9orf72S or Myc-C9orf72L. 24 h post transfection cells were lysed and Myc-C9orf72 immunoprecipitated using 9B11 anti-Myc antibodies. Immune pellets were analysed by SDS-PAGE and immunoblot, and endogenous FIP200 detected. Endogenous FIP200 was found to co-immunoprecipitate with both isoforms of C9orf72 (Fig. 3.5C). A double band corresponding to endogenous FIP200 was co-immunoprecipitated with C9orf72S and to a greater extent with C9orf72L (Fig. 3.5C). Higher molecular weights suggest a degree of post-translational modification, possibly by ubiquitin or phosphorylation.

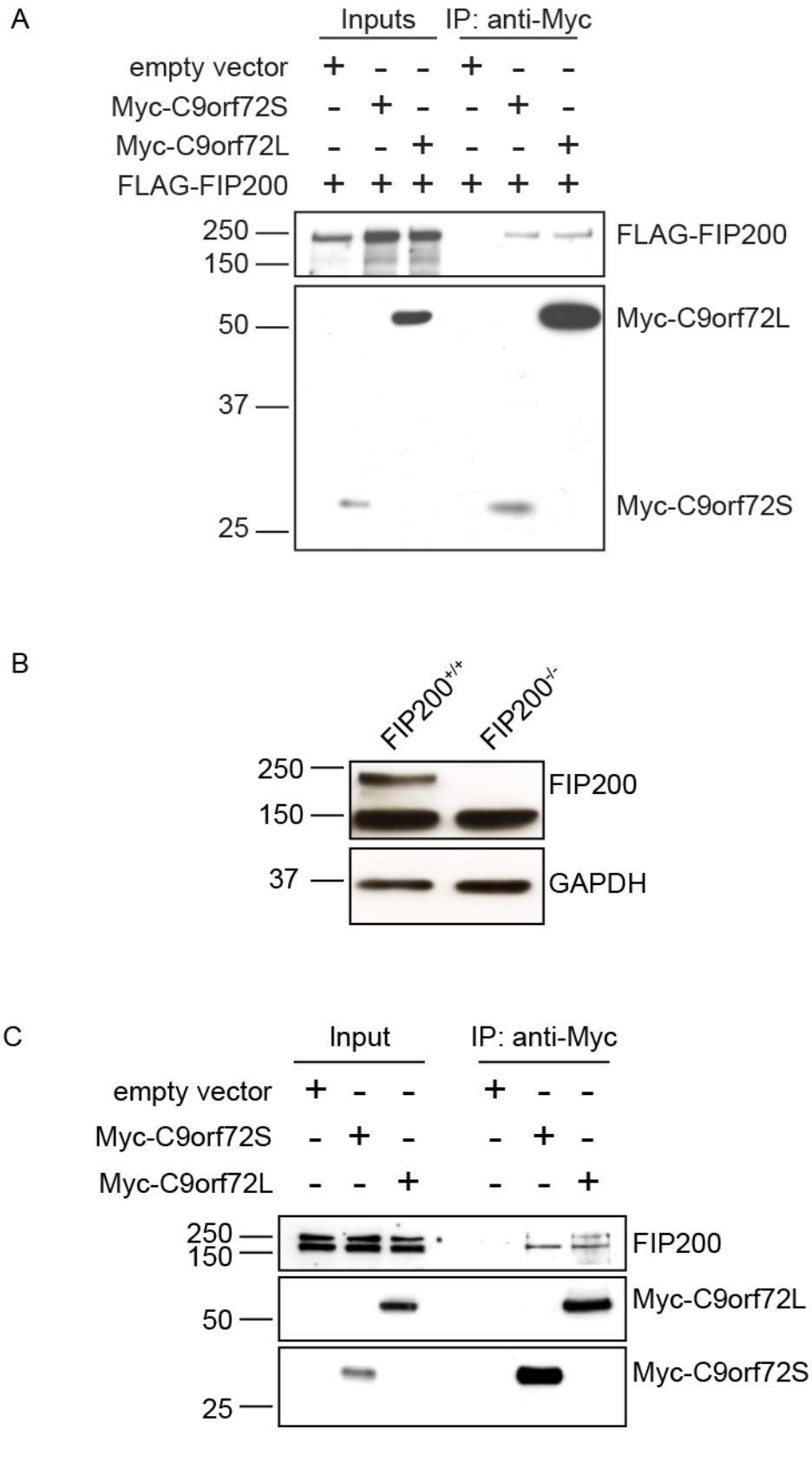

Figure 3.5 C9orf72 interacts with FIP200. (A) Whole cell lysates of HEK293 cells co-transfected with FLAG-FIP200 and either empty vector control, Myc-C9orf72S or Myc-C9orf72L were subjected to immunoprecipitation with rabbit

anti-Myc 9106 antibodies. Immune pellets were probed for Myc-C9orf72 (bottom panel) with 9B11 anti-Myc antibodies and FLAG-FIP200 (top panel) using M2 anti-FLAG antibodies on immunoblot. (B) Whole cell lysates of FIP200$^{+/+}$ and FIP200 $^{-/-}$ MEFs were analysed by SDS-PAGE and immunobot. Blots were probed with anti-FIP200 antibodies to check specificity and GAPDH as a loading control. (C) Whole cell lysates of HEK293 cells transfected with empty vector control, Myc-C9orf72S or Myc-C9orf72 were subjected to immunoblot with 9B11 anti-Myc antibodies. Immune pellets were probed for Myc-C9orf72 (using rabbit anti-Myc 9106 antibodies) and endogenous FIP200 on immunoblot. In all cases 20 µg (2%) of the immunoprecipitation was loaded as Input.

To investigate whether C9orf72 was directly interacting with FIP200, *in vitro* binding assays were performed. Recombinant GST-tagged C9orf72 protein produced in bacteria was incubated with *in vitro* translated S^{35}-labelled fragments of FIP200, corresponding to the N-terminus (NT-FIP200), Middle domain (MD-FIP200) and C-terminus (CT-FIP200) (Fig. 3.6A) (Abbi et al., 2002). GST control and GST-tagged C9orf72 proteins were pulled down using glutathione beads and proteins eluted using excess glutathione. Samples were analysed by SDS-PAGE and radiolabelled protein detected using a phosphoimager. The N-terminus of FIP200 was found to directly interact with both C9orf72S and C9orf72L, but not with the GST control (Fig. 3.6B). The middle domain of FIP200 did not interact with GST, C9orf72S or C9orf72L (Fig. 3.6C), while the C-terminus of FIP200 interacted with both C9orf72S and C9orf72L, but also with the GST control (Fig. 3.6D). When taken together these results suggest that the N-terminal region of C9orf72 directly binds the N-terminal of FIP200. Thus these data identify C9orf72 as a direct binding partner of FIP200, an interaction that occurs between the N-terminus of FIP200 and a region within the first 222 amino acids of C9orf72.

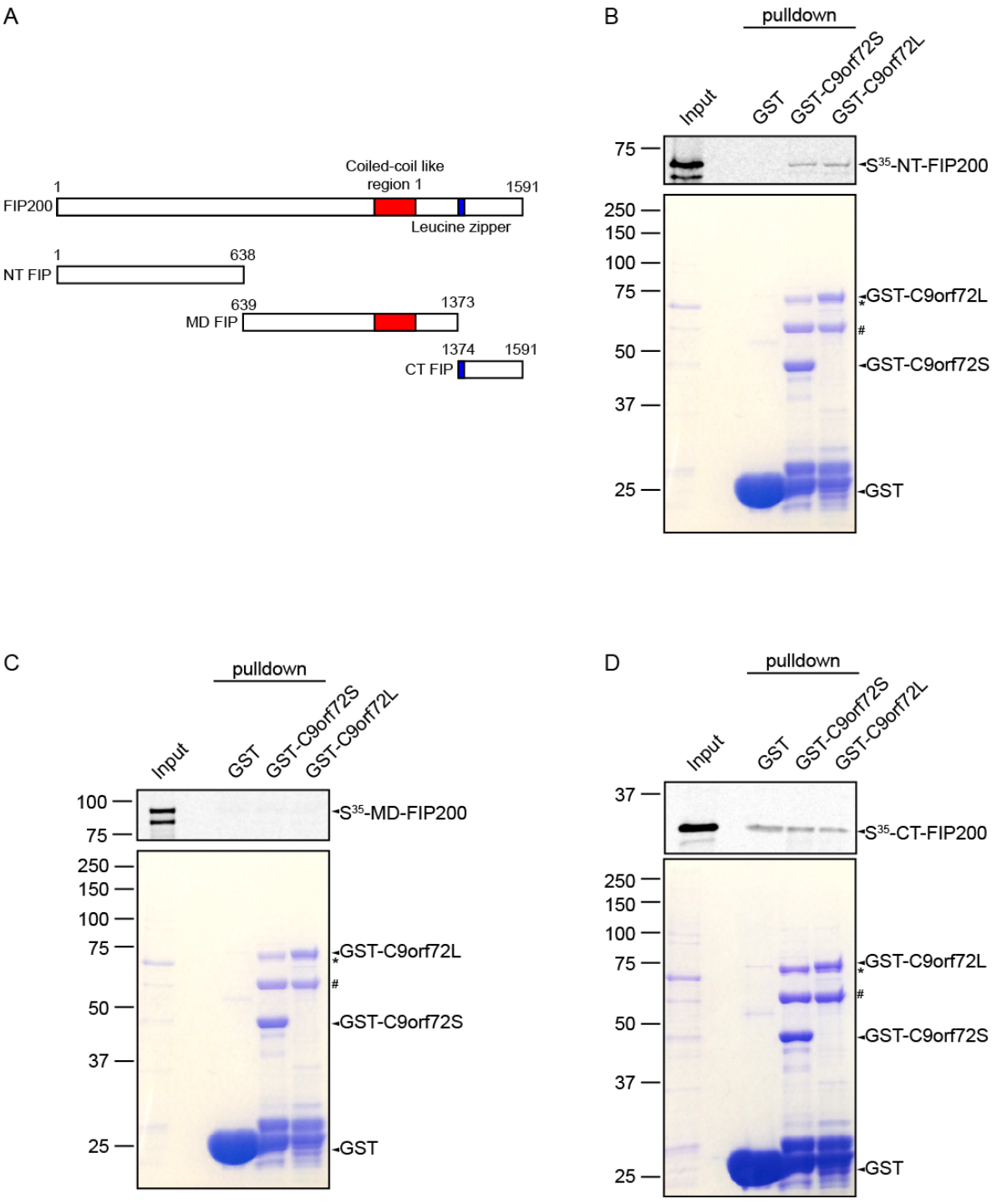

Figure 3.6 C9orf72 directly interacts with the N terminus of FIP200. (A) Schematic of the FIP200 fragments that were generated by PCR, showing how the N-terminus, the middle domain and the C-terminus of FIP200 fragments relate to full length FIP200. ^{35}S-radiolabelled recombinant FIP200 fragments correlating to the N-terminus (B), the middle domain (C) and the C-terminus (D) were incubated with GST, GST-C9orf72S or GST-C9orf7L immobilized on glutathione-coated beads. ^{35}S-radiolabelled recombinant FIP200 fragments

were visualised on a phosphoplate (top panel: B, C and D). Coomassie-stained GST, GST-C9orf72S and GST-C9orf72L from the pull down are shown (bottom panel; B, C and D). The identity of the Coomassie protein bands were confirmed by mass spectrometry (* = CH60 *E. coli*, 60kD Chaperonin, # = DnaK Chaperonin *E.coli*).

3.2.3 C9orf72 interacts with ULK1

The autophagy initiation complex is comprised of FIP200, ULK1, ATG13 and ATG101 (Ganley et al., 2009; Hara et al., 2008; Hosokawa et al., 2009b; Jung et al., 2009; Mercer et al., 2009). FIP200 directly interacts with ULK1 to mediate its correct localisation during autophagy induction (Ganley et al., 2009). The direct interaction of C9orf72 with FIP200 presented in section 3.2.2, therefore raised the possibility that C9orf72 was also capable of binding ULK1. Thus, the interaction between C9orf72 and ULK1 was investigated by co-immunoprecipitation and *in vitro* binding assays.

HEK293 cells were co-transfected with HA-tagged ULK1 and either empty vector, Myc-C9orf72S or Myc-C9orf72L. C9orf72 was immunoprecipitated from cell lysates with 9B11 anti-Myc antibodies and immune pellets were subjected to SDS-PAGE and immunoblot. HA-ULK1 was found to efficiently co-immunoprecipitate with both C9orf72S and C9orf72L (Fig. 3.7A).

As with FIP200, the interaction of C9orf72 with endogenous ULK1 was investigated. The specificity of the ULK1 antibody was firstly confirmed by western blot. The antibody detected a single band at the predicted molecular weight that was reduced after targeted ULK1 siRNA knock down (Fig. 3.7B). HEK293 cells were then transfected with empty vector, Myc-C9orf72S or Myc-C9orf72L were lysed and Myc-C9orf72 immunoprecipitated with anti-Myc antibodies. Immune pellets were subjected to SDS-PAGE and immunoblot and endogenous ULK1 detected. Endogenous ULK1 was found to co-immunoprecipitate with both isoforms of C9orf72, but to a greater extent with C9orf72L (Fig. 3.7C). Again, a higher molecular weight band corresponding to endogenous ULK1 was observed when ULK1 was co-immunoprecipitated with C9orf72L, suggesting C9orf72 was preferentially binding a post-translationally modified version of ULK1.

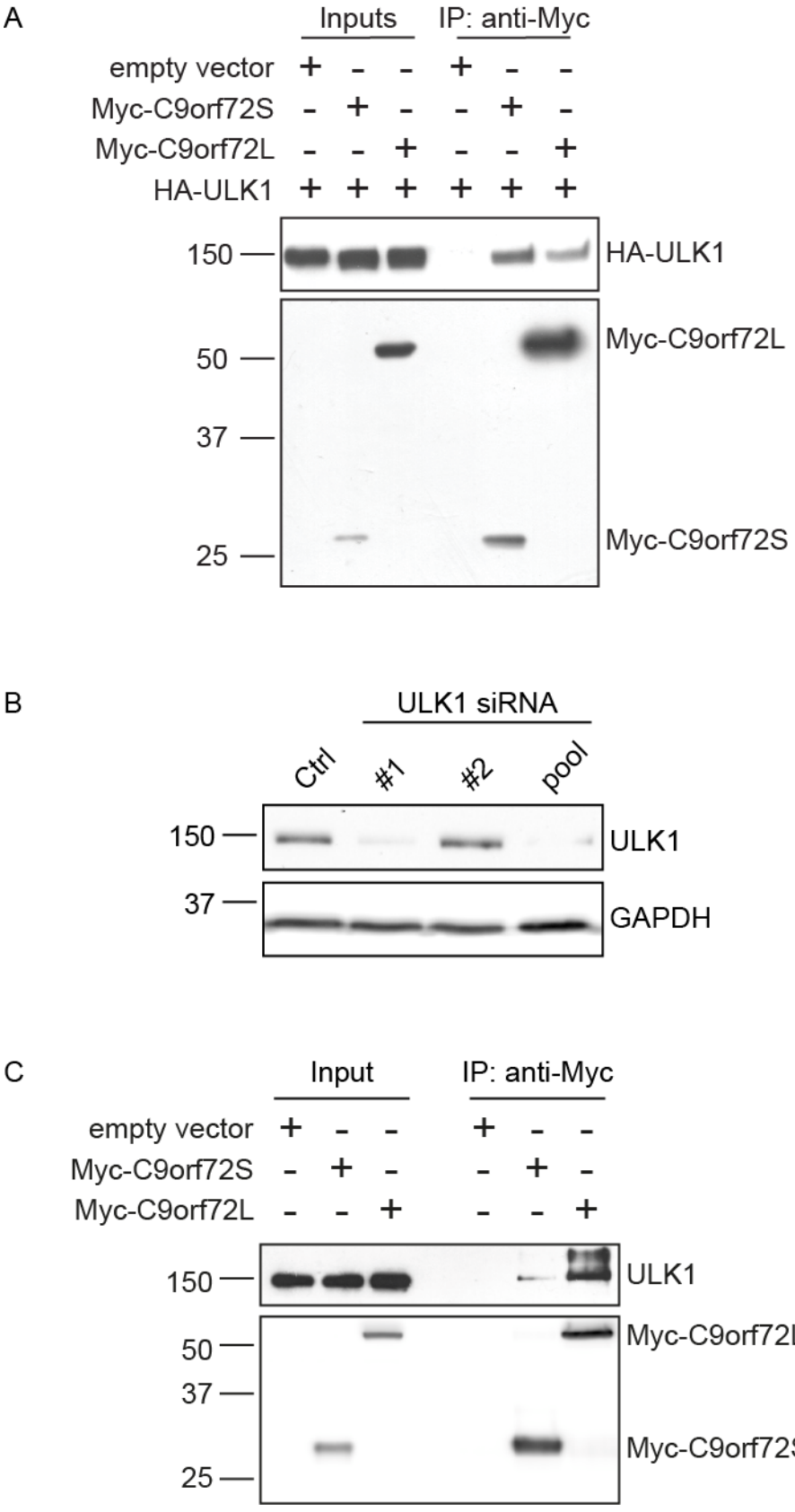

Figure 3.7 C9orf72 interacts with ULK1. (A) Whole cell lysates of HEK293 cells co-transfected with HA-ULK1 and either empty vector control, Myc-C9orf72S or

Myc-C9orf72L were subjected to immunoprecipitation with 9B11 mouse anti-Myc antibodies. Immune pellets were probed for Myc-C9orf72 (using rabbit 9106 anti-Myc antibodies) and HA-ULK1 (using rabbit anti-HA antibodies) on immunoblot. (B) Whole cell lysates of HEK293 cells treated with non-targeting control (Ctrl) siRNA, two individual ULK1 targeted siRNAs or a pool of both ULK1 targeted siRNAs were subjected to SDS-PAGE and immuoblot to test the specificity of the endogenous ULK1 antibody. (C) Whole cell lysates of HEK293 cells transfected with empty vector control, Myc-C9orf72S or Myc-C9orf72L were subjected to immunoprecipitation with 9B11 mouse anti-Myc antibodies. Immune pellets were probed for Myc-C9orf72 (using rabbit anti-Myc 9106 antibodies) and endogenous ULK1 on immunoblot. In all cases 20 µg (2%) of the immunoprecipitation was loaded as Input.

The direct interaction of C9orf72 and ULK1 was investigated using *in vitro* binding assays. Recombinant GST-tagged C9orf72 was incubated with *in vitro* translated S^{35}-labelled ULK1. GST proteins were pulled down using glutathione beads and eluted using excess glutathione. Samples were analysed by SDS-PAGE and radiolabelled proteins detected via a phosphoimager. ULK1 was found to directly interact with C9orf72S and C9orf72L but not with the GST control (Fig. 3.8).

These data show that the N-terminus of C9orf72 directly interacts with ULK1, the main regulator of the autophagy initiation complex.

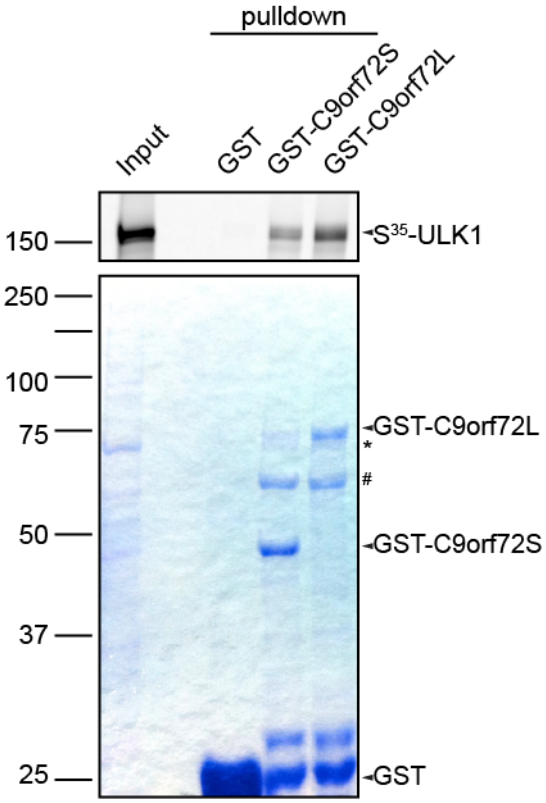

Figure 3.8 C9orf72 directly interacts with ULK1. ^{35}S-radiolabelled recombinant HA-ULK1 protein was incubated with GST, GST-C9orf72S or GST-C9orf7L immobilized on glutathione-coated beads. ^{35}S-radiolabelled recombinant HA-ULK1 protein was visualised on a phosphoplate (top panel). Coomassie-stained GST, GST-C9orf72S and GST-C9orf72L from the pull down are shown (bottom panel). The identity of the Coomassie protein bands were confirmed by mass spectrometry (* = CH60 *E. coli*, 60kD Chaperonin, # = DnaK Chaperonin *E.coli*).

3.2.4 C9orf72 interacts with ATG13

Finally, the interaction with ATG13 was investigated. ATG13 functions as a scaffold of the autophagy initiation complex, mediating the interaction between ULK1 and FIP200, ATG101 and ULK1 and also enhancing the kinase activity of ULK1 on FIP200 (Ganley et al., 2009; Jung et al., 2009; Mercer et al., 2009). HEK293 cells were co-transfected with Myc-tagged ATG13 and either empty vector, FLAG-tagged C9orf72S or FLAG-tagged C9orf72L. C9orf72 was immunoprecipitated from cell lysates with anti-FLAG antibodies. FLAG-tagged proteins were eluted from the protein G beads using excess FLAG peptide. Immune pellets were subjected to SDS-PAGE and immunoblot. Myc-ATG13 was found to efficiently co-immunoprecipitate with both C9orf72S and C9orf72L (Fig. 3.9A).

The interaction of endogenous ATG13 with Myc-C9orf72 was investigated by co-immunoprecipitation. The specificity of the ATG13 antibody was confirmed by western blot. The antibody detected a single band at the predicted molecular weight of ATG13. This band was reduced when cells were transfected with targeted ATG13 siRNA (Fig. 3.9B). Next, HEK293 cells were transfected with Myc-C9orf72. After lysis, Myc-C9orf72 was immunoprecipitated with anti-Myc antibodies. The immune pellets were subjected to SDS-PAGE and immunoblot and blots probed for endogenous ATG13. ATG13 was found to co-immunoprecipitate with both isoforms of C9orf72 (Fig. 3.9C), thus identifying C9orf72 as a novel binding partner of ATG13. Unlike the endogenous FIP200 and ULK1 interactions with C9orf72, which suggested higher molecular weight species co-immunoprecipitation with C9orf72L, a lower molecular weight species of endogenous ATG13 (indicated with * in Fig. 3.9C) was found to co-immunoprecipitate with C9orf72S and C9orf72L (Fig. 3.9C). This endogenous ATG13 species could relate to a proteolytic processed form of ATG13, although no such processing has been reported, or a degradation product of the full-length protein. Alternatively, ATG13 has been shown to undergo alternative splicing (Alers et al., 2011), and so this lower molecular weight species of ATG13 could relate to one of these smaller, alternatively spliced forms.

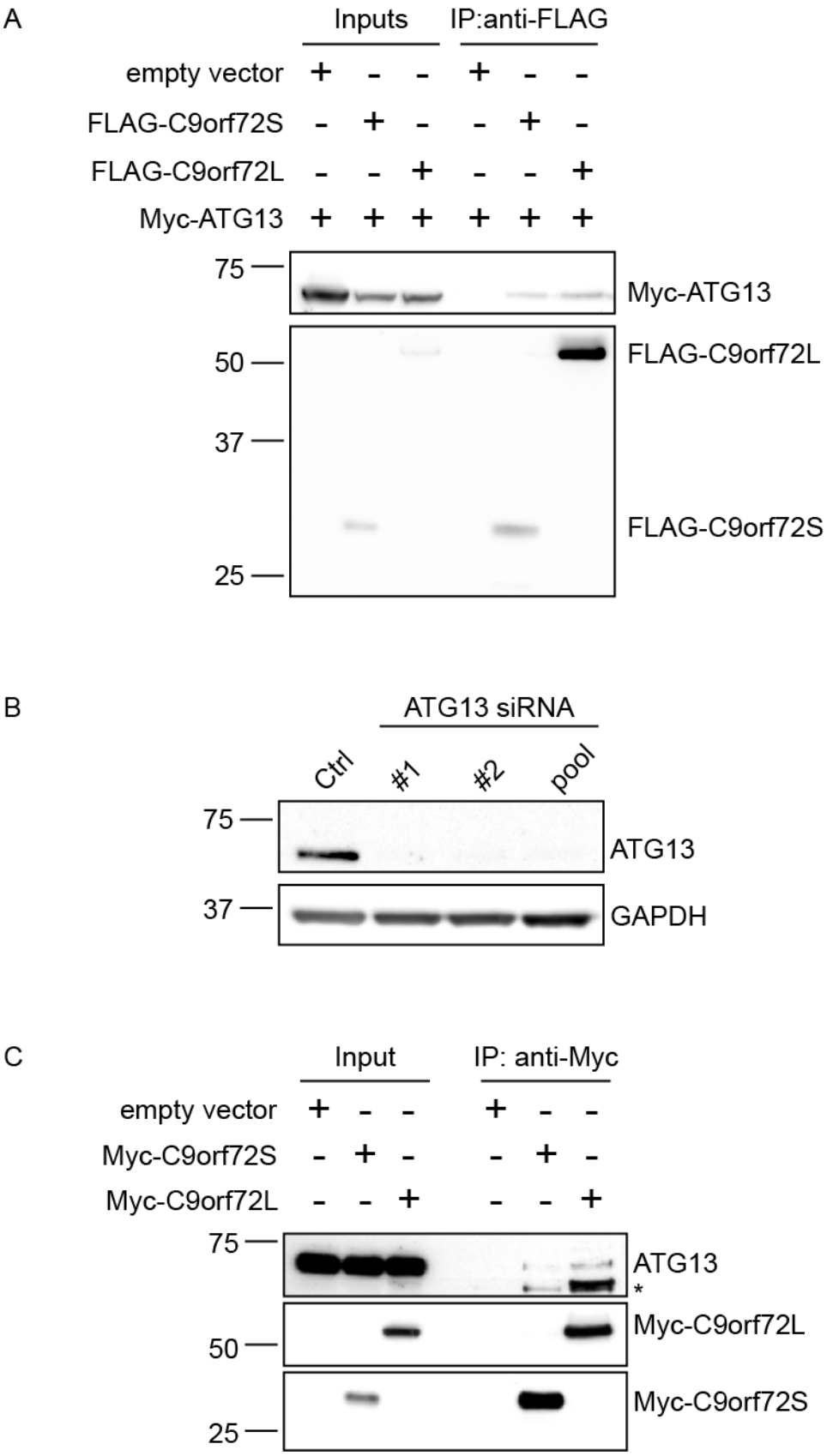

Figure 3.9 C9orf72 interacts with ATG13. (A) Whole cell lysates of HEK293 cells co-transfected with Myc-ATG13 and either empty vector control, FLAG-

C9orf72S or FLAG-C9orf72L were subjected to immunoprecipitation with M2 mouse anti-FLAG antibodies. Immune pellets were probed for FLAG-C9orf72 (using M2 anti-FLAG antibodies) and Myc-ATG13 (using 9B11 anti-Myc antibodies) on immunoblot. (B) Whole cell lysates of HEK293 cells treated with non-targeting control (Ctrl) siRNA, two individual ATG13 targeted siRNAs or a pool of both ATG13 targeted siRNAs were subjected to SDS-PAGE and immuoblot to test the specificity of the endogenous ATG13 antibody. (C) Whole cell lysates of HEK293 cells transfected with empty vector control, Myc-C9orf72S or Myc-C9orf72L were subjected to immunoblot with anti-Myc antibodies. Immune pellets were probed for Myc-C9orf72 and endogenous ATG13 on immunoblot. In all cases 20 µg (2%) of the immunoprecipitation was loaded as Input.

To test if C9orf72 was also directly interacting with ATG13 *in vitro* binding assays were performed using recombinant GST-tagged C9orf72 incubated with *in vitro* translated S^{35}-labeleld ATG13. GST negative control and GST-C9orf72 were pulled down using glutathione beads. Samples were analysed by SDS-PAGE and radiolabelled ATG13 detected using a phosphoimager. ATG13 was found to interact with C9orf72S and C9orf72L in this assay, suggesting a direct interaction (Fig. 3.10). Thus C9orf72 directly interacts with three members of the autophagy initiation complex: FIP200, ULK1 and ATG13.

Along with the data from sections 3.2.2, 3.2.3 C9orf72 has been identified as a novel binding partner of the ULK1 autophagy initiation complex, strongly supporting the idea that C9orf72 is involved in the autophagy pathway, perhaps specifically at autophagy initiation. This was investigated further in Chapter 4.

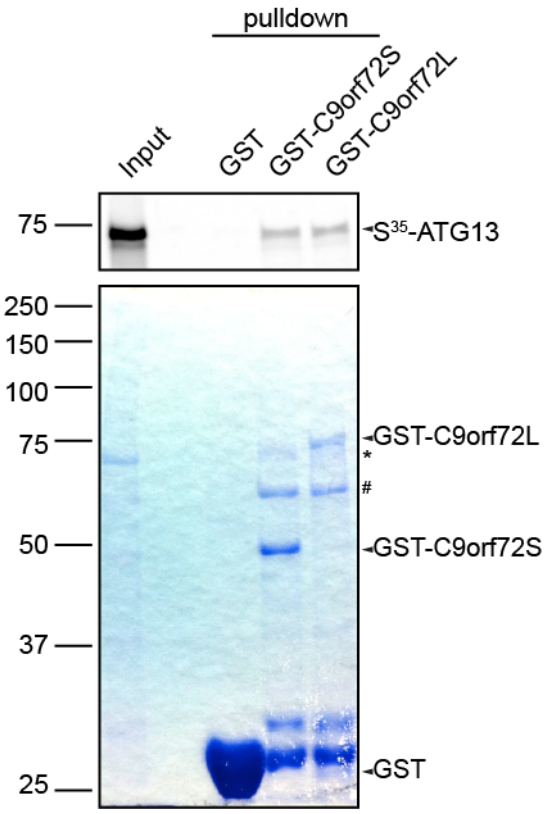

Figure 3.10 C9orf72 directly interacts with ATG13. ^{35}S-radiolabelled recombinant Myc-ATG13 protein was incubated with GST, GST-C9orf72S or GST-C9orf7L immobilized on glutathione-coated beads. ^{35}S-radiolabelled recombinant Myc-ATG13 protein was visualised on phosphoplate (top panel). Coomassie-stained GST, GST-C9orf72S and GST-C9orf72L from the pull down are shown (bottom panel). The identity of the Coomassie protein bands were confirmed by mass spectrometry (* = CH60 *E. coli*, 60kD Chaperonin, # = DnaK Chaperonin *E.coli*).

3.2.5 Unbiased mass spec identification of C9orf72 binding partners

In an indirect approach to identify C9orf72 binding proteins, Dr. Mathew Walsh from the Sheffield Institute for Translational Neuroscience conducted a mass-spec analysis of proteins that were co-immunoprecipitated with C9orf72L. Using a stable FLAG-tagged C9orf72L inducible HEK293 cell line, and a HEK FlpIN control line, FLAG-C9orf72L was immunoprecipitated from cell lysates using an anti-FLAG antibody. Immunpellets were either subjected to SDS-PAGE and immunoblot to show enrichment of C9orf72L (Fig. 3.11A), or separated via SDS-PAGE and the gel stained in colloidal coomassie, in preparation for mass spec analysis (Fig. 3.11B). After coomassie staining of the gel, bands were excised and subjected to ms/ms mass-spec analysis to identify C9orf72L interacting proteins (Fig. 3.11B). The identities of the bands labeled in Figure 3.11B are detailed in table 5.1. From the list of proteins that were identified specifically from the FlpIN FLAG-C9orf72L cell line, FIP200 was identified as a potential binding partner, supporting the results seen in Fig. 3.5 and 3.6.

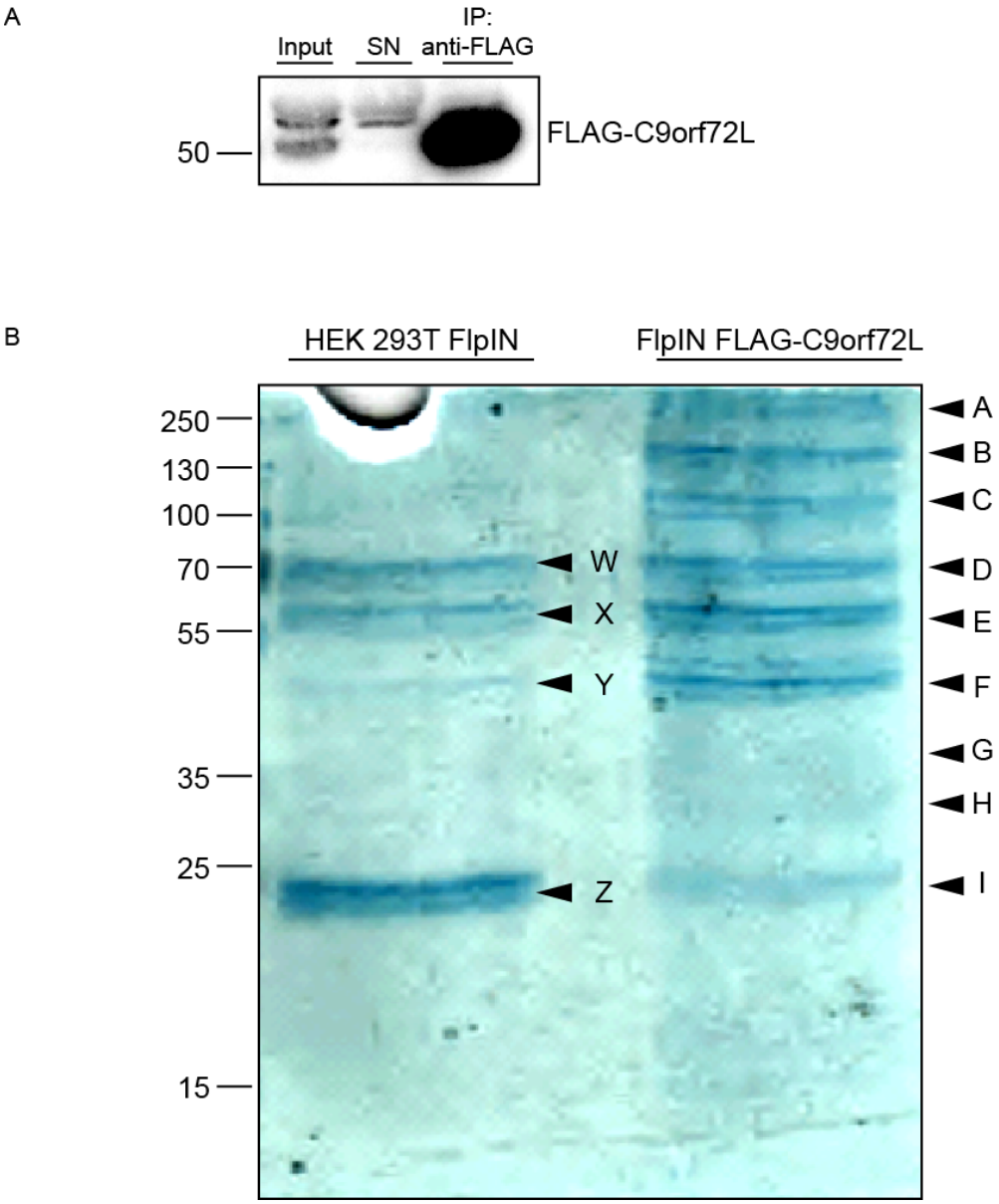

Figure 3.11 Mass spectrometry analysis of C9orf72L binding partners (A) Pull down of C9orf72L from a Flp-In inducible cell line to investigate binding partners by mass spec. FLAG-C9orf72L Flp-In cells were lysed and subjected to immunoprecipitation with anti-FLAG antibodies. Samples were analysed by SDS-PAGE and immunoblots probed with anti-FLAG antibodies. IP sample shows the enrichment of FLAG-C9orf72L from the input. (B) Flp-In Ctrl and FLAG-C9orf72 Flp-In cells were lysed and subjected to immunoprecipitation with anti-FLAG antibodies. Immune pellets were subjected to SDS-PAGE and the gel stained with colloidal coomassie. Bands were excised and analysed by ms/ms mass spec. The excised bands are labelled A-I in the FLAG-C9orf72 Flp-In cells and W-Z in the Ctrl Flp-In cells. Mass spectrometry was conducted by Dr Mathew Walsh and Dr Guillaume Hautbergue.

Table 3.1: Identities of the bands from C9orf72L pulldown

Green indicates Flp-In C9orf72L specific – Orange indicates Ctrl specific – Red indicates protein was isolated from Flp-In C9orf72L and Ctrl lines

Region of gel	Identifier	Score	Protein Name	Common Symbol
A	FLNA_HUMAN	298	Filamin-A	FLNA
A	WDR41_HUMAN	276	WD repeat-containing protein 41	WDR41
A	MAP1B_HUMAN	139	Microtubule-associated protein 1B	MAP1B
A	PRKDC_HUMAN	106	DNA-dependent protein kinase catalytic subunit	PRKDC
A	GCN1L_HUMAN	99	Translational activator GCN1	GCN1L
A	PYR1_HUMAN	61	CAD protein	CAD
A	TITIN_HUMAN	54	Titin	TTN
A	CAND1_HUMAN	49	Cullin-associated NEDD8-dissociated protein 1	CAND1
A	ZC3HE_HUMAN	41	Zinc finger CCCH domain-containing protein 14	ZC3H14
A	DAPLE_HUMAN	41	Protein Daple	CCDC88C
A	S12A1_HUMAN	38	Solute carrier family 12 member 1	SLC12A1
B	**SMCR8_HUMAN**	**2080**	**Smith-Magenis syndrome chromosomal region candidate gene 8 protein**	**SMCR8**
B	CLH1_HUMAN	246	Clathrin heavy chain 1	CLTC
B	SYIC_HUMAN	85	Isoleucine--tRNA ligase, cytoplasmic	IARS
B	WDR41_HUMAN	67	WD repeat-containing protein 41	WDR41
B	PUR2_HUMAN	55	Trifunctional purine biosynthetic protein adenosine-3	GART
B	**RBCC1_HUMAN**	**47**	**RB1-inducible coiled-coil protein 1**	**RB1CC1 / FIP200**
B	AKAP9_HUMAN	44	A-kinase anchor protein 9	AKAP9
B	DYH9_HUMAN	40	Dynein heavy chain 9, axonemal	DNAH9
B	HDGR2_HUMAN	39	Hepatoma-derived growth factor-related protein 2	HDGFRP2
C	HS90B_HUMAN	259	Heat shock protein HSP 90-beta	HSP90AB1
C	HS90A_HUMAN	185	Heat shock protein HSP 90-alpha	HSP90AA1
C	NUCL_HUMAN	143	Nucleolin	NCL
C	**SMCR8_HUMAN**	**127**	**Smith-Magenis syndrome chromosomal region candidate gene 8 protein**	**SMCR8**
C	EF2_HUMAN	69	Elongation factor 2	EEF2
C	TITIN_HUMAN	66	Titin	TTN
C	ENPL_HUMAN	42	Endoplasmin	HSP90B1
C	KDM4B_HUMAN	37	Lysine-specific demethylase 4B	KDM4B
D	HSP71_HUMAN	924	Heat shock 70 kDa protein 1A/1B	HSPA1A
D	HSP7C_HUMAN	643	Heat shock cognate 71 kDa protein	HSPA8
D	CI072_HUMAN	147	Uncharacterized protein C9orf72	C9orf72
D	**SMCR8_HUMAN**	**102**	**Smith-Magenis syndrome chromosomal region candidate gene 8 protein**	**SMCR8**
D	GRP75_HUMAN	82	Stress-70 protein, mitochondrial	HSPA9
D	HNRPK_HUMAN	49	Heterogeneous nuclear ribonucleoprotein K	HNRNPK
D	TCPG_HUMAN	46	T-complex protein 1 subunit gamma	CCT3
D	K2022_HUMAN	45	Uncharacterized protein KIAA2022	KIAA2022
D	DAPK1_HUMAN	44	Death-associated protein kinase 1	DAPK1
D	PRKDC_HUMAN	42	DNA-dependent protein kinase catalytic subunit	PRKDC
D	UNC80_HUMAN	41	Protein unc-80 homolog	UNC80
D	KDM4A_HUMAN	40	Lysine-specific demethylase 4A	KDM4A
E	CI072_HUMAN	1079	Uncharacterized protein C9orf72	C9orf72
E	STK38_HUMAN	578	Serine/threonine-protein kinase 38	STK38
E	COR1C_HUMAN	166	Coronin-1C	CORO1C
E	**SMCR8_HUMAN**	**117**	**Smith-Magenis syndrome chromosomal region candidate gene 8 protein**	**SMCR8**
E	KPYM_HUMAN	90	Pyruvate kinase isozymes M1/M2	PKM
E	ATPA_HUMAN	89	ATP synthase subunit alpha, mitochondrial	ATP5A1
E	ABCC8_HUMAN	75	ATP-binding cassette sub-family C member 8	ABCC8
E	TCPQ_HUMAN	66	T-complex protein 1 subunit theta	CCT8
E	HNRPK_HUMAN	60	Heterogeneous nuclear ribonucleoprotein K	HNRNPK
E	SERA_HUMAN	60	D-3-phosphoglycerate dehydrogenase	PHGDH
E	VIME_HUMAN	56	Vimentin	VIM
E	VIP2_HUMAN	45	Inositol hexakisphosphate and diphosphoinositol-pentakisphosphate kinase 2	PPIP5K2
E	PIM3_HUMAN	42	Serine/threonine-protein kinase pim-3	PIM3
E	EPIPL_HUMAN	42	Epiplakin	EPPK1
E	CENPF_HUMAN	40	Centromere protein F	CENPF
E	CD53_HUMAN	39	Leukocyte surface antigen CD53	CD53
E	UBR4_HUMAN	38	E3 ubiquitin-protein ligase UBR4	UBR4
E	ADCYA_HUMAN	38	Adenylate cyclase type 10	ADCY10
F	WDR41_HUMAN	959	WD repeat-containing protein 41	WDR41
F	MEP50_HUMAN	417	Methylosome protein 50	WDR77
F	EF1A1_HUMAN	398	Elongation factor 1-alpha 1	EEF1A1
F	CI072_HUMAN	253	Uncharacterized protein C9orf72	C9orf72
F	IF4A1_HUMAN	253	Eukaryotic initiation factor 4A-I	EIF4A1
F	ILF2_HUMAN	103	Interleukin enhancer-binding factor 2	ILF2
F	PSD11_HUMAN	55	26S proteasome non-ATPase regulatory subunit 11	PSMD11
F	PA2G4_HUMAN	40	Proliferation-associated protein 2G4	PA2G4
F	RSSA_HUMAN	40	40S ribosomal protein SA	RPSA
F	ZN551_HUMAN	39	Zinc finger protein 551	ZNF551
F	NMD3A_HUMAN	38	Glutamate [NMDA] receptor subunit 3A	GRIN3A
F	UB2E2_HUMAN	37	Ubiquitin-conjugating enzyme E2 E2	UBE2E2
G	RLA0_HUMAN	238	60S acidic ribosomal protein P0	RPLP0
G	GBB1_HUMAN	85	Guanine nucleotide-binding protein G(I)/G(S)/G(T) subunit beta-1	GNB1
G	PRPS1_HUMAN	63	Ribose-phosphate pyrophosphokinase 1	PRPS1
G	ICLN_HUMAN	50	Methylosome subunit pICln	CLNS1A
G	PLCB2_HUMAN	42	1-phosphatidylinositol 4,5-bisphosphate phosphodiesterase beta-2	PLCB2
H	RS3_HUMAN	234	40S ribosomal protein S3	RPS3
H	ADT2_HUMAN	232	ADP/ATP translocase 2	SLC25A5
H	RS4X_HUMAN	194	40S ribosomal protein S4, X isoform	RPS4X
H	1433E_HUMAN	164	14-3-3 protein epsilon	YWHAE
H	RL7_HUMAN	145	60S ribosomal protein L7	RPL7
H	RL7A_HUMAN	87	60S ribosomal protein L7a	RPL7A
H	RL8_HUMAN	75	60S ribosomal protein L8	RPL8
H	TAGAP_HUMAN	42	T-cell activation Rho GTPase-activating protein	TAGAP
H	SN_HUMAN	41	Sialoadhesin	SIGLEC1
H	RYR1_HUMAN	41	Ryanodine receptor 1	RYR1

Table 3.1 continued

I	RL13A_HUMAN	61	60S ribosomal protein L13a	RPL13A
I	MIA3_HUMAN	50	Melanoma inhibitory activity protein 3	MIA3
I	UACA_HUMAN	43	Uveal autoantigen with coiled-coil domains and ankyrin repeats	UACA
I	NOTC3_HUMAN	41	Neurogenic locus notch homolog protein 3	NOTCH3
I	FRAS1_HUMAN	39	Extracellular matrix protein FRAS1	FRAS1
I	RL15_HUMAN	37	60S ribosomal protein L15	RPL15
W	HSP71_HUMAN	128	Heat shock 70 kDa protein 1A/1B	HSPA1A
W	PRKDC_HUMAN	72	DNA-dependent protein kinase catalytic subunit	PRKDC
W	AKAP9_HUMAN	64	A-kinase anchor protein 9	AKAP9
W	HSP7C_HUMAN	62	Heat shock cognate 71 kDa protein	HSPA8
W	PCLO_HUMAN	58	Protein piccolo	PCLO
W	TDRD1_HUMAN	52	Tudor domain-containing protein 1	TDRD1
W	ATM_HUMAN	47	Serine-protein kinase ATM	ATM
W	SRBS2_HUMAN	44	Sorbin and SH3 domain-containing protein 2	SORBS2
W	ATOH8_HUMAN	43	Protein atonal homolog 8	ATOH8
W	DYHC2_HUMAN	42	Cytoplasmic dynein 2 heavy chain 1	DYNC2H1
W	MBP_HUMAN	42	Myelin basic protein	MBP
W	CJ079_HUMAN	41	WD repeat-containing protein 96	WDR96
W	SPG17_HUMAN	39	Sperm-associated antigen 17	SPAG17
W	ABHD8_HUMAN	38	Abhydrolase domain-containing protein 8	ABHD8
X	STK38_HUMAN	332	Serine/threonine-protein kinase 38	STK38
X	AKAP9_HUMAN	40	A-kinase anchor protein 9	AKAP9
X	ATS6_HUMAN	37	A disintegrin and metalloproteinase with thrombospondin motifs 6	ADAMTS6
Y	MEP50_HUMAN	253	Methylosome protein 50	WDR77
Y	ASH1L_HUMAN	46	Histone-lysine N-methyltransferase ASH1L	ASH1L
Y	TLL1_HUMAN	43	Tolloid-like protein 1	TLL1
Y	ATG2B_HUMAN	43	Autophagy-related protein 2 homolog B	ATG2B
Z	KI13B_HUMAN	43	Kinesin-like protein KIF13B	KIF13B
Z	TITIN_HUMAN	42	Titin	TTN
Z	CDK13_HUMAN	41	Cyclin-dependent kinase 13	CDK13
Z	TPX2_HUMAN	40	Targeting protein for Xklp2	TPX2
Z	PPWD1_HUMAN	39	Peptidylprolyl isomerase domain and WD repeat-containing protein 1	PPWD1
Z	LRRK2_HUMAN	38	Leucine-rich repeat serine/threonine-protein kinase 2	LRRK2
Z	ADA28_HUMAN	37	Disintegrin and metalloproteinase domain-containing protein 28	ADAM28

The top hit and interacting partner identified from this mass spec screen was the Smith-Magenis syndrome chromosome region candidate 8 protein (SMCR8). Little is known about the function of the SMCR8 protein. In a link to C9orf72, the autophagy network screen conducted by Behrends et al, identified SMCR8 as a potential FIP200 interacting protein, similar to C9orf72 (Behrends et al., 2010). Interestingly SMCR8 was also identified as a novel DENN domain containing protein in the same study that identified C9orf72 as a potential DENN protein (Zhang et al., 2012). Therefore, this link to FIP200 and the DENN homology suggests that SMCR8 may function in the autophagy pathway. To confirm the interaction, HEK293 cells were co-transfected with Myc-C9orf72S or Myc-C9orf72L and either empty vector or Myc-DDK-tagged SMCR8. After lysis, SMCR8-Myc-DDK was immunoprecipitated from samples with anti-FLAG antibodies and immune pellets were subjected to SDS-PAGE and immunoblot. Both isoforms of C9orf72 were found to co-immunoprecipitate with SMCR8 (Fig. 3.12A and B). The binding of SMCR8 and C9orf72L appeared to be particularly strong, supporting the finding from the mass spec analysis.

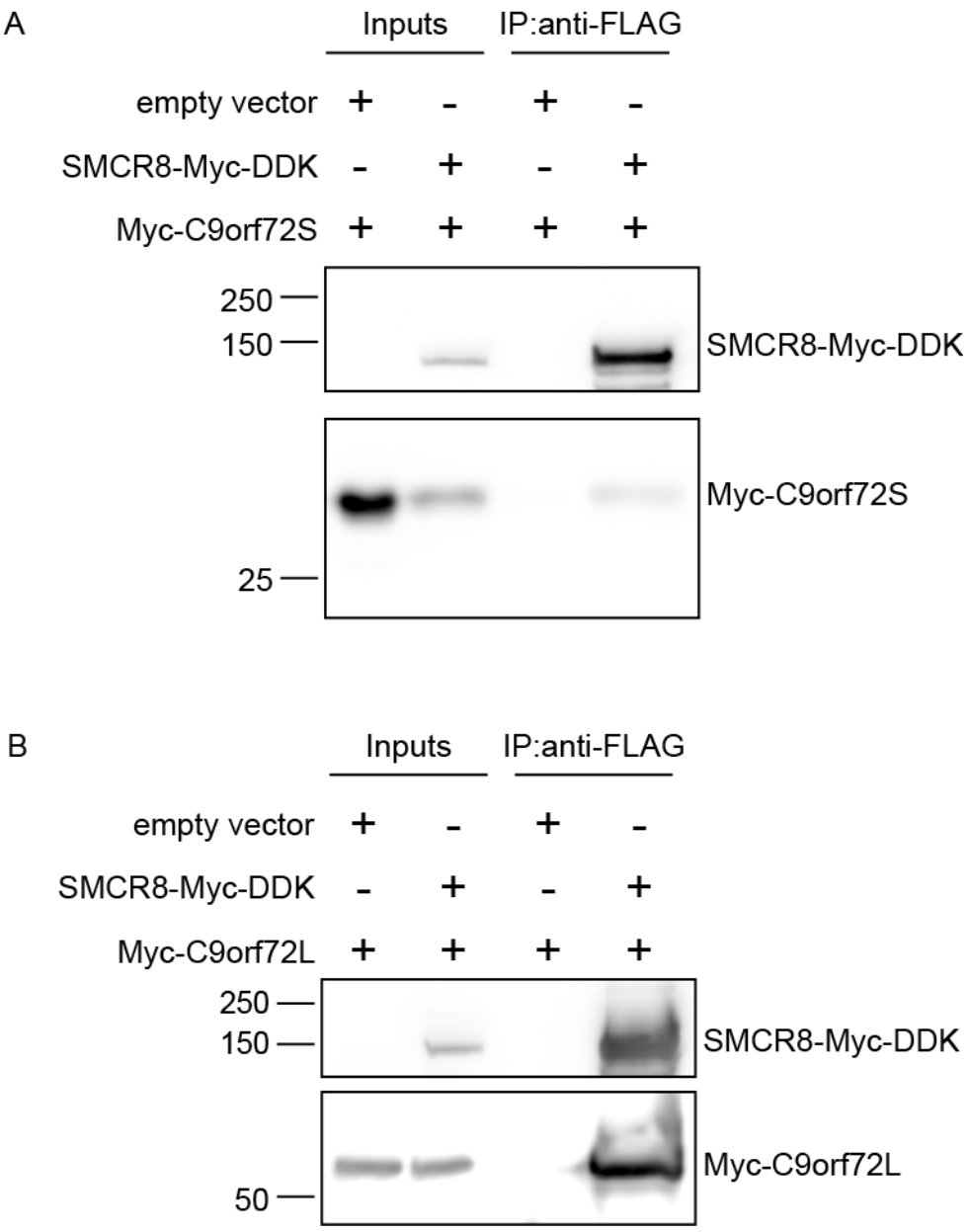

Figure 3.12 C9orf72 interacts with SMCR8. Whole cell lysates of HEK293 cells co-transfected with Myc-C9orf72S (A) or Myc-C9orf72L (B) and either empty vector control or SMCR8-Myc-DDK were subjected to immunoprecipitation with mouse M2 anti-FLAG antibodies. Immune pellets were probed for SMCR8-Myc-DDK and Myc-C9orf72 on immunoblot using rabbit 9106 anti-Myc antibodies. 20 µg (2%) of the immunoprecipitation was loaded as Input.

3.2.6 Unbiased Y2H screen

As a second method of identifying novel C9orf72 binding partners, a Y2H screen was conducted. Essentially a complementation assay, Y2H screens involve a bait protein fused with the DNA binding domain of a transcription factor and prey proteins fused to the activation domain of the transcription factor. Only if the bait and prey interact is a functional transcription formed. The functional transcription factor binds upstream of a reporter gene, therefore allowing for selection. C9orf72S and C9orf72L were cloned into the pGBKT7 vector for high levels of expression in yeast. The screen, performed by Protein Interaction Screening of the Genomics and Proteomics Core Facilities, German Cancer Research Centre, Heidelberg, Germany, used these C9orf72S and C9orf72L constructs as bait proteins to screen a human brain cDNA library comprising of cDNA fragments as well as full length ORFs to identify prey proteins, which could correspond to potential binding partners. In a second round of screening C9orf72L was used as bait in a full length ORF library. Y2H screens can identify false positives, where physical interactions are observed that cannot be replicated in an independent system (Brückner et al., 2009). To account for this error rate, only preys that were pulled out more than once were considered as positive "hits". As there are often a number of false positives with this type of method it has been possible to identify commonly promiscuous preys, i.e. preys that are often found as positive hits in screens and are therefore more likely than not false positives. These highly promiscuous or "sticky" hits were rejected based on this principle (Brückner et al., 2009). From this screen a number of novel potential C9orf72 binding proteins were identified. These are highlighted from the full list in table 3.2. These interactions were then confirmed or rejected by co-immunoprecipitation experiments. The interaction with USP8 will be discussed in more detail in chapter 5. Of the other hits, the Coilin interaction is being investigated by Miss Yolanda Gibson within the lab, Decorin was not investigated further at this time due to its role in the extracellular matrix formation, and mitochondrial ribosomal protein L48 and Claudin 10 were rejected based on the fact that the peptide regions of these preys were located in the 5' UTRs.

Table 3.2 Clones identified from the Y2H screen

Bait	Gene	Times prey isolated	Times fragment starts in the 5' UTR	Times fragments starts in coding region	Times fragment starts in the 3' UTR	Number of bases of the 5' UTR that are part of the prey protein	Prey promiscuity	Gene description
C9orf72_L	COX6C	2	0	2	0	0	4	cytochrome c oxidase subunit VIc
C9orf72_L	SYN3	37	0	37	0	0	1	synapsin III
C9orf72_L	COIL	5	0	5	0	0	1	coilin
C9orf72_L	HRK	1	0	0	0	0	1	Activator of apoptosis harakiri (Neuronal death protein DP5)
C9orf72_L	LOC100506746	1	0	1	0	0	1	LOC100506746 uncharacterized LOC100506746 [Homo sapiens (human)]
C9orf72_L	na-Hs.633061	1	0	0	0	0	1	NCBI UniGene cluster: Hs.633061
C9orf72_L	RALA	1	1	0	0	252	1	v-ral simian leukemia viral oncogene homolog A (ras related)
C9orf72_L	SNTA1	1	0	1	0	0	4	syntrophin, alpha 1 (dystrophin-associated protein A1, 59kDa, acidic component)
C9orf72_S	MRPL48	3	3	0	0	93	3	mitochondrial ribosomal protein L48
C9orf72_S	CLDN10	2	2	0	0	32	4	claudin 10
C9orf72_S	DCN	2	0	2	0	0	4	decorin
C9orf72_S	USP8	2	0	2	0	0	6	ubiquitin specific peptidase 8
C9orf72_S	OAT	2	0	2	0	0	7	ornithine aminotransferase (gyrate atrophy)
C9orf72_S	ADPRM	1	0	1	0	0	1	ADPRM ADP-ribose/CDP-alcohol diphosphatase, manganese-dependent
C9orf72_S	ATP5I	1	1	0	0	9	1	ATP synthase, H+ transporting, mitochondrial F0 complex, subunit E
C9orf72_S	BEX1	1	1	0	0	213	1	brain expressed, X-linked 1
C9orf72_S	CACTIN	1	0	1	0	0	1	CACTIN cactin, spliceosome C complex subunit [Homo sapiens (human)]
C9orf72_S	ERI1	1	0	1	0	0	1	ERI1 exoribonuclease 1 [Homo sapiens (human)]
C9orf72_S	EXOSC10	1	0	1	0	0	1	exosome component 10
C9orf72_S	IGIP	1	1	0	0	639	1	IGIP IgA-inducing protein homolog (Bos taurus) [Homo sapiens (human)]
C9orf72_S	JAKMIP2	1	0	1	0	0	1	janus kinase and microtubule interacting protein 2
C9orf72_S	LOC100130938	1	0	1	0	0	1	hypothetical protein LOC100130938
C9orf72_S	LOC645513	1	0	1	0	0	1	hypothetical LOC645513
C9orf72_S	PITRM1	1	0	1	0	0	1	pitrilysin metallopeptidase 1
C9orf72_S	PPP2R2B	1	0	1	0	0	1	protein phosphatase 2 (formerly 2A), regulatory subunit B, beta isoform
C9orf72_S	RAD54B	1	0	1	0	0	1	RAD54 homolog B (S. cerevisiae)
C9orf72_S	TJP2	1	0	1	0	0	1	tight junction protein 2 (zona occludens 2)
C9orf72_S	UBA3	1	0	1	0	0	1	ubiquitin-like modifier activating enzyme 3
C9orf72_S	USP48	1	0	1	0	0	1	ubiquitin specific peptidase 48
C9orf72_S	ANXA7	1	0	1	0	0	2	annexin A7
C9orf72_S	DARS	1	0	1	0	0	2	aspartyl-tRNA synthetase
C9orf72_S	HERC2P9	1	0	1	0	0	2	HERC2P9 hect domain and RLD 2 pseudogene 9 [Homo sapiens]
C9orf72_S	HSPD1	1	0	1	0	0	2	heat shock 60kDa protein 1 (chaperonin)
C9orf72_S	KCNMB4	1	0	1	0	0	2	potassium large conductance calcium-activated channel, subfamily M, beta member 4
C9orf72_S	WAC	1	0	1	0	0	2	WW domain containing adaptor with coiled-coil
C9orf72_S	ZDHHC6	1	0	1	0	0	2	zinc finger, DHHC-type containing 6
C9orf72_S	ZDHHC9	1	0	1	0	0	2	zinc finger, DHHC-type containing 9
C9orf72_S	ZNF585A	1	0	1	0	0	2	zinc finger protein 585A
C9orf72_S	CXXC5	1	0	1	0	0	3	CXXC finger 5
C9orf72_S	NDUFA10	1	0	1	0	0	3	NADH dehydrogenase (ubiquinone) 1 alpha subcomplex, 10, 42kDa
C9orf72_S	RPE	1	1	0	0	5	3	ribulose-5-phosphate-3-epimerase
C9orf72_S	SENP6	1	0	1	0	0	3	SUMO1/sentrin specific peptidase 6

C9orf72_S	ANXA2	1	0	1	0	0	4	annexin A2
C9orf72_S	ITM2A	1	0	1	0	0	4	integral membrane protein 2A
C9orf72_S	LDHA	1	0	1	0	0	4	lactate dehydrogenase A
C9orf72_S	RAB1A	1	0	1	0	0	4	RAB1A, member RAS oncogene family
C9orf72_S	STMN2	1	1	0	0	104	4	stathmin-like 2
C9orf72_S	TCP1	1	0	1	0	0	4	t-complex 1
C9orf72_S	ALDOA	1	1	0	0	131	5	aldolase A, fructose-bisphosphate
C9orf72_S	COL5A2	1	0	1	0	0	6	collagen, type V, alpha 2
C9orf72_S	FEZ1	1	0	1	0	0	6	fasciculation and elongation protein zeta 1 (zygin I)
C9orf72_S	RAD1	1	0	1	0	0	6	RAD1 homolog (S. pombe)
C9orf72_S	DSTN	1	0	1	0	0	7	destrin (actin depolymerizing factor)
C9orf72_S	NR1D2	1	0	1	0	0	7	nuclear receptor subfamily 1, group D, member 2

Green indicates preys that were isolated more than once

Yellow indicates preys that were only isolated once

3.2.7 C9orf72 interacts with Cox6C

Cytochrome c oxidase subunit VIc (Cox6C) was identified as a C9orf72L interacting protein from the Y2H screen. Cytochrome c oxidase is the final complex of the electron transport chain, complex IV, and is comprised of 13 different subunits (Yoshikawa et al., 1998). Of the 13 subunits, subunits 1-3 are encoded on mitochondrial DNA, while the other 10 are nuclear encoded (Lazarou et al., 2009) Cox6C has been shown to assemble into an intermediate complex that may be necessary for the formation of mature, functional and complete holo-Complex IV (Lazarou et al., 2009). Cox6C is a 75 amino acid mitochondrial transmembrane protein, with a peptide segment within the mitochondrial matrix and a 4-turn α helix on the cytosolic side (Tsukihara et al., 1996). The exact function of Cox6C is not fully understood but it is thought to provide structural integrity to complex IV as a whole (Musatov and Robinson, 2002). Cox6C was isolated as a C9orf72L prey twice in this screen, with the same Cox6C fragment identified in each case. The known domains of Cox6C and the peptide sequence interacting with C9orf72L are detailed in Figure 3.13.

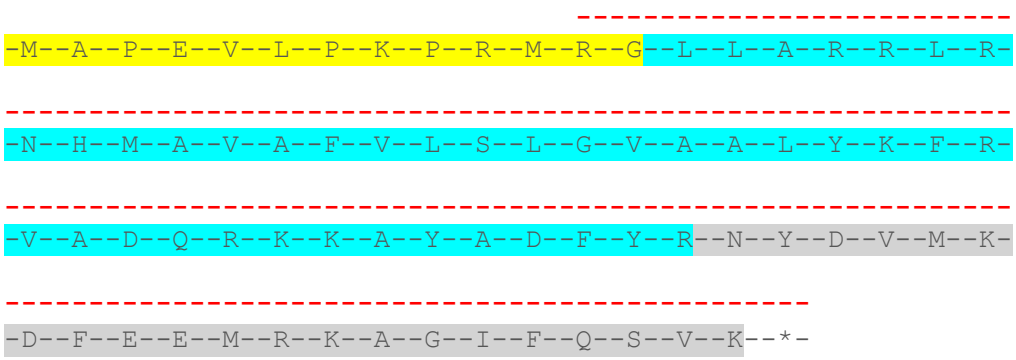

Key:

Matrix domain
Helical Transmembrane domain
Mitochondrial intermembrane domain
------ = Cox6C prey region interacting with C9orf72L

Figure 3.13 The Cox6C clones identified from the Y2H screen map across the transmembrane domain of Cox6C. Two Cox6C clones identified as prey of the C9orf72L bait protein map across the transmembrane domain of Cox6C. The Matrix domain is indicated in yellow, the transmembrane domain in cyan and the mitochondrial intermembrane domain in grey. The dotted red dashes indicate the peptide sequence of the clone identified in the Y2H screen.

The interaction of C9orf72 with Cox6C was investigated by co-immunoprecipitation. HEK293 cells were co-transfected with Myc-C9orf72S or Myc-C9orf72L and either empty vector or Myc-DDK-tagged Cox6C. Cox6C-Myc-DDK was immunoprecipitated using anti-FLAG antibodies and immune pellets analyse by SDS-PAGE and immunoblot. Cox6C-Myc-DDK was enriched in the immunoprecipitated samples. In these assays, C9orf72L was found to efficiently co-immunoprecipitate with Cox6C (Fig. 3.14B). However, C9orf72S did not (Fig. 3.14A). The fact that C9orf72L interacted with Cox6C, while C9orf72S did not, suggested that the interaction required a region within the C terminus of C9orf72L, i.e. between amino acids 222-481; the region lacking in C9orf72S (DeJesus-Hernandez et al., 2011; Renton et al., 2011). Thus, these data identify Cox6C as a novel interacting partner of C9orf72L. This interaction of C9orf72 and Cox6C, and the possible role of C9orf72 in mitochondrial biology, is being further characterised by Miss Emma Smith within the lab.

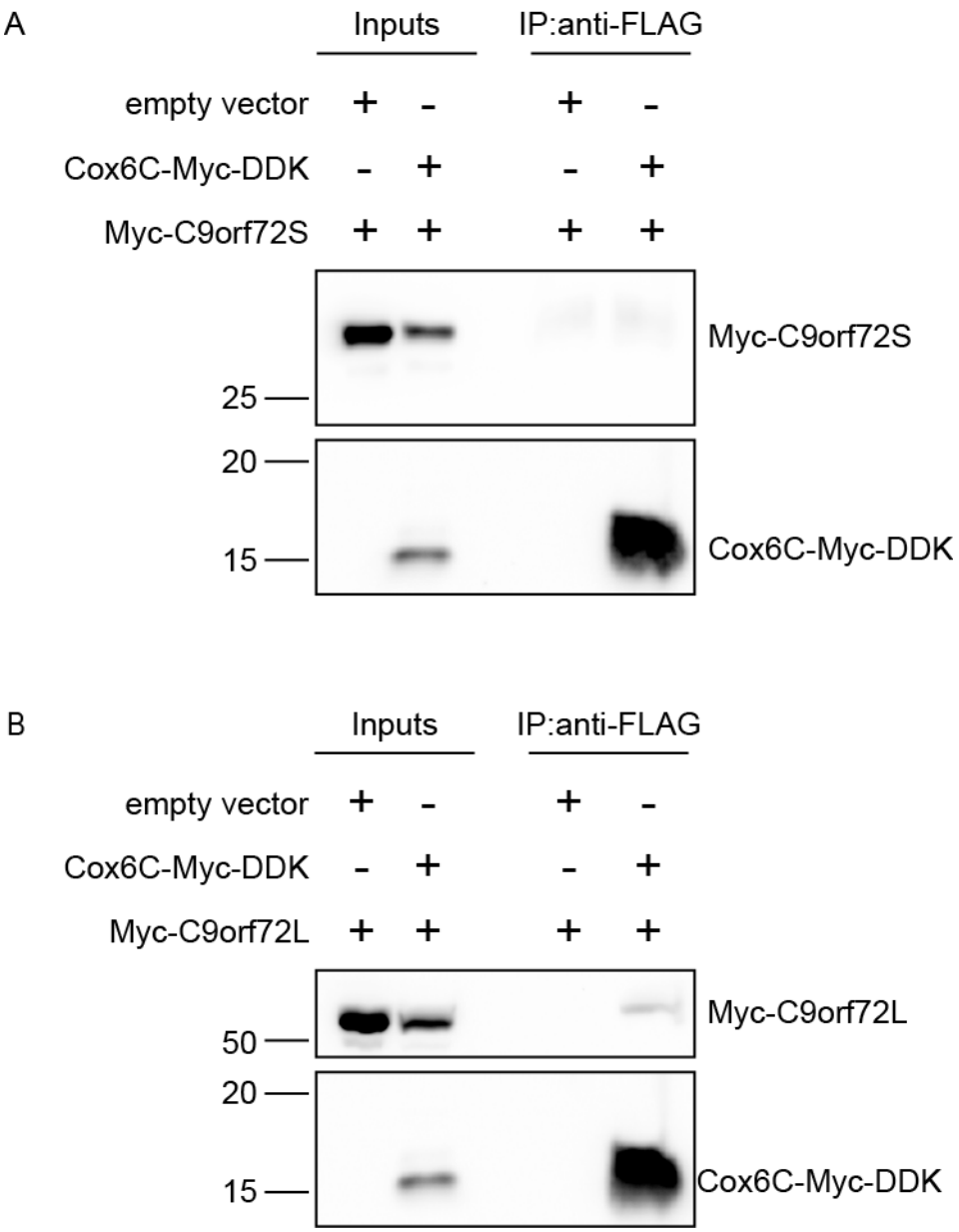

Figure 3.14 C9orf72L interacts with Cox6C. Whole cell lysates of HEK293 cells co-transfected with Myc-C9orf72S (A) or Myc-C9orf72L (B) and either empty vector control or Cox6C-Myc-DDK were subjected to immunoprecipitation with M2 mouse anti-FLAG antibodies. Immune pellets were probed for Cox6C-Myc-DDK with rabbit 9106 anti-Myc antibodies and Myc-C9orf72 with rabbit sc-138763 anti-C9orf72 antibodies on immunoblot. 20 µg (2%) of the immunoprecipitation was loaded as Input.

3.2.8 C9orf72 does not interact with OAT

A second mitochondrial protein identified from the Y2H screen was Ornithine aminotransferase (OAT). OAT is a nuclear encoded 45 kDa mitochondrial matrix enzyme responsible for arginine catabolism as well as proline biosynthesis (Aral and Kamoun, 1997; Shah et al., 1997). Mutations to OAT, leading to OAT deficiency, are a known cause of familial inherited gyrate atrophy of the choroid and retina (Brody et al., 1992). OAT was identified twice from this screen as a C9orf72S prey, with the same peptide region identified in each case. The peptide region of OAT identified from this screen is detailed in Figure 3.15.

The interaction of OAT with C9orf72 was investigated by co-immunoprecipitation. HEK293 cells were co-transfected with Myc-C9orf72S or Myc-C9orf72L and either empty vector or OAT-Myc-DDK. OAT-Myc-DDK was immunoprecipitated with anti-FLAG antibodies and immune pellets analysed by SDS-PAGE and immunoblot. OAT-Myc-DDK was enriched in the immunoprecipitated samples. In these assays, neither C9orf72S nor C9orf72L was found to co-immunoprecipitate with OAT (Fig. 3.16A and B), suggesting this was a false positive hit from the Y2H screen.

-M--F--S--K--L--A--H--L--Q--R--F--A--V--L--S--R--G--V--H--S-

-S--V--A--S--A--T--S--V--A--T--K--K--T--V--Q--G--P--P--T--S-

-D--D--I--F--E--R--E--Y--K--Y--G--A--H--N--Y--H--P--L--P--V-

-A--L--E--R--G--K--G--I--Y--L--W--D--V--E--G--R--K--Y--F--D-

-F--L--S--S--Y--S--A--V--N--Q--G--H--C--H--P--K--I--V--N--A-

-L--K--S--Q--V--D--K--L--T--L--T--S--R--A--F--Y--N--N--V--L-

-G--E--Y--E--E--Y--I--T--K--L--F--N--Y--H--K--V--L--P--M--N-

-T--G--V--E--A--G--E--T--A--C--K--L--A--R--K--W--G--Y--T--V-

-K--G--I--Q--K--Y--K--A--K--I--V--F--A--A--G--N--F--W--G--R-

-T--L--S--A--I--S--S--S--T--D--P--T--S--Y--D--G--F--G--P--F-

-M--P--G--F--D--I--I--P--Y--N--D--L--P--A--L--E--R--A--L--Q-

-D--P--N--V--A--A--F--M--V--E--P--I--Q--G--E--A--G--V--V--V-

-P--D--P--G--Y--L--M--G--V--R--E--L--C--T--R--H--Q--V--L--F-

-I--A--D--E--I--Q--T--G--L--A--R--T--G--R--W--L--A--V--D--Y-

-E--N--V--R--P--D--I--V--L--L--G--K--A--L--S--G--G--L--Y--P-

-V--S--A--V--L--C--D--D--D--I--M--L--T--I--K--P--G--E--H--G-

-S--T--Y--G--G--N--P--L--G--C--R--V--A--I--A--A--L--E--V--L-

-E--E--E--N--L--A--E--N--A--D--K--L--G--I--I--L--R--N--E--L-

-M--K--L--P--S--D--V--V--T--A--V--R--G--K--G--L--L--N--A--I-

-V--I--K--E--T--K--D--W--D--A--W--K--V--C--L--R--L--R--D--N-

-G--L--L--A--K--P--T--H--G--D--I--I--R--F--A--P--P--L--V--I-

-K--E--D--E--L--R--E--S--I--E--I--I--N--K--T--I--L--S--F--*-

Key

---- = OAT prey region interacting with C9orf72S

Figure 3.15 Mapping of the OAT clones identified from the Y2H screen to the OAT amino acid sequence. Two OAT clones were identified as prey of C9orf72S bait protein in the Y2H screen. The dotted red line indicates the peptide sequence of the clones that were identified.

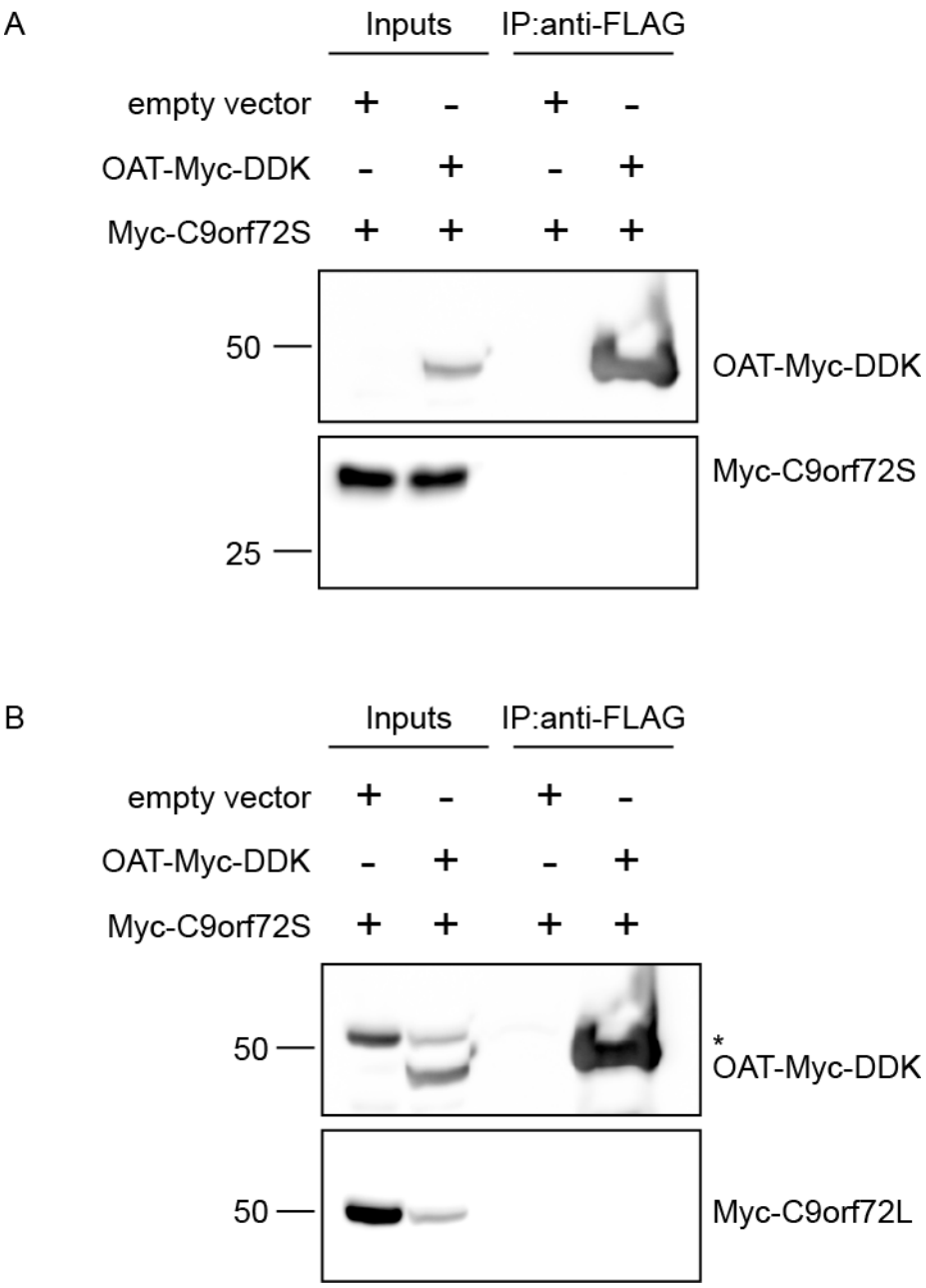

Figure 3.16 C9orf72 does not interact with OAT. Whole cell lysates of HEK293 cells co-transfected with Myc-C9orf72S (A) or Myc-C9orf72L (B) and either empty vector control or OAT-Myc-DDK were subjected to immunoprecipitation with M2 mouse anti-FLAG antibodies. Immune pellets were probed for OAT-Myc-DDK using rabbit anti-Myc 9106 antibodies and Myc-C9orf72 using rabbit sc-138763 anti-C9orf72 antibodies on immunoblot. * indicates Myc-C9orf72L bands in the input. To detect Myc-C9orf72L alone first, blots were probed with rabbit sc-138763 anti-C9orf72 antibodies. The same blot was then re-probed with 9106 rabbit anti-Myc antibodies to show both Myc-C9orf72 and OAT-Myc-DDK. 20 µg (2%) of the immunoprecipitation was loaded as Input.

3.2.9 C9orf72 interacts with Synapsin III

Synapsin III was identified as a potential C9orf72L binding partner from the Y2H screen. The family of synapsin proteins are important phosphoproteins associated with synaptic vesicles (Rosahl et al., 1993). The actual function of the synapsins is currently unknown but knockout mouse models have revealed they are required for synaptic vesicle regulation and formation (Rosahl et al., 1995; Ryan et al., 1996). The function of synapsin III is relatively unknown, but it shares homology with synapsins I and II (Hosaka and Südhof, 1998a). As with synapsin I and II, synapsin III has been shown to bind ATP, suggesting a possible enzymatic role (Hosaka and Südhof, 1998a, b). However, unlike synapsin I, where the presence of Ca^{2+} ions increases ATP binding, Ca^{2+} inhibits ATP binding by synapsin III (Hosaka and Südhof, 1998a). Synapsin III was identified as a C9orf72L prey 37 times from this screen, with the same peptide region identified each time. The peptide region interacting with C9orf72L in this screen is detailed in Figure 3.17, along with the domain structure shared by the synapsin family of proteins (Hosaka and Südhof, 1998a) (Fig. 3.17).

The interaction of Synapsin III (SynIII) with C9orf72 was investigated by co-immunoprecipitation. HEK293 cells were co-transfected with Myc-C9orf72S or Myc-C9orf72L and either empty vector or SynIII-Myc-DDK. SynIII-Myc-DDK was immunoprecipitated with anti-FLAG antibodies and immune pellets analysed by SDS-PAGE and immunoblot. SynIII-Myc-DDK was enriched in the immunoprecipitated samples. In these assays both isoforms of C9orf72 were found to co-immunoprecipitiate with Synapsin III (Fig. 3.18A and B). However, the interaction with C9orf72S appeared much weaker than that of C9orf72L. The interaction of C9orf72 with the synapsin family, and the role of C9orf72 in synaptic vesicle formation, is being further investigated by Miss Rebecca Cohen within the lab.

-M--N--F--L--R--R--R--L--S--D--S--S--F--M--A--N--L--P--N--G-

-Y--M--T--D--L--Q--R--P--D--S--S--T--S--S--P--A--S--P--A--M-

-E--R--R--H--P--Q--P--L--A--A--S--F--S--S--P--G--S--S--L--F-

-S--S--L--S--S--A--M--K--Q--A--P--Q--A--T--S--G--L--M--E--P-

-P--G--P--S--T--P--I--V--Q--R--P--R--I--L--L--V--I--D--D--A-

-H--T--D--W--S--K--Y--F--H--G--K--K--V--N--G--E--I--E--I--R-

-V--E--Q--A--E--F--S--E--L--N--L--A--A--Y--V--T--G--G--C--M-

-V--D--M--Q--V--V--R--N--G--T--K--V--V--S--R--S--F--K--P--D-

-F--I--L--V--R--Q--H--A--Y--S--M--A--L--G--E--D--Y--R--S--L-

-V--I--G--L--Q--Y--G--G--L--P--A--V--N--S--L--Y--S--V--Y--N-

-F--C--S--K--P--W--V--F--S--Q--L--I--K--I--F--H--S--L--G--P-

-E--K--F--P--L--V--E--Q--T--F--F--P--N--H--K--P--M--V--T--A-

-P--H--F--P--V--V--V--K--L--G--H--A--H--A--G--M--G--K--I--K-

-V--E--N--Q--L--D--F--Q--D--I--T--S--V--V--A--M--A--K--T--Y-

-A--T--T--E--A--F--I--D--S--K--Y--D--I--R--I--Q--K--I--G--S-

-N--Y--K--A--Y--M--R--T--S--I--S--G--N--W--K--A--N--T--G--S-

-A--M--L--E--Q--V--A--M--T--E--R--Y--R--L--W--V--D--S--C--S-

-E--M--F--G--G--L--D--I--C--A--V--K--A--V--H--S--K--D--G--R-

-D--Y--I--I--E--V--M--D--S--S--M--P--L--I--G--E--H--V--E--E-

-D--R--Q--L--M--A--D--L--V--V--S--K--M--S--Q--L--P--M--P--G-

-G--T--A--P--S--P--L--R--P--W--A--P--Q--I--K--S--A--K--S--P-

-G--Q--A--Q--L--G--P--Q--L--G--Q--P--Q--P--R--P--P--P--Q--G-

-G--P--R--Q--A--Q--S--P--Q--P--Q--R--S--G--S--P--S--Q--Q--R-

-L--S--P--Q--G--Q--Q--P--L--S--P--Q--S--G--S--P--Q--Q--Q--R-

-S--P--G--S--P--Q--L--S--R--A--S--S--G--S--S--P--N--Q--A--S-

-K--P--G--A--T--L--A--S--Q--P--R--P--P--V--Q--G--R--S--T--S-

-Q--Q--G--E--E--S--K--K--P--A--P--P--H--P--H--L--N--K--S--Q-

-S--L--T--N--S--L--S--T--S--D--T--S--Q--R--G--T--P--S--E--D-

-E--A--K--A--E--T--I--R--N--L--R--K--S--F--A--S--L--F--S--D-

-*-

Key

A domain B domain C domain ----- = SynIII prey region interacting with C9orf72

Figure 3.17 The Synapsin III clones identified from the Y2H screen map across the conserved C domain of Synapsin III. 37 Synapsin III clones were identified as prey of C9orf72L bait protein in the Y2H screen. The conserved A (cyan), B (green) and C (yellow) domains of the synapsin family members are indicated. The red dotted line indicates the peptide sequence of the clones that were identified.

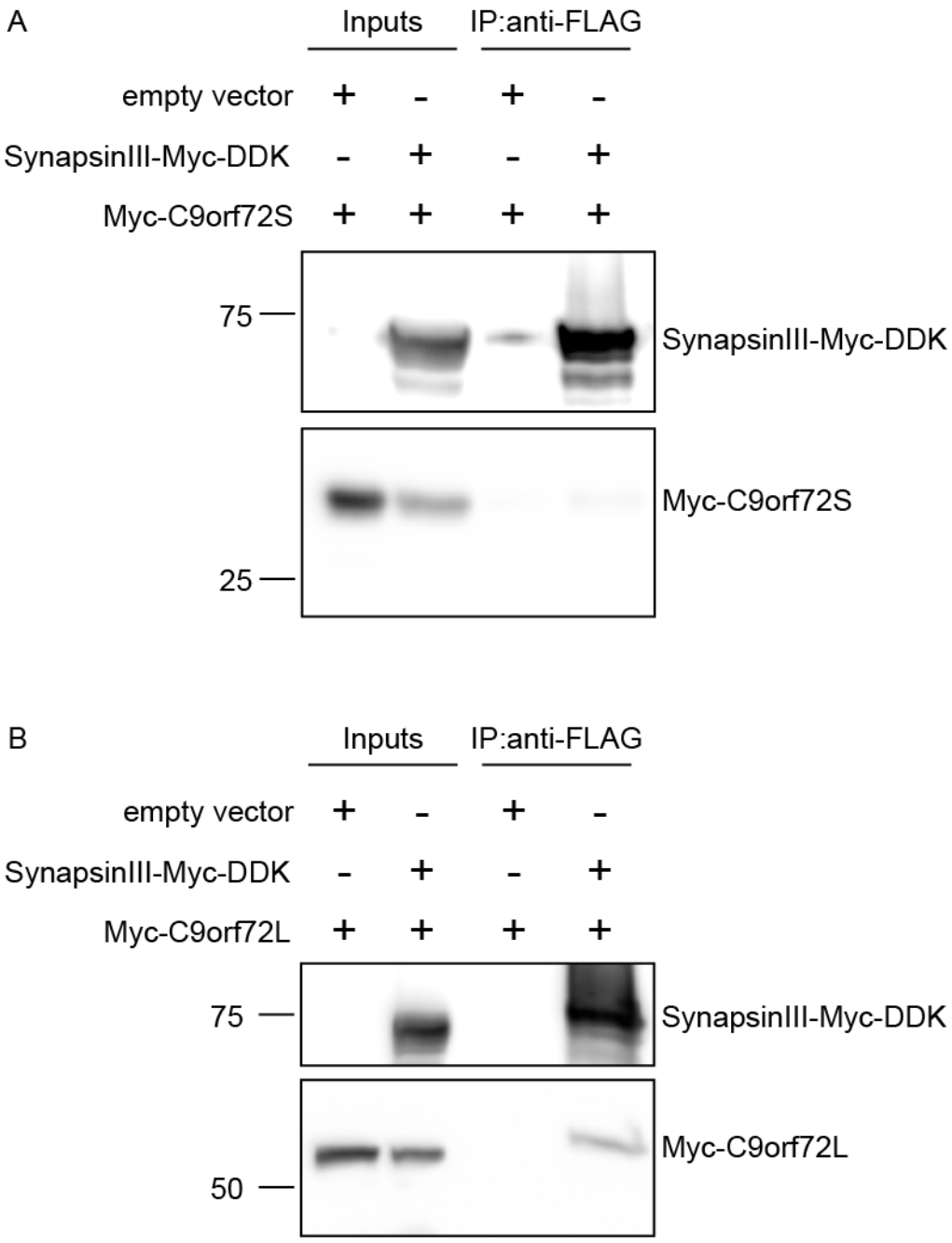

Figure 3.18 C9orf72 interacts with Synapsin III. Whole cell lysates of HEK293 cells co-transfected with Myc-C9orf72S (A) or Myc-C9orf72L (B) and either empty vector control or Myc-DDK-SynIII were subjected to immunoprecipitation with M2 mouse anti-FLAG antibodies. Immune pellets were probed for SynIII-Myc-DDK and Myc-C9orf72 on immunoblot using rabbit anti-Myc 9106 antibodies. 20 µg (2%) of the immunoprecipitation was loaded as Input.

3.3 Discussion

The purpose of this chapter was to identify novel C9orf72 interacting partners with the aim of shedding light on the possible biological function of C9orf72. In a hypothesis driven approach, the interaction of C9orf72 with the autophagy initiation complex was investigated. Furthermore, in an unbiased approach, a mass spec screen was conducted on C9orf72L immunoprecipitates to identify C9orf72L interacting proteins and a Y2H screen was also performed using C9orf72S and C9orf72L as bait proteins.

A previous screen of the autophagy regulation network identified C9orf72 as a possible interacting partner of FIP200 (Behrends et al., 2010). The pathology associated with C9ALS/FTD, also suggested a possible autophagy deficit in these patients (Al-Sarraj et al., 2011; Cooper-Knock et al., 2012). In this Chapter C9orf72 was found to directly interact with FIP200, ULK1 and ATG13 (Figs 3.5 – 3.10), all of which are important members of the autophagy initiation complex (Ganley et al., 2009; Hosokawa et al., 2009a; Jung et al., 2009), thus suggesting that C9orf72 may play a role at the initiation stage of autophagy. Endogenous FIP200, ULK1 and ATG13 were all found to co-immunoprecipitate with Myc-C9orf72S and Myc-C9orf72L (Figs 3.5, 3.7 and 3.9). In the case of FIP200 and ULK1, a higher molecular weight species was found to be the most prominent band co-immunoprecipitating with C9orf72L (Fig. 3.5C and 3.7C). ULK1 phosphorylates a number of targets after autophagy induction, including itself, FIP200 and ATG13 (Ganley et al., 2009; Hosokawa et al., 2009a; Jung et al., 2009). Thus, the higher molecular weight bands of FIP200 and ULK1 that were found to interact with C9orf72L could be phosphorylated forms of these proteins, raising the possibility that C9orf72L interacts with FIP200 and ULK1 predominantly after autophagy induction. Phosphatase treatment of the immunoprecipitates from these endogenous experiments would confirm whether these bands were indeed phosphorylated forms of either protein. The lower molecular weight species of endogenous ATG13 that was found to co-immunoprecipitate with C9orf72 (Fig. 3.9C) could be related to the 7 alternatively spliced isoforms of ATG13 (Alers et al., 2011). Full length ATG13 (isoform A) and isoform B, which is alternatively spliced to skip exon 8, are the predominant splice variants found in cells based on their relative mRNA levels (Alers et al., 2011). Thus, the lower molecular weight variant found to co-immunoprecipitate with C9orf72 in Fig 3.9C could be related to ATG13 isoform

B. Interestingly, isoform B is one of only two isoforms that is capable of interacting with FIP200 (Alers et al., 2011). The lack of reliable commercial C9orf72 antibodies prevented the investigation of endogenous C9orf72 with its binding partners. While this is an obvious limitation of these studies, the fact that the interaction was confirmed firstly via overexpression immunoprecipitation assays, then via co-immunoprecipitation of endogenous binding partners and finally via *in-vitro* binding assays, gave confidence to the results. Xiao et al recently developed isoform specific antibodies towards C9orf72S and C9orf72L (Xiao et al., 2015). The use of such antibodies in future may allow the detection and investigation of endogenous C9orf72 and its binding partners.

All interaction studies detailed in this Chapter were conducted on HEK293 cells. Due to its role in ALS/FTD, studies of the interaction partners in a more neuronal cell line would be of benefit, making the findings potentially more relevant for the understanding of the disease. To further investigate the binding partners of C9orf72, as well as the subcellular localisation of C9orf72 within intact cells, the proximity ligation assay could be employed (Soderberg et al., 2006), as could fluorescent resonance energy transfer (FRET) microscopy (Broussard et al., 2013). Again, conducting such studies on more neuronal cell types would beneficial to the understanding of this protein.

Bioinformatics analysis has revealed C9orf72 to be structurally related to the DENN family of proteins and may function in Rab activity (Levine et al., 2013; Zhang et al., 2012). This is supported by another study showing that C9orf72 co-localises with a number of Rab proteins (Farg et al., 2014). SMCR8 was identified as the top hit from the mass spec screen of C9orf7L interacting proteins, which was then confirmed by co-immunoprecipitation (Fig. 3.11 and 3.12). SMCR8 was also identified as a novel DENN domain protein in the same screen as C9orf72 (Zhang et al., 2012). The DENN domain proteins are known GEFs for the Rab GTPases (Levine et al., 2013; Yoshimura et al., 2010; Zhang et al., 2012). The involvement of Rab proteins in the autophagy pathway has been discussed in section 1.5.2.5. Interestingly, SMCR8 was also identified in the same autophagy screen as C9orf72 as a possible FIP200 interacting protein (Behrends et al., 2010). Thus, as potential DENN Rab GEFs, C9orf72 and SMCR8 could be important for regulation of the autophagy initiation complex and the induction of autophagy.

The identification of Cox6C and OAT as potential C9orf72 interacting proteins, suggested the C9orf72 protein might in part have some link to the mitochondrial network. While C9orf72 did not show any interaction with OAT (Fig. 3.16A and B), Cox6C was shown to co-immunoprecipitate with C9orf72L (Fig. 3.14B). As a mitochondrial transmembrane protein, only the short 4-turn helix structure of Cox6C is exposed to the cytoplasm, with another peptide segment within the mitochondrial matrix (Tsukihara et al., 1996). The peptide sequence of Cox6C found to interact with C9orf72L in the Y2H screen mapped across this transmembrane domain and the mitochondrial matrix domain (Fig. 3.13). The immunofluorescence data presented in Figure 3.3 suggested C9orf72 was relatively diffuse throughout the cell. However, this does not rule out the possibility that C9orf72 could be associated with the mitochondria. Assuming C9orf72 is only present within the cytoplasm would mean C9orf72 could only interact with Cox6C en route to the mitochondria, or with the short 4-turn helix structure exposed to the cytoplasm, as suggested by the Y2H data (Fig. 3.13). On the other hand, if it is assumed C9orf72 could be present within mitochondria then C9orf72 could interact with the mitochondrial matrix portion of Cox6C, which was also suggested by the clones identified in the Y2H screen (Fig. 3.13). The interaction of C9orf72 with Cox6C suggests C9orf72 may play a role in mitochondrial biology, whether it be delivery of nuclear encoded mitochondrial proteins, as in the case of Cox6C, or even regulation of the mitochondrial network, including mitochondrial morphology and clearance.

The interaction of C9orf72 with synapsin III (Fig. 3.18) suggests C9orf72 plays an important role in neuronal biology, as the synapsin family are important for synaptic vesicle regulation in neurons (Rosahl et al., 1993; Rosahl et al., 1995; Ryan et al., 1996). Synapsins I, II and III share a common domain structure, comprising of A, B, C, D and E domains (Hosaka and Südhof, 1998a, b). The C domain of synapsins is thought to be involved in ATP binding, and possibly phosphotransfer to other protein targets (Esser et al., 1998; Hosaka and Südhof, 1998b). The protein region of synapsin III interacting with C9orf72 in the Y2H screen was mapped to the B and C domains (Fig. 3.17) As a simplistic model, synapsin III could therefore be involved in phosphotransfer to C9orf72, or C9orf72 could be involved in directing synapsin III to its correct protein target and aiding in correct phosphotransfer. Ca^{2+} levels are known to inhibit the binding of ATP by synapsin III (Hosaka and Südhof, 1998a). As Ca^{2+} levels are

important in synaptic transmission this could impact on the binding of C9orf72 with synapsin III during neurotransmission.

The involvement of autophagy in C9ALS/FTD is supported by the pathology that is specifically associated with these patients, namely the accumulation of p62 (Al-Sarraj et al., 2011; Cooper-Knock et al., 2012; Mahoney et al., 2012). As discussed previously in section 1.5.2.3, p62 is involved in substrate delivery to the autophagosome and so accumulations of p62 suggest a dysfunctional autophagy pathway (Mathew et al., 2009; Pankiv et al., 2007). Having shown C9orf72 interacts with a number of autophagy related proteins, loss of C9orf72 protein in patients due to the expanded repeat could lead to a dysfunctional autophagy pathway and, in turn, the specific pathology associated with this disease. As the interacting proteins identified in this Chapter were members of the autophagy initiation complex, the role of C9orf72 in autophagy initiation was investigated more specifically. The next Chapter looks at the effect loss of C9orf72 could have on the autophagy pathway, investigating how C9orf72 knock down could affect the different steps, and also what effect over expression of C9orf72 can have on autophagy induction.

4 C9orf72 regulates the initiation of autophagy

4.1 Introduction

The ULK1 initiation complex controls the induction of autophagy as shown in Figure 1.4 and 1.5 (Ganley et al., 2009; Hosokawa et al., 2009a; Jung et al., 2009). Upon inhibition of mTOR, the ULK1 kinase becomes active, phosphorylating the other members of the complex, leading to further downstream signalling and the activation of autophagy (Hosokawa et al., 2009a; Jung et al., 2009; Russell et al., 2013). In chapter 3 C9orf72 was shown to directly interact with the autophagy initiation complex (Figs. 3.5 – 3.10) suggesting C9orf72 may play a role in this pathway. Since C9orf72 was interacting with the initiation complex and haploinsufficiency of *C9orf72* may be involved in C9ALS/FTD, the aim of this chapter was to investigate what effect modulating C9orf72 protein levels would have on autophagy induction, with the final aim of placing C9orf72 in the pathway and describing its functional role.

4.2 Results

4.2.1 Loss of C9orf72 disrupts the initiation of autophagy

To investigate the role of C9orf72 in autophagy, a number of techniques were employed, as described by Klionsky et al. 2012 (Klionsky et al., 2012). As a marker of the autophagosomes, LC3-II conversion assays were used to evaluate the level of autophagy induction following targeted knock down or overexpression of C9orf72. Firstly, LC3-II positive autophagosomes and lysosomes were measured via immunofluorescence assays to monitor autophagic flux. Secondly, LC3-II levels were monitored via immunoblot to determine cellular levels of autophagy. Upon autophagy induction the cytosolic form of LC3, LC3-I, is lipidated to form LC3-II, which is localised to the autphagosomes and is required for their formation (Kabeya, 2000; Kabeya et al., 2004), see section 1.5.2.2 and Fig. 1.4. LC3-II remains membrane bound until autophagosome, lysosome fusion, and is then degraded along with the other autophagic cargos (Tanida et al., 2005). Thus quantification of LC3-II levels is indicative of the level of autophagy. In a final approach, other fluorescently labelled autophagy related proteins were monitored by immunofluorescence to investigate specific stages of the pathway, namely the translocation stage of autophagy, which is associated with autophagic induction. Details of these assays will be discussed below.

To address if C9orf72 plays a role in the initiation of autophagy, the levels of C9orf72 were reduced in cells with targeted siRNA and the levels of autophagy investigated after induction. Firstly, the effect of C9orf72 knock down on the level of autophagy was measured by quantifying the number of autophagosomes and autolysosomes by counting mCherry-EGFP-LC3 positive puncta by fluorescence microscopy. The mCherry-EGFP-LC3 construct allows for the distinction between autophagosomes and autolysosomes as the acid environment of the autolysosome quenches the EGFP signal, while the mCherry signal is unaffected. Therefore, autophagosomes fluoresce red and green, while the autolysosomes fluoresce only red (Pankiv et al., 2007). Therefore, quantifying the number of red and green puncta compared to red only puncta allows the quantification of autophagic flux (Klionsky et al., 2012).

Hela cells treated with Ctrl or C9orf72 siRNA were transfected with mCherry-GFP-LC3. Autophagy was induced by treatment with Torin1. In Ctrl siRNA treated cells, Torin1 lead to a significant increase in the level of autophagosomes as well as autolysosomes (Fig. 4.1A). In comparison, Torin1 no longer increased the numbers of autophagosomes in C9orf72 siRNA treated cells, and the number of autolysosomes was significantly reduced (Fig. 4.1A). Thus loss of C9orf72 appeared to affect autophagy induction. To directly investigate the level of induction, HeLa cells transfected with Ctrl or C9orf72 siRNA were treated with Torin1 in the presence of bafilomycin A_1, a specific inhibitor of the vacuolar ATPase (V-ATPase), which inhibits acidification of the lysosome, preventing fusion of the autophagosome with the lysosome (Klionsky et al., 2008; Yamamoto et al., 1998). This therefore allows for the quantification of the number of autophagosomes formed specifically after induction (Tanida et al., 2005). In Ctrl siRNA transfected cells, these conditions lead to a significant increase in the number of autophagosomes (Fig. 4.1B). However, in C9orf72 siRNA treated cells no increase in the number of autophagosomes was detected indicating that loss of C9orf72 prevents the correct induction of autophagy (Fig 4.1B). The level of C9orf72 knockdown was quantified by RT-qPCR (Fig. 4.1C).

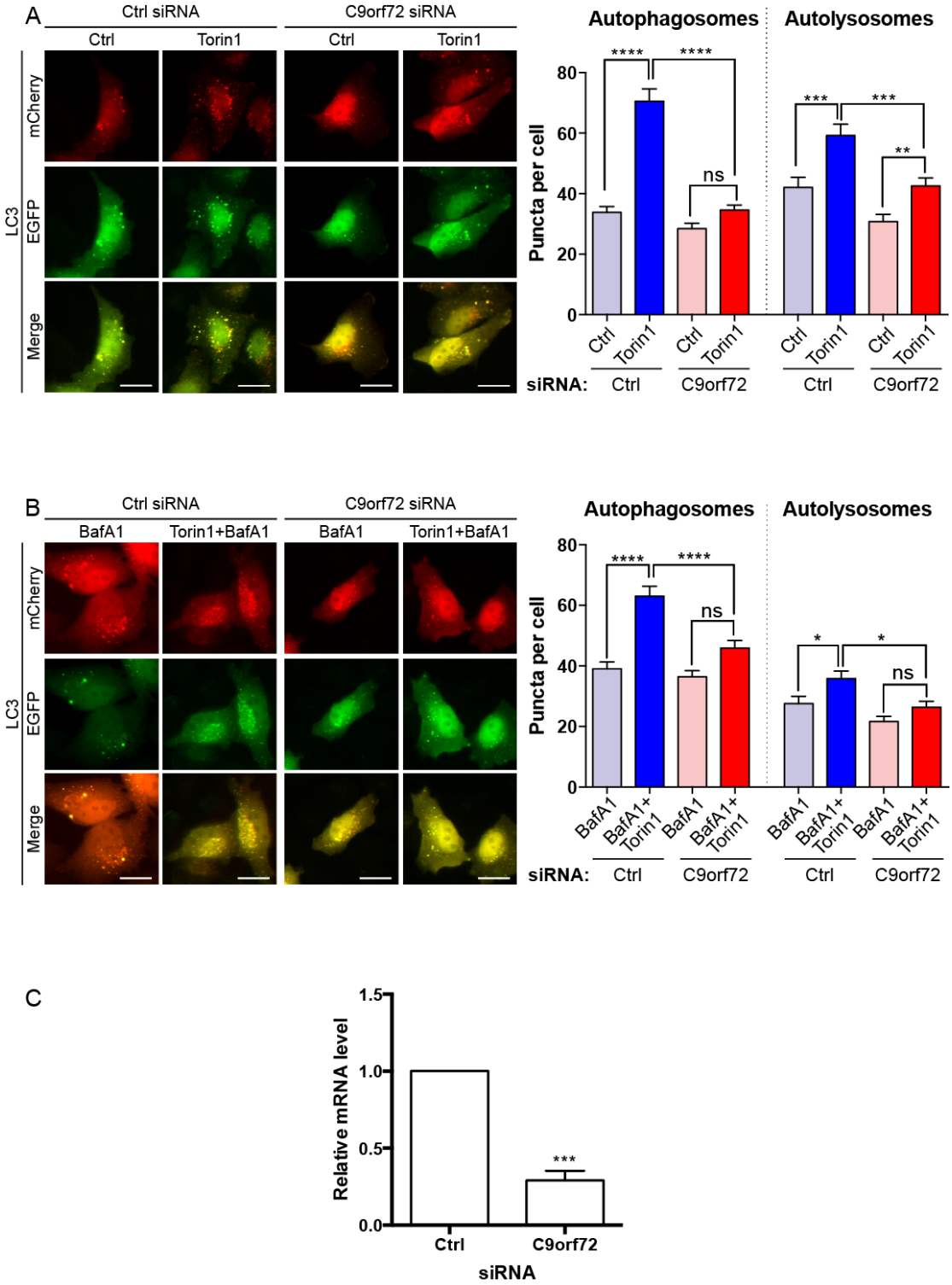

Figure 4.1 Loss of C9orf72 prevents autophagy induction. HeLa cells treated with non-targeting control (Ctrl) or C9orf72 siRNA and transfected with mCherry-EGFP-LC3 were incubated as indicated with vehicle (Ctrl), Torin1 (250 nM; 3 h), Bafilomycin A_1 (BafA1; 100 nM: 6 h) or combinations thereof. Autophagosomes (green+red) and autolysosomes (red only) were quantified per cell and are shown as mean±SEM from 3 replicate experiments. Statistical significance was

determined by one-way ANOVA with Fisher's LSD test, * $p \leq 0.05$, ** $p \leq 0.01$, *** $p \leq 0.001$, **** $p \leq 0.0001$; N (cells) = Ctrl/Ctrl 120; Ctrl/Torin1 101; C9orf72/Ctrl 99; C9orf72/Torin1 106; Ctrl/BafA1 116; Ctrl/BafA1+Torin1 118; C9orf72/BafA1 109; C9orf72/BafA1+Torin1 106. Representative images show EGFP (green), mCherry (red) and merged EGFP and mCherry. Scale bar = 20 µm. C9orf72 knock down was confirmed by RT-qPCR.

In a second approach, the levels of endogenous LC3-II were measured via immunoblot. HEK293 cells treated with either non-targeting control (Ctrl) or C9orf72 targeted siRNA were untreated, treated with Torin1 alone, rapamycin alone, bafilomycin A_1 alone, bafilomycin A_1 and Torin1 or bafilomycin A_1 and rapamycin together to, again, specifically investigate induction. Although, autophagy was induced with rapamycin or Torin1 alone, there was no accumulation of LC3-II possibly due to the fact that the pathway was still able to progress and LC3-II was degraded (Fig. 4.2A and B). Inhibition of basal autophagy with bafilomycin A_1 caused the accumulation of LC3-II in all samples (Fig. 4.2A and B). In HEK293 cells treated with Ctrl siRNA, rapamycin or Torin1 in the presence of bafilomycin A_1 led to a significant increase in the level of LC3-II compared to bafilomycin A_1 treatment alone (Fig. 4.2A and B), indicating that rapamycin and Torin1 were effectively inducing autophagy. However, in HEK293 cells treated with C9orf72 siRNA the level of LC3-II did not increase after rapamycin or Torin1 treatment indicating that in these cells, autophagy was no longer induced above basal levels (Fig. 4.2A and B). Consistent with the data obtained from the mCherry-EGFP-LC3 flux assay, this suggested that loss of C9orf72 was preventing autophagy induction.

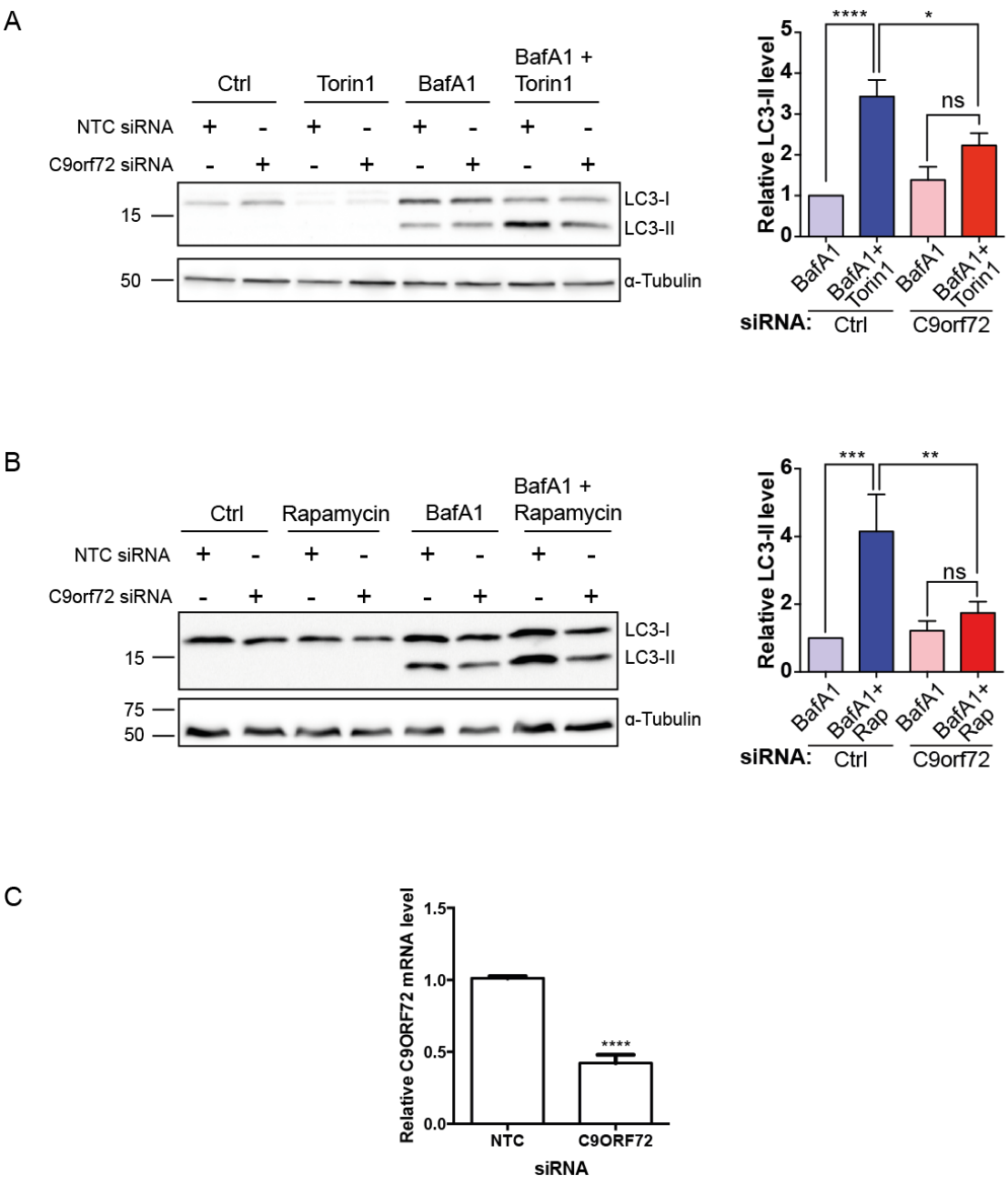

Figure 4.2 Loss of C9orf72 inhibits LC3-II formation. HEK293 cells treated with non targeting control (Ctrl) or C9orf72 siRNA were incubated with Bafilomycin A_1 (BafA1 100 nM; 6 h), BafA1 and Torin1 (BafA1; 100nM; 6 h; Torin1; 250 nM; 3 h) (A) or BafA1 and Rapamycin (BafA1; 100 nM; 6 h; Rapamycin; 500 nM; 6 h) (B) and the levels of LC3-I and LC3-II determined on immunoblot. Levels of LC3-II were normalised to tubulin and are shown relative to the BafA1 only sample (Mean±SEM; one-way ANOVA with Fisher's LSD test, ** $p \leq 0.01$, *** $p \leq 0.001$; N = 6 experiments). C9orf72 knock down was confirmed by RT-qPCR.

4.2.2 C9orf72 over expression induces autophagy

As loss of C9orf72 inhibited the induction of autophagy, the effect of C9orf72 overexpression on the autophagy pathway was investigated. HEK293 cells were co-transfected with EGFP-LC3 and either empty vector, Myc-C9orf72S or Myc-C9orf72L. Monitoring the conversion of EGFP-LC3 meant autophagy was only assessed in cells that were co-transfected with either the empty vector control, C9orf72S or C9orf72L. Empty vector control cells were either untreated, treated with Torin1 alone, treated with bafilomycin A_1 alone or treated with both Torin1 and bafilomycin A_1 together. Myc-C9orf72 transfected samples were either untreated, or treated with bafilomycin A_1. Bafilomycin A_1 treatment alone (lane 3, Fig. 4.3) lead to a significant accumulation of EGFP-LC3-II compared to untreated samples (lane 1, Fig. 4.3), and Torin1 treatment alone samples (lane 2, Fig. 4.3). Torin1 treatment in the presence of bafilomycin A_1 (lane 4, Fig. 4.3) significantly increased the amount of EGFP-LC3-II compared to bafilomycin A_1 treatment alone (lane 3, Fig. 4.3), indicating Torin1 was inducing autophagy (Fig. 4.3). Overexpression of Myc-C9orf72S or Myc-C9orf72L in the presence of bafilomycin A_1 (lanes 6 and 8, Fig. 4.3) also significantly increased the level of EGFP-LC3-II compared to bafilomycin A_1 treatment alone (lane 3, Fig. 4.3), similar to that of Torin1 treatment (lane 4, Fig. 4.3), indicating overexpression of C9orf72 was inducing autophagy to a similar extent to that of Torin1.

In a second approach the number of EGFP-LC3 positive puncta were counted in cells co-transfected with empty vector, Myc-C9orf72S or Myc-C9orf72L. Empty vector transfected cells were treated with Torin1 to induce autophagy. As expected, Torin1 treatment significantly increased the number of EGFP-LC3 puncta per cell (Fig. 4.4). Overexpression of either C9orf72S or C9orf72L also significantly increased the number of EGFP-LC3 puncta to a similar level to that of Torin1 treatment (Fig. 4.4). Thus overexpression of C9orf72 induces the formation of autophagosomes.

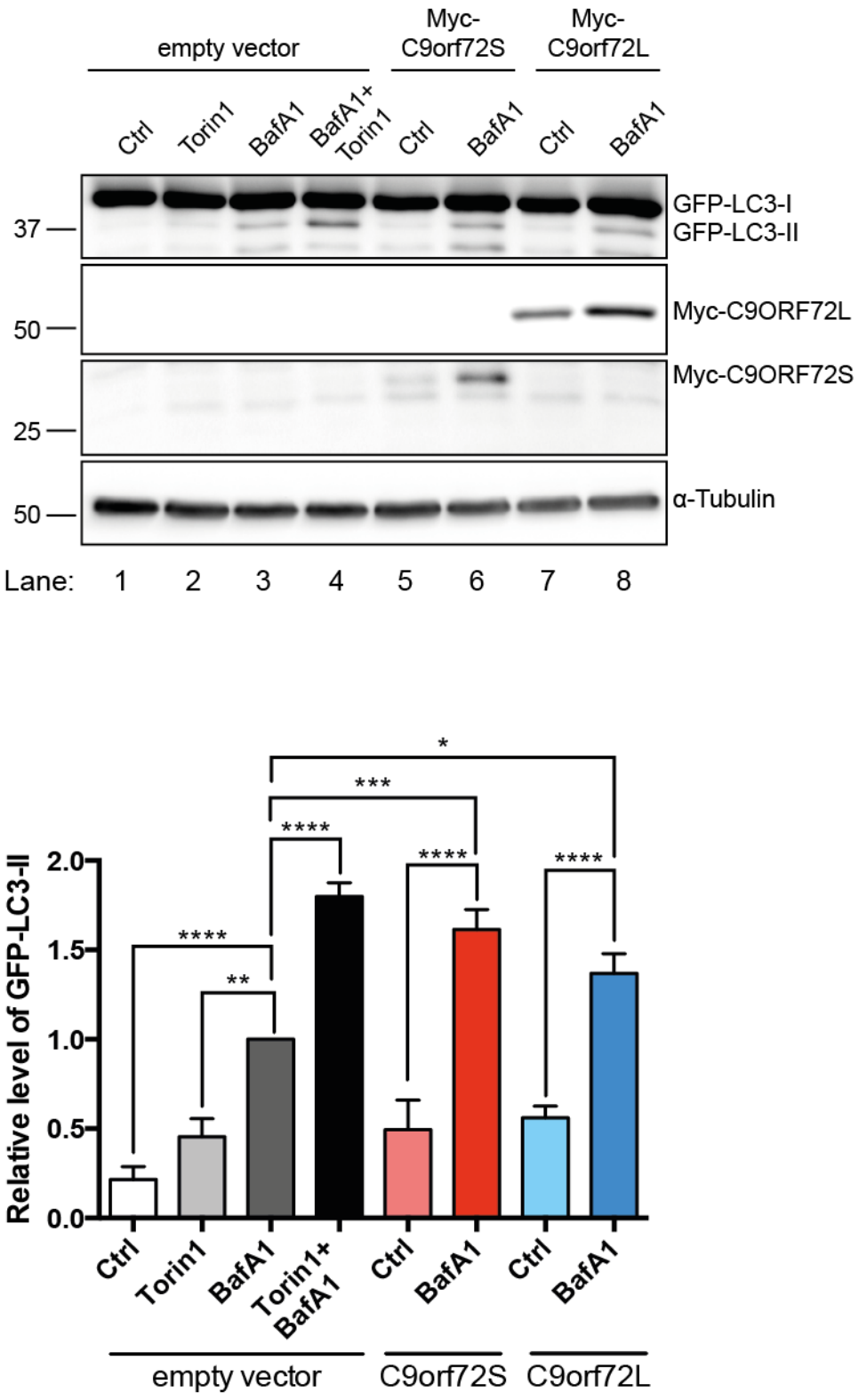

Figure 4.3. C9orf72 induces EGFP-LC3-II. HEK293 cells were co-transfected with EGFP-LC3 and either empty vector, Myc-C9orf72S or Myc-C9orf72L. 24 h post transfection cells empty vector transfected cells were incubated with vehicle (Ctrl), Torin1, Bafilomycin A_1 (BafA1) or both Bafilomycin A_1 and Torin1.

Myc-C9orf72 transfected cells were incubated with vehicle (Ctrl) or BafA1 only. Levels of autophagy were determined by immunoblot for EGFP-LC3-I and II. C9orf72 expression was confirmed with anti-Myc antibodies. Levels of EGF-LC3-II were normalised to tubulin and are shown relative to empty vector vehicle treated samples. (Mean±SEM; one-way ANOVA with Fisher's LSD test, ** $p \leq 0.01$, *** $p \leq 0.001$; N = 4 experiments).

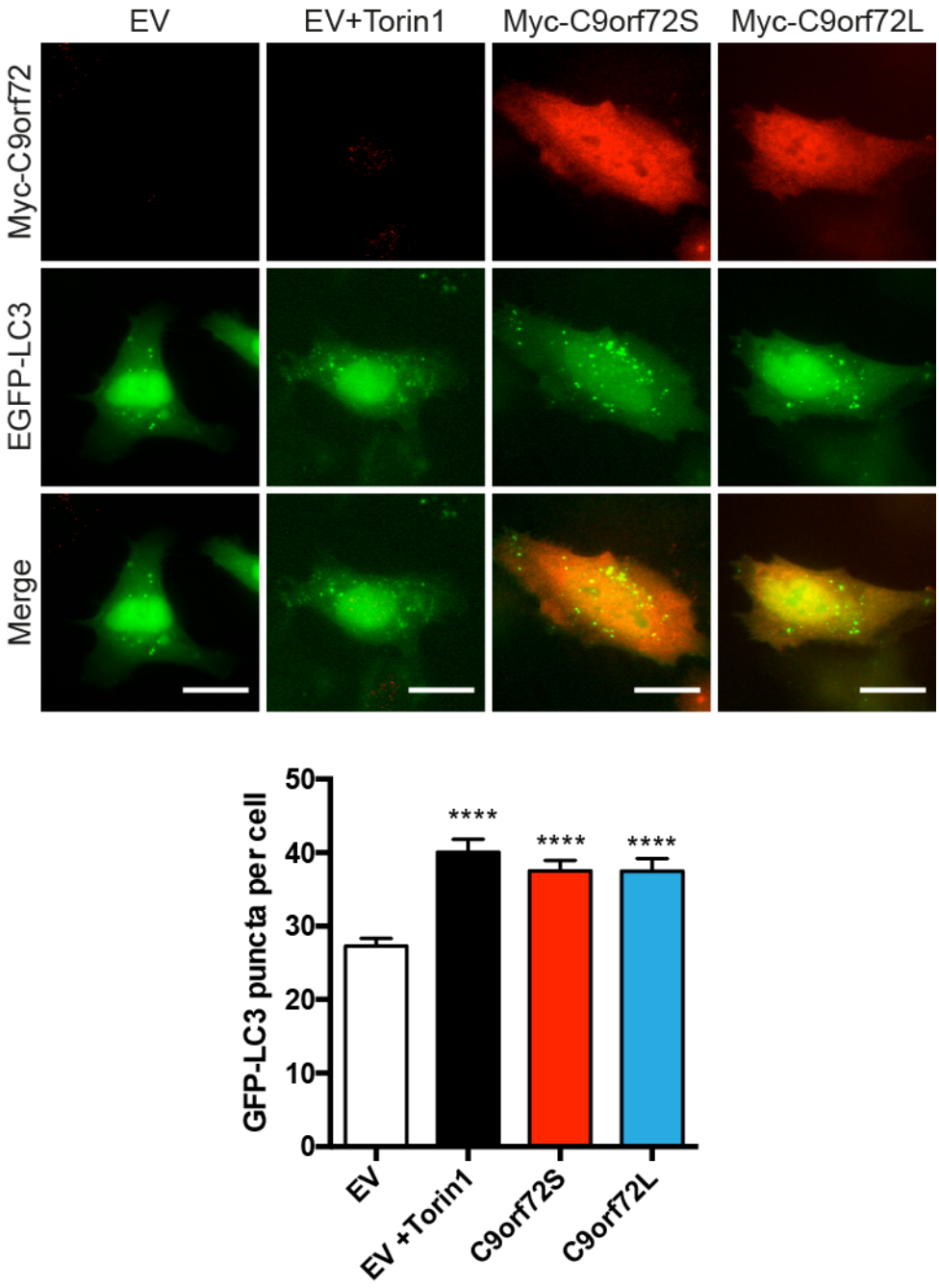

Figure 4.4 C9orf72 induces autophagy. HeLa cells were co-transfected with EGFP-LC3 (green) and either empty vector (EV), Myc-C9orf72S or Myc-C9orf72L (red). As a positive control, EV transfected cells were treated with Torin1 (250 nM; 3 h). Autophagy was quantified as the number of EGFP-LC3 positive autophagosomes per cell from 3 replicate experiments. (Mean±SEM; one-way ANOVA with Fisher's LSD test, **** $p \leq 0.0001$, N (cells) = EV 75; EV+Torin1 63; C9orf72S 79, C9orf72L 85. Scale bar = 20 µm.

4.2.3 C9orf72 induces autophagy via the ULK1 initiation complex

FIP200 is essential for autophagy induction (Ganley et al., 2009; Hara et al., 2008; Hosokawa et al., 2009a; Jung et al., 2009). Loss of FIP200 can completely abolish autophagy, leading to the accumulation of protein aggregates that are associated with defective autophagy (Hara et al., 2006; Hara et al., 2008; Komatsu et al., 2006; Liang et al., 2010; Wei et al., 2011). Thus, FIP200 siRNA can disrupt the ULK1 initiation complex, inhibiting autophagy (Hara et al., 2008). To determine if the induction of autophagy by C9orf72 overexpression was via the ULK1 initiation complex, C9orf72 was overexpressed in cells treated with non-targeting control (Ctrl) or FIP200 siRNA. Autophagy induction was monitored by the conversion of co-transfected EGFP-LC3 on immunoblot (Fig. 4.5A) or by quantifying the number of EGFP-LC3 puncta (Fig. 4.5B). As before overexpression of C9orf72S or C9orf72L increased the level of EGFP-LC3-II as well as the number of EGFP-LC3 positive autophagosomes in Ctrl siRNA treated cells, similar to the treatment with Torin1 (Fig. 4.5A and B). FIP200 siRNA completely prevented the induction of autophagy by C9orf72 overexpression in both assays (Fig. 4.5A and B). Thus C9orf72 induces autophagy via the ULK1 initiation complex.

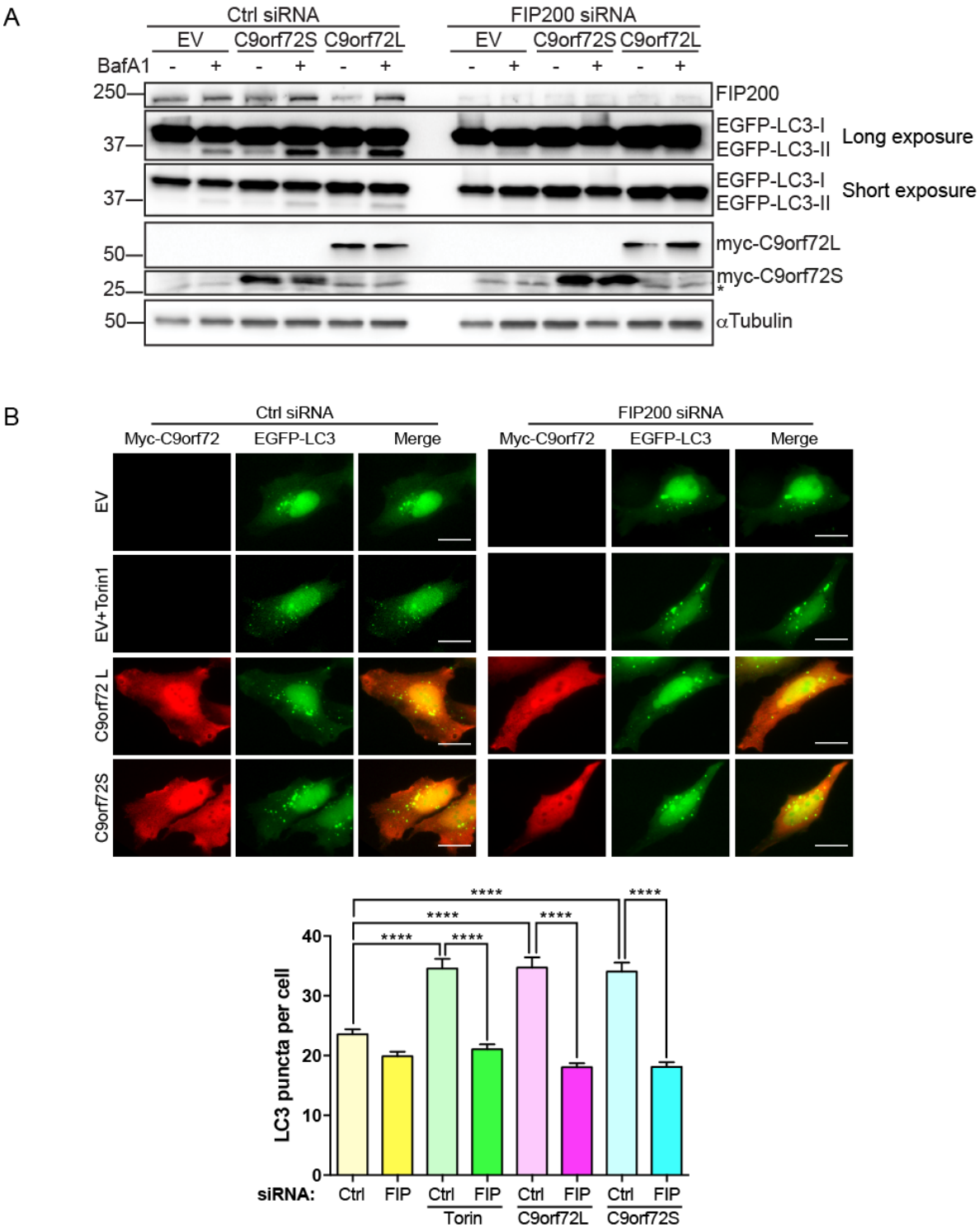

Figure 4.5 C9orf72 induces autophagy via the ULK1 initiation complex. (A) HEK293 cells treated with non-targeting control (Ctrl) or FIP200 siRNA were co-transfected with EGFP-LC3 and either empty vector control (EV), Myc-C9orf72S or Myc-C9orf72L. 24 h post transfection cells were treated with vehicle or BafA1 for 6 h. Samples were lysed and subjected to SDS-PAGE and immunoblot. Autophagy levels were determined by immunoblot for EGFP-LC3-I and II. Expression of C9orf72 was confirmed using anti-Myc antibodies (* indicates

aspecific band). FIP200 knock down was confirmed using anti-FIP200 antibodies. α-Tubulin was used as a loading control. (B) HeLa cells treated with non-targeting (Ctrl) or FIP200 siRNA were co-transfected with empty vector (EV), myc-C9orf72S or myc-C9orf72L (red) and EGFP-LC3 (green) to label autophagosomes. As positive control EV transfected cells were treated with Torin1 (250 nM; 3 h). Autophagy was quantified as the number of EGFP-LC3 positive autophagosomes per cell from 3 replicate experiments (Mean±SEM; one-way ANOVA with Fisher's LSD test, ** $p \leq 0.01$, *** $p \leq 0.001$; **** $P \leq 0.0001$, N (cells) = Ctrl/EV: 73; FIP200/EV: 76; Ctrl/EV/Torin1: 73, FIP200/EV/Torin1: 70; Ctrl/C9orf72L: 71; FIP200/C9orf72L: 74; Ctrl/C9orf72S: 72; FIP200/C9orf72S: 72). Scale bar = 20 µm. FIP200 knockdown was confirmed by immunoblot.

4.2.4 Loss of C9orf72 does not affect ULK1 activation

Under basal condition mTOR phosphorylates ULK1 at serine 757, rendering the initiation complex inactive (Jung et al., 2009; Kim et al., 2011), see section 1.5.2.1 and Figs. 1.4 and 1.5. Induction of autophagy releases the ULK1 initiation complex from mTOR resulting in loss of ULK1 Ser757 phosphorylation and the activation of ULK1 kinase activity (Ganley et al., 2009; Jung et al., 2009; Kim et al., 2011). Thus, the level of ULK1 Ser757 phosphorylation is indicative of the activation state of ULK1. To investigate whether loss of C9orf72 affected the activation of ULK1, the level of ULK1 Ser757 phosphorylation was assessed in HEK293 cells treated with non-targeting (Ctrl) or C9orf72 siRNA. Autophagy was induced with rapamycin or Torin1 and the level of ULK1 Ser757 phosphorylation determined by using phosphospecific antibodies. Inhibition of mTOR with rapamycin or Torin1 led to a decrease in ULK1 Ser757 phosphorylation in both control and C9orf72 siRNA treated cells (Fig. 4.6A and B), indicating that loss of C9orf72 did not prevent ULK1 activation. C9orf72 knockdown was quantified by qPCR (Fig. 4.6C). As loss of C9orf72 inhibits autophagy induction, but does not affect the activation of ULK1, loss of C9orf72 therefore most likely affects a step further downstream.

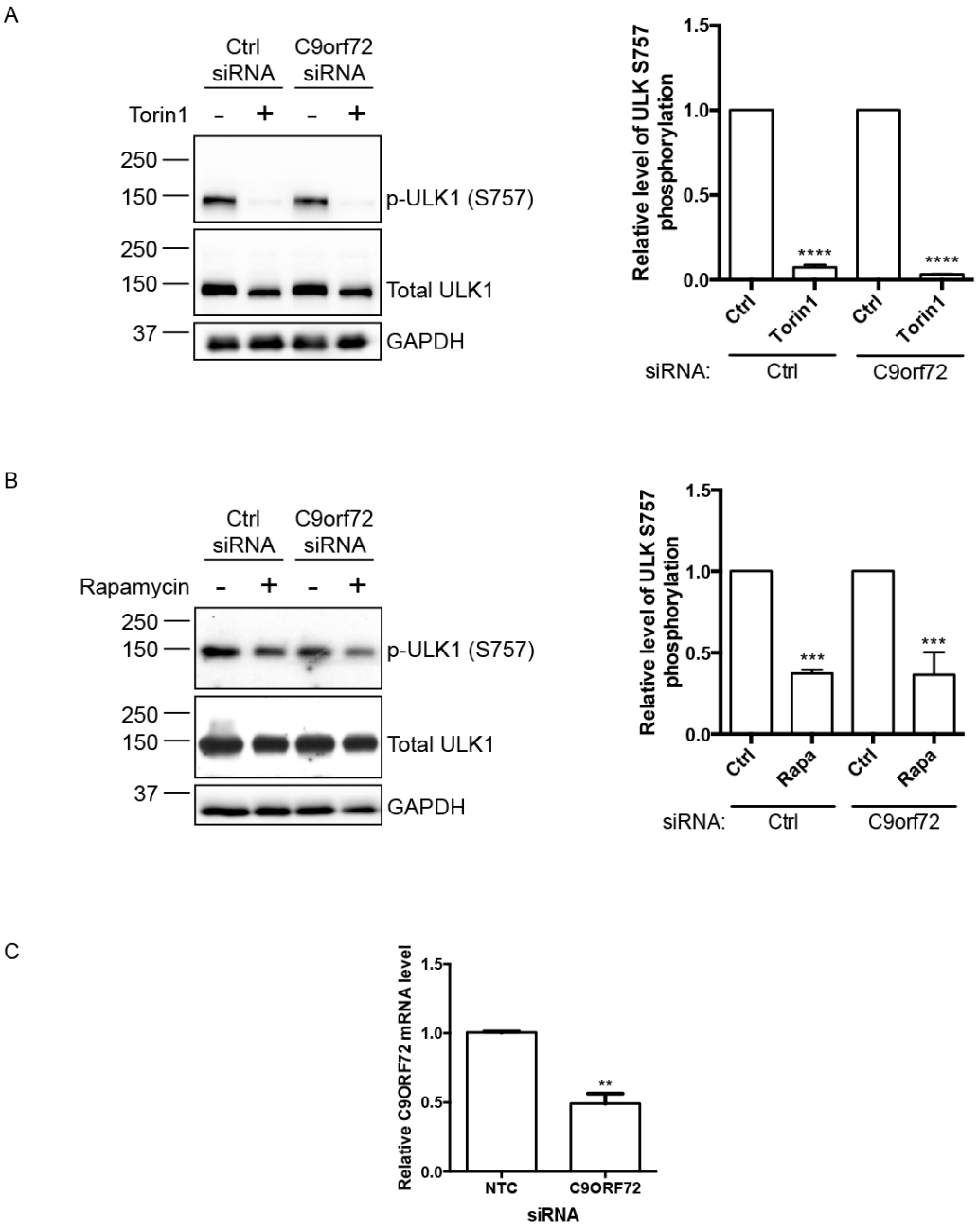

Figure 4.6 Loss of C9orf72 does not affect activation of ULK1. HEK293 cells treated with non-targeting control or C9orf72 siRNA were treated with vehicle, Torin1 (250 nM; 3 h) (A) or rapamycin (500 nM; 6 h) (B) to induce autophagy. Activation of ULK1 was determined via immunoblots using phopho-ULK1 (S757) and total ULK antibodies. Phospho-ULK1 (S757) levels were normalised to total ULK1 and are shown relative to the vehicle treated samples. GAPDH was used as a loading control. (Mean±SEM; one-way ANOVA with Fisher's LSD test, *** $p \leq 0.001$, **** $p \leq 0.0001$. (C) C9orf72 knock down was confirmed by RT-qPCR (Mean±SEM; one-way ANOVA with Fisher's LSD test, ** $p \leq 0.01$). (N = 3 experiments).

4.2.5 C9orf72 regulates translocation of the ULK1 initiation complex to the phagophore via Rab1a

Upon autophagy induction, the active ULK1 initiation complex translocates to the phagophore to initiate formation of the autophagosome (Hara et al., 2008), see section 1.5.2.1 and Fig. 1.4. Thus, the formation of ULK1, FIP200 or ATG13 positive puncta can be monitored by immunofluorescent microscopy to assess translocation of the initiation complex to the phagophore (Ganley et al., 2009). To investigate whether C9orf72 could affect translocation of the initiation complex, mCherry-tagged FIP200 translocation was monitored in HeLa cells transfected with non-targeting (Ctrl) or C9orf72 siRNA and treated with Torin1 to induce autophagy. In untreated Ctrl siRNA and C9orf72 siRNA transfected cells, mCherry-FIP200 was diffusely distributed throughout the cytoplasm, with a small number of bright puncta (Fig. 4.7A). Torin1 treatment in Ctrl siRNA cells lead to a significant increase in the number of mCherry-FIP200 puncta, indicating translocation of the initiation complex after autophagy induction (Fig. 4.7A). However, Torin1 treatment had no effect on the number of mCherry-FIP200 puncta in cells treated with C9orf72 siRNA, indicating that loss of C9orf72 prevents translocation of the initiation complex (Fig. 4.7A). Thus C9orf72 is required for translocation of the autophagy initiation complex. The knockdown of C9orf72 was quantified by qPCR (Fig. 4.7B).

As C9orf72 overexpression was capable of inducing autophagy, and C9orf72 was required for translocation of the initiation complex, it was reasoned that increasing C9orf72 levels would actively drive translocation of the autophagy initiation complex to bring about the induction of autophagy as seen in Fig. 4.3 and Fig. 4.4. To test this possibility, Hela cells were co-transfected with mCherry-FIP200 and either empty vector, Myc-C9orf72S or Myc-C9orf72L. Torin1 treatment of empty vector transfected cells significantly increased the number of co-transfected mCherry-FIP200 puncta compared to untreated cells (Fig. 4.7C). As expected, overexpression of C9orf72S or C9orf72L also significantly increased the number of mCherry-FIP200 puncta similar to the effect seen with Torin1 treatment (Fig. 4.7C).

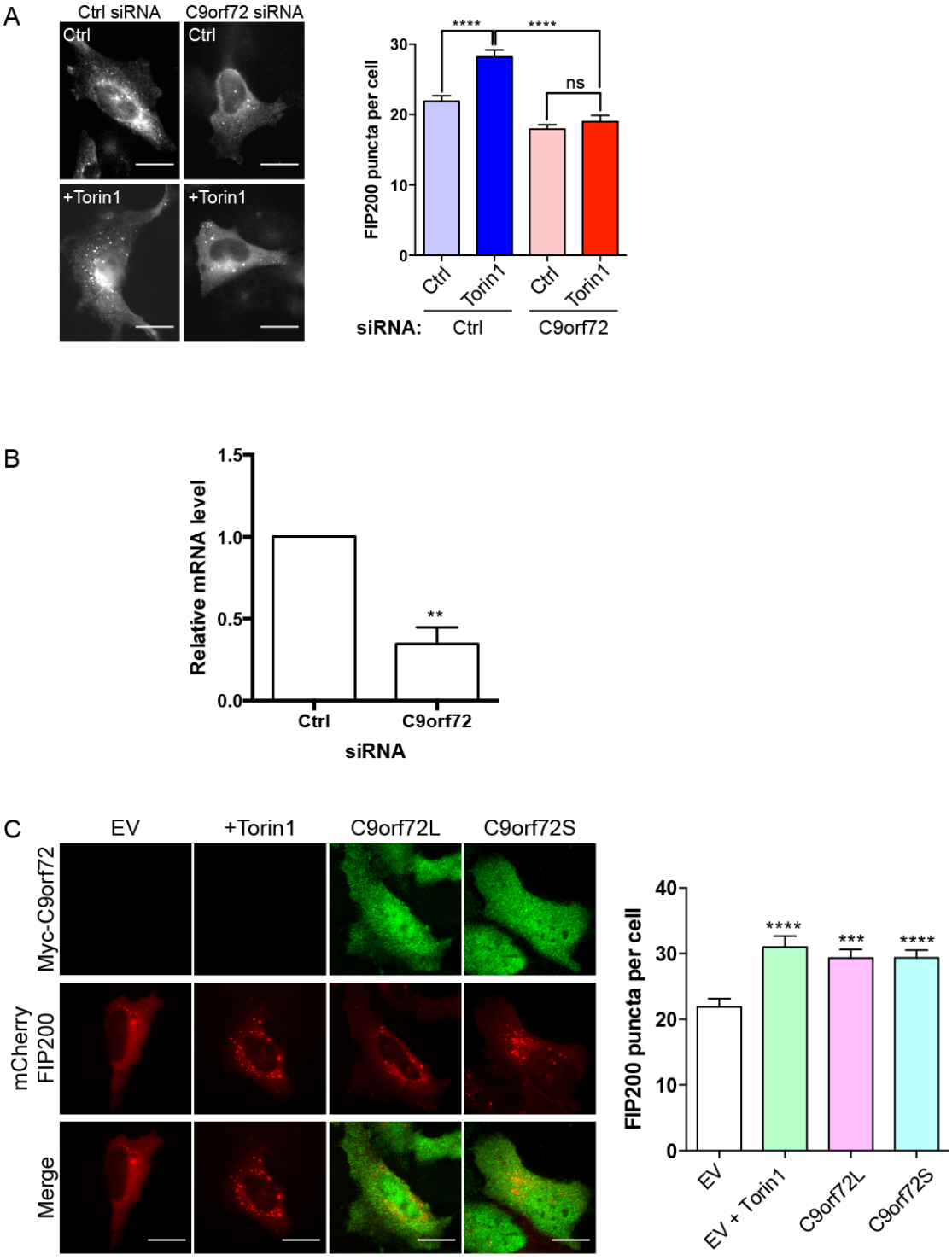

Figure 4.7 C9orf72 regulates translocation of the ULK1 complex. (A) HeLa cells treated with non-targeting (Ctrl) or C9orf72 siRNA were transfected with mCherry-FIP200. 24 h post transfection cells were treated with vehicle (Ctrl) or Torin1 (250 nM; 3 h) to induce autophagy. Translocation of the ULK1 complex was quantified as the number of mCherry-FIP200 positive puncta per cell from 3 replicate experiments (Mean±SEM; one-way ANOVA with Fisher's LSD test, ns:

not significant, **** P ≤ 0.0001; N (cells) = Ctrl/Ctrl: 65; Ctrl/Torin1: 60; C9orf72/Ctrl: 54; C9orf72/Torin1: 49). C9orf72 knockdown was determined by RT-qPCR. Scale bar = 10 µm. (B) HeLa cells were co-transfected with mCherry-FIP200 (red) and either empty vector (EV), FLAG-C9orf72L or FLAG-C9orf72S (green). As positive control EV transfected cells were treated with Torin1 (250 nM; 3 h) to induce autophagy. Translocation of the ULK1 complex was quantified as the number of mCherry-FIP200 positive puncta per cell from 3 replicate experiments (Mean±SEM; one-way ANOVA with Fisher's LSD test, *** P ≤ 0.001, **** P ≤ 0.0001); N (cells) = EV: 47, EV + Torin1: 31, C9orf72L: 46, C9orf72S: 45). Scale bar = 10µm.

In yeast Ypt1 regulates the translocation ATG1, the homologue of ULK1, to the PAS to induce autophagy (Lynch-Day et al., 2010; Wang et al., 2013). To determine if the mammalian homologue of Ypt1, Rab1, was able to regulate the translocation of the initiation complex in mammalian cells, the translocation of mCherry-FIP200 in HeLa cells was investigated after depletion of Rab1a with targeted siRNA. Rab1a was chosen as Rab1a had previously been shown to regulate autophagy induction (Winslow et al., 2010). Targeted knock down of Rab1a by siRNA completely prevented the translocation of mCherry-FIP200 induced by Torin1 (Fig. 4.8A), suggesting that Rab1a may regulate the translocation of the autophagy initiation complex in mammalian cells. To determine if C9orf72 acted via Rab1a to induce translocation of the initiation complex and induce autophagy, the effect of C9orf72 overexpression on mCherry-FIP200 translocation was also quantified in Rab1a depleted cells. As previously, overexpression of Myc-tagged C9orf72S and C9orf72L induced the translocation of the mCherry-FIP200 to similar levels seen with Torin1 induction (Fig. 4.8A). However, in cells treated with Rab1a siRNA, overexpression of Myc-C9orf72S and Myc-C9orf72L was no longer able to induce translocation of mCherry-FIP200 (Fig. 4.8A). The knockdown of Rab1a was confirmed by qPCR (Fig. 4.8B). Thus C9orf72 required Rab1a to induce the translocation of the autophagy initiation complex.

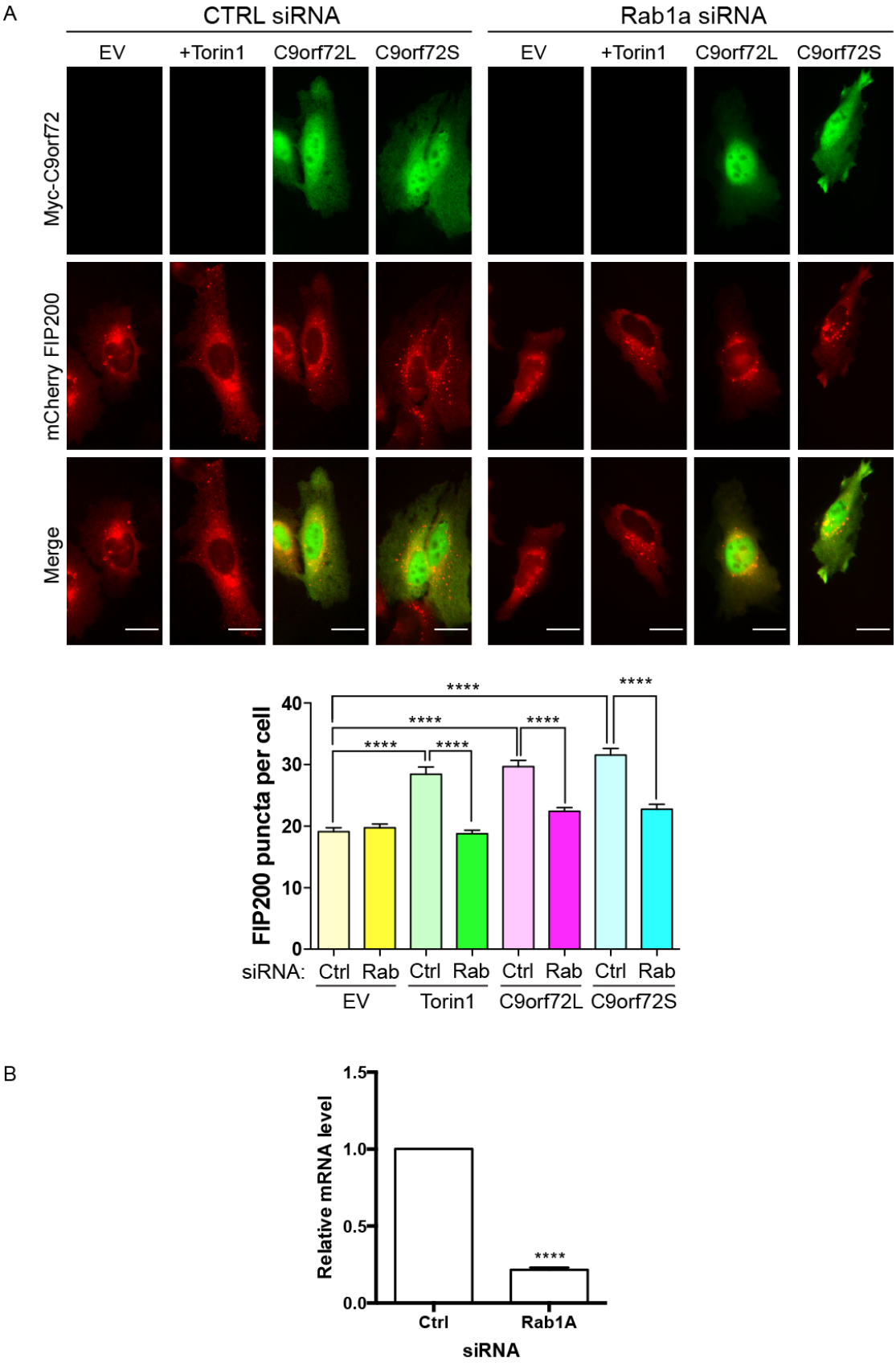

Figure 4.8 C9orf72 regulates translocation of the ULK1 initiation complex via Rab1a. HeLa cells treated with non-targeting (Ctrl) or Rab1a siRNA were co-

transfected with mCherry-FIP200 (red) and empty vector (EV), myc-C9orf72L or myc-C9orf72S (green). As positive control EV transfected cells were treated for 3 h with Torin1 (250 nM). Translocation of the ULK1 complex was quantified as the number of mCherry-FIP200 positive puncta per cell from 3 replicate experiments (Mean±SEM; one-way ANOVA with Fisher's LSD test, **** $P \leq 0.0001$); N (cells) = Ctrl/EV: 81; Ctrl/EV/Torin1: 48; Ctrl/C9orf72L: 86; Ctrl/C9orf72S: 48; Rab1a/EV: 79; Rab1a/EV/Torin1: 68; Rab1a/C9orf72L: 78; Rab1a/C9orf72S: 52). Rab1a knockdown was confirmed by RT-qPCR. Scale bar = 10µm.

4.2.6 C9orf72 interacts with Rab1a

There are 2 isoforms of Rab1, Rab1a and Rab1b, which share approximately 92% homology (Vielh et al., 1989). Rab1 and its yeast counterpart, Ypt1, are required for ER to Golgi transport (Pind SN, 1994), but both have also been implicated in the autophagy pathway (Lipatova et al., 2012; Winslow et al., 2010; Zoppino et al., 2010). The data in section 4.2.5, along with the structural homology of C9orf72 with the DENN domain Rab GEF proteins, suggested C9orf72 may interact with Rab1a. Further to this, the Y2H screen conducted in Chapter 3 section 3.2.6 identified Rab1a as a potential C9orf72S interacting protein. One clone, encoding a partial Rab1a sequence (aa 46-205), was identified while using C9orf72S as bait. To confirm this interaction, HEK293 cells were co-transfected with Myc-Rab1a and either empty vector, FLAG-C9orf72S or FLAG-C9orf72L. FLAG-C9orf72 was immunoprecipitated with anti-FLAG antibodies and the immunepellets analysed by SDS-PAGE and immunoblot. Myc-Rab1a was found to efficiently co-immunoprecipitate with both C9orf72S and C9orf72L (Fig. 4.9A).

To test if Rab1a was directly interacting with C9orf72 *in vitro* binding assays were performed using recombinant GST-tagged C9orf72 incubated with *in vitro* translated S^{35}-labelled Rab1a protein. GST proteins were pulled down using glutathione beads and samples analysed by SDS-PAGE. Radiolabelled Rab1a was detected using a phosphoimager. Rab1a was found to directly interact with both C9orf72S and C9orf72L (Fig. 4.9B). Thus Rab1a was confirmed as a direct binding partner of C9orf72.

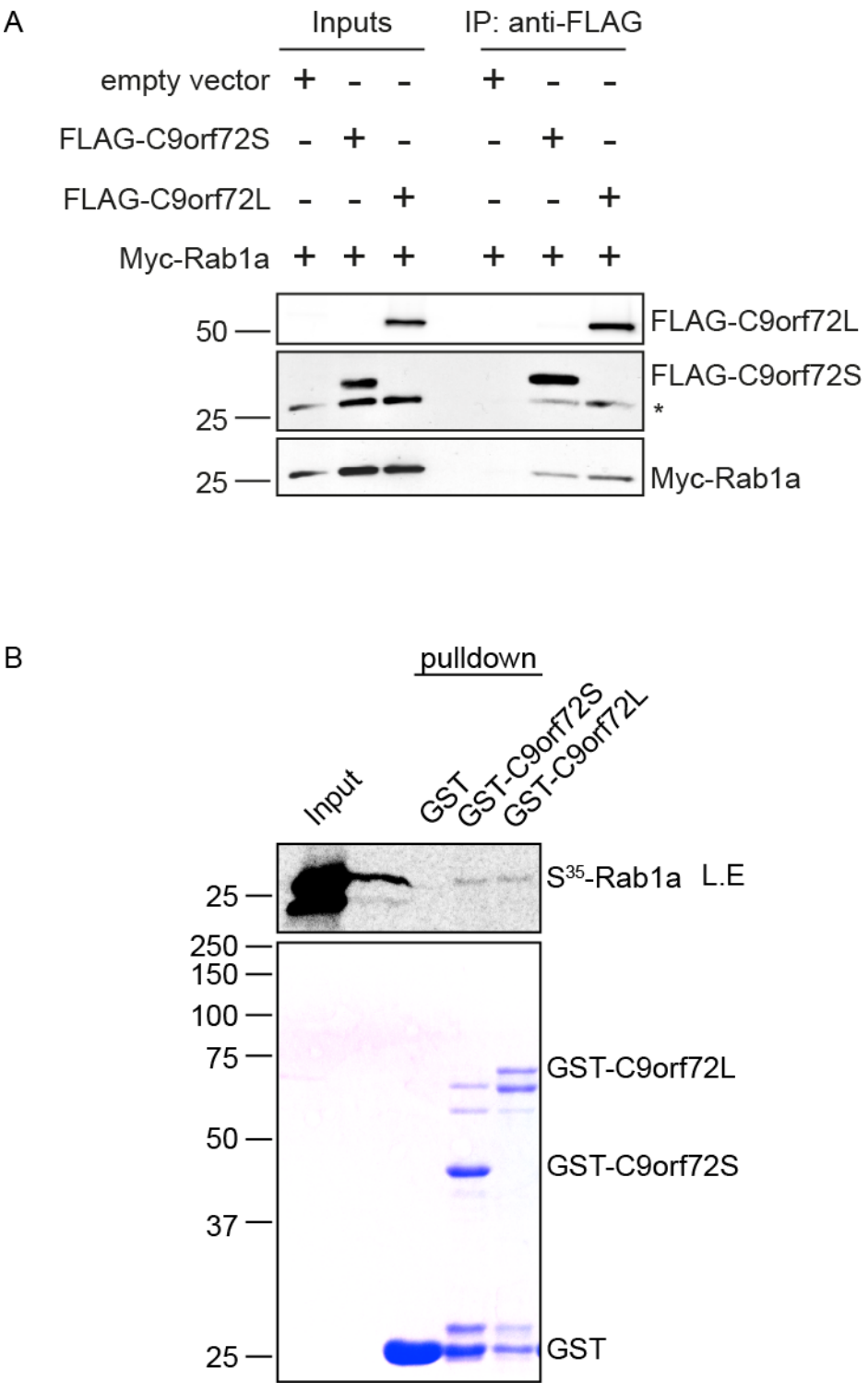

Figure 4.9 C9orf72 directly interacts with Rab1a. (A) Whole cell lysates of HEK293 cells co-transfected with Myc-Rab1a and either empty vector control, FLAG-C9orf72S or FLAG-C9orf72L were subjected to immunoprecipitation with anti-FLAG antibodies. Immune pellets were probed for FLAG-C9orf72 and Myc-Rab1a on immunoblot. Blots were initially probed with 9B11 mouse anti-Myc to detect Myc-Rab1a. Blots were then re-probed with M2 mouse anti-FLAG to

detect FLAG-C9orf72. The * in the middle panel indicates Myc-Rab1a bands that were present after re-probing of the membrane for FLAG-C9orf72S. (B) C9orf72 directly interacts with Rab1a. ^{35}S-radiolabelled recombinant Myc-Rab1a protein was incubated with GST, GST-C9orf72S or GST-C9orf7L immobilized on glutathione-coated beads. ^{35}S-radiolabelled recombinant Myc-Rab1a protein was visualised by autoradiography (top panel: S.E = short exposure, L.E = long exposure). Coomassie-stained GST, GST-C9orf72S and GST-C9orf72L from the pull down are shown (bottom panel). The identities of the Coomassie protein bands were confirmed by mass spectrometry (* = CH60 *E. coli*, 60kD Chaperonin, # = DnaK Chaperonin *E.coli*).

4.2.7 C9orf72 mediates the interaction between Rab1a and the ULK1 initiation complex

The structural homology of C9orf72 with DENN domain proteins suggested that C9orf72 might function as a GEF for the Rab GTPases (Levine et al., 2013; Zhang et al., 2012). The interaction with Rab1a, therefore suggested that the C9orf72 could function as a GEF for Rab1a, allowing for translocation of the initiation complex and the induction of autophagy. To function as a GEF, C9orf72 would be expected to bind preferentially to the GDP-bound version of Rab1a and mediate the exchange of GDP for GTP, thus activating the Rab GTPase.

To investigate the binding affinity of C9orf72 to GDP-bound Rab1a, *in vitro* binding assays were conducted between GST-tagged C9orf72 and *in vitro* translated S^{35}-radiolabelled Rab1a. Recombinant GST-tagged C9orf72 was incubated with *in vitro* translated S^{35}-labelled Rab1a, S^{35}-labelled Rab1a pre-loaded with GDP or S^{35}-labelled Rab1a preloaded with a non-hydrolysable version of GTP. GST tagged proteins were pulled down with glutathione beads and samples analysed by SDS-PAGE. The gel was exposed to a phosphoimager plate to detect S^{35}-Rab1a. Preloading Rab1a with GDP, to mimic the inactive form of Rab1a, did not alter the binding with C9orf72 (Fig. 4.11). However, preloading Rab1a with a non-hydrolysable form of GTP (GMP-PNP), thus mimicking the active form of Rab1a, significantly increased the amount of Rab1a interacting with C9orf72S and C9orf72L (Fig.4.10). The preferential interaction between GTP-Rab1a and C9orf72 suggests that C9orf72 is a Rab1a effector protein rather than a Rab1a GEF.

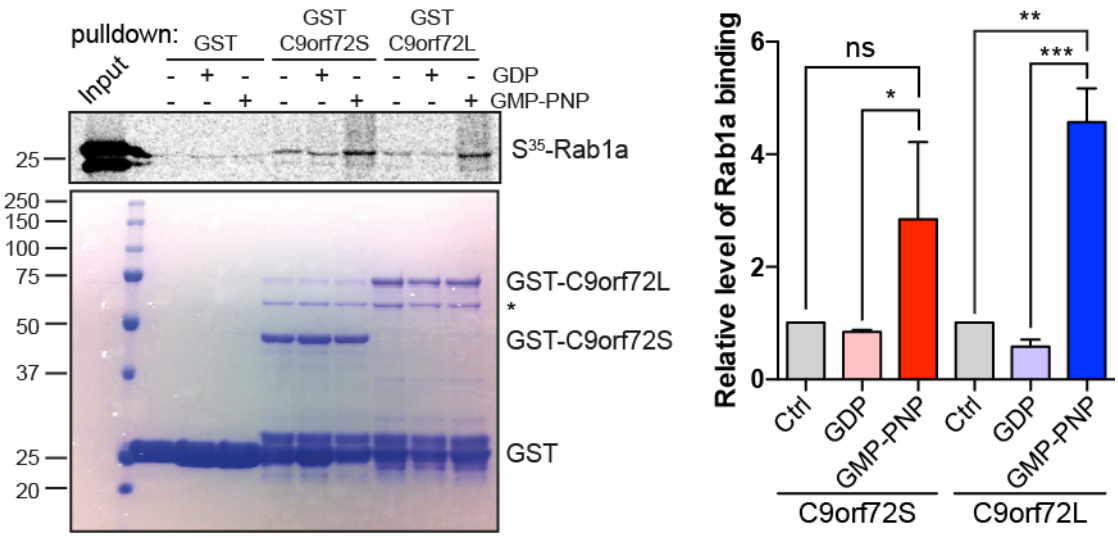

Figure 4.10 C9orf72 preferentially binds GTP-bound Rab1a. ^{35}S-radiolabelled recombinant Myc-Rab1a protein loaded with vehicle, GDP or GMP-PNP was added to GST, GST-C9orf72S and GST-C9orf72L immobilized on glutathione-coated beads. ^{35}S-radiolabelled recombinant Myc-Rab1a protein was visualized by autoradiography (top panel). Coomassie-stained GST, GST-C9orf72S and GST-C9orf72L in the pull-down samples are shown (bottom panel). The identity of the Coomassie protein bands was confirmed by mass spectrometry (* = CH60 *E. coli*, 60kD Chaperonin; Fig. S3). Relative binding of Rab1A to C9orf72 was quantified from 3 independent experiments (Mean±SEM; one-way ANOVA with Fisher's LSD test; ns, not significant; * P ≤ 0.05; ** P ≤ 0.01; *** P ≤ 0.001).

In yeast, the active GTP-loaded Ypt1 is brought into contact with ATG1 by the action of the PAS scaffold protein, ATG11 (Lipatova et al., 2012). To investigate whether C9orf72 was required for the interaction of active Rab1a with the ULK1 initiation complex, the interaction between Rab1a and ULK1 was investigated in HeLa cells that were treated with non-targeting (Ctrl) or C9orf72 siRNA by an *in situ* proximity ligation assay (PLA) (Soderberg et al., 2006). In PLA, cells are fixed and the two proteins of interest stained with primary antibodies. Secondary antibodies are then added, which are conjugated with complementary oligonucleotide probes. If the two proteins are in close enough proximity (i.e. less than 50 nm) the oligonucleotide probes can be ligated. This closed circle formation of the probes allows for rolling circle amplification, which can be detected by using complementary fluorescently labelled oligonucleotides. The signal from these fluorescent oligonucleotides can be detected by fluorescence microscopy (Soderberg et al., 2006). In control siRNA transfected cells, proximity signals were observed in all cells transfected with HA-ULK and Myc-Rab1a, while only low numbers of proximity signals were observed in cells transfected with Myc-Rab1a or HA-ULK alone (Fig. 4.11). In comparison, C9orf72 siRNA treated cells showed significantly less proximity signals when co-transfected with HA-ULK and Myc-Rab1a (Fig. 4.11). Thus, Rab1a interacts with ULK1 in a C9orf72 dependent manner.

To test whether C9orf72 was indeed required for the Rab1a dependent induction of autophagy, the effect of constitutively active Rab1a (Rab1aQ70L) overexpression on mCherry-FIP200 translocation was investigated in HeLa cells treated with C9orf72 siRNA. Consistent with the Rab1a dependent translocation of the autophagy initiation complex, overexpression of constitutively active Rab1a (Q70L) was able to induce translocation of the autophagy initiation complex as measured by mCherry-FIP200 puncta formation in HeLa cells treated with control siRNA (Fig. 4.12A). However, in C9orf72 siRNA treated cells, Rab1a (Q70L) was no longer able to induce translocation of mCherry-FIP200 (Fig. 4.12). The knockdown of C9orf72 was confirmed by RT-qPCR (Fig. 4.12B)

In conclusion these data indicate that C9orf72 acts as a Rab1a effector, recruiting active GTP bound Rab1a to the initiation complex to bring about translocation of the autophagy initiation complex and initiate formation of the autophagosome.

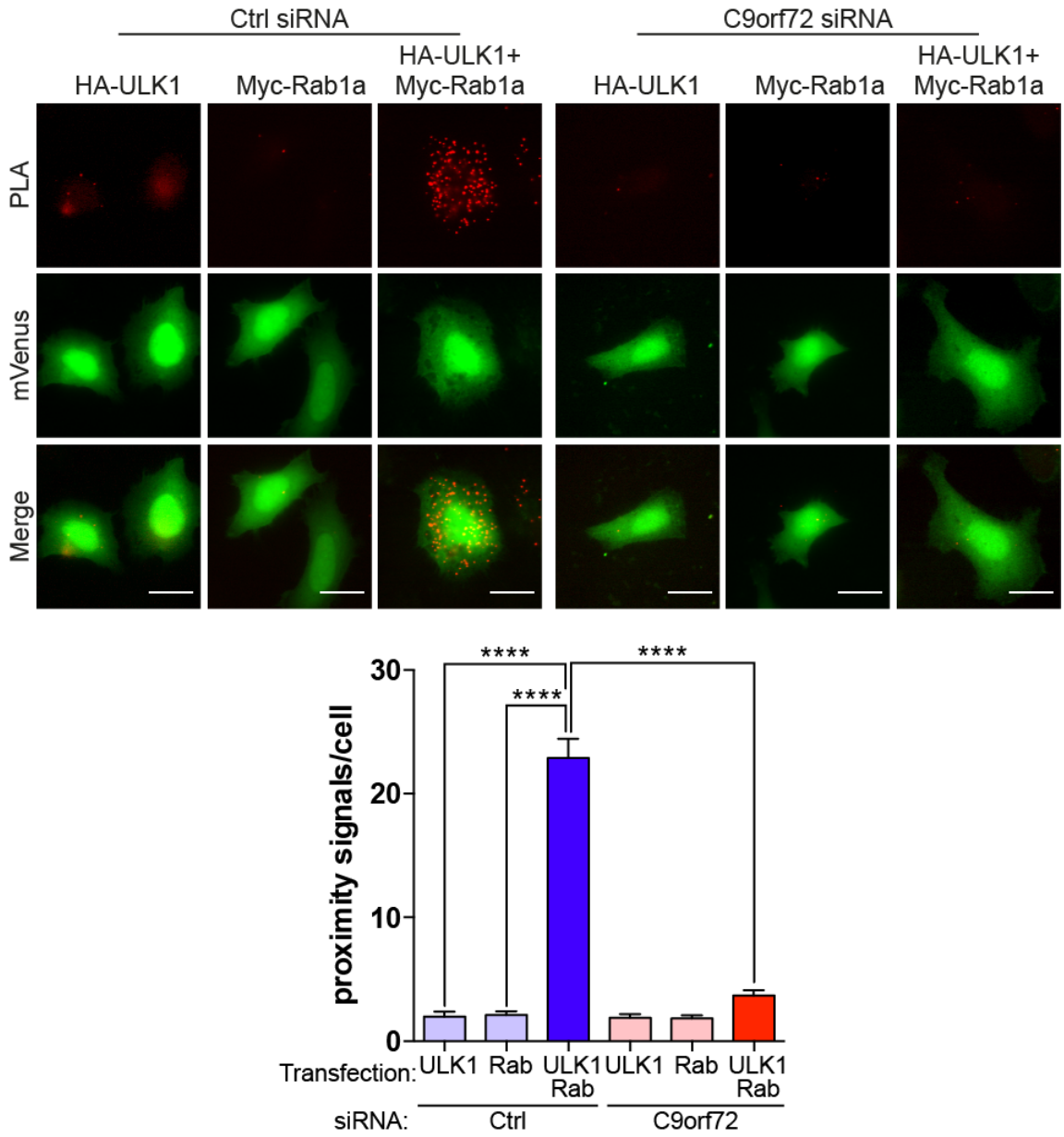

Figure 4.11 C9orf72 regulates the interaction between Rab1a and ULK1. HeLa cells treated with non-targeting (Ctrl) or C9orf72 siRNA were transfected with HA-ULK, Myc-Rab1a or HA-ULK1 + Myc-Rab1a as indicated. Transfections were laced with mVenus to enable identification of transfected cells for analysis (green). Transfected cells were probed with both anti-HA and anti-myc antibodies and processed for PLA. PLA proximity signals per cell (red) were determined from 3 replicate experiments (Mean±SEM; one-way ANOVA with Fisher's LSD test, **** $P \leq 0.0001$); N (cells) = Ctrl/HA-ULK1: 125, Ctrl/Myc-Rab1a: 149, Ctrl/HA-ULK1+Myc-Rab1a: 163, C9orf72/HA-ULK1: 136, C9orf72/Myc-Rab1a: 133, C9orf72/HA-ULK1+Myc-Rab1a: 155). Scale bar = 20µm.

A

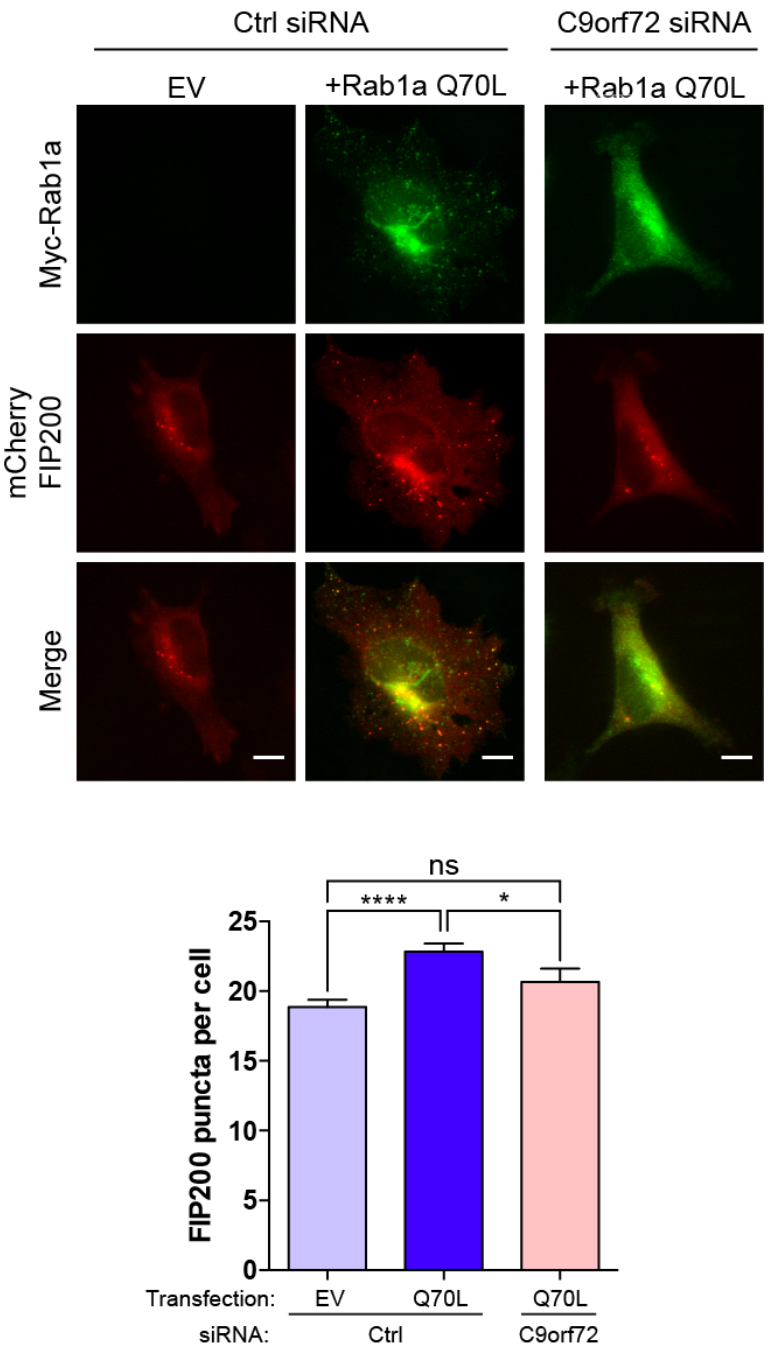
Ctrl siRNA
C9orf72 siRNA
EV
+Rab1a Q70L
+Rab1a Q70L
Myc-Rab1a
mCherry FIP200
Merge
ns
****
*
FIP200 puncta per cell
25
20
15
10
5
0
Transfection:
EV
Q70L
Q70L
siRNA:
Ctrl
C9orf72

B

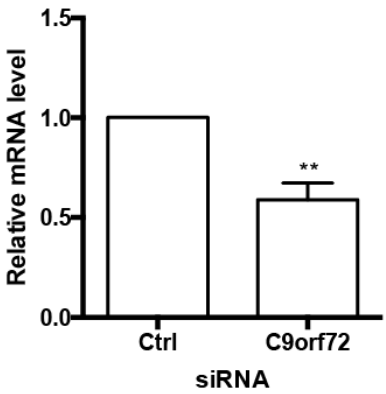
Relative mRNA level
1.5
1.0
0.5
0.0
**
Ctrl
C9orf72
siRNA

Figure 4.12 C9orf72 is required for the Rab1a dependent induction of autophagy. HeLa cells treated with non-targeting (Ctrl) or C9orf72 siRNA were co-transfected with mCherry-FIP200 (red) and empty vector (EV) or myc-Rab1a (Q70L). Translocation of the ULK1 complex was quantified as the number of mCherry-FIP200 positive puncta per cell from 4 replicate experiments (Mean±SEM; one-way ANOVA with Fisher's LSD test, * $P \leq 0.05$, **** $P \leq 0.0001$); N (cells) = Ctrl/EV: 101; Ctrl/Q70L: 106; C9/Q70L: 42. C9orf72 knockdown was determined by RT-qPCR.

4.2.8 C9orf72 depletion induces p62 accumulation

The accumulation of p62 specific pathology in C9ALS/FTD patients is indicative of defective autophagy. The link between C9orf72 and autophagy induction therefore suggests that haploinsufficiency of C9orf72 could lead to autophagy deficiency in patients and the associated C9ALS/FTD pathology. To investigate whether loss of C9orf72 was sufficient to cause accumulation of p62, the accumulation of p62 were monitored by immunofluorescence in cells treated with non-targeting (Ctrl) siRNA or C9orf72 siRNA. In Ctrl siRNA treated cells, p62 was diffusely distributed throughout the cytoplasm, but was also present in a number of p62 cytoplasmic puncta (Fig. 4.13A). In contrast, there were significantly more p62 puncta in cells transfected with C9orf72 siRNA, suggesting that loss of C9orf72 led to the accumulation of p62 in these puncta or aggregates (Fig. 4.13A). Thus loss of C9orf72 is sufficient to cause the accumulation of p62, mimicking the pathology associated with C9ALS/FTD *in vitro.* The knockdown of C9orf72 was confirmed by RT-qPCR (Fig. 4.13B).

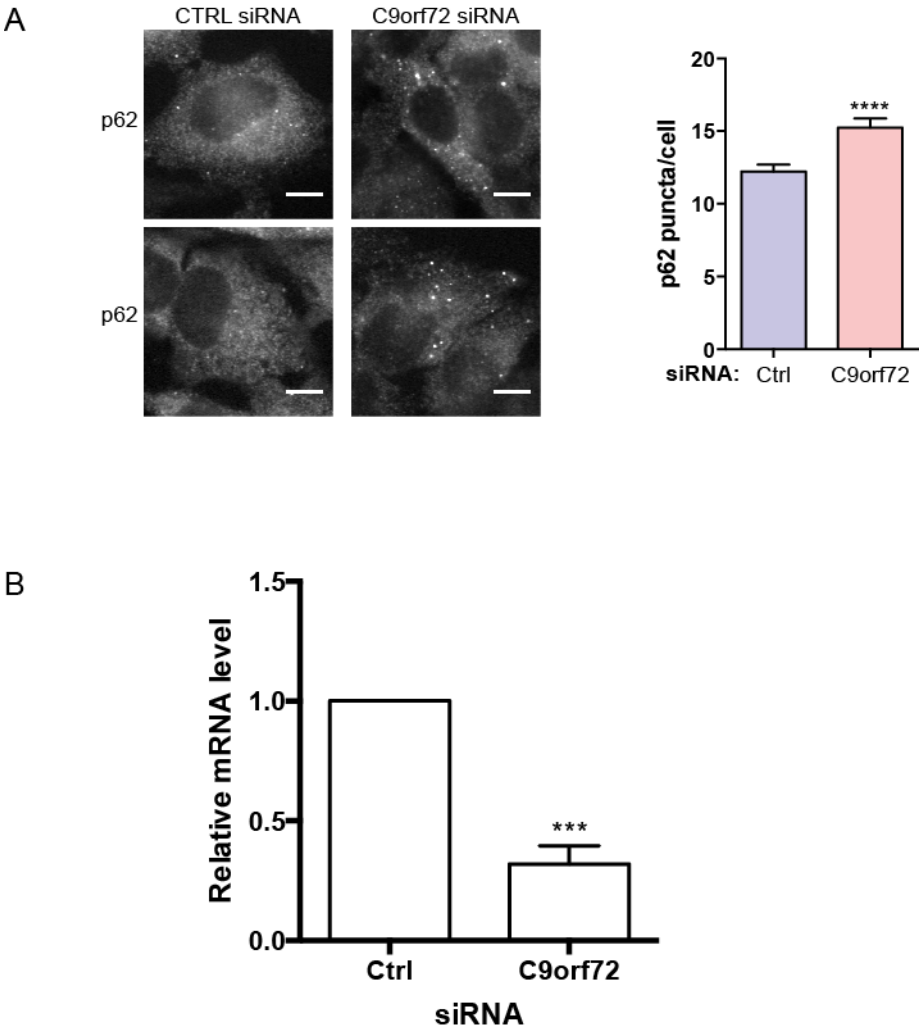

Figure 4.13 Loss of C9orf72 induces p62 accumulation. HeLa cells treated with non-targeting (Ctrl) or C9orf72 siRNA were immunostained for endogenous p62. Accumulation of p62 was quantified by counting p62 positive puncta per cell from 3 replicate experiments (Mean±SEM; Mann-Whitney test, **** $P \leq 0.0001$); N (cells) = Ctrl: 74, C9orf72: 55). C9orf72 knockdown was confirmed by RT-qPCR. Scale bar = 10µm.

4.2.9 C9orf72 ALS/FTD patient derived iNeurons show defective autophagy

To investigate the possibility that C9ALS/FTD patients are deficient in autophagy, the basal levels of autophagy were analysed in C9ALS/FTD patient derived iNeurons. iNeurons were generated by differentiation of induced neural progenitor cells from two C9ALS/FTD patients and their age and sex matched controls. Analysis of the C9orf72 mRNA by RT-qPCR revealed that patients had significantly less C9orf72 mRNA compared to controls, consistent with the idea that the C9orf72 repeat expansion causes haploinsufficiency of C9orf72 (Fig. 4.14C). Such a marked reduction in C9orf72 mRNA levels in patients compared to controls was even greater then the knockdown achieved in many of siRNA experiments detailed previously. To investigate basal levels of autophagy, cells were either untreated or treated with bafilomycin A_1 to inhibit progression of basal autophagy (Fig. 4.14A and B). LC3-I and LC3-II were detected in both controls, and both accumulated upon treatment with bafilomycin A_1 (Fig 4.14A and B). In line with reduced levels of autophagy, LC3-I was readily detected in untreated in C9ALS/FTD patient cells, while LC3-II was not (Fig. 4.14A and B). Treatment of patient cells with bafilomycin A_1 led to an accumulation of LC3-II, suggesting that autophagy was not completely inhibited in these cells (Fig. 4.14A and B). However, the levels of LC3-II were significantly lower than the levels of LC3-II in control iNeurons (Fig. 4.14A and B). Thus there was a clear deficit in basal autophagy in C9ALS/FTD patient iNeurons compared to controls.

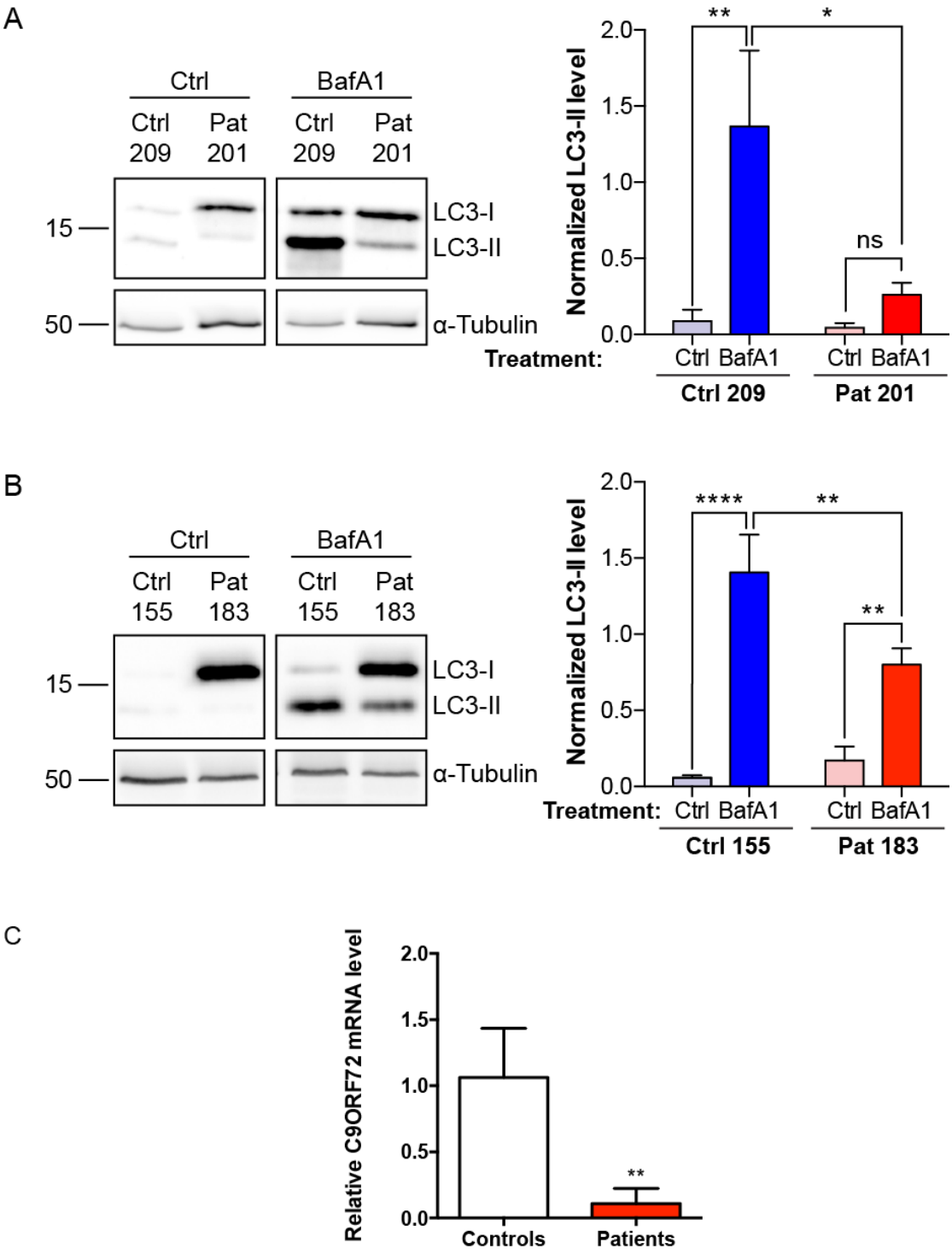

Figure 4.14 C9ALS/FTD patients have reduced basal autophagy. iPSC derived iNeurons from 2 controls (C155 and C209) and 2 confirmed C9orf72 patients (P183, and P201) were incubated with vehicle or BafA1 (100 nM; 6 h) to inhibit autophagy progression. Levels of LC3-I and LC3-II were determined on immunoblot. Levels of LC3-II were normalised to tubulin are shown. (Mean±SEM; 2-way ANOVA with Fisher's LSD test; * $p \leq 0.05$, ** $p \leq 0.01$, **** p

≤ 0.0001, N = 4 experiments). iNeurons were prepared by Dr. Laura Ferraiuolo and Miss Monika Myszczynska.

4.3 Discussion

In this chapter, C9orf72 was shown to regulate the induction of autophagy by mediating Rab1a dependent translocation of the ULK1 autophagy initiation complex.

The structural homology of C9orf72 with the DENN family of proteins suggested that C9orf72 might be a GEF for the Rab family of GTPases. In line with this, C9orf72 was shown to directly interact with Rab1a (Fig. 4.9). However, C9orf72 was found to preferentially interact with the active GTP-Rab1a rather than GDP-Rab1a, behaviour more associated with a Rab effector rather than a Rab GEF (Fig. 4.10). As reviewed by Grosshans et al 2006, there are multiple examples of Rab effector proteins binding their specific Rab (Grosshans et al., 2006). For example, the localisation of Rab5 to the endocytic vesicles is dependent upon its effector protein, Rabaptin-5, which binds GTP-Rab5 and brings it into contact with its partner Rab4 on endocytic vesicles (Korobko et al., 2005; Rubino et al., 2000).

In yeast, GTP bound Ypt1, the homologue of Rab1, is brought into contact with ATG1, the homologue of ULK1, by the action of ATG11 (Lipatova et al., 2012). As such, ATG11 functions as a Ypt1 effector protein. The fact that C9orf72 carries out many of the roles performed by ATG11 suggests C9orf72 may be the mammalian counterpart of ATG11 in terms of function. There is also evidence that Rab effectors and Rab GEFs work together in feedback mechanism, whereby the active Rab is brought to its correct site of action by its effector and maintained in the active state by the continued presence of the GEF. In the case of Ypt1 and ATG11, the transport protein particle (TRAPP) III complex functions as the autophagy specific GEF for Ypt1 (Lynch-Day et al., 2010; Wang et al., 2013). The TRAPPIII GEF complex is targeted to the PAS to maintain Ypt1 activity, possibly by the interaction of the TRAPPIII subunit Trs85, and ATG17, the yeast homologue of FIP200 (Kakuta et al., 2012; Lynch-Day et al., 2010; Wang et al., 2013). Indeed, the importance of Trs85 in autophagy is demonstrated by the fact that loss of Trs85 results in a decreased autophagic rate (Meiling-Wesse et al., 2005; Nazarko et al., 2005). The organisation of a Rab GTPase, a Rab effector and a Rab GEF is also found in the case of Rab5. While Rabaptin-5 localises active Rab5 to the endocytic vesicles, Rabaptin-5 can also bind and recruit the Rab5 GEF Rebex5 (Lippé et al., 2001). Thus, a

positive feedback loop is established, maintaining active Rab5 at the endocytic vesicle (Lippé et al., 2001). If C9orf72 were functioning as the mammalian homologue of ATG11, then the presence of a Rab1a GEF would also be expected to bind in this complex.

In mammalian cells, the TRAPPC8 protein has been identified as a distant homologue of Trs85, and is also important for autophagy induction (Behrends et al., 2010; Choi et al., 2011). However, unlike Trs85, which is known to bind ATG17, TRAPPC8 has not been identified as a FIP200 interacting protein. This potential difference in the binding partners of Trs85 and TRAPPC8 could suggest other autophagy related GEFs are required for the activation of Rab1a. From the same study that identified the potential interaction of C9orf72 and FIP200, as well as the role of TRAPPC8 in autophagy, SMCR8 was also identified as a potential FIP200 interacting protein (Behrends et al., 2010). As SMCR8 was shown to interact with C9orf72 in Chapter 3, this could suggest that, in a similar fashion to the Ypt1-ATG11-Trs85 module, SMCR8 functions as the autophagy specific GEF for Rab1a, interacting with the Rab1a effector protein, C9orf72, as well as the autophagy initiation protein FIP200, to maintain active Rab1a at the site of autophagosome formation.

ATG11 has a number of diverse roles in yeast. As detailed above, ATG11 recruits a number of essential autophagy proteins to the newly forming PAS, but also acts as a scaffold for the formation of the autophagosome, recruiting the ATG9 positive membranes (He et al., 2006). Recruitment of ATG9 vesicles appears to be essential for autophagosome formation (Mari et al., 2010). The mammalian homologue of ATG9, mATG9, is located within the trans-Golgi network, and redistributes to LC3 positive autophagosomes upon autophagy induction (Young et al., 2006). Rab1a is also located within similar Golgi structures and loss of Rab1 was shown to disrupt the redistribution of mATG9 to autophagosomes (Winslow et al., 2010). Thus as C9orf72 was shown to regulate the translocation of Rab1a to ULK1 in this Chapter, C9orf72, via its interaction with Rab1a, could also regulate the translocation of mATG9-positive vesicles to the ULK1 initiation complex and the autophagosomes. As Golgi derived membranes have also been implicated in autophagosome formation (Yen et al., 2010), the interaction between C9orf72 and Rab1a, as well as the possible regulation of mATG9, could be required for the delivery of double

membrane structures and the formation of functional autophagosomes during autophagy initiation.

The use of more then one method to investigate the autophagy pathway gave confidence that the results observed were reliable, which is standard procedure with such assays (Klionsky et al., 2012). The same approach was taken for many other experiments within this thesis. Unfortunatly, the interaction between Rab1a and ULK1 was only investigated by PLA. Proximity signals only indicate two potential binding partners are within 50 nm of each other, and do not confirm an actual interaction. As such this interaction should be investigated in more detail, potentially via co-immunoprecipitation or *in vitro* binding assays.

Although this chapter identified C9orf72 as a Rab1a effector protein, it cannot be ruled out that C9orf72 is also capable of acting as a GEF for another autophagy related Rab. A common feature of the Rab GTPase family is the so-called Rab cascade whereby one activated Rab recruits a further downstream Rab (Ortiz et al., 2002). In this sense, while C9orf72 may be important for Rab1a recruitment to the ULK1 initiation complex, it may also be required for GEF activity on another Rab. These other targets could include other autophagy related Rabs as detailed in section 1.5.2.5, or those suggested to co-localise with C9orf72 in previous studies (Farg et al., 2014).

C9orf72 is not the only Rab associated protein known to be involved in the pathogenesis of ALS. The Rab5 GEF Alsin (ALS2) is associated with juvenile onset ALS (Hadano et al., 2001a; Hadano et al., 2010; Hadano et al., 2001b). As mentioned above, Rab5 is classically thought to function in the endocytic pathway, aiding the homotypic fusion of endocytic vesicles (Lippé et al., 2001; Rubino et al., 2000; Topp et al., 2004). However, Rab5 is also linked to the autophagy pathway, regulating the formation of the Vps34 class III PI3K complex and also inhibiting mTORC1 (Ao et al., 2014; Dou et al., 2013; Li et al., 2010; Ravikumar et al., 2008; Su et al., 2011). While Rab1a functions in translocation of the initiation complex, Rab5 appears to act further downstream, regulating the elongation of the autophagosome membrane (Ravikumar et al., 2008). Mutations to Alsin, which disrupt correct GEF activity to Rab5, therefore also lead to dysfunctional autophagy (Otomo et al., 2011). Loss of Alsin and dysfunctional autophagy may therefore lead to the development of ALS. The role of autophagy in neuronal health is well established (Komatsu et al., 2006).

Beside the fact that the post-mitotic nature of neurons means they must have effective recycling and maintenance pathways, neural specific loss of many autophagy genes is has been shown to lead to neurodegeneration. Neural specific loss of *RB1CC1* (FIP200), *ATG7* or *ATG5* in mice leads to neurodegeneration, progressive motor defects as well as the accumulation of cytoplasmic neural inclusion bodies (Hara et al., 2006; Komatsu et al., 2006; Liang et al., 2010). The cerebellum of these mice appears to be particularly effected by loss of these genes and the subsequent disruption to autophagy, suggesting a high autophagic demand by this tissue. Interestingly, C9ALS/FTD patients also develop p62 specific accumulations in the cerebellum suggesting an autophagy defect (Al-Sarraj et al., 2011; Cooper-Knock et al., 2012; Mahoney et al., 2012), which was replicated by C9orf72 knockdown in Fig. 4.13. Thus, as C9orf72 has been identified as a regulator of autophagy initiation, loss of C9orf72 in patients would result in a defective autophagy pathway. This is supported by the fact that iNeurons from C9ALS/FTD patients, who showed reduced C9orf72 mRNA levels, were also found to be deficient in basal levels of autophagy (Fig. 4.14). It would be interesting to determine whether the relative level of C9orf72 in patients gives any indication of disease severity, or age of onset. The marked reduction in C9orf72 mRNA levels in patient iNeurons compared to controls was consistent with previous reports (Belzil et al., 2013; Cooper-Knock et al., 2012; Gijselinck et al., 2012; Xi et al., 2013). However, whether the two patients used in this study are representative of all C9ALS/FTD patients remains to be seen. Whether such a significant difference between the level of C9orf72 mRNA in patients and the controls is always present and whether this leads to a worsening effect should be investigated and documented further.

While basal autophagy in these iNeurons was investigated, the ability of these cells to induce autophagy above basal levels was not. Aside from the mTOR inhibitors used in this Chapter, the level of autophagy induction after a more physiologically relevant induction should be investigated, namely starvation.

The evidence from the patient iNeurons supports the role of C9orf72 in autophagy in C9ALS/FTD as identified by the siRNA knock down studies. However, there is potential for off target effects when using siRNA (Fedorov et al., 2006). For this reason the gold standard in siRNA experiments would be to rescue the defect by overexpression of an siRNA-resistant form C9orf72

(Cullen, 2006). If the resistant over-expression construct is able to alleviate the defect, then one can be confident that the effect observed by knock down is specific. As with the previous Chapter, conducting such experiments on more neuronal cell populations or, better still, primary neuronal cells would greatly support the role of C9orf72 in the autophagy pathway and its relevance to C9ALS/FTD.

5 C9orf72 turnover and stability

5.1 Introduction

If haploinsufficiency of C9orf72 is an underlying cause of C9ALS/FTD, possibly by inhibition of autophagy induction (see Chapter 4), then restoring/increasing C9orf72 protein levels could be of therapeutic benefit.

Protein levels are controlled by balancing their synthesis and breakdown, referred to as protein turnover. As discussed in Chapter 1, two pathways mediate protein degradation in eukaryotic systems: the ubiquitin proteasome system (UPS) and autophagy. Both UPS and autophagy-mediated degradation involves substrate ubiquitination. Much like phosphorylation, ubiquitination is a dynamic and reversible post-translational modification (Komander et al., 2009). The removal of ubiquitin from protein substrates is mediated by the de-ubiquitinating enzymes (DUBs). Under physiological conditions ubiquitination levels are controlled by the opposing action of E3 Ubiquitin ligases and DUBs. Thus both classes of enzymes could be possible therapeutic targets for the treatment of C9orf72 haploinsufficiency.

In this chapter the half-life of C9orf72 was determined and the role of the UPS and autophagy in its degradation investigated. Using bioinformatics approaches the predicted possible regulatory ubiquitination sites on C9orf72 were investigated and one mutated to investigate its effect on C9orf72 turnover. Finally, the interaction of C9orf72 and USP8 was investigated, as was the role of USP8 in the regulation of C9orf72 turnover.

5.2 Results

5.2.1. Determination of the half-life of C9orf72

Firstly, the stability of C9orf72S and C9orf72L was characterised using cycloheximide (CHX) chase assays. The principle of these assays is to inhibit protein translation using CHX, which functions by binding to the 60S ribosome (Schneider-Poetsch et al., 2010) and measure protein levels over time after inhibition. As no new protein is synthesised after addition of CHX it is possible to determine the rate of degradation of a protein with the protein level at the time of CHX addition being 100%. Protein degradation is exponential and so to gain a more accurate value for protein half-life, the natural log (ln) of the calculated

protein levels is plotted against time to produce a straight-line curve. According to the laws of exponential decay, the gradient of this line is equal to the decay constant of the substance of interest, in this case the decay constant of C9orf72. This decay constant (λ) can then be used to solve the decay law equation ($N = N_0 e^{-\lambda t}$) with respect to $t_{1/2}$ or half-life, where λ is the decay constant, N is the amount of protein remaining at time t and N_0 is the amount of protein at time 0. Solving this equation with respect to $t_{1/2}$ gives: $t_{1/2} = \ln(2)/\lambda$. This method of half-life calculation was previously described (Belle et al., 2006).

To determine the half-life of C9orf72, HEK293 cells were transfected with Myc-C9orf72S or Myc-C9orf72L. 24 h post transfection protein translation was inhibited with CHX and the levels of C9orf72S or C9orf72L measured over time on immunoblots to detect the Myc tag. The half-life of C9orf72L was calculated as 2.29 h ± 0.37 h (mean ± SEM) (Fig. 5.1A and C). C9orf72S was found to have a half-life of 1.12 h ± 0.18 h (mean ± SEM) (Fig. 5.1B and C), which was significantly shorter than the half-life of C9orf72L (Fig. 5.1C).

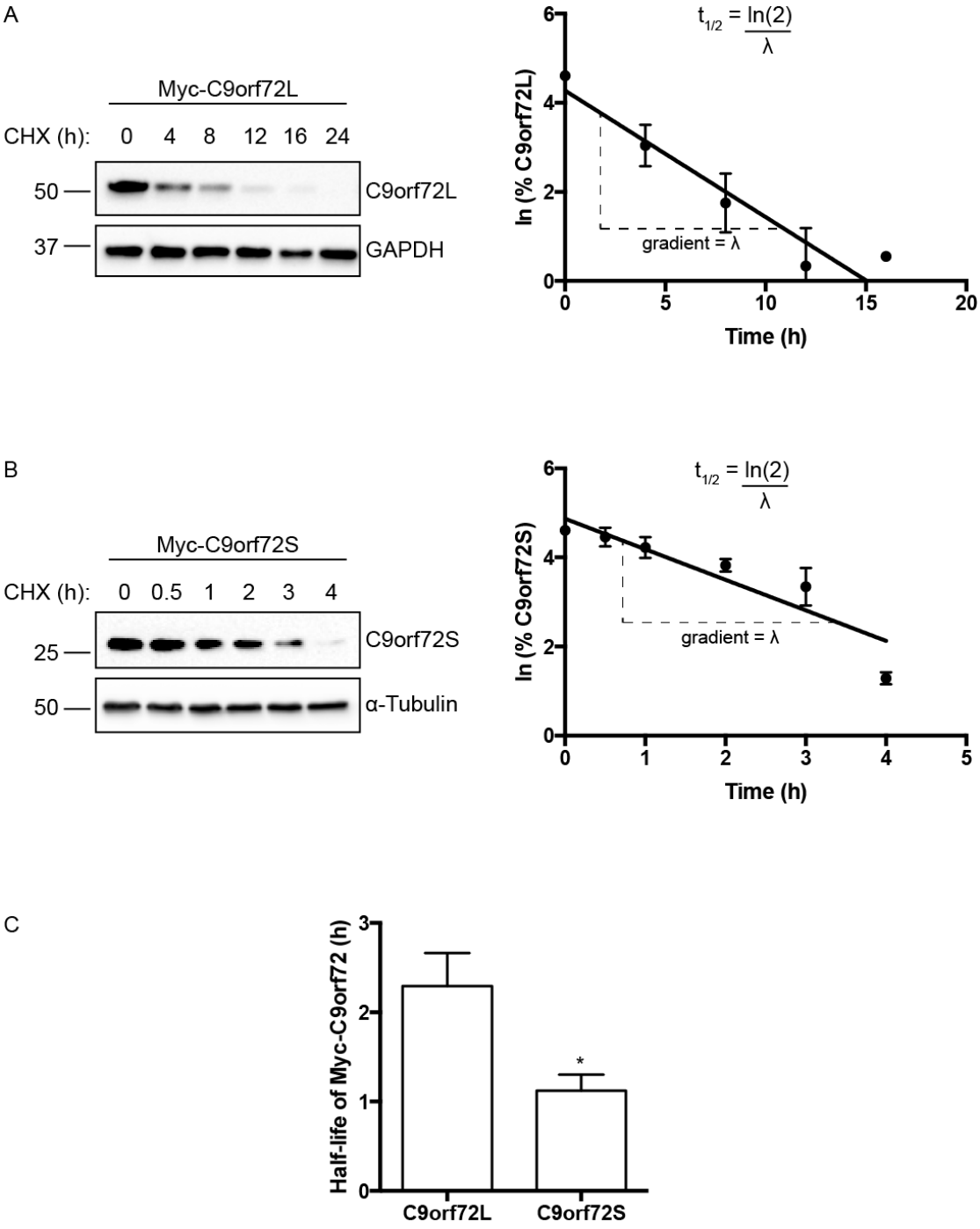

Figure 5.1 Half-life of C9orf72. HEK293 cells were transfected with Myc-C9orf72L (A) or Myc-C9orf72S (B). 24 h post transfection cells were treated with the translational inhibitor cycloheximide (CHX) for the indicated times. After treatments cells were lysed and subjected to SDS-PAGE and immunoblot. Blots were probed for Myc-C9orf72 and either GAPDH or α-Tubulin as loading controls. Relative levels of C9orf72L (A) and C9orf72S (B) were taken as a percentage and the natural log (ln) of these values plotted against time to produce the corresponding graphs. (C) Using the gradient of the decay curve

graph and the decay equation, ($t_{1/2}$ = ln(2)/decay constant, the half-life of C9orf72L and C9orf72S was calculated across the 3 experiments. The bar graph shows the comparison of the half-life of C9orf72L with C9orf72S. (Mean±SEM; unpaired t-test, * $p \leq 0.05$; N = 3 experiments).

5.2.2. C9orf72 is a substrate of the proteasome

To determine whether C9orf72 was a substrate of the UPS or the autophagy pathway, C9orf72 CHX chase assays were conducted in the presence of the selective proteasome inhibitor MG132 or the autophagy inhibitor bafilomycin A_1.

HEK293 cells were transfected with Myc-C9orf72S or Myc-C9orf72L and 24 h post transfection protein translation was blocked with CHX alone, CHX in the presence of bafilomycin A_1 or CHX in the presence of MG132. The levels of C9orf72 protein were measured over time on immunoblots using 9B11 anti-Myc antibodies to detect the Myc tag. As above, both C9orf72S and C9orf72L were rapidly degraded after addition of cycloheximide alone (Fig. 5.2 and 5.3). The addition of bafilomycin A_1 during treatment with cycloheximide had no effect on the stability of C9orf72S (Fig. 5.2) or C9orf72L (Fig. 5.3). However, the addition of MG132 significantly delayed the degradation of C9orf72S (Fig. 5.2) and completely halted the degradation of C9orf72L during the 24h time period analysed (Fig. 5.3). Thus, C9orf72 is mainly degraded via the UPS.

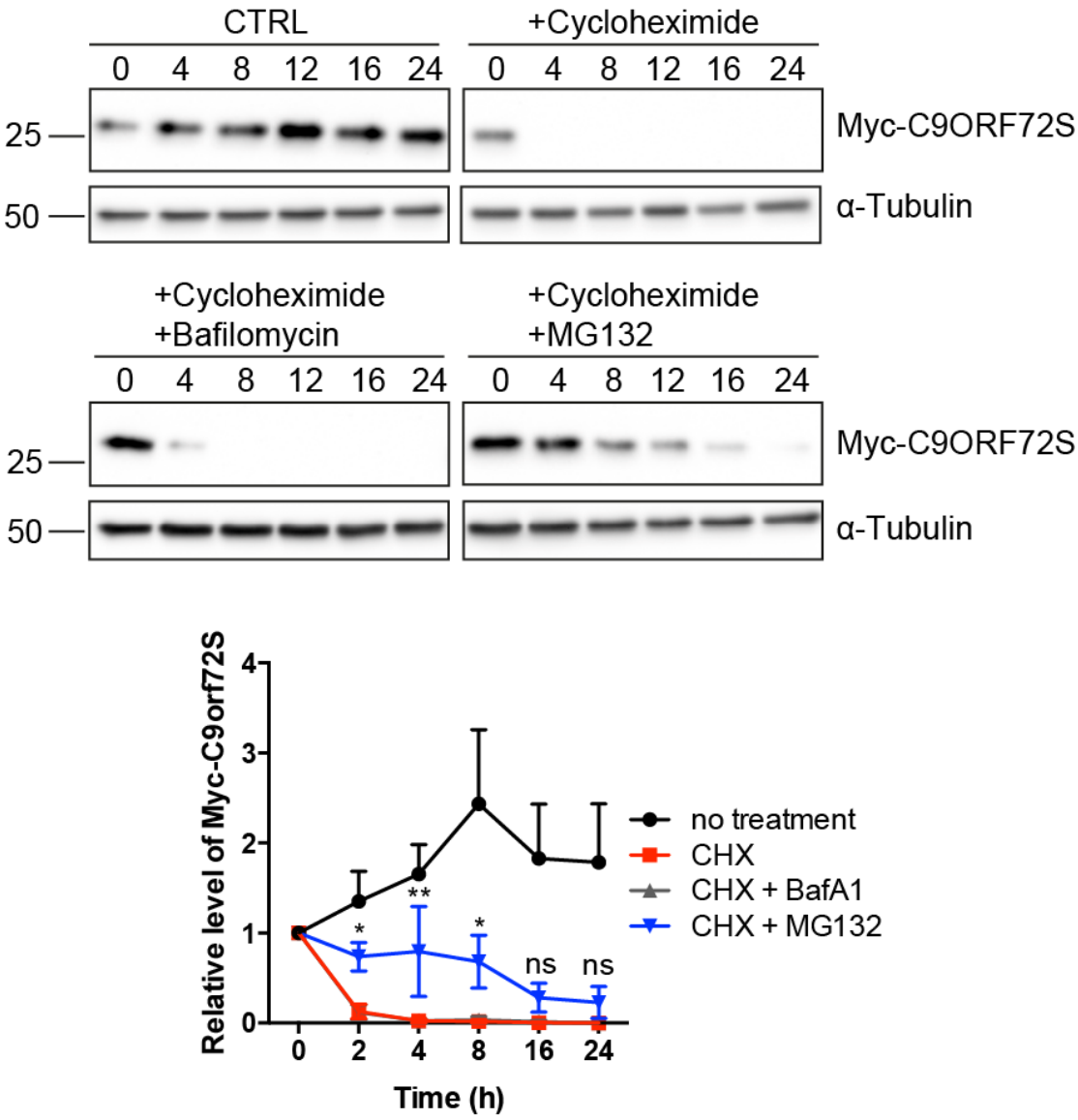

Figure 5.2 C9orf72S is a substrate of the proteasome. HEK293 cells were transfected with Myc-C9orf72S. 24 h post transfection cells were untreated, treated with cycloheximide, cycloheximide and bafilomycin A_1 or cycloheximide and MG132 for the indicated times (h). After treatments cells were lysed and subjected to SDS-PAGE and immunoblot. Blots were probed for anti-Myc-C9orf72 and α-Tubulin as a loading control. Line graph depicts mean relative levels of Myc-C9orf72S (normalised to α-Tubulin) at the indicated times of no-treatment (black circles), cycloheximide treatment (red squares), cycloheximide and bafilomycin A_1 treatment (grey triangles) or cycloheximide and MG132 treatment (blue triangles) (Mean±SEM; two-way ANOVA with Fisher's LSD test; * $p \leq 0.05$, ** $p \leq 0.01$; N = 3 experiments).

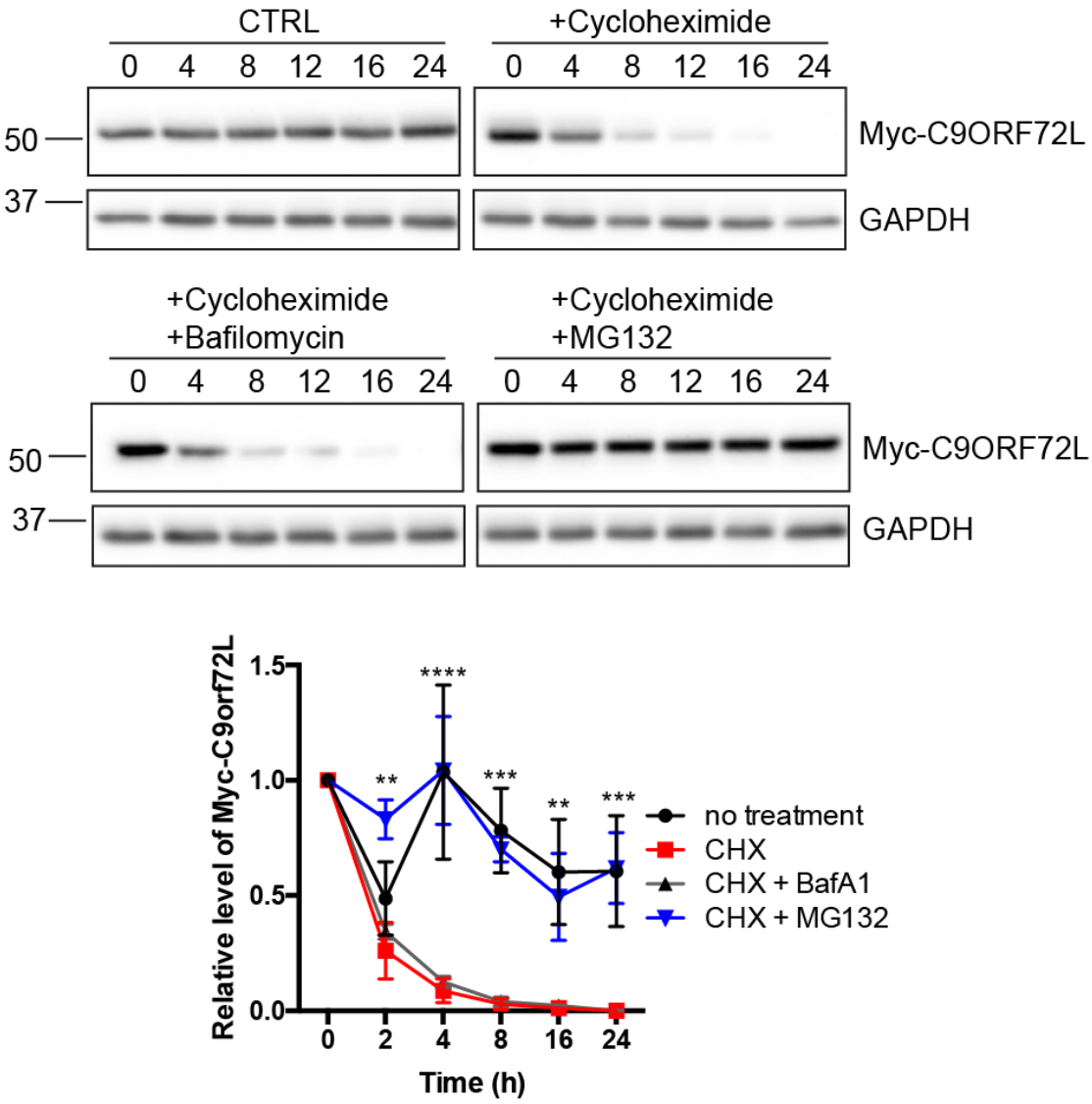

Figure 5.3 C9orf72L is a substrate of the proteasome. HEK293 cells were transfected with Myc-C9orf72L. 24 h post transfection cells were untreated, treated with cycloheximide, cycloheximide and bafilomycin A_1 or cycloheximide and MG132 for the indicated times (h). After treatments cells were lysed and subjected to SDS-PAGE and immunoblot. Blots were probed for Myc-C9orf72 and GAPDH as a loading control. Line graph depicts mean relative levels of Myc-C9orf72L (normalised to GAPDH) at the indicated times of no-treatment (black circles), cycloheximide treatment (red squares), cycloheximide and bafilomycin A_1 treatment (grey triangles) or cycloheximide and MG132 treatment (blue triangles) (Mean±SEM; two-way ANOVA with Fisher's LSD test; ** $p \leq 0.01$, *** $p \leq 0.001$, **** $p \leq 0.0001$; N = 3 experiments).

5.2.3. Mutation of Lysine 14 extends the half-life of C9orf72L

Substrates of the proteasome are targeted for degradation by addition of ubiquitin moieties to their lysine residues. These residues become poly-ubiquitinated by the addition of more ubiquitin moieties to internal lysine residues within the initial ubiquitin molecule, most commonly at lysine 48. The size and type of these ubiquitin chains plays a critical role in the fate of the protein. Tetra ubiquitination of a substrate linked through lysine 48 appears to be the minimum signal for degradation of a substrate by the proteasome (Thrower et al., 2000).

C9orf72 contains 26 lysine residues as detailed in Fig. 5.4. To analyse which of these lysines was the most likely to be ubiquitinated, the C9orf72L protein sequence was entered into the ubiquitination site prediction software, UbPred. UbPred uses a database consisting of 266 experimentally verified ubiquitination sites to predict potential ubiquitination sites within a target sequence of interest (Radivojac et al., 2010). Of all possible lysines UbPred identified lysine 14 as the most likely site for ubiquitination (Figure 5.4 and Table 5.1).

MSTLCPPPSPAVAKTEIALSGKSPLLAATFAYWDNILGPRVRHIWAPKTEQVLL
SDGEITFLANHTLNGEILRNAESGAIDVKFFVLSEKGVIIVSLIFDGNWNGDRST
YGLSIILPQTELSFYLPLHRVCVDRLTHIIRKGRIWMHKERQENVQKIILEGTERM
EDQGQSIIPMLTGEVIPVMELLSSMKSHSVPEEIDIADTVLNDDDIGDSCHEGFL
LNAISSHLQTCGCSVVVGSSAEKVNKIVRTLCLFLTPAERKCSRLCEAESSFKY
ESGLFVQGLLKDSTGSFVLPFRQVMYAPYPTTHIDVDVNTVKQMPPCHEHIYN
QRRYMRSELTAFWRATSEEDMAQDTIIYTDESFTPDLNIFQDVLHRDTLVKAFL
DQVFQLKPGLSLRSTFLAQFLLVLHRKALTLIKYIEDDTQKGKKPFKSLRNLKID
LDLTAEGDLNIIMALAEKIKPGLHSFIFGRPFYTSVQERDVLMTF

Figure 5.4 UbPred predicted ubiquitination sites of C9orf72L. The C9orf72L amino acid sequence was entered into the UbPred ubiquitination site prediction software. All 26 lysine residues are indicated with lysine 14 marked in blue. Lysine 14 was scored with medium confidence as a potential ubiquitination site.

Table 5.1: C9orf72L lysine residues and UbPred scores

Residue	Score	Ubiquitinated
14	0.79	Yes Medium confidence
22	0.61	No
48	0.47	No
83	0.61	No
90	0.53	No
141	0.41	No
148	0.4	No
156	0.52	No
191	0.55	No
243	0.44	No
246	0.29	No
261	0.38	No
273	0.59	No
285	0.52	No
316	0.39	No
378	0.51	No
388	0.32	No
408	0.52	No
414	0.3	No
422	0.18	No
424	0.09	No
425	0.14	No
428	0.22	No
434	0.48	No
454	0.41	No
456	0.27	No

Label	Score range	Sensitivity	Specificity
Low confidence	0.62 ≤ s ≤ 0.69	0.464	0.903
Medium confidence	0.69 ≤ s ≤ 0.84	0.346	0.950
High confidence	0.84 ≤ s ≤ 1.00	0.197	0.989

Lysine (K) to arginine (R) mutation is a common method to prevent ubiquitination of a protein (Rodriguez et al., 2000; Rufini et al., 2011). Therefore, to investigate whether ubiquitination on lysine 14 was involved in C9orf72 degradation via the proteasome, the lysine 14 residue was mutated to arginine and the half-life of C9orf72L K14R determined in CHX chase assays. The cloning of C9orf72L K14R is detailed in section 2.2.1.6.

HEK293 cells were transfected with either Myc-C9orf72L or Myc-C9orf72L K14R. 24 h post transfection protein translation was inhibited using CHX and the levels of C9orf72 protein were measured over time on immunoblots. The half-life of C9orf72L is this experiment was calculated as 3.2 h ± 0.29 h (mean ± SEM) (Fig. 5.5), similar to the value calculated in previously (Fig. 5.1A). The K14R mutation significantly extended the half-life of C9orf72L to 5.46 h ± 0.02 h (mean ± SEM; Fig. 5.5) suggesting that K14 ubiquitination is involved in C9orf72 degradation by the proteasome.

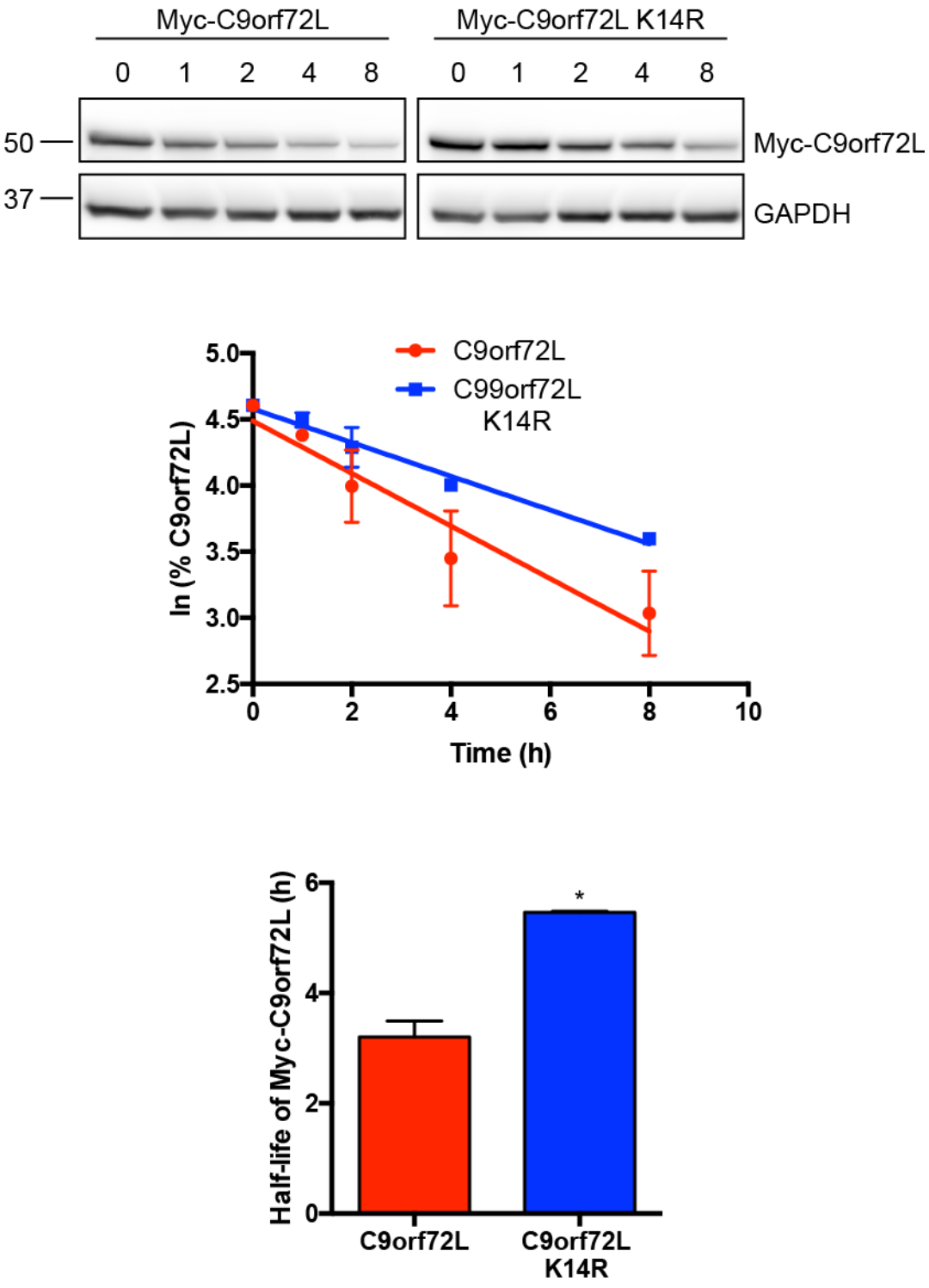

Figure 5.5 Mutation of lysine 14 extends the half-life of C9orf72L. HEK293 cells were transfected with Myc-C9orf72L or Myc-C9orf72L K14R. 24 h post transfection cells were treated with cycloheximide for the indicated times. After treatment cells were lysed and subjected to SDS-PAGE and immunoblot. Blots were probed for Myc-C9orf72L and GAPDH as a loading control. Decay curve

depicts mean relative levels of C9orf72L (red circles) and C9orf72 K14R (blue squares) at the indicated times of cycloheximide treatment. Bar chart depicts the comparison of the half-life of C9orf72L or C9orf72 K14R. (Mean±SEM; unpaired t-test, * $p \leq 0.05$; N = 2 experiments).

5.2.4. C9orf72 interacts with USP8

The Y2H screen conducted in Chapter 3 identified USP8 as a possible interaction partner of C9orf72S (Table 3.2). USP8, also known as Ubiquitin-specific protease Y (UBPy), is a ubiquitin isopeptidase of the USP family of cysteine proteases and is particularly abundant in the brain and testis (Gnesutta et al., 2001; Naviglio et al., 1998). USP8 has been shown to interact with a number of proteins substrates including the Ras nucleotide exchange factor CDC25, TrkA and NRDP1, leading to their subsequent deubiquitination (Ceriani et al., 2015; Gnesutta et al., 2001; Wu et al., 2004). USP8 depletion in cells leads to increased global ubiquitination and enlargement of MVBs and endosomal structures. (Row et al., 2006). Thus USP8 may function to regulate the ubiquitination and stability of C9orf72.

To confirm the interaction between C9orf72 and USP8, co-immunoprecipitation experiments were conducted. HEK293 cells were co-transfected with EGFP or EGFP-USP8 and either empty vector, Myc-C9orf72S or Myc-C9orf72L. C9orf72 was isolated using anti-Myc antibodies and immune pellets analyzed by SDS-PAGE and immunoblot. C9orf72 was specifically enriched in the immunoprecipitated samples. EGFP did not co-immunoprecipitate with either C9orf72 isoform, while EGFP-tagged USP8 specifically co-immunoprecipitated with both C9orf72 isoforms (Fig. 5.6). Thus C9orf72 interacts with the DUB enzyme USP8.

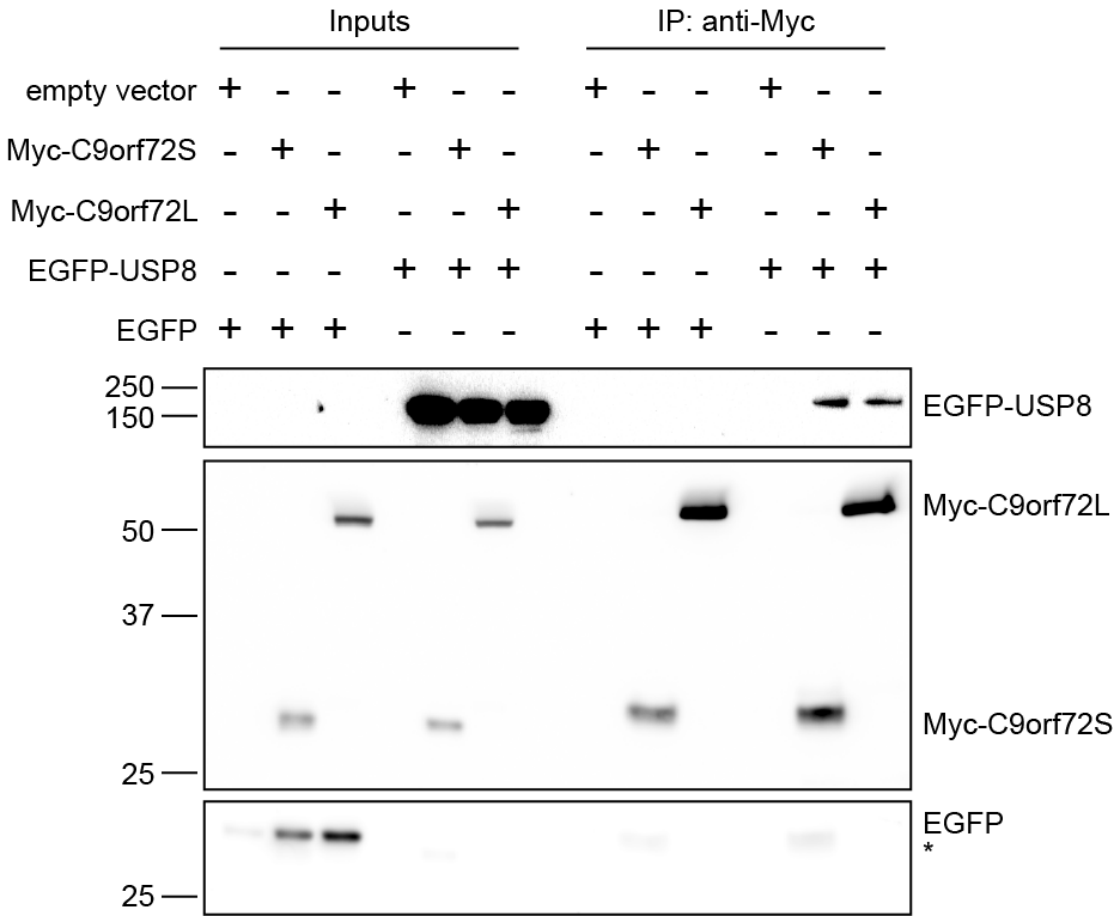

Figure 5.6 C9orf72 interacts with USP8. Whole cell lysates of HEK293 cells co-transfected with empty vector, Myc-C9orf72S or Myc-C9orf72L and either EGFP or EGFP-USP8 were subjected to immunoprecipitation with rabbit anti-Myc 9106 antibodies. Immune pellets were probed for Myc-C9orf72 with mouse anti-Myc 9B11 antibodies and EGFP and EGFP-USP8 using mouse JL8 anti-GFP antibodies on immunoblot. Blots were initially cut at approximately 75 – 100 kDa. The top section was probed with mouse JL8 mouse anti-GFP antibodies (top panel) and the lower section probed with 9B11 mouse anti-Myc antibodies (middle panel). This lower section was then re-probed with JL8 mouse anti-JL8 antibodies to detect GFP control (bottom panel). The * indicates the Myc-C9orf72S bands present in the IP samples after the initial detection with anti-Myc antibodies.

5.2.5. USP8 extends the half-life of C9orf72L

To investigate whether USP8 regulates the stability of C9orf72 by deubiquitination, the half-life of C9orf72 was investigated in cells overexpressing USP8 using CHX chase assays.

HEK293 cells were co-transfected with Myc-C9orf72L or Myc-C9orf72S and either EGFP or EGFP-USP8. 24 h post transfection protein translation was inhibited with CHX and the levels of C9orf72 measured over time on immunoblots. USP8 overexpression caused an increase in C9orf72S and C9orf72L protein levels at time 0, indicating that USP8 can stabilize and increase C9orf72 protein levels (Fig. 5.7 and 5.8). This was confirmed in the half-life analysis.

The half-life of C9orf72L co-transfected with only the EGFP control was calculated as 2.82 h ± 0.1 h (mean ± SEM) (Fig 5.7), similar to the half-life calculated in Fig. 5.1 and 5.5. USP8 overexpression significantly increased the half-life of C9orf72L to 5.87 h ± 0.64 h (mean ± SEM) (Fig. 5.7) suggesting that USP8 is able to stabilize C9orf72L possibly by deubiquitinating C9orf72L and preventing its degradation by the proteasome. The half-life of C9orf72S co-transfected with EGFP control was more than double that seen in cells transfected with only Myc-C9orf72S (2.86 h v 1.12 h; see Fig. 5.1B and C). Nevertheless, as was the case for C9orf72L, USP8 overexpression significantly increased the half-life of C9orf72S from 2.86 h ± 0.05 (mean ± SEM) to 3.45 h ± 0.22 h (mean ± SEM) (Fig. 5.8).

Taken together these data implicate USP8 in the turnover of C9orf72.

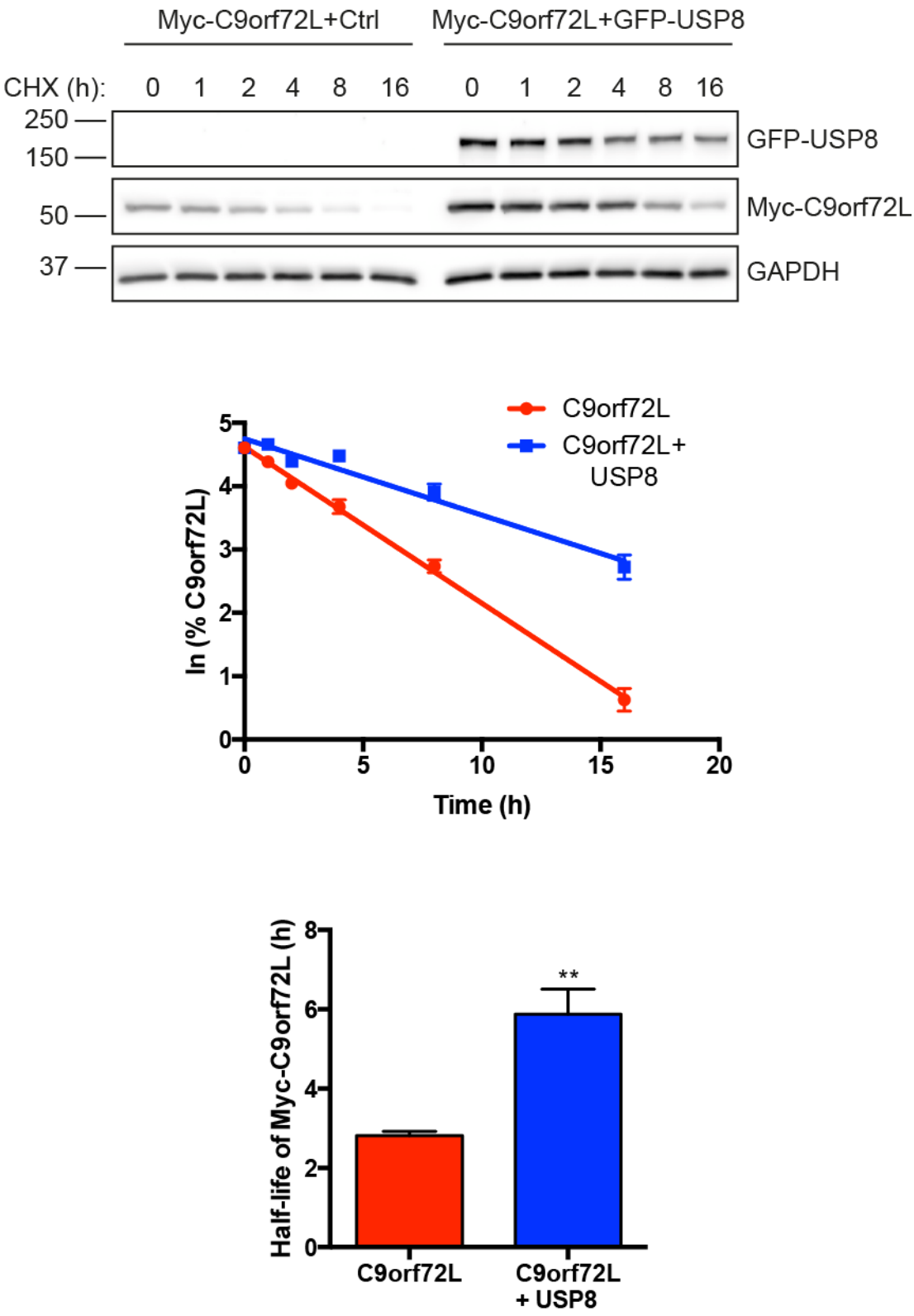

Figure 5.7 USP8 extends the half-life of C9orf72L. HEK293 cells were co-transfected with Myc-C9orf72L and either EGFP or EGFP-USP8. 24 h post transfection cells were treated with cycloheximide (CHX) for the indicated times. After treatments cells were lysed and subjected to SDS-PAGE and immunoblot.

Blots were probed for Myc-C9orf72L, EGFP, EGFP-USP8 and GAPDH as a loading control. Decay curve depicts ln of relative percentages of Myc-C9orf72L (red circles) or Myc-C9orf72L in the presence of USP8 (blue squares) at the indicated times of cycloheximide treatment. Bar chart depicts the comparison of the half-life of C9orf72L alone or in the presence of USP8 overexpression. (Mean±SEM; unpaired t-test, ** $p \leq 0.01$; N = 3 experiments).

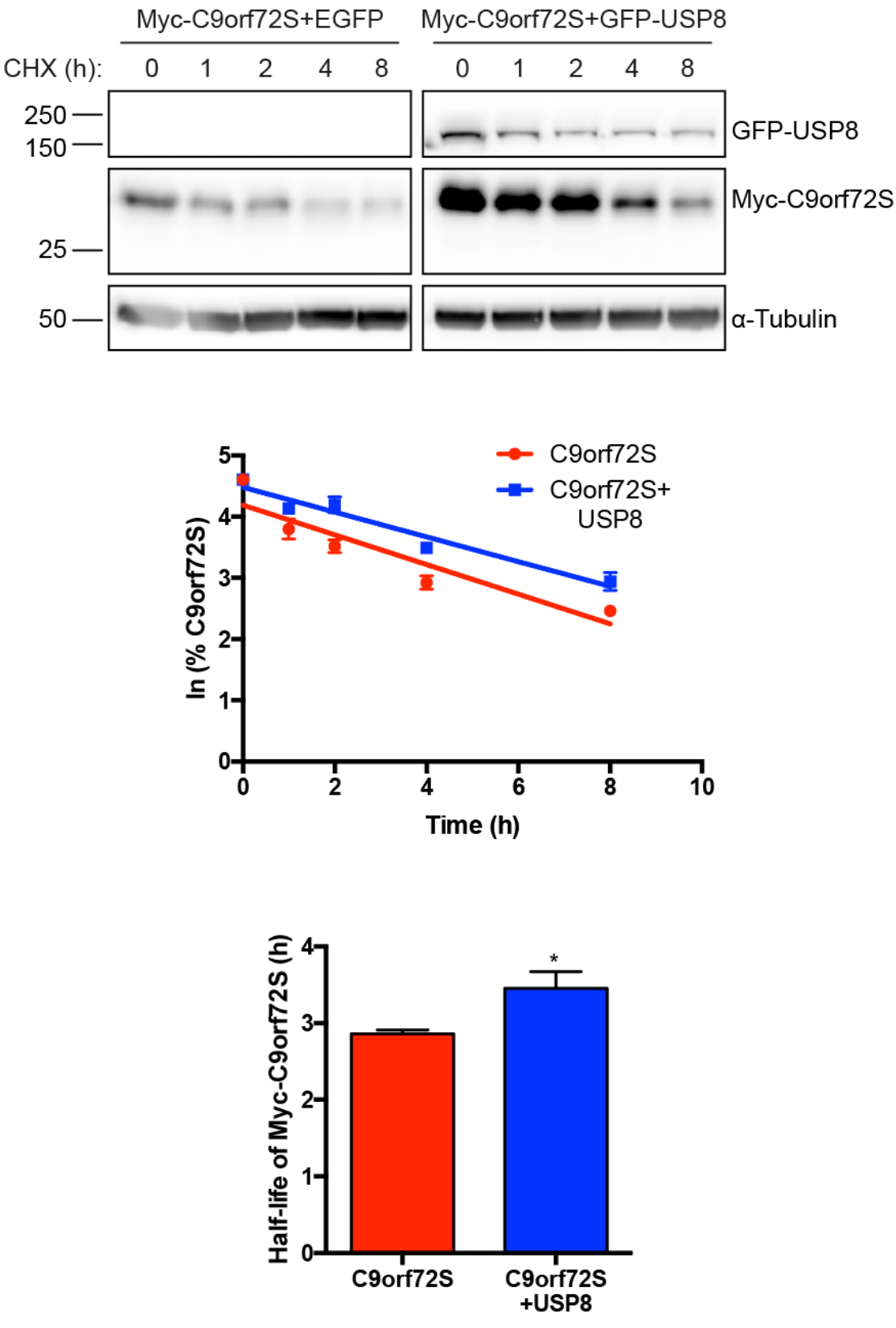

Figure 5.8 USP8 extends the half-life of C9orf72S. HEK293 cells were co-transfected with Myc-C9orf72S and either EGFP or EGFP-USP8. 24 h post transfection cells were treated with cycloheximide (CHX) for the indicated times.

After treatments cells were lysed and subjected to SDS-PAGE and immunoblot. Blots were probed for Myc-C9orf72S, EGFP, EGFP-USP8 and α-Tubulin as a loading control. Decay curve depicts ln of relative percentages of Myc-C9orf72S (red circles) or Myc-C9orf72S in the presence of USP8 (blue squares) at the indicated times of cycloheximide treatment. Bar chart depicts the comparison of the half-life of C9orf72S alone or in the presence of USP8 overexpression. (Mean±SEM; unpaired t-test, * $p \leq 0.05$; N = 3 experiments).

5.3. Discussion

This chapter has identified C9orf72 as a substrate of the proteasome and implicates K14 ubiquitination and the DUB USP8 as regulators of C9orf72 turnover.

The involvement of C9orf72 in autophagy initiation detailed in Chapter 4, therefore suggests that USP8, via its regulation of C9orf72, could also be involved in autophagy regulation. USP8 has previously been implicated in endocytic trafficking events, mediating the stability of the endosomal protein, hepatocyte growth factor-regulated tyrosine kinase substrate (Hrs) binding protein (Hbp), which is involved in growth factor receptor degradation via the endosome (Kato et al., 2000). USP8 appears to be localized to the endosomal compartment by the interaction of its N-terminal microtubule interacting and transport (MIT) domain with the CHMP family of proteins of the ESCRT machinery (Row et al., 2007). Endosomal enlargement resulting from USP8 knockdown suggests loss of USP8 leads to disruption of endocytic trafficking events and degradation (Row et al., 2006).

The catalytic activity of USP8 is regulated by Src-dependent phosphorylation (Meijer et al., 2013; Mizuno et al., 2007). The phosphorylation status of USP8 also regulates the binding of 14-3-3 proteins, which negatively regulate the catalytic activity of USP8, potentially by changing the conformation of the USP8 active site (Meijer et al., 2013; Mizuno et al., 2007). 14-3-3ζ has been shown to negatively regulate autophagy by binding the PI3K, Vps34 (Pozuelo-Rubio, 2011). Upon autophagy initiation 14-3-3ζ dissociates from Vps34, allowing for progression of autophagy (Pozuelo-Rubio, 2011). Thus in a similar fashion, autophagy induction could also release 14-3-3 from USP8, leading to activation of USP8 and the deubiquitination of C9orf72. By preventing the turnover of C9orf72 and increasing C9orf72 protein levels, this may facilitate the ULK1-Rab1a interaction and the induction of autophagy as described in Chapter 4. USP8 is further implicated in autophagy due to its interaction with Nbr1, a ubiquitin scaffold protein that functions in a similar way to p62 (Waters et al., 2009).

USP8 is also implicated in mitophagy by regulating Parkin ubiquitination; de-ubiquitination of Parkin by USP8 allows for the correct recruitment of Parkin to

dysfunctional mitochondria, thus mediating their clearance by the PINK1/Parkin pathway and mitophagy (Durcan et al., 2014). The data presented in this Chapter directly links C9orf72, which regulates the initiation of autophagy (Chapter 4) with a known regulator of mitophagy. As C9orf72 was shown to interact with the mitochondrial Cox6C protein (Chapter 3), it may be that C9orf72 delivers USP8 to mitochondria, via its interaction with Cox6C, to allow for the effective stabilisation of Parkin and efficient mitophagy. Thus in a positive feedback mechanism, USP8 could deubiquitinate and stabilise C9orf72, leading to an increase in C9orf72 levels, which allows for the increased recruitment of USP8 to the mitochondria via the interaction of C9orf72 and Cox6C. C9orf72 could therefore be the regulator of USP8 delivery to the mitochondrial network. If the interaction of C9orf72 with Cox6C were promoted under conditions of mitochondrial depolarisation then C9orf72 would increase the delivery of USP8 to depolarised mitochondria to increase the stabilisation of Parkin, and the induction of mitophagy.

The ability for C9orf72 to function as the homologue of ATG11 (Chapter 4) is also relevant for the role of C9orf72 and USP8 in mitophagy. Upon the induction of mitophagy in yeast, ATG11 localises to the mitochondria, via its interaction with ATG32, and recruits the mitochondrial fission machinery to bring about isolation of the damaged organelles from the mitochondrial network (Mao et al., 2013). Thus, if C9orf72 is able to function as ATG11, then C9orf72 may be involved in isolation of damaged mitochondria from the network via the interaction with Cox6C and the recruitment of USP8, and ultimately the ULK1 initiation complex.

The idea of stabilising C9orf72 or modulating C9orf72 levels is particularly interesting in terms of treatment for C9ALS/FTD. If indeed the autophagy defect associated with loss of C9orf72 described in this thesis is a contributing factor to disease, then modulating C9orf72 stability and half-life could be one method to increase C9orf72 protein levels. This Chapter shows that ubiquitination is important for the regulation of C9orf72. Consequently both E3 ligases and DUBs are candidates to help modulate C9orf72 protein levels. Increasing the activity of a DUB could prove to be more complicated than inhibiting the action of an E3 ligase. Furthermore, as there are fewer DUBs relative to the E3 ligases, DUBs may be considered to be more promiscuous in terms of protein targets. Therefore, increasing DUB activity could have more detrimental off target effects

that targeting an E3 ligase with a specific protein target. For example, while increasing the activity of USP8 in C9ALS/FTD patients may help to restore C9orf72 protein levels and the induction of autophagy, this could also promote an increase in mitophagy and the aberrant clearance of healthy mitochondria. Unfortunately, a candidate E3 ligase for C9orf72 was not identified during this thesis. Analysis of the C9orf72 sequence should be conducted to identify possible recognition motifs for the different E3 ligases that may be responsible for C9orf72 ubiquitination and clearance by the proteasome.

Although the data presented in this Chapter indicate that C9orf72 is indeed ubiquitinated, further work would be required to confirm this. Co-immunoprecipitation experiments between a tagged ubiquitin construct and C9orf72 would allow this. Alternatively mass spectrometry analysis of C9orf72 immunoprecipitates would highlight all potential ubiquitination sites (Udeshi et al., 2013). These experiments would also indicate whether C9orf72 K14R is unable to be ubiquitinated as would be predicted.

While cycloheximide is commonly used to investigate protein turnover, radioactive pulse chase assays may provide a more accurate estimate of half-life (Simon and Kornitzer, 2014). The use of radioactive pulse chase allows the investigation of turnover without global disruptions to cellular protein translation caused by cycloheximide. The inhibition of translation by cycloheximide may also lead to an artificially extended half-life due to the fact that all protein translation is inhibited, including any relevant E3 ligases that may be responsible for ubiquitination of C9orf72. Furthermore regulatory feedback loops may prevent further protein degradation and maintain certain cellular pools of essential proteins due to the fact that no new protein can be translated.

6 Discussion

6.1 Summary

A hexanucleotide repeat expansion of GGGGCC in *C9orf72* is the most common genetic defect associated with ALS and FTD. As detailed in section 1.7, there are multiple possible mechanisms by which this expansion may cause disease, but it has been shown to correlate with reduced *C9orf72* expression, suggesting C9orf72-associated ALS/FTD may be a result of *C9orf72* haploinsufficiency (Belzil et al., 2013; Cooper-Knock et al., 2012; DeJesus-Hernandez et al., 2011). As reduced C9orf72 protein may therefore contribute to disease, it is important to determine the cellular function of C9orf72 to aid understanding of disease pathogenesis.

The aim of this thesis was to discover the cellular function of C9orf72. As a method to indicate possible function, the interaction partners of C9orf72 were investigated. The p62 specific pathology associated with C9ALS/FTD indicated that C9orf72 might be involved in the autophagy pathway. Searches of the literature highlighted FIP200 as a potential binding partner of C9orf72, which led to the investigation of C9orf72 and the autophagy initiation complex. These data presented in Chapter 3 strongly linked C9orf72 to the autophagy pathway. Parallel to this, two unbiased approaches were conducted to identify novel interacting proteins: a mass spec screen conducted on immunoprecipitated C9orf72L and a Y2H screen conducted using C9orf72S and C9orf72L as bait. These different approaches were able to identify a number of novel C9orf72 interacting partners, which were confirmed by co-immunoprecipitation studies.

Chapter 4 investigated what effect altering C9orf72 protein levels could have on the autophagy pathway. Knock down of C9orf72 with targeted siRNA led to an inhibition of autophagy, specifically at the stage of induction (Figures 4.1 and 4.2). These data fitted with the binding data obtained in Chapter 3, which showed C9orf72 was interacting with the autophagy initiation complex (Figures 3.5-3.10). Further in depth analysis of the autophagy pathway showed that C9orf72 was important for translocation of the ULK1 complex, and that loss of C9orf72 inhibited translocation and thus the induction of autophagy (Figures 4.1, 4.2, 4.5, and 4.7). Conversely, overexpression of C9orf72 was able to actively induce autophagy (Figures 4.3, 4.4 and 4.7).

This ability of C9orf72 to regulate autophagy induction via the ULK1 initiation complex was Rab1a dependent (Figure 4.8). Analysis of the interaction of C9orf72 with Rab1a identified C9orf72 as an effector of Rab1a biology, with C9orf72 mediating the interaction between active GTP-bound Rab1a and ULK1, thus facilitating the translocation of the initiation complex to the PAS to initiate autophagosome formation (Figures 4.9-4.11).

The clinical relevance of this data linking loss of C9orf72 to reduced autophagy induction was investigated in C9ALS/FTD patient iNPC derived iNeurons, which showed reduced levels of basal autophagy compared to controls (Figure 4.14). Thus, these data were in support of the idea that haploinsufficiency of C9orf72 may be a contributing factor to the development of C9ALS/FTD due to the decreased levels of autophagy. The data showing that knock down of C9orf72 was also able to replicate the p62 aggregation seen in patients supported this idea (Figure 4.13).

Thus increasing C9orf72 protein levels could be therapeutic. The aim of Chapter 5 was to investigate the stability of the C9orf72 protein. The data presented here identified C9orf72 as a substrate of the ubiquitin proteasome system (Figure 5.2 and 5.3). Analysis of the C9orf72 amino acid sequence highlighted lysine residue 14 as a potential ubiquitination site (Figure 5.4 and Table 5.1). Mutation of lysine 14 was able to increase the stability of C9orf72L, suggesting C9orf72 was ubiquitinated at this residue (Figure 5.5). The Y2H data presented in Chapter 3 identified the DUB USP8 as a potential C9orf72S interacting protein. Here it was shown that USP8 was indeed an interacting partner of C9orf72S and C9orf72L and that USP8 was able to increase the stability of C9orf72, increasing the half-life of both C9orf72 isoforms (Figure 5.6, 5.7 and 5.8).

6.2 Defective autophagy and ALS/FTD

The data reported in this thesis places C9orf72 at the initiation stage of autophagy, showing that loss of C9orf72 leads to defective autophagy induction and the accumulation of p62 positive structures, similar to the pathology specifically associated with C9ALS/FTD (Al-Sarraj et al., 2011; Cooper-Knock et al., 2012). Several groups have reported reduced C9orf72 mRNA in C9ALS/FTD patients and reduced C9orf72 protein frontal cortex of C9ALS/FTD patients has

also been described (Waite et al., 2014). Consequently, the data presented in this thesis suggest haploinsufficiency of C9orf72 could result in the development of C9ALS/FTD in part due to the defect in autophagy initiation. This is summarised in figure 6.1.

The model predicts that loss of function C9orf72 prevents the delivery of active GTP-Rab1a to the ULK1 initiation complex. Without active Rab1a the ULK1 initiation complex then fails to translocate to the site of autophagosome formation. Without functional autophagosomes, autophagy receptors cannot target their ubiquitinated substrates, thus leading to their accumulation, which may be toxic to the cell. Thus this thesis has identified the molecular mechanism by which reduced C9orf72 leads to defective autophagy and potentially the development of C9ALS/FTD.

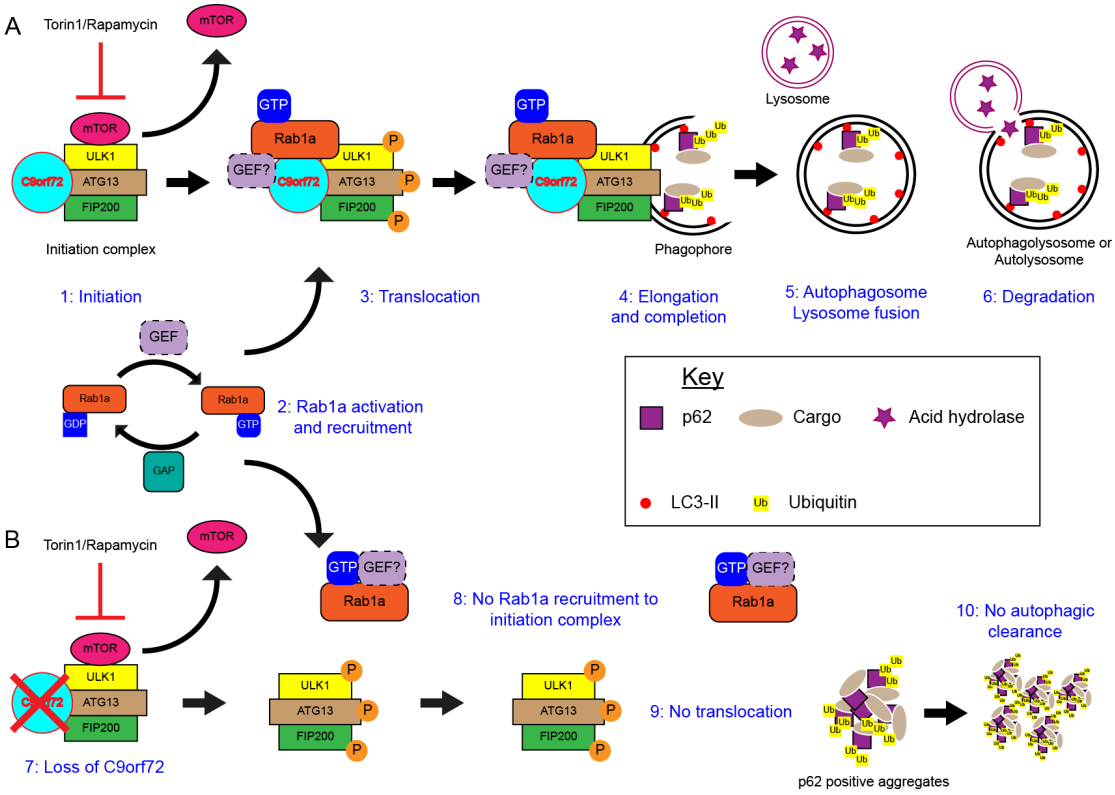

Figure 6.1 The role of C9orf72 in autophagy initiation. (A) Under normal conditions, C9orf72 binds to the autophagy initiation complex **(1)**. The Rab1a protein is activated by the action of an unknown GEF, forming GTP-Rab1a **(2)**. Via its interaction with Rab1a and ULK1, C9orf72 mediates the interaction between these two proteins allowing for translocation of the autophagy initiation complex to the phagophore. C9orf72 may also bind the Rab1a GEF to maintain active GTP-Rab1a at its site of action **(3)**. Once at the phagophore the initiation complex promotes the further downstream signalling events leading to formation and elongation of the autophagosome. During this time, substrates are delivered to the autophagosome by the action of autophagy receptor proteins such as p62 and OPTN **(4)**. Autophagosomes may then be translocated before fusing with the lysosome **(5)**. Finally, the acid hydrolases degrade the contents of the autolysosome **(6)**. (B) In C9ALS/FTD, haploinsufficiency of *C9orf72* may result in reduced C9orf72 protein **(7)**. Without C9orf72 at the ULK1 complex, active GTP-Rab1a cannot be recruited to the initiation complex **(8)**. Without the Rab1a-ULK1 interaction the initiation complex cannot translocate to the phagophore and so autophagosome formation decreases **(9)**. Without the formation of the autophagosomes, the autophagic substrates accumulate, as they cannot be

cleared. This leads to further aggregates and accumulations possibly leading to cellular toxicity and cell death **(10)**.

As discussed in Chapter 1, Rab proteins play a number of vital roles in autophagy induction. The interaction between Rab1a and C9orf72 identifies C9orf72 as the second Rab associated protein linked to the development of ALS. Alsin (ALS2) is a Rab5 GEF (Topp et al., 2004), with loss of function mutations known to cause juvenile onset ALS (Hadano et al., 2001a; Hadano et al., 2001b). While Rab1a appears to regulate translocation of the ULK1 initiation complex, Rab5 acts via the Vps34-Atg6/Beclin 1 complex to regulate autophagosome formation (Ravikumar et al., 2008), suggesting both C9orf72 and Alsin regulate trafficking events in the autophagy pathway. Loss of function mutations in Alsin therefore result in the inactivation of Rab5 and the inhibition of autophagosome formation leading to the development of ALS. Indeed, loss of Alsin has been shown to exacerbate motor dysfunction in a SOD1 mouse model of ALS, possibly due to the accumulation of autophagic substrates (Hadano et al., 2010). Thus regulation of autophagy and particularly Rab biology may be a common contributing factor to the development of ALS.

The neuronal cytoplasmic inclusions of ubiquitin and hyperphosphorylated TDP-43 are hallmarks of ALS and FTD (Arai et al., 2006; Neumann et al., 2006). These inclusions are also suggestive of defective autophagy as ubiquitinated protein aggregates are readily cleared via autophagy (Filimonenko et al., 2010; Pankiv et al., 2007). There is also further evidence linking this hallmark of disease to autophagy. Firstly, TDP-43 has been shown to be a substrate of autophagy, with autophagy induction enhancing the clearance of mutant TDP-43 and increasing cell survival in ALS neuronal models (Barmada et al., 2014). Secondly, TDP-43 aggregate formation may involve p62 as well as HDAC6, both of which are considered receptors for autophagy substrates (Brady et al., 2011; Cohen et al., 2015). Furthermore, TDP-43 has been shown to regulate expression of HDAC6, with loss of functional TDP-43 down regulating HDAC6 expression (Fiesel et al., 2010). Mutant TDP-43 may therefore establish a toxic feed forward mechanism whereby aggregates of mutant TDP-43, lead to loss of functional TDP-43 subsequently downregulating HDAC6 expression and therefore disrupting its own autophagic clearance.

Impaired and defective autophagy has also been implicated in other cases of non-C9orf72 ALS and FTD, as discussed in section 1.6. The study of familial inherited forms of ALS and FTD indicates many of the disease associated gene products are involved in the autophagy process. Figure 6.2, which includes the

effects of C9orf72 haploinsufficiency, highlights the steps of autophagy that are affected. For example, optineurin, p62 and Tbk1, all of which are mutated in certain cases of FALS and FTD (Freischmidt et al., 2015; Ito et al., 2011; Rubino et al., 2012; Teyssou et al., 2013), are all involved in autophagy substrate recognition and delivery to the autophagosome (Matsumoto et al., 2015; Pankiv et al., 2007; Pilli et al., 2012; Wong and Holzbaur, 2014). These disease-associated mutations, which lead to loss of functional protein, result in reduced substrate delivery to autophagosomes, increased aggregate formation and the development of disease (Freischmidt et al., 2015; Ito et al., 2011; Rubino et al., 2012; Teyssou et al., 2013; Wong and Holzbaur, 2014). Interestingly, patients harbouring both C9orf72 repeat expansions and p62 mutations have recently been described, possibly suggesting that the two mutations act synergistically to affect disease pathogenesis (Almeida et al., 2015).

Furthermore, several ALS/FTD related genes are linked to autophagosome maturation. For example, mutations to *Ubiquilin-2* cause a subset of ALS and FTD cases (Deng et al., 2011; Osaka et al., 2015). Ubiquilin-2 is thought to function in autophagosome maturation due to its ability of co-localising with p62, optineurin and ULK1 positive vesicles (N'Diaye et al., 2009b; Osaka et al., 2015; Rothenberg et al., 2010). Mutant Ubiquilin-2 disrupts the localisation of optineurin; again suggesting a synergistic effect between these two ALS/FTD associated mutations (Osaka et al., 2015). Loss of VCP leads to accumulation of p62, ubiquitin and LC3-II positive structures (Ju et al., 2009; Tresse et al., 2010), suggesting that the accumulation and aggregate formation seen in VCP F155H ALS and Paget's disease of bone and FTD (Johnson et al., 2010; Ju et al., 2009) is due to accumulations of immature autophagosome structures. Similarly, loss of FIG4 leads to accumulations of p62 and LC3-II in FIG4$^{-/-}$ mice (Chow et al., 2007). Loss of function mutations in *FIG4* account for approximately 1-2% of FALS cases, supporting the idea that loss of autophagosome maturation or clearance is a contributing factor to the development of ALS.

The discovery of TMEM106B as a known modifier of C9ALS/FTD supports the idea that C9orf72 regulates autophagy initiation (Gallagher et al., 2014; Van Blitterswijk et al., 2014). TMEM106B is a transmembrane protein that localises to the endo-lysosomal compartment and has been implicated in lysosomal biology (Brady et al., 2013; Stagi et al., 2014). How TMEM106B modifies

C9ALS/FTD is unknown, but the identification of a known lysosomal protein as a modifier of C9ALS/FTD suggests that lysosomal biology, and therefore autophagy, are potential pathways at play, supporting the outcome of this thesis. Single nucleotide polymorphisms within TMEM106B appear to regulate expression and turnover of this protein (Nicholson et al., 2013). There is conflicting evidence for the effect of TMEM106B levels on lysosomal function. On one hand overexpression of TMEM106B has been reported to disrupt lysosomal function (Brady et al., 2013), while on the other, increased levels are reported to improve lysosomal function and stress signalling (Stagi et al., 2014). Thus as a modifier of C9ALS/FTD the levels of TMEM106B may contribute to an autophagy related defect associated with reduced C9orf72 and therefore increase or reduce the risk of developing C9ALS/FTD.

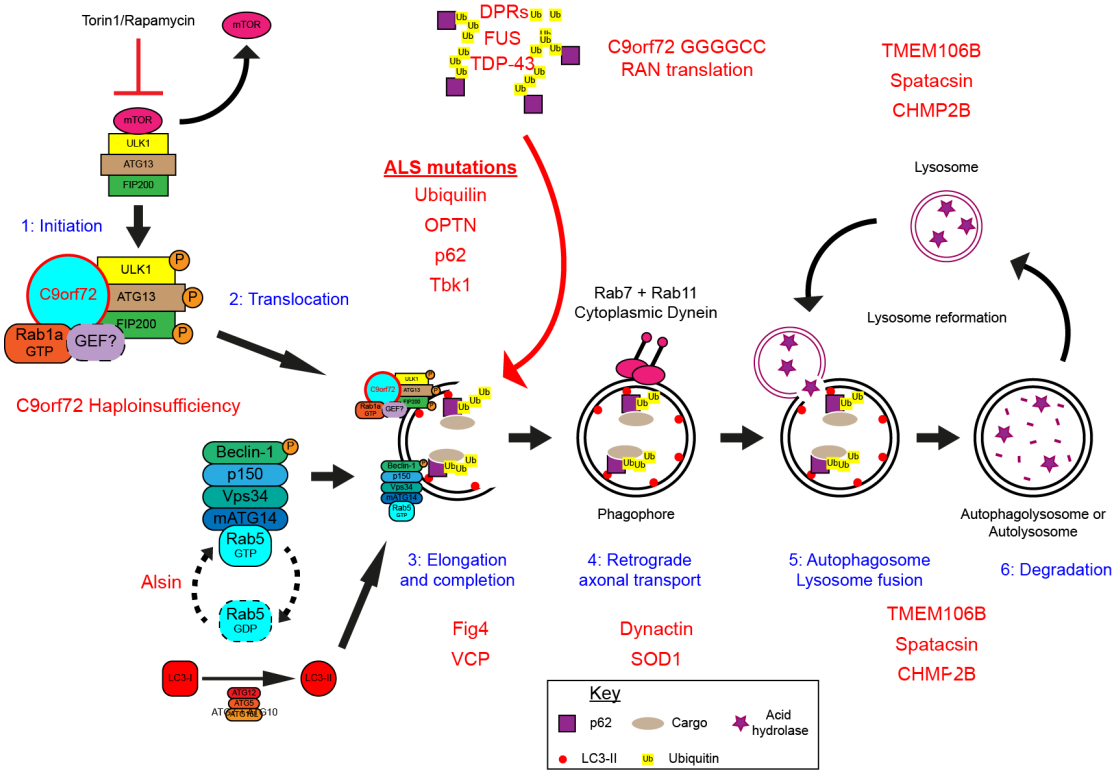

Figure 6.2 Impact of ALS associated genes on the autophagy pathway. As described above, loss of C9orf72 prevents correct translocation of the initiation complex, inhibiting autophagy induction. Mutation to the autophagy receptor proteins such as p62, OPTN, and their activator Tbk1, may lead to reduced substrate delivery to the autophagosome resulting in increased aggregate formation. Mutations to Fig4, VCP and Alsin are all likely to disrupt formation of the lysosome leading to a failure to clear autophagic substrates. ALS associated mutations to Dynactin or SOD1 may disrupt the retrograde transport of autophagosomes, a step known to be important for autophagosome lysosome fusion. A number of ALS genes are thought to impact on the autophagosome lysosome fusion event. Spatacsin mutations may impact on lysosome biogenesis thus disrupting lysosome fusion, while the mutation to CHMP2B may affect maturation of the autophagosomes and the final fusion with the lysosome. TMEM106B is a genetic modifier of C9ALS/FTD and is involved in lysosomal biology. Mutations or SNPs within TMEM may negatively impact lysosomal biology thus exacerbating C9ALS/FTD.

It is well established that loss of neuronal autophagy can result in neuronal degeneration. The neural specific knockout of essential autophagy genes in mice, such as *ATG7, ATG5* and *Rb1cc1 (FIP200),* leads to neuronal degeneration, progressive motor defects, such as reduced coordinated movement, and increased neuronal cytoplasmic inclusion body formation (Hara et al., 2006; Komatsu et al., 2006; Liang et al., 2010). Interestingly, the cerebellum appears to be particularly susceptible to loss of autophagy in these models, suggesting a high autophagic demand (Komatsu et al., 2006; Liang et al., 2010). The specific p62 positive, TDP-43 negative, structures characteristic of C9ALS/FTD are also largely associated with the cerebellum and hippocampus (Al-Sarraj et al., 2011; Cooper-Knock et al., 2012; Mahoney et al., 2012). These p62 positive accumulations in the cerebellum are also seen with neuron specific knockout of FIP200 (Liang et al., 2010). Such a bono fide defect in neuronal autophagy giving rise to a similar pathology to that of C9ALS/FTD supports the idea that defective autophagy is factor in the development of C9ALS/FTD.

In the only reported *C9orf72* knockout mouse model, developed by Koppers et al. 2015, neuronal specific ablation of C9orf72 did not lead to motor neuron degeneration (Koppers et al., 2015), suggesting that, unlike *ATG7, ATG5* or *FIP200,* C9orf72 is not essential for neuronal autophagy in mice. While there may be redundancy of the *C9orf72* gene in mice, C9orf72 may be involved at a more specific level of autophagy initiation. Dysregulated innate immunity and inflammation have been implicated in the pathogenesis of ALS (Goldknopf et al., 2006; Zhang et al., 2009). Whether defective or prolonged inflammation is found in these *C9orf72* knockout mice is yet to be established, but ULK1 activation has been shown to reduce the inflammatory response, preventing sustained, aberrant inflammation (Konno et al., 2013a). Indeed, suppression of autophagy has been shown to increase the inflammatory response (Yoshizaki et al., 2012). In support of this, SNPs that increase ATG16L1 turnover and degradation are strongly linked to Crohn's disease, a type of inflammatory bowl disease (Murthy et al., 2014). Thus, one could speculate that without functional C9orf72, the correct action of ULK1 may be perturbed, leading to prolonged and harmful inflammation. Autophagy defects or neuronal p62 accumulations have not been investigated in these *C9orf72* knockout mice. However, C9orf72 knockout did result in reduced body weight, a feature that is also found in the $ATG7^{-/-}$ mice (Komatsu et al., 2006). Knock-out of *ATG7* in hypothalamic agouti-related

peptide neurons also leads to significantly reduced body weight (Kaushik et al., 2011). This suggests that reduced body weight in these C9orf72 neural specific knockout mice could be related to defective autophagy.

Aside from C9orf72 haploinsufficiency there are two other possible mechanisms of disease associated with C9ALS/FTD: toxic RNA foci formation and aberrant DPR protein production. The production of aggregating DPR proteins from the repeat expansion has been shown to be toxic in a number of models. The arginine containing DPR proteins, poly-GR and poly-PR, are particularly toxic when overexpressed in a *Drosophila* model (Mizielinska et al., 2014), while the poly-GA species are toxic to primary cortical neurons (May et al., 2014). These DPR protein species are also a component of the p62 positive inclusions in C9ALS/FTD patients (Mann et al., 2013), suggesting that, similar to p62, their accumulation is could be due to defective autophagic clearance. If DPR proteins are considered substrates of the autophagy pathway this could put a greater burden on the autophagy system. There is therefore the potential for a synergistic effect between the production of DPRs and haploinsufficiency of C9orf72. This hypothesis is outlined in figure 6.2. With an already defective autophagy pathway, caused by C9orf72 haploinsufficiency, increased autophagic substrate production would exacerbate the problem. Inflicting further pressure on the autophagy pathway would promoting further aggregate formation and ultimately lead to cellular toxicity and possibly cell death. In this case the DPR proteins and haploinsufficiency of C9orf72 could function in a two hit scenario, where individually they may not have the potential to cause disease, but together their effects are cumulative, leading to the development of C9ALS/FTD.

A number of mouse models have been developed to investigate the effect of the C9orf72 hexanucleotide repeat expansion (Chew et al., 2015; Hukema et al., 2014; O'Rourke et al., 2015; Peters et al., 2015). These models are able to replicate the RNA nuclear inclusions, TDP-43 positive inclusions, ubiquitinated aggregates, DPR proteins aggregation (Chew et al., 2015; Hukema et al., 2014; O'Rourke et al., 2015; Peters et al., 2015) and in some cases cortical neuronal loss (Chew et al., 2015). However, there are no reports of motor neuron loss, muscle wasting, paralysis or other classical ALS phenotypes (Chew et al., 2015; Hukema et al., 2014; O'Rourke et al., 2015; Peters et al., 2015). Crucially these models do not report the presence of specific p62 positive, TDP-43 negative,

inclusions in the cerebellum and hippocampus, the phenotype most strongly linked to C9ALS/FTD. While these models mimic many features of C9ALS/FTD, it also suggests that the repeat expansion alone does not completely replicate the C9ALS/FTD pathology or phenotype. It would be predicted that, due to the function of C9orf72 outlined in this thesis, the knockout model of C9orf72 is the most likely to develop the p62 pathology, as well as other autophagy related defects. It would be interesting to determine which phenotypes are specifically associated with haploinsufficiency, DPR protein production or RNA foci formation. One would predict that a model that is able to reproduce all three mechanisms would more fully replicate C9ALS/FTD.

As the C9orf72 repeat expansion is the most common genetic cause of ALS and FTD, this, along with the evidence from other ALS associated mutations, therefore supports the idea that defective autophagy is a common and important pathogenic mechanism associated with the development of ALS and FTD.

6.3 Consequences for the treatment of ALS/FTD

The range of evidence for the three mechanisms associated with C9orf72 ALS suggests the three are likely to be non mutually exclusive. However, having identified the cellular function of the C9orf72 protein, it is important to recognise that if haploinsufficiency is a mechanism of disease then mediating C9orf72 levels, or modulating the autophagy pathway, has the potential to be a therapeutic target in the treatment of C9orf72 ALS/FTD. Autophagy treatments have already been suggested to be beneficial in the treatment of ALS (Barmada et al., 2014; Castillo et al., 2013). However, simply inducing autophagy in C9ALS/FTD may not be beneficial due to the role of C9orf72 at autophagy initiation. On the other hand, treatments that could enhance autophagy via a different route would certainly be an attractive possible therapy for C9ALS/FTD, as would the modulation of endogenous C9orf72 protein levels. As described in Chapter 5, C9orf72 is a substrate of the UPS with USP8 possibly functioning as the deubiquitinating enzyme responsible for stabilising C9orf72. Therefore targeting proteins such as USP8 could act as a therapeutic target to increase C9orf72 protein levels and ameliorate disease. Alternatively, determining the E3 ubiquitin ligase responsible for C9orf72 ubiquitination, possibly at lysine 14, could also provide a method of regulating C9orf72 levels. Identification of a small molecule inhibitor of an E3 ligase is possibly a more realistic target compared to finding an activator of a DUB, as E3 inhibitors are already in clinical

trials for the treatment of some cancers (Patel and Player, 2008). By inhibiting the action of the E3 ligase, endogenous levels of C9orf72 would be increased; potentially ameliorating the problems associated with decreased C9orf72 protein levels. Targeting the E3 ligase may prove a more attractive target due to the specificity of E3 ligases to their substrate compared to that of the DUBs.

As discussed in section 6.2, variants of *TMEM106B* are known modifiers of FTLD and C9ALS/FTD (Gallagher et al., 2014; Van Blitterswijk et al., 2014; Vass et al., 2011). Understanding how these variants modulate risk of C9orf72 may provide potential targets for the treatment of C9ALS/FTD and FTLD. Identification of other genetic modifiers of C9ALS/FTD could be investigated in a similar fashion.

6.4 C9orf72 as an effector of Rab biology

Secondary structural analysis has revealed C9orf72 to have structural homology with the DENN domain family of proteins, which are GEFs for the Rab GTPases (Levine et al., 2013; Zhang et al., 2012). In line with this evidence C9orf72 was shown to co-localise with a number of Rab proteins (Farg et al., 2014). In this thesis, C9orf72 was shown to directly interact with Rab1a, consistent with the idea that C9orf72, as a DENN domain protein, could be a GEF for the Rab GTPases. However, *in vitro* binding assays conducted in Chapter 4 revealed that C9orf72 had a higher affinity for the active GTP-bound Rab1a (Fig. 4.10), a concept more in line with a Rab effector protein (Grosshans et al., 2006). Rab effector proteins preferentially bind GTP-bound Rabs and target them to their site of action (Grosshans et al., 2006). In some cases, these effectors are also capable of binding the GEF associated with the Rab, meaning the active Rab is targeted to its correct site of action by the effector and also kept active by the presence of the GEF (Horiuchi et al., 1997; Korobko et al., 2005; Lipatova et al., 2012). This scenario of a Rab module comprising of a GEF, and effector and a Rab is detailed in Figure 6.3.

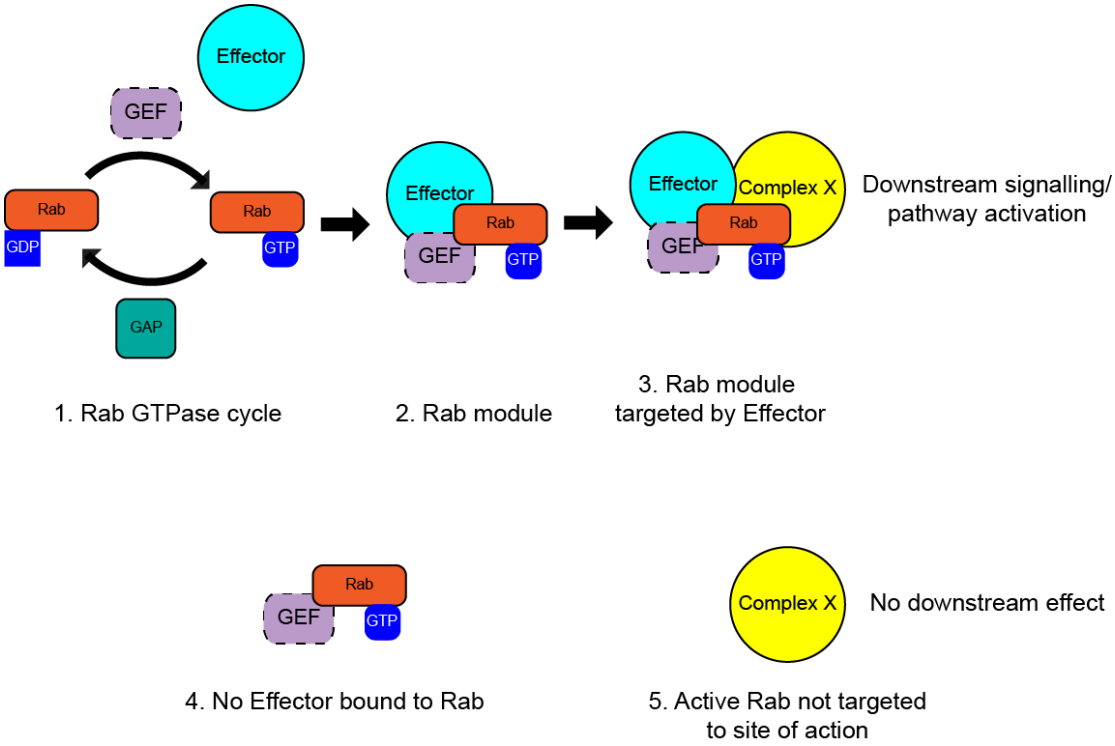

Figure 6.3 The Rab module. 1) The Rab GTPases cycle from an inactive GDP bound state to an active GTP-bound state. The exchange of GDP for GTP is mediated by the guanine nucleotide exchange factors (GEFs). The intrinsic GTPase activity of the Rabs can be enhance by GTPase activating proteins (GAPs) promoting the hydrolysis of GTP to GDP, thus inactivating the Rab GTPase. 2) Rab effectors bind active GTP-Rabs to bring them to their site of action. Rab effectors are also capable of binding the GEF responsible for Rab activation, meaning the active Rab is brought to its site of action and maintained in an active state by the presence of the GEF. This Rab module therefore comprises a GEF, an effector and a Rab GTPase. 3) The active Rab module is targeted to its site of action, (a cellular compartment, a membrane or a complex) via the interaction of the effector. Localisation of the correct Rab and the correct site leads to downstream effects and pathway activation. 4) Without an effector protein the Rab module is not established. 5) The active Rab cannot be targeted to its site of action meaning there is no pathway activation or downstream signalling.

The yeast Rab1a homologue, Ypt1, regulates the translocation of the ULK1 homologue, ATG1, to the PAS, allowing for autophagosome formation (Lipatova et al., 2012; Wang et al., 2013). Data presented in Chapter 4 showed Rab1a has a similar role in mammalian cells, as Rab1a was required for translocation of the ULK1 initiation complex upon autophagy induction (Figure 4.8). C9orf72 was shown to mediate the interaction between Rab1a and ULK1 (Figure 4.11). Thus by binding active, GTP-bound Rab1a, C9orf72 is able to mediate the further downstream interaction with ULK1, therefore leading to translocation of the autophagy initiation complex and the induction of autophagy. The interaction between GTP-loaded Ypt1 and ATG1 in yeast is mediated by the ATG11 protein; however, in mammalian systems there is no known homologue of ATG11 (Lipatova et al., 2012). The data presented here show that, much like ATG11, C9orf72 is required for the interaction of ULK1 and Rab1a, by binding GTP-loaded Rab1a and ULK1. These data suggest C9orf72 may be functioning as the mammalian homologue of ATG11. ATG11 is thought to interact with Ypt1, as well as the Ypt1 GEF complex and Ypt1 activator, TRAPPIII, on ATG9 positive membranes, mediating the interaction of this complex with ATG1 (Lipatova et al., 2012). This module is then targeted to the PAS either by the interaction of ATG11 with ATG17, the yeast homologue of FIP200, or by the interaction of TRAPPIII subunit, Trs85, with ATG17 (Lipatova et al., 2012; Lynch-Day et al., 2010; Wang et al., 2013). The delivery of this complex to the PAS brings about the interaction of ATG1 and ATG17, Ypt1 with ATG1, as well as delivery of ATG9 positive membranes to the PAS, all of which are essential for the formation of the autophagosome (Kakuta et al., 2012; Lipatova et al., 2012; Lynch-Day et al., 2010; Wang et al., 2013). Again similarly to yeast ATG11, the data presented here show that C9orf72 is also able to bind FIP200, supporting the idea that C9orf72 may be functioning as the mammalian homologue of ATG11, by binding GTP-loaded Rab1a and bringing it into contact with the ULK1 initiation complex. This is detailed in Figure 6.1. By binding the initiation complex as well as the GTP-bound Rab1a, C9orf72 mediates the interaction between active Rab1a and ULK1. This allows the correct translocation of the autophagy initiation complex to the phagophore, and thus the formation of the autophagosome. Loss of C9orf72 prevents active GTP-bound Rab1a from binding ULK1, therefore preventing the translocation of the initiation complex and preventing the formation of the autophagosome. By preventing autophagosome formation, autophagy is effectively inhibited. Autophagy receptor proteins such as p62 still bind their associated substrates,

but the lack of newly formed autophagosomes prevents their clearance. This in turn leads to the accumulation of ubiquitin and p62 positive aggregates.

TRAPPC8 has been identified as the mammalian homologue of Trs85 (Choi et al., 2011; Zong et al., 2011), the subunit that targets the TRAPPIII GEF complex to Ypt1 in yeast (Lipatova et al., 2012; Lynch-Day et al., 2010). While TRAPPC8 has been shown to be important for autophagy induction (Behrends et al., 2010), no direct TRAPPIII GEF complex able to active Rab1a in mammalian cells has been identified (Huang et al., 2011). In yeast, Trs85 is able to bind Ypt1 as well ATG17 at the PAS, but also co-localises with ATG11 (Lipatova et al., 2012; Lynch-Day et al., 2010; Wang et al., 2013). If C9orf72 were taken to function in a similar way to ATG11, then one would expect a GEF protein to interact with C9orf72, FIP200 as well as Rab1a, which would be responsible for the activation of Rab1a. The same study that identified C9orf72 as a possible FIP200 interacting protein also found SMCR8 to be the most likely interactor of FIP200 (Behrends et al., 2010). Interestingly, SMCR8 was then further identified as a novel DENN domain protein in the same study that identified C9orf72 as a potential DENN protein (Zhang et al., 2012). A mass spec screen conducted by Dr Mathew Walsh within the department suggested SMCR8 was also a binding partner of C9orf72L (Figure 3.11 and table 3.1). Having confirmed the C9orf72 and SMCR8 interaction by co-immunoprecipitation experiments (Figure 3.12), it is not inconceivable to imagine that through its interaction with C9orf72 and its likely interaction with FIP200, SMCR8 could function as a GEF for Rab1a, in a similar method to TRAPPIII in yeast. Future work would seek to address this. Thus in an arrangement similar to that seen in yeast, C9orf72 may function in a Rab1a module, with C9orf72 as the effector, Rab1a as the GTPase and SMCR8 as the GEF, regulating the initiation stages of autophagy.

This module type arrangement of a GEF, an effector and a Rab GTPase is commonly seen with Rab biology. For example, the Rab5 GEF Rabex5 is in complex with Rab5 and the Rab5 effector, Rabaptin5, meaning active Rab5 is brought to its site of action by the effector and maintained in an active state by the GEF, ensuring efficient endosomal trafficking (Horiuchi et al., 1997). In yeast, transport of secretory vesicles required for exocytosis requires the Rab GTPase Sec4p, which associates with its effector Sec15p and its exchange factor Sec2p to ensure correct and efficient activity during exocytosis (Medkova et al., 2006).

With the exception of Cox6C, C9orf72 appears to interact with all identified binding partners through its N-terminal domain, shown in Chapter 1 to correspond to the u-DENN region of the full DENN domain (Figure 1.8). The u-DENN region of DENN domain proteins appears to be important in GEF cascade pathways, as it may mediate the interaction between other Rab proteins without necessarily facilitating GDP/GTP exchange. In the case of the Rab6 GEF, Rab6IP1, the u-DENN domain of Rab6IP1 is likely the region required for Rab11 binding (Miserey-Lenkei et al., 2007). By interacting with GTP-bound Rab11 as well as acting as a GEF for Rab6, Rab6IP1 can mediate the interaction between the late endosomes and the Golgi (Marat et al., 2011; Miserey-Lenkei et al., 2007). Another example of the uDENN region involved in Rab binding and GEF cascade formation is the Rab3 GEF, DENN/MADD. The u-DENN region of DENN/MADD, also known as Rab3-GEP, interacts with GTP-bound Rab3, which is found on synaptic vesicles, potentially to mediate motor dependent transport of Rab3 positive vesicles (Marat et al., 2011; Niwa et al., 2008). In terms of the cascade, DENN/MADD then acts as a functional GEF for the Rab27 (Figueiredo et al., 2008; Yoshimura et al., 2010), which, similar to Rab3, is involved in exocytosis. The requisite for a DENN protein to function in a GEF cascade appears to be the ability to bind an active GTP-bound Rab, effectively functioning as an effector protein, before coming into contact with its actual Rab target. This situation has obvious similarities with the action of C9orf72 described here. By binding GTP-Rab1a and mediating the interaction with the ULK1 initiation complex, perhaps C9orf72 is able to function as a GEF for another autophagy related Rab, such as Rab5 or Rab7 (Ao et al., 2014; Blümer et al., 2013; Ravikumar et al., 2008; Su et al., 2011). It would be of interest to dissect the pathway further and identify the possible Rab requiring C9orf72 for activation. Thus, via its u-DENN region, C9orf72 could be functioning in a GEF cascade involving Rab1a.

6.5 C9orf72 and mitophagy

Mitochondrial quality control and removal of dysfunctional mitochondria is essential to maintain a healthy mitochondrial network (Poole et al., 2008; Whitworth and Pallanck, 2009). The mitochondrial localised serine/threonine kinase PTEN-induced kinase 1 (PINK1) and the E3 ubiquitin ligase Parkin are the main regulators of mitophagy. USP8 been identified as a de-ubiquitinating enzyme for Parkin, mediating removal of K6-linked ubiquitin and promoting

Parkin recruitment to depolarised mitochondria (Durcan et al., 2014). The interaction of C9orf72 with USP8, detailed in Chapter 5, and its proposed role in autophagy induction, therefore links C9orf72 to mitophagy. A potential role of C9orf72 in mitochondrial biology is further supported by its interaction with Cox6C, as identified in Chapter 3. Considering the evidence presented in Chapter 4, showing C9orf72 regulates the delivery of active Rab1a to the ULK1 complex, C9orf72 could function as an adaptor protein in other cellular situations. Via its interaction with Cox6C, C9orf72 could aid in the delivery of USP8 to the mitochondria thereby enhancing the ability of USP8 to deubiquitinate Parkin and promote mitophagy of dysfunctional mitochondria. It could also be that C9orf72 binds Cox6C more readily after mitochondrial depolarisation allowing for enhanced recruitment of USP8 to damaged mitochondria and therefore more efficient mitophagy. The PINK1/Parkin pathway essentially functions to isolate dysfunctional mitochondria and therefore the autophagy machinery is still required for their removal. Thus, as C9orf72 was shown to regulate translocation of the ULK1 initiation complex, C9orf72 may be involved in the recruitment of the autophagy machinery to dysfunctional, isolated, mitochondria. The concept of C9orf72 functioning as the ATG11 homologue discussed in section 6.4 supports this idea. ATG11 has been shown to have an important role in mitophagy (Mao et al., 2013), binding to the mitochondrial associated protein ATG32 and aiding in recruitment of the mitochondrial fission machinery and also the core autophagy proteins to the mitochondrial surface (Aoki et al., 2011; Kondo-Okamoto et al., 2012; Mao et al., 2013).

As with autophagy, Rab proteins are also involved in mitophagy. Rab7 and Rab32 have both been implicated in autophagosome formation and specifically mitophagy (Alto et al., 2002; Hirota and Tanaka, 2009; Yamano et al., 2014). Thus, via its DENN homology, C9orf72 may act as a GEF for these mitophagy related Rabs, promoting the clearance of dysfunctional mitochondria.

Mitochondrial dysfunction in the pathogenesis of ALS is well documented (De Vos et al., 2007; Menzies et al., 2002). Beyond the predicted autophagy dysfunction described here, haploinsufficiency of C9orf72 could therefore, also promote mitochondrial dysfunction providing a further insult to neurons and potentially contributing to disease pathogenesis.

6.6 Future directions

This thesis has identified the role of C9orf72 in autophagy. However, understanding this function of C9orf72 has also raised further questions and ideas that should be addressed. These are outlined in this section.

Data presented in Chapter 5 suggested USP8 was a DUB enzyme for C9orf72. Future work should make use of co-immunoprecipitation experiments between C9orf72 and tagged ubiquitin, firstly to show that C9orf72 is ubiquitinated and that, secondly, USP8 is able to deubiquitinate C9orf72. Similar methods should be employed to investigate whether the K14 residue is indeed a ubiquitination site. Studies should also be undertaken to identify the E3 ligase responsible for C9orf72 ubiquitination. Many E3 ligases rely on consensus sequences within their target protein for binding. Analysis of the C9orf72 sequence may yield potential sites specific for certain E3 ligases. Potential E3 ligases would then be confirmed by interaction studies. Identification of the E3 ligase could then form part of the basis for investigating methods to modulate C9orf72 levels, with the idea of alleviating the problems caused by C9orf72 haploinsufficiency by inhibiting the E3 ligase responsible for C9orf72 degradation.

The interaction of C9orf72 with USP8 also suggests a potential role in mitophagy, as discussed in section 6.5. As mitochondrial morphology defects and mitochondrial dysfunction is observed in ALS, future experiments should assess the effect alterations in C9orf72 protein levels can have on these aspects of mitochondrial biology. C9orf72 was also speculated to deliver USP8 to dysfunctional mitochondria possibly via its interaction with Cox6C. Therefore the interaction of USP8 and Cox6C with C9orf72 should be investigated after depolarisation of the mitochondrial network to determine whether these interactions are promoted under such conditions and whether they are required for efficient mitochondrial clearance by mitophagy.

Future work should seek to assess the subcellular localisation of C9orf72 in more detail. Fractionation experiments would help to determine if C9orf72 is present within the mitochondrial fraction supporting the idea that C9orf72 could be interacting with Cox6C within the mitochondrial environment.

The data obtained from the C9orf72 patient derived iNeurons in Chapter 4 suggests a defect in basal autophagy. If reduced C9orf72 levels caused this defect then overexpression of C9orf72 could act as a rescue. Viral transduction of these iNeurons with C9orf72 construct would be one method of delivering a functional *C9orf72* gene. Rescuing the autophagy defect by overexpression of C9orf72 would support the idea that modulating C9orf72 levels in patients would be an attractive therapy for the treatment of C9ALS/FTD.

Further work would be required to confirm the existence of the C9orf72-Rab1a module. The yeast ATG11-Ypt1 module also comprises the GEF complex, TRAPPIII. It is speculated here that SMCR8 could function as the Rab1a GEF, mainly due to the predicted interaction with FIP200 (Behrends et al., 2010), a characteristic of the yeast module, but also its interaction with C9orf72. Future work should establish if SMCR8 has the ability to interact with Rab1a and also whether SMCR8 is able to promote GDP-GTP exchange on Rab1a.

Identifying C9orf72 as part of the Rab1a module raises the possibility that C9orf72 is functioning as the mammalian homologue of ATG11. Complementation experiments in ATG11$^{-/-}$ yeast could help to identify C9orf72 as the definitive homologue of ATG11. Expression of *beclin-1* in the vps30 mutant yeast can rescue the associated autophagy defect (Liang et al., 1999). It would be interesting to see whether expression of *C9orf72* in ATG11$^{-/-}$ yeast would be sufficient to rescue the associated autophagy defects.

The interaction of C9orf72 with GTP-bound Rab1a suggests C9orf72 is a Rab1a effector. However, C9orf72 could also function in a GEF cascade, activating another downstream autophagy related Rab. Future work should determine whether C9orf72 has the potential to act as a GEF for another Rab protein. GDP release assays could be conducted to determine this. Possible candidates would include known autophagy related Rabs such as Rab5, Rab7, Rab32 and Rab33B (Ao et al., 2014; Dou et al., 2013; Gutierrez et al., 2004; Hirota and Tanaka, 2009; Itoh et al., 2008; Jäger et al., 2004; Ravikumar et al., 2008).

Rab1 is known to be Golgi associated (Jin et al., 1996; Pind SN, 1994). In Rab biology, the Rab GTPases are located within a specific membrane compartment by their specific prenylation motif (Gomes et al., 2003). In relation to Rab1a and C9orf72, this suggests that C9orf72 could be responsible for the delivery of

Rab1a, within its Golgi derived membranes, to the ULK1 initiation complex to bring about autophagosome formation. Golgi derived membranes have been suggested as the precursor to autophagosome membrane (Geng et al., 2010; Yen et al., 2010). In line with this, ATG9 positive membranes are required for autophagosome formation (Chan et al., 2009; Young et al., 2006) and ATG9 is located within the Golgi network (Winslow et al., 2010; Yen et al., 2010; Young et al., 2006). In this case, C9orf72 could be responsible for the delivery of Golgi membrane compartments required for the formation of the autophagosome. ATG11 appears to be responsible for this activity in yeast (He et al., 2006). To investigate whether C9orf72 is required for Golgi-derived membrane delivery to the autophagosome, the inclusion of Golgi related proteins in newly synthesised membranes could be investigated after C9orf72 targeted siRNA. The effect of C9orf72 siRNA on ATG9-positive membrane distribution should also be investigated, as Rab1a siRNA was shown to disrupt the localisation of ATG9 to LC3 positive vesicles (Winslow et al., 2010).

Upon activation, ULK1 phosphorylate a number of targets, including its initiation complex partners FIP200 and ATG13, as well as further downstream targets such as Beclin-1 (Alers et al., 2011; Ganley et al., 2009; Jung et al., 2009; Russell et al., 2013). Recently, a consensus motif for the ULK1 phosphorylation site has been identified. ULK1 has a preference for serine residues surrounded by hydrophobic residues, particularly at the -3, +1 and +2 sites in relation to the serine target (Egan et al., 2015). This gives the general consensus motif as (L/M,X,X,**S**,Z,Z), where X appears to be any amino acid and Z is any aliphatic or hydrophobic amino acid, including methionine (Egan et al., 2015). Serine 189 within C9orf72 appears to be a potential candidate as an ULK1 target site. The -3 position is taken by leucine, while position +1 is taken by methionine, both of which fit the suggested consensus motif (Egan et al., 2015). Further to this, position -1 is taken by serine, which also appears beneficial to the ULK1 recognition motif. This raises the possibility that, like the other ULK1 interacting proteins FIP200 and ATG13 (Alers et al., 2011; Jung et al., 2009), C9orf72 could also be a target of activated ULK1 phosphorylation upon autophagy induction. Future work could utilise *in vitro* kinase assays to determine whether C9orf72 is a substrate of ULK1 and, if so, whether the serine 189 residue is particularly important for this phosphorylation.

Throughout this thesis experiments have been conducted on both the short and long isoforms of C9orf72. In many cases, both C9orf72S and C9orf72L were shown to bind the same protein partners, or indeed have the same effect. As C9orf72S essential lacks the majority of the DENN domain as well as the entire dDENN domain (See Fig 1.8), future work should investigate the differential actions of C9orf72S and C9orf72L, such as whether C9orf72S is a functional GEF as it lacks the C-terminal region. Other Rab GEF proteins are known to dimerize for efficient GEF activity, possibly via their longin (uDENN) domains (Nordmann et al.). Thus, as C9orf72S contains the longin domain, it may have the potential to interact and dimerize with C9orf72L. This interaction should be investigated further.

As described in Chapter 3, endogenous FIP200, ULK1 and ATG13 were found to co-immunoprecipitate with C9orf72. However, endogenous bands of FIP200, ULK1 and ATG13 of different molecular weights also co-immunoprecipitated. It was speculated that the bands of FIP200 and ULK1, could be phosphorylated species, in response to ULK1 activation. Thus the identities of these other species should be investigated, to confirm whether they are phosphorylate forms. Alternatively, these endogenous co-immunoprecipitation experiments could be conducted after Torin1 treatment of the cells to activate ULK1. The lower molecular weight band of ATG13 was speculated to be a splice variant. This could be confirmed by mass spec analysis of this co-immunoprecipitant.

7 References

Abbi, S., Ueda, H., Zheng, C., Cooper, L.A., Zhao, J., Christopher, R., and Guan, J.L. (2002). Regulation of focal adhesion kinase by a novel protein inhibitor FIP200. Mol Biol Cell *13*, 3178-3191.

Abel, O., Powell, J.F., Andersen, P.M., and Al-Chalabi, A. (2012). ALSoD: A user-friendly online bioinformatics tool for amyotrophic lateral sclerosis genetics. Human Mutation *33*, 1345-1351.

Abràmoff M. D, M.P.J., Ram S. J. (2004). Image Processing with ImageJ. Biophotonics International.

Ackerley, S., Grierson, A.J., Brownlees, J., Thornhill, P., Anderton, B.H., Nigel Leigh, P., Shaw, C.E., and Miller, C.C.J. (2000). Glutamate slows axonal transport of neurofilaments in transfected neurons. Journal of Cell Biology *150*, 165-175.

Ackerley, S., Thornhill, P., Grierson, A.J., Brownlees, J., Anderton, B.H., Leigh, P.N., Shaw, C.E., and Miller, C.C.J. (2003). Neurofilament heavy chain side arm phosphorylation regulates axonal transport of neurofilaments. Journal of Cell Biology *161*, 489-495.

Al-Chalabi, A., Fang, F., Hanby, M.F., Leigh, P.N., Shaw, C.E., Ye, W., and Rijsdijk, F. (2010). An estimate of amyotrophic lateral sclerosis heritability using twin data. Journal of neurology, neurosurgery, and psychiatry *81*, 1324-1326.

Al-Hakim, A.K., Zagorska, A., Chapman, L., Deak, M., Peggie, M., and Alessi, D.R. (2008). Control of AMPK-related kinases by USP9X and atypical Lys(29)/Lys(33)-linked polyubiquitin chains. Biochem J *411*, 249-260.

Al-Mahdawi, S., Pinto, R.M., Ismail, O., Varshney, D., Lymperi, S., Sandi, C., Trabzuni, D., and Pook, M. (2008). The Friedreich ataxia GAA repeat expansion mutation induces comparable epigenetic changes in human and transgenic mouse brain and heart tissues. Human Molecular Genetics *17*, 735-746.

Al-Saif, A., Al-Mohanna, F., and Bohlega, S. (2011). A mutation in sigma-1 receptor causes juvenile amyotrophic lateral sclerosis. Annals of Neurology *70*, 913-919.

Al-Sarraj, S., King, A., Troakes, C., Smith, B., Maekawa, S., Bodi, I., Rogelj, B., Al-Chalabi, A., Hortobágyi, T., and Shaw, C.E. (2011). P62 positive, TDP-43 negative, neuronal cytoplasmic and intranuclear inclusions in the cerebellum and hippocampus define the pathology of C9orf72-linked FTLD and MND/ALS. Acta Neuropathol *122*, 691-702.

Alers, S., Löffler, A.S., Paasch, F., Dieterle, A.M., Keppeler, H., Lauber, K., Campbell, D.G., Fehrenbacher, B., Schaller, M., Wesselborg, S.*, et al.* (2011). Atg13 and FIP200 act independently of Ulk1 and Ulk2 in autophagy induction. Autophagy *7*, 1424-1433.

Almeida, M.R., Letra, L., Pires, P., Santos, A., Rebelo, O., Guerreiro, R., van der Zee, J., Van Broeckhoven, C., and Santana, I. (2015). Characterization of an FTLD-PDB family with the coexistence of SQSTM1 mutation and hexanucleotide (GC) repeat expansion in C9orf72 gene. Neurobiol Aging.

Alonso, A., Logroscino, G., Jick, S.S., and Hernan, M.A. (2009). Incidence and lifetime risk of motor neuron disease in the United Kingdom: a population-based study. Eur J Neurol *16*, 745-751.

Alto, N.M., Soderling, J., and Scott, J.D. (2002). Rab32 is an A-kinase anchoring protein and participates in mitochondrial dynamics. J Cell Biol *158*, 659-668.

Andersson, M.K., Stahlberg, A., Arvidsson, Y., Olofsson, A., Semb, H., Stenman, G., Nilsson, O., and Aman, P. (2008). The multifunctional FUS, EWS and TAF15 proto-oncoproteins show cell type-specific expression patterns and involvement in cell spreading and stress response. BMC Cell Biol *9*, 37.

Ao, X., Zou, L., and Wu, Y. (2014). Regulation of autophagy by the Rab GTPase network. Cell death and differentiation *21*, 348-358.

Aoki, Y., Kanki, T., Hirota, Y., Kurihara, Y., Saigusa, T., Uchiumi, T., and Kang, D. (2011). Phosphorylation of Serine 114 on Atg32 mediates mitophagy. Molecular Biology of the Cell *22*, 3206-3217.

Arai, T., Hasegawa, M., Akiyama, H., Ikeda, K., Nonaka, T., Mori, H., Mann, D., Tsuchiya, K., Yoshida, M., Hashizume, Y.*, et al.* (2006). TDP-43 is a component of ubiquitin-positive tau-negative inclusions in frontotemporal lobar degeneration and amyotrophic lateral sclerosis. Biochemical and Biophysical Research Communications *351*, 602-611.

Arai, T., Nonaka, T., Hasegawa, M., Akiyama, H., Yoshida, M., Hashizume, Y., Tsuchiya, K., Oda, T., and Ikeda, K. (2003). Neuronal and glial inclusions in frontotemporal dementia with or without motor neuron disease are immunopositive for p62. Neuroscience Letters *342*, 41-44.

Aral, B., and Kamoun, P. (1997). The proline biosynthesis in living organisms. Amino Acids *13*, 189-217.

Atkin, J.D., Farg, M.A., Turner, B.J., Tomas, D., Lysaght, J.A., Nunan, J., Rembach, A., Nagley, P., Beart, P.M., Cheema, S.S.*, et al.* (2006). Induction of the unfolded protein response in familial amyotrophic lateral sclerosis and association of protein-disulfide isomerase with superoxide dismutase 1. Journal of Biological Chemistry *281*, 30152-30165.

Atkin, J.D., Farg, M.A., Walker, A.K., McLean, C., Tomas, D., and Horne, M.K. (2008). Endoplasmic reticulum stress and induction of the unfolded protein response in human sporadic amyotrophic lateral sclerosis. Neurobiology of Disease *30*, 400-407.

Axe, E.L., Walker, S.A., Manifava, M., Chandra, P., Roderick, H.L., Habermann, A., Griffiths, G., and Ktistakis, N.T. (2008). Autophagosome formation from membrane compartments enriched in phosphatidylinositol 3-phosphate and dynamically connected to the endoplasmic reticulum. Journal of Cell Biology *182*, 685-701.

Backer, J.M. (2008). The regulation and function of Class III PI3Ks: novel roles for Vps34. The Biochemical journal *410*, 1-17.

Bamsey, C., Mayeenuddin, L.H., Cheung, R., and Mitchell, J. (2000). Dissociation of G-protein alpha from rhabdomeric membranes decreases its interaction with rhodopsin and increases its degradation by calpain. Comp Biochem Physiol B Biochem Mol Biol *127*, 75-83.

Barmada, S.J., Serio, A., Arjun, A., Bilican, B., Daub, A., Ando, D.M., Tsvetkov, A., Pleiss, M., Li, X., Peisach, D.*, et al.* (2014). Autophagy induction enhances TDP43 turnover and survival in neuronal ALS models. Nature chemical biology *10*, 677-685.

Baron, D.M., Kaushansky, L.J., Ward, C.L., Sama, R.R.K., Chian, R.-J., Boggio, K.J., Quaresma, A.J.C., Nickerson, J.A., and Bosco, D.A. (2013). Amyotrophic lateral sclerosis-linked FUS/TLS alters stress granule assembly and dynamics. Molecular Neurodegeneration *8*, 1-18.

Behrends, C., Sowa, M.E., Gygi, S.P., and Harper, J.W. (2010). Network organization of the human autophagy system. Nature *466*, 68-76.

Belle, A., Tanay, A., Bitincka, L., Shamir, R., and O'Shea, E.K. (2006). Quantification of protein half-lives in the budding yeast proteome. Proc Natl Acad Sci U S A *103*, 13004-13009.

Belly, A., Moreau-Gachelin, F., Sadoul, R., and Goldberg, Y. (2005). Delocalization of the multifunctional RNA splicing factor TLS/FUS in hippocampal neurones: exclusion from the nucleus and accumulation in dendritic granules and spine heads. Neurosci Lett *379*, 152-157.

Belzil, V.V., Bauer, P.O., Prudencio, M., Gendron, T.F., Stetler, C.T., Yan, I.K., Pregent, L., Daughrity, L., Baker, M.C., Rademakers, R.*, et al.* (2013). Reduced C9orf72 gene expression in c9FTD/ALS is caused by histone trimethylation, an epigenetic event detectable in blood. Acta Neuropathol *126*, 895-905.

Bensimon, G., Lacomblez, L., and Meininger, V. (1994). A controlled trial of riluzole in amyotrophic lateral sclerosis. ALS/Riluzole Study Group. Paper presented at: The New England journal of medicine.

Benussi, L., Rossi, G., Glionna, M., Tonoli, E., Piccoli, E., Fostinelli, S., Paterlini, A., Flocco, R., Albani, D., Pantieri, R.*, et al.* (2014). C9ORF72 hexanucleotide repeat number in frontotemporal lobar degeneration: a genotype-phenotype correlation study. J Alzheimers Dis *38*, 799-808.

Berndsen, C.E., and Wolberger, C. (2014). New insights into ubiquitin E3 ligase mechanism. Nat Struct Mol Biol *21*, 301-307.

Berridge, M.J. (1993). Inositol trisphosphate and calcium signalling. Nature *361*, 315-325.

Bilsland, L.G., Sahai, E., Kelly, G., Golding, M., Greensmith, L., and Schiavo, G. (2010). Deficits in axonal transport precede ALS symptoms in vivo. Proceedings of the National Academy of Sciences of the United States of America *107*, 20523-20528.

Bjørkøy, G., Lamark, T., Brech, A., Outzen, H., Perander, M., Øvervatn, A., Stenmark, H., and Johansen, T. (2005). p62/SQSTM1 forms protein aggregates degraded by autophagy and has a protective effect on huntingtin-induced cell death. Journal of Cell Biology *171*, 603-614.

Blümer, J., Rey, J., Dehmelt, L., Maze, T., Wu, Y.W., Bastiaens, P., Goody, R.S., and Itzen, A. (2013). RabGEFs are a major determinant for specific Rab membrane targeting. Journal of Cell Biology *200*, 287-300.

Boston-Howes, W., Gibb, S.L., Williams, E.O., Pasinelli, P., Brown, R.H., and Trotti, D. (2006). Caspase-3 cleaves and inactivates the glutamate transporter EAAT2. Journal of Biological Chemistry *281*, 14076-14084.

Boxer, A.L., Mackenzie, I.R., Boeve, B.F., Baker, M., Seeley, W.W., Crook, R., Feldman, H., Hsiung, G.Y., Rutherford, N., Laluz, V.*, et al.* (2011). Clinical, neuroimaging and neuropathological features of a new chromosome 9p-linked FTD-ALS family. J Neurol Neurosurg Psychiatry *82*, 196-203.

Bradford, M.M. (1976). A rapid and sensitive method for the quantitation of microgram quantities of protein utilizing the principle of protein-dye binding. Anal Biochem *72*, 248-254.

Brady, O.A., Meng, P., Zheng, Y., Mao, Y., and Hu, F. (2011). Regulation of TDP-43 aggregation by phosphorylation and p62/SQSTM1. J Neurochem *116*, 248-259.

Brady, O.A., Zheng, Y., Murphy, K., Huang, M., and Hu, F. (2013). The frontotemporal lobar degeneration risk factor, TMEM106B, regulates lysosomal morphology and function. Human Molecular Genetics *22*, 685-695.

Brody, L.C., Mitchell, G.A., Obie, C., Michaud, J., Steel, G., Fontaine, G., Robert, M.F., Sipila, I., Kaiser-Kupfer, M., and Valle, D. (1992). Ornithine delta-aminotransferase mutations in gyrate atrophy. Allelic heterogeneity and functional consequences. Journal of Biological Chemistry *267*, 3302-3307.

Broussard, J.A., Rappaz, B., Webb, D.J., and Brown, C.M. (2013). Fluorescence resonance energy transfer microscopy as demonstrated by measuring the activation of the serine/threonine kinase Akt. Nat Protocols *8*, 265-281.

Brückner, A., Polge, C., Lentze, N., Auerbach, D., and Schlattner, U. (2009). Yeast Two-Hybrid, a Powerful Tool for Systems Biology. International Journal of Molecular Sciences *10*, 2763-2788.

Bucciantini, M., Giannoni, E., Chiti, F., Baroni, F., Formigli, L., Zurdo, J., Taddei, N., Ramponi, G., Dobson, C.M., and Stefani, M. (2002). Inherent toxicity of aggregates implies a common mechanism for protein misfolding diseases. Nature *416*, 507-511.

Buchan, J.R., and Parker, R. (2009). Eukaryotic Stress Granules: The Ins and Out of Translation. Molecular cell *36*, 932.

Buchman, V.L., Cooper-Knock, J., Connor-Robson, N., Higginbottom, A., Kirby, J., Razinskaya, O.D., Ninkina, N., and Shaw, P.J. (2013). Simultaneous and independent detection of C9ORF72 alleles with low and high number of GGGGCC repeats using an optimised protocol of Southern blot hybridisation. Molecular neurodegeneration *8*, 12.

Bunina, T.L. (1962). [On intracellular inclusions in familial amyotrophic lateral sclerosis]. Zh Nevropatol Psikhiatr Im S S Korsakova *62*, 1293-1299.

Byrne, S., Heverin, M., Elamin, M., Walsh, C., and Hardiman, O. (2013). Intermediate repeat expansion length in C9orf72 may be pathological in amyotrophic lateral sclerosis. Amyotrophic lateral sclerosis & frontotemporal degeneration, 1-3.

Byrne, S., Walsh, C., Lynch, C., Bede, P., Elamin, M., Kenna, K., McLaughlin, R., and Hardiman, O. (2011). Rate of familial amyotrophic lateral sclerosis: a systematic review and meta-analysis. Journal of neurology, neurosurgery, and psychiatry *82*, 623-627.

Cadenas, E., Boveris, A., Ragan, C.I., and Stoppani, A.O. (1977). Production of superoxide radicals and hydrogen peroxide by NADH-ubiquinone reductase and ubiquinol-cytochrome c reductase from beef-heart mitochondria. Archives of biochemistry and biophysics *180*, 248-257.

Cardenas, C., Miller, R.A., Smith, I., Bui, T., Molgo, J., Muller, M., Vais, H., Cheung, K.H., Yang, J., Parker, I.*, et al.* (2010). Essential regulation of cell bioenergetics by constitutive InsP3 receptor Ca2+ transfer to mitochondria. Cell *142*, 270-283.

Carriedo, S.G., Sensi, S.L., Yin, H.Z., and Weiss, J.H. (2000). AMPA exposures induce mitochondrial Ca(2+) overload and ROS generation in spinal motor neurons in vitro. J Neurosci *20*, 240-250.

Carriedo, S.G., Yin, H.Z., and Weiss, J.H. (1996). Motor neurons are selectively vulnerable to AMPA/kainate receptor-mediated injury in vitro. J Neurosci *16*, 4069-4079.

Castillo, K., Nassif, M., Valenzuela, V., Rojas, F., Matus, S., Mercado, G., Court, F.A., van Zundert, B., and Hetz, C. (2013). Trehalose delays the progression of amyotrophic lateral sclerosis by enhancing autophagy in motoneurons. Autophagy *9*, 1308-1320.

Ceriani, M., Amigoni, L., D'Aloia, A., Berruti, G., and Martegani, E. (2015). The deubiquitinating enzyme UBPy/USP8 interacts with TrkA and inhibits neuronal differentiation in PC12 cells. Exp Cell Res *333*, 49-59.

Chan, E.Y.W., Kir, S., and Tooze, S.A. (2007). siRNA screening of the kinome identifies ULK1 as a multidomain modulator of autophagy. Journal of Biological Chemistry *282*, 25464-25474.

Chan, E.Y.W., Longatti, A., McKnight, N.C., and Tooze, S.A. (2009). Kinase-inactivated ULK proteins inhibit autophagy via their conserved C-terminal domains using an Atg13-independent mechanism. Molecular and cellular biology *29*, 157-171.

Chang, J., Lee, S., and Blackstone, C. (2014). Spastic paraplegia proteins spastizin and spatacsin mediate autophagic lysosome reformation. *124*, 5249-5262.

Chang, L., and Monteiro, M.J. (2015). Defective Proteasome Delivery of Polyubiquitinated Proteins by Ubiquilin-2 Proteins Containing ALS Mutations. Plos One *10*, e0130162.

Chau, V., Tobias, J.W., Bachmair, A., Marriott, D., Ecker, D.J., Gonda, D.K., and Varshavsky, A. (1989). A multiubiquitin chain is confined to specific lysine in a targeted short-lived protein. Science *243*, 1576-1583.

Cheah, B.C., Vucic, S., Krishnan, A.V., and Kiernan, M.C. (2010). Riluzole, neuroprotection and amyotrophic lateral sclerosis. Current medicinal chemistry *17*, 1942-1199.

Chen, H.-J., Anagnostou, G., Chai, A., Withers, J., Morris, A., Adhikaree, J., Pennetta, G., and de Belleroche, J.S. (2010). Characterization of the Properties of a Novel Mutation in VAPB in Familial Amyotrophic Lateral Sclerosis. Journal of Biological Chemistry *285*, 40266-40281.

Chen, Y.-Z., Bennett, C.L., Huynh, H.M., Blair, I.P., Puls, I., Irobi, J., Dierick, I., Abel, A., Kennerson, M.L., Rabin, B.a.*, et al.* (2004). DNA/RNA helicase gene mutations in a form of juvenile amyotrophic lateral sclerosis (ALS4). American journal of human genetics *74*, 1128-1135.

Cheng, X.T., Zhou, B., Lin, M.Y., Cai, Q., and Sheng, Z.H. (2015). Axonal autophagosomes recruit dynein for retrograde transport through fusion with late endosomes. J Cell Biol *209*, 377-386.

Chew, J., Gendron, T.F., Prudencio, M., Sasaguri, H., Zhang, Y.-j., Castanedes-casey, M., Lee, C.W., Jansen-west, K., Kurti, A., Murray, M.E.*, et al.* (2015). C9ORF72 repeat expansions in mice cause TDP-43 pathology, neuronal loss, and behavioral deficits. 1-5.

Chiò, A., Borghero, G., Restagno, G., Mora, G., Drepper, C., Traynor, B.J., Sendtner, M., Brunetti, M., Ossola, I., Calvo, A.*, et al.* (2012). Clinical characteristics of patients with familial amyotrophic lateral sclerosis carrying the pathogenic GGGGCC hexanucleotide repeat expansion of C9ORF72. Brain *135*, 784-793.

Chio, A., Schymick, J.C., Restagno, G., Scholz, S.W., Lombardo, F., Lai, S.L., Mora, G., Fung, H.C., Britton, A., Arepalli, S.*, et al.* (2009). A two-stage genome-wide association study of sporadic amyotrophic lateral sclerosis. Hum Mol Genet *18*, 1524-1532.

Choi, C., Davey, M., Schluter, C., Pandher, P., Fang, Y., Foster, L.J., and Conibear, E. (2011). Organization and Assembly of the TRAPPII Complex. Traffic *12*, 715-725.

Chow, C.Y., Landers, J.E., Bergren, S.K., Sapp, P.C., Grant, A.E., Jones, J.M., Everett, L., Lenk, G.M., McKenna-Yasek, D.M., Weisman, L.S.*, et al.* (2009). Deleterious Variants of FIG4, a Phosphoinositide Phosphatase, in Patients with ALS. American Journal of Human Genetics *84*, 85-88.

Chow, C.Y., Zhang, Y., Dowling, J.J., Jin, N., Adamska, M., Shiga, K., Szigeti, K., Shy, M.E., Li, J., Zhang, X.*, et al.* (2007). Mutation of FIG4 causes neurodegeneration in the pale tremor mouse and patients with CMT4J. Nature *448*, 68-72.

Ciechanover, A., Elias, S., Heller, H., and Hershko, A. (1982). "Covalent affinity" purification of ubiquitin-activating enzyme. J Biol Chem *257*, 2537-2542.

Ciechanover, A., Heller, H., Katz-Etzion, R., and Hershko, A. (1981). Activation of the heat-stable polypeptide of the ATP-dependent proteolytic system. Proc Natl Acad Sci U S A *78*, 761-765.

Ciechanover, A., Hod, Y., and Hershko, A. (1978). A heat-stable polypeptide component of an ATP-dependent proteolytic system from reticulocytes. Biochemical and Biophysical Research Communications *81*, 1100-1105.

Cirulli, E.T., Lasseigne, B.N., Petrovski, S., Sapp, P.C., Dion, P.A., Leblond, C.S., Couthouis, J., Lu, Y.-F., Wang, Q., Krueger, B.J.*, et al.* (2015). Exome sequencing in amyotrophic lateral sclerosis identifies risk genes and pathways. Science (New York, NY) *347*, 1436-1441.

Ciura, S., Lattante, S., Le Ber, I., Latouche, M., Tostivint, H., Brice, A., and Kabashi, E. (2013). Loss of function of C9orf72 causes motor deficits in a zebrafish model of amyotrophic lateral sclerosis. Annals of Neurology *74*, 180-187.

Cohen, T.J., Hwang, A.W., Restrepo, C.R., Yuan, C.-X., Trojanowski, J.Q., and Lee, V.M.Y. (2015). An acetylation switch controls TDP-43 function and aggregation propensity. Nat Commun *6*.

Collard, J.F., Côté, F., and Julien, J.P. (1995). Defective axonal transport in a transgenic mouse model of amyotrophic lateral sclerosis. Nature *375*, 61-64.

Colombrita, C., Zennaro, E., Fallini, C., Weber, M., Sommacal, A., Buratti, E., Silani, V., and Ratti, A. (2009). TDP-43 is recruited to stress granules in conditions of oxidative insult. J Neurochem *111*, 1051-1061.

Constantine, R., Zhang, H., Gerstner, C.D., Frederick, J.M., and Baehr, W. (2012). Uncoordinated (UNC)119: Coordinating the trafficking of myristoylated proteins. Vision Research *75*, 26-32.

Cooper-Knock, J., Hewitt, C., Highley, J.R., Brockington, A., Milano, A., Man, S., Martindale, J., Hartley, J., Walsh, T., Gelsthorpe, C.*, et al.* (2012). Clinico-pathological features in amyotrophic lateral sclerosis with expansions in C9ORF72. Brain *135*, 751-764.

Cooper-Knock, J., Walsh, M.J., Higginbottom, A., Highley, J.R., Dickman, M.J., Edbauer, D., Ince, P.G., Wharton, S.B., Wilson, S.A., Kirby, J.*, et al.* (2014). Sequestration of multiple RNA recognition motif-containing proteins by C9orf72 repeat expansions. Brain *137*, 2040-2051.

Cox, L.E., Ferraiuolo, L., Goodall, E.F., Heath, P.R., Higginbottom, A., Mortiboys, H., Hollinger, H.C., Hartley, J.A., Brockington, A., Burness, C.E.*, et al.* (2010). Mutations in CHMP2B in lower motor neuron predominant amyotrophic lateral sclerosis (ALS). PLoS ONE *5*.

Cuervo, A.M., and Dice, J.F. (1996). A receptor for the selective uptake and degradation of proteins by lysosomes. Science *273*, 501-503.

Cullen, B.R. (2006). Enhancing and confirming the specificity of RNAi experiments. Nat Meth *3*, 677-681.

Dai, R.M., and Li, C.C. (2001). Valosin-containing protein is a multi-ubiquitin chain-targeting factor required in ubiquitin-proteasome degradation. Nature cell biology *3*, 740-744.

Damiano, M., Starkov, A.A., Petri, S., Kipiani, K., Kiaei, M., Mattiazzi, M., Flint Beal, M., and Manfredi, G. (2006). Neural mitochondrial Ca2+ capacity impairment precedes the onset of motor symptoms in G93A Cu/Zn-superoxide dismutase mutant mice. Journal of Neurochemistry *96*, 1349-1361.

Danbolt, N.C. (2001). Glutamate uptake. Prog Neurobiol *65*, 1-105.

De Stefani, D., Bononi, A., Romagnoli, A., Messina, A., De Pinto, V., Pinton, P., and Rizzuto, R. (2012). VDAC1 selectively transfers apoptotic Ca2+ signals to mitochondria. Cell Death Differ *19*, 267-273.

De Vos, K.J., Allan, V.J., Grierson, A.J., and Sheetz, M.P. (2005). Mitochondrial Function and Actin Regulate Dynamin-Related Protein 1-Dependent Mitochondrial Fission. Current Biology *15*, 678-683.

De Vos, K.J., Chapman, A.L., Tennant, M.E., Manser, C., Tudor, E.L., Lau, K.F., Brownlees, J., Ackerley, S., Shaw, P.J., Mcloughlin, D.M.*, et al.* (2007). Familial

amyotrophic lateral sclerosis-linked SOD1 mutants perturb fast axonal transport to reduce axonal mitochondria content. Human Molecular Genetics *16*, 2720-2728.

De Vos, K.J., Mórotz, G.M., Stoica, R., Tudor, E.L., Lau, K.F., Ackerley, S., Warley, A., Shaw, C.E., and Miller, C.C.J. (2012). VAPB interacts with the mitochondrial protein PTPIP51 to regulate calcium homeostasis. Human Molecular Genetics *21*, 1299-1311.

De Vos, K.J., and Sheetz, M.P. (2007). Visualization and quantification of mitochondrial dynamics in living animal cells. Methods Cell Biol *80*, 627-682.

DeJesus-Hernandez, M., Mackenzie, I.R., Boeve, B.F., Boxer, A.L., Baker, M., Rutherford, N.J., Nicholson, A.M., Finch, N.A., Flynn, H., Adamson, J.*, et al.* (2011). Expanded GGGGCC Hexanucleotide Repeat in Noncoding Region of C9ORF72 Causes Chromosome 9p-Linked FTD and ALS. Neuron *72*, 245-256.

Deng, H.-X., Chen, W., Hong, S.-T., Boycott, K.M., Gorrie, G.H., Siddique, N., Yang, Y., Fecto, F., Shi, Y., Zhai, H.*, et al.* (2011). Mutations in UBQLN2 cause dominant X-linked juvenile and adult-onset ALS and ALS/dementia. Nature *477*, 211-215.

Devereaux, K., Dall'Armi, C., Alcazar-Roman, A., Ogasawara, Y., Zhou, X., Wang, F., Yamamoto, A., de Camilli, P., and Di Paolo, G. (2013). Regulation of Mammalian Autophagy by Class II and III PI 3-Kinases through PI3P Synthesis. PLoS ONE *8*.

Dice, J.F. (1990). Peptide sequences that target cytosolic proteins for lysosomal proteolysis. Trends in biochemical sciences *15*, 305-309.

Diekstra, F.P., Van Deerlin, V.M., van Swieten, J.C., Al-Chalabi, A., Ludolph, A.C., Weishaupt, J.H., Hardiman, O., Landers, J.E., Brown, R.H., van Es, M.A.*, et al.* (2014). C9orf72 and UNC13A are shared risk loci for ALS and FTD: a genome-wide meta-analysis. Annals of neurology *76*, 120-133.

Dingledine, R., Borges, K., Bowie, D., and Traynelis, S.F. (1999). The glutamate receptor ion channels. Pharmacol Rev *51*, 7-61.

Dols-Icardo, O., García-Redondo, A., Rojas-García, R., Sánchez-Valle, R., Noguera, A., Gó mez-Tortosa, E., Pastor, P., Hernández, I., Esteban-Pérez, J., Suárez-Calvet, M.*, et al.* (2014). Characterization of the repeat expansion size in C9orf72 in amyotrophic lateral sclerosis and frontotemporal dementia. Human Molecular Genetics *23*, 749-754.

Donnelly, C.J., Zhang, P.W., Pham, J.T., Heusler, A.R., Mistry, N.a., Vidensky, S., Daley, E.L., Poth, E.M., Hoover, B., Fines, D.M.*, et al.* (2013). RNA Toxicity from the ALS/FTD C9ORF72 Expansion Is Mitigated by Antisense Intervention. Neuron *80*, 415-428.

Dormann, D., Rodde, R., Edbauer, D., Bentmann, E., Fischer, I., Hruscha, A., Than, M.E., Mackenzie, I.R.A., Capell, A., Schmid, B.*, et al.* (2010). ALS-associated fused in sarcoma (FUS) mutations disrupt Transportin-mediated nuclear import. The EMBO journal *29*, 2841-2857.

Dou, Z., Pan, J.A., Dbouk, H.A., Ballou, L.M., DeLeon, J.L., Fan, Y., Chen, J.S., Liang, Z., Li, G., Backer, J.M.*, et al.* (2013). Class IA PI3K p110β Subunit Promotes Autophagy through Rab5 Small GTPase in Response to Growth Factor Limitation. Molecular Cell *50*, 29-42.

Driscoll, J., and Goldberg, A.L. (1990). The proteasome (multicatalytic protease) is a component of the 1500-kDa proteolytic complex which degrades ubiquitin-conjugated proteins. J Biol Chem *265*, 4789-4792.

Duan, W., Li, X., Shi, J., Guo, Y., Li, Z., and Li, C. (2010). Mutant TAR DNA-binding protein-43 induces oxidative injury in motor neuron-like cell. Neuroscience *169*, 1621-1629.

Dupre, D.J., Robitaille, M., Ethier, N., Villeneuve, L.R., Mamarbachi, A.M., and Hebert, T.E. (2006). Seven transmembrane receptor core signaling complexes are assembled prior to plasma membrane trafficking. J Biol Chem *281*, 34561-34573.

Durcan, T.M., Tang, M.Y., Pérusse, J.R., Dashti, E.a., Aguileta, M.a., Mclelland, L., Gros, P., Shaler, T.a., Faubert, D., Coulombe, B.*, et al.* (2014). USP 8

regulates mitophagy by removing K 6 -linked ubiquitin conjugates from parkin. Embo, 1-19.

Edelstein, A.D., Tsuchida, M.A., Amodaj, N., Pinkard, H., Vale, R.D., and Stuurman, N. (2014). Advanced methods of microscope control using muManager software. J Biol Methods *1*.

Egan, Daniel F., Chun, Matthew G.H., Vamos, M., Zou, H., Rong, J., Miller, Chad J., Lou, Hua J., Raveendra-Panickar, D., Yang, C.-C., Sheffler, Douglas J.*, et al.* (2015). Small Molecule Inhibition of the Autophagy Kinase ULK1 and Identification of ULK1 Substrates. Molecular Cell *59*, 285-297.

Elden, A.C., Kim, H.-J., Hart, M.P., Chen-Plotkin, A.S., Johnson, B.S., Fang, X., Armakola, M., Geser, F., Greene, R., Lu, M.M.*, et al.* (2010). Ataxin-2 intermediate-length polyglutamine expansions are associated with increased risk for ALS. Nature *466*, 1069-1075.

Esser, L., Wang, C.R., Hosaka, M., Smagula, C.S., Sudhof, T.C., and Deisenhofer, J. (1998). Synapsin I is structurally similar to ATP-utilizing enzymes. EMBO J *17*, 977-984.

Eytan, E., Ganoth, D., Armon, T., and Hershko, A. (1989). ATP-dependent incorporation of 20S protease into the 26S complex that degrades proteins conjugated to ubiquitin. Proc Natl Acad Sci U S A *86*, 7751-7755.

Fader, C.M., Sánchez, D., Furlán, M., and Colombo, M.I. (2008). Induction of autophagy promotes fusion of multivesicular bodies with autophagic vacuoles in K562 cells. Traffic *9*, 230-250.

Fader, C.M., Sánchez, D.G., Mestre, M.B., and Colombo, M.I. (2009). TI-VAMP/VAMP7 and VAMP3/cellubrevin: two v-SNARE proteins involved in specific steps of the autophagy/multivesicular body pathways. Biochimica et Biophysica Acta - Molecular Cell Research *1793*, 1901-1916.

Fallini, C., Zhang, H., Su, Y., Silani, V., Singer, R.H., Rossoll, W., and Bassell, G.J. (2011). The Survival of Motor Neuron (SMN) Protein Interacts with the mRNA-Binding Protein HuD and Regulates Localization of Poly(A) mRNA in

Primary Motor Neuron Axons. The Journal of neuroscience : the official journal of the Society for Neuroscience *31*, 3914-3925.

Fang, Y.S., Tsai, K.J., Chang, Y.J., Kao, P., Woods, R., Kuo, P.H., Wu, C.C., Liao, J.Y., Chou, S.C., Lin, V.*, et al.* (2014). Full-length TDP-43 forms toxic amyloid oligomers that are present in frontotemporal lobar dementia-TDP patients. Nat Commun *5*, 4824.

Farg, M.A., Sundaramoorthy, V., Sultana, J.M., Yang, S., Atkinson, R.A.K., Levina, V., Halloran, M.A., Gleeson, P.A., Blair, I.P., Soo, K.Y.*, et al.* (2014). C9ORF72, implicated in amytrophic lateral sclerosis and frontotemporal dementia, regulates endosomal trafficking. Human Molecular Genetics *23*, 3579-3595.

Fecto, F., Yan, J., Vemula, S.P., Liu, E., Yang, Y., Chen, W., Zheng, J.G., Shi, Y., Siddique, N., Arrat, H.*, et al.* (2011). SQSTM1 mutations in familial and sporadic amyotrophic lateral sclerosis. Archives of neurology *68*, 1440-1446.

Fedorov, Y., Anderson, E.M., Birmingham, A., Reynolds, A., Karpilow, J., Robinson, K., Leake, D., Marshall, W.S., and Khvorova, A. (2006). Off-target effects by siRNA can induce toxic phenotype. RNA *12*, 1188-1196.

Ferguson, C.J., Lenk, G.M., and Meisler, M.H. (2009). Defective autophagy in neurons and astrocytes from mice deficient in PI(3,5)P2. Human Molecular Genetics *18*, 4868-4878.

Ferrante, R.J., Browne, S.E., Shinobu, L.A., Bowling, A.C., Baik, M.J., MacGarvey, U., Kowall, N.W., Brown, R.H., and Beal, M.F. (1997). Evidence of increased oxidative damage in both sporadic and familial amyotrophic lateral sclerosis. Journal of neurochemistry *69*, 2064-2074.

Ferrari, R., Kapogiannis, D., Huey, E.D., and Momeni, P. (2011). FTD and ALS: A Tale of Two Diseases. Current Alzheimer research *8*, 273-294.

Fiesel, F.C., Voigt, A., Weber, S.S., Van den Haute, C., Waldenmaier, A., Gorner, K., Walter, M., Anderson, M.L., Kern, J.V., Rasse, T.M.*, et al.* (2010).

Knockdown of transactive response DNA-binding protein (TDP-43) downregulates histone deacetylase 6. EMBO J *29*, 209-221.

Figueiredo, A.C., Wasmeier, C., Tarafder, A.K., Ramalho, J.S., Baron, R.A., and Seabra, M.C. (2008). Rab3GEP is the non-redundant guanine nucleotide exchange factor for Rab27a in melanocytes. J Biol Chem *283*, 23209-23216.

Filimonenko, M., Isakson, P., Finley, K.D., Anderson, M., Melia, T.J., Jeong, H., Bartlett, B.J., Myers, K.M., Birkeland, H.C.G., Lamark, T.*, et al.* (2010). The selective macroautophagic degradation of aggregated proteins requires the phosphatidylinositol 3-phosphate binding protein Alfy. Molecular cell *38*, 265-279.

Filimonenko, M., Stuffers, S., Raiborg, C., Yamamoto, A., Malerød, L., Fisher, E.M.C., Isaacs, A., Brech, A., Stenmark, H., and Simonsen, A. (2007). Functional multivesicular bodies are required for autophagic clearance of protein aggregates associated with neurodegenerative disease. Journal of Cell Biology *179*, 485-500.

Fiszman, M.L., Ricart, K.C., Latini, A., Rodríguez, G., and Sica, R.E.P. (2010). In vitro neurotoxic properties and excitatory aminoacids concentration in the cerebrospinal fluid of amyotrophic lateral sclerosis patients. Relationship with the degree of certainty of disease diagnoses. Acta Neurologica Scandinavica *121*, 120-126.

Fray, A.E., Ince, P.G., Banner, S.J., Milton, I.D., Usher, P.A., Cookson, M.R., and Shaw, P.J. (1998). The expression of the glial glutamate transporter protein EAAT2 in motor neuron disease: an immunohistochemical study. The European journal of neuroscience *10*, 2481-2489.

Freischmidt, A., Wieland, T., Richter, B., Ruf, W., Schaeffer, V., Müller, K., Marroquin, N., Nordin, F., Hübers, A., Weydt, P.*, et al.* (2015). Haploinsufficiency of TBK1 causes familial ALS and fronto-temporal dementia. Nature Neuroscience *18*.

Fujii, R., Okabe, S., Urushido, T., Inoue, K., Yoshimura, A., Tachibana, T., Nishikawa, T., Hicks, G.G., and Takumi, T. (2005). The RNA binding protein

TLS is translocated to dendritic spines by mGluR5 activation and regulates spine morphology. Curr Biol *15*, 587-593.

Fujita, N., Itoh, T., Omori, H., Fukuda, M., Noda, T., and Yoshimori, T. (2008). The Atg16L complex specifies the site of LC3 lipidation for membrane biogenesis in autophagy. Molecular biology of the cell *19*, 2092-2100.

Furuta, N., Fujita, N., Noda, T., Yoshimori, T., and Amano, A. (2010). Combinational soluble N-ethylmaleimide-sensitive factor attachment protein receptor proteins VAMP8 and Vti1b mediate fusion of antimicrobial and canonical autophagosomes with lysosomes. Molecular biology of the cell *21*, 1001-1010.

Furuya, N., Yu, J., Byfield, M., Pattingre, S., and Levine, B. (2005). The evolutionarily conserved domain of Beclin 1 is required for Vps34 binding, autophagy and tumor suppressor function. Autophagy *1*, 46-52.

Gallagher, M.D., Suh, E., Grossman, M., Elman, L., McCluskey, L., Van Swieten, J.C., Al-Sarraj, S., Neumann, M., Gelpi, E., Ghetti, B.*, et al.* (2014). TMEM106B is a genetic modifier of frontotemporal lobar degeneration with C9orf72 hexanucleotide repeat expansions. Acta Neuropathol *127*, 407-418.

Gammoh, N., Florey, O., Overholtzer, M., and Jiang, X. (2013). Interaction between FIP200 and ATG16L1 distinguishes ULK1 complex-dependent and -independent autophagy. Nat Struct Mol Biol *20*, 144-149.

Ganley, I.G., Lam, D.H., Wang, J., Ding, X., Chen, S., and Jiang, X. (2009). ULK1·ATG13·FIP200 complex mediates mTOR signaling and is essential for autophagy. Journal of Biological Chemistry *284*, 12297-12305.

Gendron, T.F., Bieniek, K.F., Zhang, Y.J., Jansen-West, K., Ash, P.E.a., Caulfield, T., Daughrity, L., Dunmore, J.H., Castanedes-Casey, M., Chew, J.*, et al.* (2013). Antisense transcripts of the expanded C9ORF72 hexanucleotide repeat form nuclear RNA foci and undergo repeat-associated non-ATG translation in c9FTD/ALS. Acta Neuropathol *126*, 829-844.

Geng, J., Nair, U., Yasumura-Yorimitsu, K., and Klionsky, D.J. (2010). Post-Golgi Sec proteins are required for autophagy in Saccharomyces cerevisiae. Mol Biol Cell *21*, 2257-2269.

Gijselinck, I., Engelborghs, S., Maes, G., Cuijt, I., Peeters, K., Mattheijssens, M., Joris, G., Cras, P., Martin, J.J., De Deyn, P.P.*, et al.* (2010). Identification of 2 Loci at chromosomes 9 and 14 in a multiplex family with frontotemporal lobar degeneration and amyotrophic lateral sclerosis. Arch Neurol *67*, 606-616.

Gijselinck, I., Van Langenhove, T., van der Zee, J., Sleegers, K., Philtjens, S., Kleinberger, G., Janssens, J., Bettens, K., Van Cauwenberghe, C., Pereson, S.*, et al.* (2012). A C9orf72 promoter repeat expansion in a Flanders-Belgian cohort with disorders of the frontotemporal lobar degeneration-amyotrophic lateral sclerosis spectrum: A gene identification study. The Lancet Neurology *11*, 54-65.

Gill, S.R., Schroer, T.A., Szilak, I., Steuer, E.R., Sheetz, M.P., and Cleveland, D.W. (1991). Dynactin, a conserved, ubiquitously expressed component of an activator of vesicle motility mediated by cytoplasmic dynein. J Cell Biol *115*, 1639-1650.

Giordana, M.T., Piccinini, M., Grifoni, S., De Marco, G., Vercellino, M., Magistrello, M., Pellerino, A., Buccinnà, B., Lupino, E., and Rinaudo, M.T. (2010). TDP-43 redistribution is an early event in sporadic amyotrophic lateral sclerosis. Brain pathology (Zurich, Switzerland) *20*, 351-360.

Gkogkas, C., Middleton, S., Kremer, A.M., Wardrope, C., Hannah, M., Gillingwater, T.H., and Skehel, P. (2008). VAPB interacts with and modulates the activity of ATF6. Human Molecular Genetics *17*, 1517-1526.

Gnesutta, N., Ceriani, M., Innocenti, M., Mauri, I., Zippel, R., Sturani, E., Borgonovo, B., Berruti, G., and Martegani, E. (2001). Cloning and Characterization of Mouse UBPy, a Deubiquitinating Enzyme That Interacts with the Ras Guanine Nucleotide Exchange Factor CDC25Mm/Ras-GRF1. Journal of Biological Chemistry *276*, 39448-39454.

Goldknopf, I.L., and Busch, H. (1977). Isopeptide linkage between nonhistone and histone 2A polypeptides of chromosomal conjugate-protein A24. Proc Natl Acad Sci U S A *74*, 864-868.

Goldknopf, I.L., Sheta, E.A., Bryson, J., Folsom, B., Wilson, C., Duty, J., Yen, A.A., and Appel, S.H. (2006). Complement C3c and related protein biomarkers in amyotrophic lateral sclerosis and Parkinson's disease. Biochem Biophys Res Commun *342*, 1034-1039.

Gomes, A.Q., Ali, B.R., Ramalho, J.S., Godfrey, R.F., Barral, D.C., Hume, A.N., and Seabra, M.C. (2003). Membrane targeting of Rab GTPases is influenced by the prenylation motif. Mol Biol Cell *14*, 1882-1899.

Gómez-Tortosa, E., Gallego, J., Guerrero-López, R., Marcos, A., Gil-Neciga, E., José Sainz, M., Díaz, A., Franco-Macías, E., Trujillo-Tiebas, M.J., Ayuso, C.*, et al.* (2013). C9ORF72 hexanucleotide expansions of 20-22 repeats are associated with frontotemporal deterioration. Neurology *80*, 366-370.

Gordon, P.H., Salachas, F., Lacomblez, L., Le Forestier, N., Pradat, P.-F., Bruneteau, G., Elbaz, A., and Meininger, V. (2012). Predicting Survival of Patients with Amyotrophic Lateral Sclerosis at Presentation: A 15-Year Experience. In Neurodegenerative Diseases.

Greenway, M.J., Andersen, P.M., Russ, C., Ennis, S., Cashman, S., Donaghy, C., Patterson, V., Swingler, R., Kieran, D., Prehn, J.*, et al.* (2006). ANG mutations segregate with familial and 'sporadic' amyotrophic lateral sclerosis. Nature genetics *38*, 411-413.

Greger, V., Passarge, E., Hopping, W., Messmer, E., and Horsthemke, B. (1989). Epigenetic changes may contribute to the formation and spontaneous regression of retinoblastoma. Hum Genet *83*, 155-158.

Grosshans, B.L., Ortiz, D., and Novick, P. (2006). Rabs and their effectors: Achieving specificity in membrane traffic. Proceedings of the National Academy of Sciences *103*, 11821-11827.

Gutierrez, M.G., Munafó, D.B., Berón, W., and Colombo, M.I. (2004). Rab7 is required for the normal progression of the autophagic pathway in mammalian cells. Journal of cell science *117*, 2687-2697.

Hadano, S., Hand, C.K., Osuga, H., Yanagisawa, Y., Otomo, A., Devon, R.S., Miyamoto, N., Showguchi-Miyata, J., Okada, Y., Singaraja, R.*, et al.* (2001a). A gene encoding a putative GTPase regulator is mutated in familial amyotrophic lateral sclerosis 2. Nature genetics *29*, 166-173.

Hadano, S., Otomo, A., Kunita, R., Suzuki-Utsunomiya, K., Akatsuka, A., Koike, M., Aoki, M., Uchiyama, Y., Itoyama, Y., and Ikeda, J.E. (2010). Loss of ALS2/Alsin exacerbates motor dysfunction in a SOD1H46R-expressing mouse ALS model by disturbing endolysosomal trafficking. PLoS ONE *5*.

Hadano, S., Yanagisawa, Y., Skaug, J., Fichter, K., Nasir, J., Martindale, D., Koop, B.F., Scherer, S.W., Nicholson, D.W., Rouleau, G.A.*, et al.* (2001b). Cloning and characterization of three novel genes, ALS2CR1, ALS2CR2, and ALS2CR3, in the juvenile amyotrophic lateral sclerosis (ALS2) critical region at chromosome 2q33-q34: candidate genes for ALS2. Genomics *71*, 200-213.

Haeusler, A.R., Donnelly, C.J., Periz, G., Simko, E.a.J., Shaw, P.G., Kim, M.-S., Maragakis, N.J., Troncoso, J.C., Pandey, A., Sattler, R.*, et al.* (2014). C9orf72 nucleotide repeat structures initiate molecular cascades of disease. Nature *507*, 195-200.

Hafezparast, M., Klocke, R., Ruhrberg, C., Marquardt, A., Ahmad-Annuar, A., Bowen, S., Lalli, G., Witherden, A.S., Hummerich, H., Nicholson, S.*, et al.* (2003). Mutations in dynein link motor neuron degeneration to defects in retrograde transport. Science *300*, 808-812.

Hailey, D.W., Rambold, A.S., Satpute-Krishnan, P., Mitra, K., Sougrat, R., Kim, P.K., and Lippincott-Schwartz, J. (2010). Mitochondria Supply Membranes for Autophagosome Biogenesis during Starvation. Cell *141*, 656-667.

Hamasaki, M., Furuta, N., Matsuda, A., Nezu, A., Yamamoto, A., Fujita, N., Oomori, H., Noda, T., Haraguchi, T., Hiraoka, Y.*, et al.* (2013). Autophagosomes form at ER-mitochondria contact sites. Nature *495*, 389-393.

Hanada, T., Noda, N.N., Satomi, Y., Ichimura, Y., Fujioka, Y., Takao, T., Inagaki, F., and Ohsumi, Y. (2007). The Atg12-Atg5 conjugate has a novel E3-like activity for protein lipidation in autophagy. Journal of Biological Chemistry *282*, 37298-37302.

Hand, C.K., Khoris, J., Salachas, F., Gros-Louis, F., Lopes, A.A., Mayeux-Portas, V., Brewer, C.G., Brown, R.H., Jr., Meininger, V., Camu, W.*, et al.* (2002). A novel locus for familial amyotrophic lateral sclerosis, on chromosome 18q. Am J Hum Genet *70*, 251-256.

Hara, T., Nakamura, K., Matsui, M., Yamamoto, A., Nakahara, Y., Suzuki-Migishima, R., Yokoyama, M., Mishima, K., Saito, I., Okano, H.*, et al.* (2006). Suppression of basal autophagy in neural cells causes neurodegenerative disease in mice. Nature *441*, 885-889.

Hara, T., Takamura, A., Kishi, C., Iemura, S.I., Natsume, T., Guan, J.L., and Mizushima, N. (2008). FIP200, a ULK-interacting protein, is required for autophagosome formation in mammalian cells. Journal of Cell Biology *181*, 497-510.

Harraz, M.M., Marden, J.J., Zhou, W., Zhang, Y., Williams, A., Sharov, V.S., Nelson, K., Luo, M., Paulson, H., Schoneich, C.*, et al.* (2008). SOD1 mutations disrupt redox-sensitive Rac regulation of NADPH oxidase in a familial ALS model. J Clin Invest *118*, 659-670.

Hayashi, T., and Su, T.P. (2007). Sigma-1 receptor chaperones at the ER-mitochondrion interface regulate Ca(2+) signaling and cell survival. Cell *131*, 596-610.

Hayashi-Nishino, M., Fujita, N., Noda, T., Yamaguchi, A., Yoshimori, T., and Yamamoto, A. (2009). A subdomain of the endoplasmic reticulum forms a cradle for autophagosome formation. Nature cell biology *11*, 1433-1437.

Hays, A.P., Naini, A., He, C.Z., Mitsumoto, H., and Rowland, L.P. (2006). Sporadic amyotrophic lateral sclerosis and breast cancer: Hyaline conglomerate inclusions lead to identification of SOD1 mutation. In Journal of the Neurological Sciences, pp. 67-69.

He, C., Song, H., Yorimitsu, T., Monastyrska, I., Yen, W.-L., Legakis, J.E., and Klionsky, D.J. (2006). Recruitment of Atg9 to the preautophagosomal structure by Atg11 is essential for selective autophagy in budding yeast. The Journal of Cell Biology *175*, 925-935.

Herman, J.G., Merlo, A., Mao, L., Lapidus, R.G., Issa, J.P., Davidson, N.E., Sidransky, D., and Baylin, S.B. (1995). Inactivation of the CDKN2/p16/MTS1 gene is frequently associated with aberrant DNA methylation in all common human cancers. Cancer Res *55*, 4525-4530.

Hershko, A., and Heller, H. (1985). Occurrence of a polyubiquitin structure in ubiquitin-protein conjugates. Biochem Biophys Res Commun *128*, 1079-1086.

Hershko, A., Heller, H., Elias, S., and Ciechanover, A. (1983). Components of ubiquitin-protein ligase system. Resolution, affinity purification, and role in protein breakdown. J Biol Chem *258*, 8206-8214.

Hetz, C. (2012). The unfolded protein response: controlling cell fate decisions under ER stress and beyond. In Nature Reviews Molecular Cell Biology.

Higgins, C.M.J., Jung, C., Ding, H., and Xu, Z. (2002). Mutant Cu, Zn superoxide dismutase that causes motoneuron degeneration is present in mitochondria in the CNS. The Journal of neuroscience : the official journal of the Society for Neuroscience *22*, RC215.

Highley, J.R., Kirby, J., Jansweijer, J.a., Webb, P.S., Hewamadduma, C.a., Heath, P.R., Higginbottom, A., Raman, R., Ferraiuolo, L., Cooper-Knock, J.*, et al.* (2014). Loss of nuclear TDP-43 in ALS causes altered expression of splicing machinery and widespread dysregulation of RNA splicing in motor neurons. Neuropathology and applied neurobiology.

Hirano, A., Donnenfeld, H., Sasaki, S., and Nakano, I. (1984). Fine structural observations of neurofilamentous changes in amyotrophic lateral sclerosis. Journal of neuropathology and experimental neurology *43*, 461-470.

Hirano, M., Nakamura, Y., Saigoh, K., Sakamoto, H., Ueno, S., Isono, C., Miyamoto, K., Akamatsu, M., Mitsui, Y., and Kusunoki, S. (2013). Mutations in

the gene encoding p62 in Japanese patients with amyotrophic lateral sclerosis. Neurology *80*, 458-463.

Hirota, Y., and Tanaka, Y. (2009). A small GTPase, human Rab32, is required for the formation of autophagic vacuoles under basal conditions. Cell Mol Life Sci *66*, 2913-2932.

Hoffman, L., Pratt, G., and Rechsteiner, M. (1992). Multiple forms of the 20 S multicatalytic and the 26 S ubiquitin/ATP-dependent proteases from rabbit reticulocyte lysate. J Biol Chem *267*, 22362-22368.

Hollmann, M., Hartley, M., and Heinemann, S. (1991). Ca2+ permeability of KA-AMPA--gated glutamate receptor channels depends on subunit composition. Science *252*, 851-853.

Horiuchi, H., Lippe, R., McBride, H.M., Rubino, M., Woodman, P., Stenmark, H., Rybin, V., Wilm, M., Ashman, K., Mann, M.*, et al.* (1997). A novel Rab5 GDP/GTP exchange factor complexed to Rabaptin-5 links nucleotide exchange to effector recruitment and function. Cell *90*, 1149-1159.

Hosaka, M., and Südhof, T.C. (1998a). Synapsin III, a Novel Synapsin with an Unusual Regulation by Ca2+. Journal of Biological Chemistry *273*, 13371-13374.

Hosaka, M., and Südhof, T.C. (1998b). Synapsins I and II Are ATP-binding Proteins with Differential Ca2+ Regulation. Journal of Biological Chemistry *273*, 1425-1429.

Hosokawa, N., Hara, T., Kaizuka, T., Kishi, C., Takamura, A., Miura, Y., Iemura, S.-i., Natsume, T., Takehana, K., Yamada, N.*, et al.* (2009a). Nutrient-dependent mTORC1 association with the ULK1-Atg13-FIP200 complex required for autophagy. Molecular biology of the cell *20*, 1981-1991.

Hosokawa, N., Sasaki, T., Iemura, S.I., Natsume, T., Hara, T., and Mizushima, N. (2009b). Atg101, a novel mammalian autophagy protein interacting with Atg13. Autophagy *5*, 973-979.

Huang, J., Birmingham, C.L., Shahnazari, S., Shiu, J., Zheng, Y.T., Smith, A.C., Campellone, K.G., Do Heo, W., Gruenheid, S., Meyer, T.*, et al.* (2011). Antibacterial autophagy occurs at PtdIns(3)P-enriched domains of the endoplasmic reticulum and requires Rab1 GTPase. Autophagy *7*, 17-26.

Huibregtse, J.M., Scheffner, M., Beaudenon, S., and Howley, P.M. (1995). A family of proteins structurally and functionally related to the E6-AP ubiquitin-protein ligase. Proc Natl Acad Sci U S A *92*, 2563-2567.

Hukema, R.K., Riemslagh, F.W., Melhem, S., van der Linde, H.C., Severijnen, L.-A.W.F.M., Edbauer, D., Maas, A., Charlet-Berguerand, N., Willemsen, R., and van Swieten, J.C. (2014). A new inducible transgenic mouse model for C9orf72-associated GGGGCC repeat expansion supports a gain-of-function mechanism in C9orf72-associated ALS and FTD. Acta Neuropathologica Communications *2*, 166.

Hume, R.I., Dingledine, R., and Heinemann, S.F. (1991). Identification of a site in glutamate receptor subunits that controls calcium permeability. Science *253*, 1028-1031.

Hyttinen, J.M.T., Amadio, M., Viiri, J., Pascale, A., Salminen, A., and Kaarniranta, K. (2014). Clearance of misfolded and aggregated proteins by aggrephagy and implications for aggregation diseases. Ageing Research Reviews *18*, 16-28.

Israelson, A., Arbel, N., Da Cruz, S., Ilieva, H., Yamanaka, K., Shoshan-Barmatz, V., and Cleveland, D.W. (2010). Misfolded mutant SOD1 directly inhibits VDAC1 conductance in a mouse model of inherited ALS. Neuron *67*, 575-587.

Itakura, E., Kishi, C., Inoue, K., and Mizushima, N. (2008). Beclin 1 forms two distinct phosphatidylinositol 3-kinase complexes with mammalian Atg14 and UVRAG. Molecular biology of the cell *19*, 5360-5372.

Itakura, E., and Mizushima, N. (2010). Characterization of autophagosome formation site by a hierarchical analysis of mammalian Atg proteins. Autophagy *6*, 764-776.

Ito, H., Nakamura, M., Komure, O., Ayaki, T., Wate, R., Maruyama, H., Nakamura, Y., Fujita, K., Kaneko, S., Okamoto, Y.*, et al.* (2011). Clinicopathologic study on an ALS family with a heterozygous E478G optineurin mutation. Acta Neuropathol *122*, 223-229.

Itoh, T., Fujita, N., Kanno, E., Yamamoto, A., Yoshimori, T., and Fukuda, M. (2008). Golgi-resident Small GTPase Rab33B Interacts with Atg16L and Modulates Autophagosome Formation. Molecular Biology of the Cell *19*, 2916-2925.

Jäger, S., Bucci, C., Tanida, I., Ueno, T., Kominami, E., Saftig, P., and Eskelinen, E.-L. (2004). Role for Rab7 in maturation of late autophagic vacuoles. Journal of cell science *117*, 4837-4848.

Jahreiss, L., Menzies, F.M., and Rubinsztein, D.C. (2008). The itinerary of autophagosomes: from peripheral formation to kiss-and-run fusion with lysosomes. Traffic *9*, 574-587.

Jin, M., Saucan, L., Farquhar, M.G., and Palade, G.E. (1996). Rab1a and multiple other Rab proteins are associated with the transcytotic pathway in rat liver. Journal of Biological Chemistry *271*, 30105-30113.

Johansson, M., Rocha, N., Zwart, W., Jordens, I., Janssen, L., Kuijl, C., Olkkonen, V.M., and Neefjes, J. (2007). Activation of endosomal dynein motors by stepwise assembly of Rab7-RILP-p150Glued, ORP1L, and the receptor betalll spectrin. J Cell Biol *176*, 459-471.

Johnson, J.O., Mandrioli, J., Benatar, M., Abramzon, Y., Van Deerlin, V.M., Trojanowski, J.Q., Gibbs, J.R., Brunetti, M., Gronka, S., Wuu, J.*, et al.* (2010). Exome Sequencing Reveals VCP Mutations as a Cause of Familial ALS. Neuron *68*, 857-864.

Johnson, J.O., Pioro, E.P., Boehringer, A., Chia, R., Feit, H., Renton, A.E., Pliner, H.a., Abramzon, Y., Marangi, G., Winborn, B.J.*, et al.* (2014). Mutations in the Matrin 3 gene cause familial amyotrophic lateral sclerosis. Nature neuroscience *17*, 664-666.

Jones, C.T., Swingler, R.J., and Brock, D.J.H. (1994). Identification of a novel S0D1 mutation in an apparently sporadic amyotrophic lateral sclerosis patient and the detection of Ile113Thr in three others. Human Molecular Genetics *3* 649-650.

Jones, P.A., and Baylin, S.B. (2002). The fundamental role of epigenetic events in cancer. Nature reviews Genetics *3*, 415-428.

Ju, J.S., Fuentealba, R.A., Miller, S.E., Jackson, E., Piwnica-Worms, D., Baloh, R.H., and Weihl, C.C. (2009). Valosin-containing protein (VCP) is required for autophagy and is disrupted in VCP disease. Journal of Cell Biology *187*, 875-888.

Jung, C.H., Jun, C.B., Ro, S.-H., Kim, Y.-M., Otto, N.M., Cao, J., Kundu, M., and Kim, D.-H. (2009). ULK-Atg13-FIP200 complexes mediate mTOR signaling to the autophagy machinery. Molecular biology of the cell *20*, 1992-2003.

Kabashi, E., Valdmanis, P.N., Dion, P., Spiegelman, D., McConkey, B.J., Vande Velde, C., Bouchard, J.-P., Lacomblez, L., Pochigaeva, K., Salachas, F.*, et al.* (2008). TARDBP mutations in individuals with sporadic and familial amyotrophic lateral sclerosis. Nature genetics *40*, 572-574.

Kabeya, Y. (2000). LC3, a mammalian homologue of yeast Apg8p, is localized in autophagosome membranes after processing. In The EMBO Journal, pp. 5720-5728.

Kabeya, Y., Mizushima, N., Yamamoto, A., Oshitani-Okamoto, S., Ohsumi, Y., and Yoshimori, T. (2004). LC3, GABARAP and GATE16 localize to autophagosomal membrane depending on form-II formation. Journal of cell science *117*, 2805-2812.

Kakuta, S., Yamamoto, H., Negishi, L., Kondo-Kakuta, C., Hayashi, N., and Ohsumi, Y. (2012). Atg9 vesicles recruit vesicle-tethering proteins Trs85 and Ypt1 to the autophagosome formation site. Journal of Biological Chemistry *287*, 44261-44269.

Kanekura, K., Nishimoto, I., Aiso, S., and Matsuoka, M. (2006). Characterization of amyotrophic lateral sclerosis-linked P56S mutation of vesicle-associated membrane protein-associated protein B (VAPB/ALS8). Journal of Biological Chemistry *281*, 30223-30233.

Kasher, P.R., De Vos, K.J., Wharton, S.B., Manser, C., Bennett, E.J., Bingley, M., Wood, J.D., Milner, R., McDermott, C.J., Miller, C.C.J.*, et al.* (2009). Direct evidence for axonal transport defects in a novel mouse model of mutant spastin-induced hereditary spastic paraplegia (HSP) and human HSP patients. Journal of Neurochemistry *110*, 34-44.

Kato, M., Miyazawa, K., and Kitamura, N. (2000). A Deubiquitinating Enzyme UBPY Interacts with the Src Homology 3 Domain of Hrs-binding Protein via a Novel Binding Motif PX(V/I)(D/N)RXXKP. Journal of Biological Chemistry *275*, 37481-37487.

Kato, T., Katagiri, T., Hirano, A., Kawanami, T., and Sasaki, H. (1989). Lewy body-like hyaline inclusions in sporadic motor neuron disease are ubiquitinated. Acta Neuropathol *77*, 391-396.

Katsumata, K., Nishiyama, J., Inoue, T., Mizushima, N., Takeda, J., and Yuzaki, M. (2010). Dynein- and activity-dependent retrograde transport of autophagosomes in neuronal axons. Autophagy *6*, 378-385.

Kaushik, S., Rodriguez-Navarro, J.A., Arias, E., Kiffin, R., Sahu, S., Schwartz, G.J., Cuervo, A.M., and Singh, R. (2011). Autophagy in hypothalamic AgRP neurons regulates food intake and energy balance. Cell metabolism *14*, 173-183.

Kawahara, Y., Ito, K., Sun, H., Aizawa, H., Kanazawa, I., and Kwak, S. (2004). Glutamate receptors: RNA editing and death of motor neurons. Nature *427*, 801.

Kieran, D., Hafezparast, M., Bohnert, S., Dick, J.R.T., Martin, J., Schiavo, G., Fisher, E.M.C., and Greensmith, L. (2005). A mutation in dynein rescues axonal transport defects and extends the life span of ALS mice. The Journal of Cell Biology *169*, 561-567.

Kiernan, M.C., Vucic, S., Cheah, B.C., Turner, M.R., Eisen, A., Hardiman, O., Burrell, J.R., and Zoing, M.C. (2011). Amyotrophic lateral sclerosis. Lancet *377*, 942-955.

Kim, H.J., Kim, N.C., Wang, Y.D., Scarborough, E.A., Moore, J., Diaz, Z., MacLea, K.S., Freibaum, B., Li, S., Molliex, A.*, et al.* (2013). Mutations in prion-like domains in hnRNPA2B1 and hnRNPA1 cause multisystem proteinopathy and ALS. Nature *495*, 467-473.

Kim, J., Kundu, M., Viollet, B., and Guan, K.-L. (2011). AMPK and mTOR regulate autophagy through direct phosphorylation of Ulk1. Nature cell biology *13*, 132-141.

Kim, P.K., Hailey, D.W., Mullen, R.T., and Lippincott-Schwartz, J. (2008). Ubiquitin signals autophagic degradation of cytosolic proteins and peroxisomes. Proceedings of the National Academy of Sciences of the United States of America *105*, 20567-20574.

Kimura, S., Noda, T., and Yoshimori, T. (2008). Dynein-dependent movement of autophagosomes mediates efficient encounters with lysosomes. Cell structure and function *33*, 109-122.

King, A.E., Dickson, T.C., Blizzard, C.A., Foster, S.S., Chung, R.S., West, A.K., Chuah, M.I., and Vickers, J.C. (2007). Excitotoxicity mediated by non-NMDA receptors causes distal axonopathy in long-term cultured spinal motor neurons. Eur J Neurosci *26*, 2151-2159.

Klionsky, D.J., Abdalla, F.C., Abeliovich, H., Abraham, R.T., Acevedo-Arozena, A., Adeli, K., Agholme, L., Agnello, M., Agostinis, P., Aguirre-Ghiso, J.A.*, et al.* (2012). Guidelines for the use and interpretation of assays for monitoring autophagy. Autophagy *8*, 445-544.

Klionsky, D.J., Elazar, Z., Seglen, P.O., and Rubinsztein, D.C. (2008). Does bafilomycin A1 block the fusion of autophagosomes with lysosomes? Autophagy *4*, 849-850.

Knecht, E., Martinez-Ramón, A., and Grisolia, S. (1988). Autophagy of mitochondria in rat liver assessed by immunogold procedures. The journal of histochemistry and cytochemistry : official journal of the Histochemistry Society *36*, 1433-1440.

Knobel, K.M., Davis, W.S., Jorgensen, E.M., and Bastiani, M.J. (2001). UNC-119 suppresses axon branching in C. elegans. Development *128*, 4079-4092.

Ko, H.S., Uehara, T., Tsuruma, K., and Nomura, Y. (2004). Ubiquilin interacts with ubiquitylated proteins and proteasome through its ubiquitin-associated and ubiquitin-like domains. FEBS Letters *566*, 110-114.

Komander, D., Clague, M.J., and Urbe, S. (2009). Breaking the chains: structure and function of the deubiquitinases. Nat Rev Mol Cell Biol *10*, 550-563.

Komatsu, M., Waguri, S., Chiba, T., Murata, S., Iwata, J.-i., Tanida, I., Ueno, T., Koike, M., Uchiyama, Y., Kominami, E.*, et al.* (2006). Loss of autophagy in the central nervous system causes neurodegeneration in mice. Nature *441*, 880-884.

Komatsu, M., Waguri, S., Koike, M., Sou, Y.s., Ueno, T., Hara, T., Mizushima, N., Iwata, J.i., Ezaki, J., Murata, S.*, et al.* (2007). Homeostatic Levels of p62 Control Cytoplasmic Inclusion Body Formation in Autophagy-Deficient Mice. Cell *131*, 1149-1163.

Kondo-Okamoto, N., Noda, N.N., Suzuki, S.W., Nakatogawa, H., Takahashi, I., Matsunami, M., Hashimoto, A., Inagaki, F., Ohsumi, Y., and Okamoto, K. (2012). Autophagy-related Protein 32 Acts as Autophagic Degron and Directly Initiates Mitophagy. The Journal of Biological Chemistry *287*, 10631-10638.

Konno, H., Konno, K., and Barber, Glen N. (2013a). Cyclic Dinucleotides Trigger ULK1 (ATG1) Phosphorylation of STING to Prevent Sustained Innate Immune Signaling. Cell *155*, 688-698.

Konno, T., Shiga, A., Tsujino, A., Sugai, A., Kato, T., Kanai, K., Yokoseki, A., Eguchi, H., Kuwabara, S., Nishizawa, M.*, et al.* (2013b). Japanese amyotrophic

lateral sclerosis patients with GGGGCC hexanucleotide repeat expansion in C9ORF72. J Neurol Neurosurg Psychiatry *84*, 398-401.

Koppers, M., Blokhuis, A.M., Westeneng, H.-J., Terpstra, M.L., Zundel, C.a.C., Vieira de Sá, R., Schellevis, R.D., Waite, A.J., Blake, D.J., Veldink, J.H.*, et al.* (2015). C9orf72 ablation in mice does not cause motor neuron degeneration or motor deficits. Annals of Neurology, n/a-n/a.

Kopperud, R., Krakstad, C., Selheim, F., and Doskeland, S.O. (2003). cAMP effector mechanisms. Novel twists for an 'old' signaling system. FEBS Lett *546*, 121-126.

Korac, J., Schaeffer, V., Kovacevic, I., Clement, A.M., Jungblut, B., Behl, C., Terzic, J., and Dikic, I. (2013). Ubiquitin-independent function of optineurin in autophagic clearance of protein aggregates. Journal of cell science *126*, 580-592.

Korobko, E., Kiselev, S., Olsnes, S., Stenmark, H., and Korobko, I. (2005). The Rab5 effector Rabaptin-5 and its isoform Rabaptin-5delta differ in their ability to interact with the small GTPase Rab4. FEBS J *272*, 37-46.

Kruman, II, Pedersen, W.A., Springer, J.E., and Mattson, M.P. (1999). ALS-linked Cu/Zn-SOD mutation increases vulnerability of motor neurons to excitotoxicity by a mechanism involving increased oxidative stress and perturbed calcium homeostasis. Exp Neurol *160*, 28-39.

Kuusisto, E., Salminen, A., and Alafuzoff, I. (2001). Ubiquitin-binding protein p62 is present in neuronal and glial inclusions in human tauopathies and synucleinopathies. Neuroreport *12*, 2085-2090.

Kuusisto, E., Salminen, A., and Alafuzoff, I. (2002). Early accumulation of p62 in neurofibrillary tangles in alzheimer's disease: Possible role in tangle formation. Neuropathology and Applied Neurobiology *28*, 228-237.

Kwak, S., Hideyama, T., Yamashita, T., and Aizawa, H. (2010). AMPA receptor-mediated neuronal death in sporadic ALS. In Neuropathology, pp. 182-188.

Kwiatkowski, T.J., Bosco, D.A., Leclerc, A.L., Tamrazian, E., Vanderburg, C.R., Russ, C., Davis, A., Gilchrist, J., Kasarskis, E.J., Munsat, T.*, et al.* (2009). Mutations in the FUS/TLS gene on chromosome 16 cause familial amyotrophic lateral sclerosis. Science (New York, NY) *323*, 1205-1208.

Kwon, I., Xiang, S., Kato, M., Wu, L., Theodoropoulos, P., Wang, T., Kim, J., Yun, J., Xie, Y., and McKnight, S.L. (2014). Poly-dipeptides encoded by the C9ORF72 repeats bind nucleoli, impede RNA biogenesis, and kill cells. Science (New York, NY), 1254917.

Lacomblez, L., Bensimon, G., Leigh, P.N., Guillet, P., and Meininger, V. (1996). Dose-ranging study of riluzole in amyotrophic lateral sclerosis. Amyotrophic Lateral Sclerosis/Riluzole Study Group II. Paper presented at: Lancet.

Lagier-Tourenne, C., Baughn, M., Rigo, F., Sun, S., Liu, P., Li, H.-R., Jiang, J., Watt, A.T., Chun, S., Katz, M.*, et al.* (2013). Targeted degradation of sense and antisense C9orf72 RNA foci as therapy for ALS and frontotemporal degeneration. Proceedings of the National Academy of Sciences of the United States of America *110*, E4530-4539.

Lagier-Tourenne, C., Polymenidou, M., and Cleveland, D.W. (2010). TDP-43 and FUS/TLS: emerging roles in RNA processing and neurodegeneration. Human Molecular Genetics *19*, R46-R64.

Lamark, T., Kirkin, V., Dikic, I., and Johansen, T. (2009). NBR1 and p62 as cargo receptors for selective autophagy of ubiquitinated targets. In Cell Cycle, pp. 1986-1990.

Layfield, R., Cavey, J.R., Najat, D., Long, J., Sheppard, P.W., Ralston, S.H., and Searle, M.S. (2006). p62 mutations, ubiquitin recognition and Paget's disease of bone. Biochem Soc Trans *34*, 735-737.

Lazarou, M., Smith, S.M., Thorburn, D.R., Ryan, M.T., and McKenzie, M. (2009). Assembly of nuclear DNA-encoded subunits into mitochondrial complex IV, and their preferential integration into supercomplex forms in patient mitochondria. FEBS J *276*, 6701-6713.

Le Ber, I., Camuzat, A., Berger, E., Hannequin, D., Laquerriere, A., Golfier, V., Seilhean, D., Viennet, G., Couratier, P., Verpillat, P.*, et al.* (2009). Chromosome 9p-linked families with frontotemporal dementia associated with motor neuron disease. Neurology *72*, 1669-1676.

Lee, J.A., Beigneux, A., Ahmad, S.T., Young, S.G., and Gao, F.B. (2007). ESCRT-III dysfunction causes autophagosome accumulation and neurodegeneration. Curr Biol *17*, 1561-1567.

Lee, S., Sato, Y., and Nixon, R.A. (2011). Lysosomal proteolysis inhibition selectively disrupts axonal transport of degradative organelles and causes an Alzheimer's-like axonal dystrophy. J Neurosci *31*, 7817-7830.

Lee, Y.B., Chen, H.J., Peres, J., Gomez-Deza, J., Attig, J., Štalekar, M., Troakes, C., Nishimura, A., Scotter, E., Vance, C.*, et al.* (2013). Hexanucleotide repeats in ALS/FTD form length-dependent RNA Foci, sequester RNA binding proteins, and are neurotoxic. Cell Reports *5*, 1178-1186.

Leigh, P.N., Anderton, B.H., Dodson, A., Gallo, J.M., Swash, M., and Power, D.M. (1988). Ubiquitin deposits in anterior horn cells in motor neurone disease. Neuroscience letters *93*, 197-203.

Levine, T.P., Daniels, R.D., Gatta, A.T., Wong, L.H., and Hayes, M.J. (2013). The product of C9orf72, a gene strongly implicated in neurodegeneration, is structurally related to DENN Rab-GEFs. Bioinformatics *29*, 499-503.

Levitskaya, J., Sharipo, A., Leonchiks, A., Ciechanover, A., and Masucci, M.G. (1997). Inhibition of ubiquitin/proteasome-dependent protein degradation by the Gly-Ala repeat domain of the Epstein-Barr virus nuclear antigen 1. Proceedings of the National Academy of Sciences of the United States of America *94*, 12616-12621.

Levivier, E., Goud, B., Souchet, M., Calmels, T.P., Mornon, J.P., and Callebaut, I. (2001). uDENN, DENN, and dDENN: indissociable domains in Rab and MAP kinases signaling pathways. Biochem Biophys Res Commun *287*, 688-695.

Levy, J.R., Sumner, C.J., Caviston, J.P., Tokito, M.K., Ranganathan, S., Ligon, L.A., Wallace, K.E., LaMonte, B.H., Harmison, G.G., Puls, I.*, et al.* (2006). A motor neuron disease-associated mutation in p150Glued perturbs dynactin function and induces protein aggregation. Journal of Cell Biology *172*, 733-745.

Li, L., Kim, E., Yuan, H., Inoki, K., Goraksha-Hicks, P., Schiesher, R.L., Neufeld, T.P., and Guan, K.-L. (2010). Regulation of mTORC1 by the Rab and Arf GTPases. The Journal of Biological Chemistry *285*, 19705-19709.

Li, W., Bengtson, M.H., Ulbrich, A., Matsuda, A., Reddy, V.A., Orth, A., Chanda, S.K., Batalov, S., and Joazeiro, C.A.P. (2008). Genome-Wide and Functional Annotation of Human E3 Ubiquitin Ligases Identifies MULAN, a Mitochondrial E3 that Regulates the Organelle's Dynamics and Signaling. PLoS ONE *3*, e1487.

Liang, C.C., Wang, C., Peng, X., Gan, B., and Guan, J.L. (2010). Neural-specific deletion of FIP200 leads to cerebellar degeneration caused by increased neuronal death and axon degeneration. Journal of Biological Chemistry *285*, 3499-3509.

Liang, X.H., Jackson, S., Seaman, M., Brown, K., Kempkes, B., Hibshoosh, H., and Levine, B. (1999). Induction of autophagy and inhibition of tumorigenesis by beclin 1. Nature *402*, 672-676.

Lipatova, Z., Belogortseva, N., Zhang, X.Q., Kim, J., Taussig, D., and Segev, N. (2012). Regulation of selective autophagy onset by a Ypt/Rab GTPase module. Proceedings of the National Academy of Sciences *109*, 6981-6986.

Lippé, R., Miaczynska, M., Rybin, V., Runge, A., and Zerial, M. (2001). Functional Synergy between Rab5 Effector Rabaptin-5 and Exchange Factor Rabex-5 When Physically Associated in a Complex. Molecular Biology of the Cell *12*, 2219-2228.

Liu, J., Lillo, C., Jonsson, P.A., Velde, C.V., Ward, C.M., Miller, T.M., Subramaniam, J.R., Rothstein, J.D., Marklund, S., Andersen, P.M.*, et al.* (2004). Toxicity of familial ALS-linked SOD1 mutants from selective recruitment to spinal mitochondria. Neuron *43*, 5-17.

Logroscino, G., Traynor, B.J., Hardiman, O., Chiò, A., Mitchell, D., Swingler, R.J., Millul, A., Benn, E., and Beghi, E. (2010). Incidence of amyotrophic lateral sclerosis in Europe. Journal of neurology, neurosurgery, and psychiatry *81*, 385-390.

Lomen-Hoerth, C., Murphy, J., Langmore, S., Kramer, J.H., Olney, R.K., and Miller, B. (2003). Are amyotrophic lateral sclerosis patients cognitively normal? Neurology *60*, 1094-1097.

Lowe, J., Lennox, G., Jefferson, D., Morrell, K., McQuire, D., Gray, T., Landon, M., Doherty, F.J., and Mayer, R.J. (1988). A filamentous inclusion body within anterior horn neurones in motor neurone disease defined by immunocytochemical localisation of ubiquitin. Neuroscience letters *94*, 203-210.

Lynch-Day, M.A., Bhandari, D., Menon, S., Huang, J., Cai, H., Bartholomew, C.R., Brumell, J.H., Ferro-Novick, S., and Klionsky, D.J. (2010). Trs85 directs a Ypt1 GEF, TRAPPIII, to the phagophore to promote autophagy. Proceedings of the National Academy of Sciences of the United States of America *107*, 7811-7816.

Ma, Q. (2013). Role of nrf2 in oxidative stress and toxicity. Annual review of pharmacology and toxicology *53*, 401-426.

Maday, S., Wallace, K.E., and Holzbaur, E.L.F. (2012). Autophagosomes initiate distally and mature during transport toward the cell soma in primary neurons. Journal of Cell Biology *196*, 407-417.

Maduro, M.F., Gordon, M., Jacobs, R., and Pilgrim, D.B. (2000). The UNC-119 family of neural proteins is functionally conserved between humans, Drosophila and C. elegans. J Neurogenet *13*, 191-212.

Mahoney, C.J., Beck, J., Rohrer, J.D., Lashley, T., Mok, K., Shakespeare, T., Yeatman, T., Warrington, E.K., Schott, J.M., Fox, N.C.*, et al.* (2012). Frontotemporal dementia with the C9ORF72 hexanucleotide repeat expansion: Clinical, neuroanatomical and neuropathological features. Brain *135*, 736-750.

Majounie, E., Renton, A.E., Mok, K., Dopper, E.G.P., Waite, A., Rollinson, S., Chiò, A., Restagno, G., Nicolaou, N., Simon-Sanchez, J.*, et al.* (2012). Frequency of the C9orf72 hexanucleotide repeat expansion in patients with amyotrophic lateral sclerosis and frontotemporal dementia: A cross-sectional study. The Lancet Neurology *11*, 323-330.

Manetto, V., Sternberger, N.H., Perry, G., Sternberger, L.A., and Gambetti, P. (1988). Phosphorylation of neurofilaments is altered in amyotrophic lateral sclerosis. Journal of neuropathology and experimental neurology *47*, 642-653.

Mann, D.M., Rollinson, S., Robinson, A., Bennion Callister, J., Thompson, J.C., Snowden, J.S., Gendron, T., Petrucelli, L., Masuda-Suzukake, M., Hasegawa, M.*, et al.* (2013). Dipeptide repeat proteins are present in the p62 positive inclusions in patients with frontotemporal lobar degeneration and motor neurone disease associated with expansions in C9ORF72. Acta neuropathologica communications *1*, 68.

Mao, K., Wang, K., Liu, X., and Klionsky, D.J. (2013). The scaffold protein Atg11 recruits fission machinery to drive selective mitochondria degradation by autophagy. Developmental cell *26*, 9-18.

Marat, A.L., Dokainish, H., and McPherson, P.S. (2011). DENN domain proteins: Regulators of Rab GTPases. In Journal of Biological Chemistry, pp. 13791-13800.

Marden, J.J., Harraz, M.M., Williams, A.J., Nelson, K., Luo, M., Paulson, H., and Engelhardt, J.F. (2007). Redox modifier genes in amyotrophic lateral sclerosis in mice. J Clin Invest *117*, 2913-2919.

Mari, M., Griffith, J., Rieter, E., Krishnappa, L., Klionsky, D.J., and Reggiori, F. (2010). An Atg9-containing compartment that functions in the early steps of autophagosome biogenesis. Journal of Cell Biology *190*, 1005-1022.

Marinković, P., Reuter, M.S., Brill, M.S., Godinho, L., Kerschensteiner, M., and Misgeld, T. (2012). Axonal transport deficits and degeneration can evolve independently in mouse models of amyotrophic lateral sclerosis. Proceedings of

the National Academy of Sciences of the United States of America *109*, 4296-4301.

Maruyama, H., Morino, H., Ito, H., Izumi, Y., Kato, H., Watanabe, Y., Kinoshita, Y., Kamada, M., Nodera, H., Suzuki, H.*, et al.* (2010). Mutations of optineurin in amyotrophic lateral sclerosis. Nature *465*, 223-226.

Marzella, L., Ahlberg, J., and Glaumann, H. (1981). Autophagy, heterophagy, microautophagy and crinophagy as the means for intracellular degradation. Virchows Archiv B, Cell pathology including molecular pathology *36*, 219-234.

Mathew, R., Karp, C.M., Beaudoin, B., Vuong, N., Chen, G., Chen, H.Y., Bray, K., Reddy, A., Bhanot, G., Gelinas, C.*, et al.* (2009). Autophagy Suppresses Tumorigenesis through Elimination of p62. Cell *137*, 1062-1075.

Matsumoto, G., Shimogori, T., Hattori, N., and Nukina, N. (2015). TBK1 controls autophagosomal engulfment of polyubiquitinated mitochondria through p62/SQSTM1 phosphorylation. Human Molecular Genetics

Matsumoto, G., Wada, K., Okuno, M., Kurosawa, M., and Nukina, N. (2011). Serine 403 phosphorylation of p62/SQSTM1 regulates selective autophagic clearance of ubiquitinated proteins. Molecular Cell *44*, 279-289.

Matsushita, M., Suzuki, N.N., Obara, K., Fujioka, Y., Ohsumi, Y., and Inagaki, F. (2007). Structure of Atg5??Atg16, a complex essential for autophagy. Journal of Biological Chemistry *282*, 6763-6772.

Mattiazzi, M., D'Aurelio, M., Gajewski, C.D., Martushova, K., Kiaei, M., Flint Beal, M., and Manfredi, G. (2002). Mutated human SOD1 causes dysfunction of oxidative phosphorylation in mitochondria of transgenic mice. Journal of Biological Chemistry *277*, 29626-29633.

May, S., Hornburg, D., Schludi, M.H., Arzberger, T., Rentzsch, K., Schwenk, B.M., Grässer, F.A., Mori, K., Kremmer, E., Banzhaf-Strathmann, J.*, et al.* (2014). C9orf72 FTLD/ALS-associated Gly-Ala dipeptide repeat proteins cause neuronal toxicity and Unc119 sequestration. In Acta Neuropathol.

Medkova, M., France, Y.E., Coleman, J., and Novick, P. (2006). The rab exchange factor Sec2p reversibly associates with the exocyst. Mol Biol Cell *17*, 2757-2769.

Meijer, I.M., Kerperien, J., Sotoca, A.M., van Zoelen, E.J., and van Leeuwen, J.E. (2013). The Usp8 deubiquitination enzyme is post-translationally modified by tyrosine and serine phosphorylation. Cell Signal *25*, 919-930.

Meiling-Wesse, K., Epple, U.D., Krick, R., Barth, H., Appelles, A., Voss, C., Eskelinen, E.-L., and Thumm, M. (2005). Trs85 (Gsg1), a Component of the TRAPP Complexes, Is Required for the Organization of the Preautophagosomal Structure during Selective Autophagy via the Cvt Pathway. Journal of Biological Chemistry *280*, 33669-33678.

Meissner, M., Lopato, S., Gotzmann, J., Sauermann, G., and Barta, A. (2003). Proto-oncoprotein TLS/FUS is associated to the nuclear matrix and complexed with splicing factors PTB, SRm160, and SR proteins. Exp Cell Res *283*, 184-195.

Melcher, T., Maas, S., Herb, A., Sprengel, R., Seeburg, P.H., and Higuchi, M. (1996). A mammalian RNA editing enzyme. Nature *379*, 460-464.

Menzies, F.M., Cookson, M.R., Taylor, R.W., Turnbull, D.M., Chrzanowska-Lightowlers, Z.M.A., Dong, L., Figlewicz, D.A., and Shaw, P.J. (2002). Mitochondrial dysfunction in a cell culture model of familial amyotrophic lateral sclerosis. Brain : a journal of neurology *125*, 1522-1533.

Mercer, C.A., Kaliappan, A., and Dennis, P.B. (2009). A novel, human Atg13 binding protein, Atg101, interacts with ULK1 and is essential for macroautophagy. Autophagy *5*, 649-662.

Metzger, M.B., Hristova, V.A., and Weissman, A.M. (2012). HECT and RING finger families of E3 ubiquitin ligases at a glance. J Cell Sci *125*, 531-537.

Meyer, K., Ferraiuolo, L., Miranda, C.J., Likhite, S., McElroy, S., Renusch, S., Ditsworth, D., Lagier-Tourenne, C., Smith, R.A., Ravits, J.*, et al.* (2014). Direct conversion of patient fibroblasts demonstrates non-cell autonomous toxicity of

astrocytes to motor neurons in familial and sporadic ALS. Proceedings of the National Academy of Sciences *111*, 829-832.

Milanese, M., Zappettini, S., Onofri, F., Musazzi, L., Tardito, D., Bonifacino, T., Messa, M., Racagni, G., Usai, C., Benfenati, F.*, et al.* (2011). Abnormal exocytotic release of glutamate in a mouse model of amyotrophic lateral sclerosis. Journal of Neurochemistry *116*, 1028-1042.

Millecamps, S., Salachas, F., Cazeneuve, C., Gordon, P., Bricka, B., Camuzat, A., Guillot-Noël, L., Russaouen, O., Bruneteau, G., Pradat, P.-F.*, et al.* (2010). SOD1, ANG, VAPB, TARDBP, and FUS mutations in familial amyotrophic lateral sclerosis: genotype–phenotype correlations. Journal of Medical Genetics *47*, 554-560.

Miserey-Lenkei, S., Waharte, F., Boulet, A., Cuif, M.-H., Tenza, D., El Marjou, A., Raposo, G., Salamero, J., Héliot, L., Goud, B.*, et al.* (2007). Rab6-interacting Protein 1 Links Rab6 and Rab11 Function. Traffic *8*, 1385-1403.

Mitsumoto, H., Santella, R.M., Liu, X., Bogdanov, M., Zipprich, J., Wu, H.-C., Mahata, J., Kilty, M., Bednarz, K., Bell, D.*, et al.* (2008). Oxidative stress biomarkers in sporadic ALS. Amyotrophic lateral sclerosis : official publication of the World Federation of Neurology Research Group on Motor Neuron Diseases *9*, 177-183.

Mizielinska, S., Grönke, S., Niccoli, T., Ridler, C.E., Clayton, E.L., Devoy, A., Moens, T., Norona, F.E., Woollacott, I.O.C., Pietrzyk, J.*, et al.* (2014). C9orf72 repeat expansions cause neurodegeneration in Drosophila through arginine-rich proteins. Science (New York, NY) *16*, 1131-1135.

Mizielinska, S., Lashley, T., Norona, F.E., Clayton, E.L., Ridler, C.E., Fratta, P., and Isaacs, A.M. (2013). C9orf72 frontotemporal lobar degeneration is characterised by frequent neuronal sense and antisense RNA foci. Acta Neuropathol *126*, 845-857.

Mizuno, E., Kitamura, N., and Komada, M. (2007). 14-3-3-dependent inhibition of the deubiquitinating activity of UBPY and its cancellation in the M phase. Exp Cell Res *313*, 3624-3634.

Mizuno, Y., Amari, M., Takatama, M., Aizawa, H., Mihara, B., and Okamoto, K. (2006a). Immunoreactivities of p62, an ubiqutin-binding protein, in the spinal anterior horn cells of patients with amyotrophic lateral sclerosis. Journal of the Neurological Sciences *249*, 13-18.

Mizuno, Y., Amari, M., Takatama, M., Aizawa, H., Mihara, B., and Okamoto, K. (2006b). Transferrin localizes in Bunina bodies in amyotrophic lateral sclerosis. Acta Neuropathol *112*, 597-603.

Mizuno, Y., Fujita, Y., Takatama, M., and Okamoto, K. (2011). Peripherin partially localizes in Bunina bodies in amyotrophic lateral sclerosis. J Neurol Sci *302*, 14-18.

Mizushima, N., Kuma, A., Kobayashi, Y., Yamamoto, A., Matsubae, M., Takao, T., Natsume, T., Ohsumi, Y., and Yoshimori, T. (2003). Mouse Apg16L, a novel WD-repeat protein, targets to the autophagic isolation membrane with the Apg12-Apg5 conjugate. Journal of cell science *116*, 1679-1688.

Mizushima, N., Noda, T., Yoshimori, T., Tanaka, Y., Ishii, T., George, M.D., Klionsky, D.J., Ohsumi, M., and Ohsumi, Y. (1998). A protein conjugation system essential for autophagy. Nature *395*, 395-398.

Moldoveanu, T., Hosfield, C.M., Lim, D., Elce, J.S., Jia, Z., and Davies, P.L. (2002). A Ca(2+) switch aligns the active site of calpain. Cell *108*, 649-660.

Moreau, K., Ravikumar, B., Renna, M., Puri, C., and Rubinsztein, D.C. (2011). Autophagosome precursor maturation requires homotypic fusion. Cell *146*, 303-317.

Moreau, K., and Rubinsztein, D.C. (2012). The plasma membrane as a control center for autophagy. In Autophagy, pp. 861-863.

Mori, K., Arzberger, T., Grässer, F.A., Gijselinck, I., May, S., Rentzsch, K., Weng, S.M., Schludi, M.H., Van Der Zee, J., Cruts, M*., et al.* (2013a). Bidirectional transcripts of the expanded C9orf72 hexanucleotide repeat are translated into aggregating dipeptide repeat proteins. Acta Neuropathol *126*, 881-893.

Mori, K., Weng, S.-M., Arzberger, T., May, S., Rentzsch, K., Kremmer, E., Schmid, B., Kretzschmar, H.a., Cruts, M., Van Broeckhoven, C.*, et al.* (2013b). The C9orf72 GGGGCC repeat is translated into aggregating dipeptide-repeat proteins in FTLD/ALS. Science (New York, NY) *339*, 1335-1338.

Morita, M., Al-Chalabi, A., Andersen, P.M., Hosler, B., Sapp, P., Englund, E., Mitchell, J.E., Habgood, J.J., de Belleroche, J., Xi, J.*, et al.* (2006). A locus on chromosome 9p confers susceptibility to ALS and frontotemporal dementia. Neurology *66*, 839-844.

Morotz, G.M., De Vos, K.J., Vagnoni, A., Ackerley, S., Shaw, C.E., and Miller, C.C. (2012). Amyotrophic lateral sclerosis-associated mutant VAPBP56S perturbs calcium homeostasis to disrupt axonal transport of mitochondria. Hum Mol Genet *21*, 1979-1988.

Mortimore, G.E., Lardeux, B.R., and Adams, C.E. (1988). Regulation of microautophagy and basal protein turnover in rat liver. Effects of short-term starvation. Journal of Biological Chemistry *263*, 2506-2512.

Münch, C., Rosenbohm, A., Sperfeld, A.D., Uttner, I., Reske, S., Krause, B.J., Sedlmeier, R., Meyer, T., Hanemann, C.O., Stumm, G.*, et al.* (2005). Heterozygous R1101K mutation of the DCTN1 gene in a family with ALS and FTD. Annals of Neurology *58*, 777-780.

Münch, C., Sedlmeier, R., Meyer, T., Homberg, V., Sperfeld, A.D., Kurt, A., Prudlo, J., Peraus, G., Hanemann, C.O., Stumm, G.*, et al.* (2004). Point mutations of the p150 subunit of dynactin (DCTN1) gene in ALS. Neurology *63*, 724-726.

Munoz, D.G., Greene, C., Perl, D.P., and Selkoe, D.J. (1988). Accumulation of phosphorylated neurofilaments in anterior horn motoneurons of amyotrophic lateral sclerosis patients. Journal of neuropathology and experimental neurology *47*, 9-18.

Murayama, S., Ookawa, Y., Mori, H., Nakano, I., Ihara, Y., Kuzuhara, S., and Tomonaga, M. (1989). Immunocytochemical and ultrastructural study of Lewy

body-like hyaline inclusions in familial amyotrophic lateral sclerosis. Acta Neuropathol *78*, 143-152.

Murthy, A., Li, Y., Peng, I., Reichelt, M., Katakam, A.K., Noubade, R., Roose-Girma, M., DeVoss, J., Diehl, L., Graham, R.R.*, et al.* (2014). A Crohn/'s disease variant in Atg16l1 enhances its degradation by caspase 3. Nature *506*, 456-462.

Musatov, A., and Robinson, N.C. (2002). Cholate-Induced Dimerization of Detergent- or Phospholipid-Solubilized Bovine Cytochrome c Oxidase†. Biochemistry *41*, 4371-4376.

N'Diaye, E.-N., Kajihara, K.K., Hsieh, I., Morisaki, H., Debnath, J., and Brown, E.J. (2009a). PLIC proteins or ubiquilins regulate autophagy-dependent cell survival during nutrient starvation. EMBO reports *10*, 173-179.

N'Diaye, E.N., Debnath, J., and Brown, E.J. (2009b). Ubiquilins accelerate autophagosome maturation and promote cell survival during nutrient starvation. Autophagy *5*, 573-575.

Naviglio, S., Mattecucci, C., Matoskova, B., Nagase, T., Nomura, N., Di Fiore, P.P., and Draetta, G.F. (1998). UBPY: a growth-regulated human ubiquitin isopeptidase. The EMBO Journal *17*, 3241-3250.

Nazarko, T.Y., Huang, J., Nicaud, J.-M., Klionsky, D.J., and Sibirny, A.A. (2005). Trs85 is Required for Macroautophagy, Pexophagy and Cytoplasm to Vacuole Targeting in Yarrowia lipolytica and Saccharomyces cerevisiae. Autophagy *1*, 37-45.

Neumann, M., Sampathu, D.M., Kwong, L.K., Truax, A.C., Micsenyi, M.C., Chou, T.T., Bruce, J., Schuck, T., Grossman, M., Clark, C.M.*, et al.* (2006). Ubiquitinated TDP-43 in frontotemporal lobar degeneration and amyotrophic lateral sclerosis. Science (New York, NY) *314*, 130-133.

Nguyen, K.T., García-Chacón, L.E., Barrett, J.N., Barrett, E.F., and David, G. (2009). The Psi(m) depolarization that accompanies mitochondrial Ca2+ uptake is greater in mutant SOD1 than in wild-type mouse motor terminals.

Proceedings of the National Academy of Sciences of the United States of America *106*, 2007-2011.

Nicholson, A.M., Finch, N.A., Wojtas, A., Baker, M.C., Perkerson, R.B., 3rd, Castanedes-Casey, M., Rousseau, L., Benussi, L., Binetti, G., Ghidoni, R.*, et al.* (2013). TMEM106B p.T185S regulates TMEM106B protein levels: implications for frontotemporal dementia. J Neurochem *126*, 781-791.

Nijman, S.M., Luna-Vargas, M.P., Velds, A., Brummelkamp, T.R., Dirac, A.M., Sixma, T.K., and Bernards, R. (2005). A genomic and functional inventory of deubiquitinating enzymes. Cell *123*, 773-786.

Nishikawa, H., Ooka, S., Sato, K., Arima, K., Okamoto, J., Klevit, R.E., Fukuda, M., and Ohta, T. (2004). Mass spectrometric and mutational analyses reveal Lys-6-linked polyubiquitin chains catalyzed by BRCA1-BARD1 ubiquitin ligase. J Biol Chem *279*, 3916-3924.

Nishimura, A.L., Mitne-Neto, M., Silva, H.C.A., Richieri-Costa, A., Middleton, S., Cascio, D., Kok, F., Oliveira, J.R.M., Gillingwater, T., Webb, J.*, et al.* (2004). A mutation in the vesicle-trafficking protein VAPB causes late-onset spinal muscular atrophy and amyotrophic lateral sclerosis. American journal of human genetics *75*, 822-831.

Nishimura, T., Kaizuka, T., Cadwell, K., Sahani, M.H., Saitoh, T., Akira, S., Virgin, H.W., and Mizushima, N. (2013). FIP200 regulates targeting of Atg16L1 to the isolation membrane. EMBO Rep *14*, 284-291.

Niwa, S., Tanaka, Y., and Hirokawa, N. (2008). KIF1Bbeta- and KIF1A-mediated axonal transport of presynaptic regulator Rab3 occurs in a GTP-dependent manner through DENN/MADD. Nat Cell Biol *10*, 1269-1279.

Noda, N.N., Fujioka, Y., Hanada, T., Ohsumi, Y., and Inagaki, F. (2013). Structure of the Atg12-Atg5 conjugate reveals a platform for stimulating Atg8-PE conjugation. EMBO reports *14*, 206-211.

Nordmann, M., Cabrera, M., Perz, A., Bröcker, C., Ostrowicz, C., Engelbrecht-Vandré, S., and Ungermann, C. The Mon1-Ccz1 Complex Is the GEF of the Late Endosomal Rab7 Homolog Ypt7. Current Biology *20*, 1654-1659.

Norman, J.M., Cohen, G.M., and Bampton, E.T. (2010). The in vitro cleavage of the hAtg proteins by cell death proteases. Autophagy *6*, 1042-1056.

O'Rourke, J.G., Bogdanik, L., Muhammad, A.K., Gendron, T.F., Kim, K.J., Austin, A., Cady, J., Liu, E.Y., Zarrow, J., Grant, S.*, et al.* (2015). C9orf72 BAC Transgenic Mice Display Typical Pathologic Features of ALS/FTD. Neuron *88*, 892-901.

Okamoto, K., Hirai, S., Amari, M., Watanabe, M., and Sakurai, A. (1993). Bunina bodies in amyotrophic lateral sclerosis immunostained with rabbit anti-cystatin C serum. Neuroscience Letters *162*, 125-128.

Okamoto, K., Mizuno, Y., and Fujita, Y. (2008). Bunina bodies in amyotrophic lateral sclerosis. In Neuropathology, pp. 109-115.

Orlacchio, A., Babalini, C., Borreca, A., Patrono, C., Massa, R., Basaran, S., Munhoz, R.P., Rogaeva, E.A., St George-Hyslop, P.H., Bernardi, G.*, et al.* (2010). SPATACSIN mutations cause autosomal recessive juvenile amyotrophic lateral sclerosis. Brain *133*, 591-598.

Ortiz, D., Medkova, M., Walch-Solimena, C., and Novick, P. (2002). Ypt32 recruits the Sec4p guanine nucleotide exchange factor, Sec2p, to secretory vesicles; evidence for a Rab cascade in yeast. The Journal of Cell Biology *157*, 1005-1016.

Osaka, M., Ito, D., Yagi, T., Nihei, Y., and Suzuki, N. (2015). Evidence of a link between ubiquilin 2 and optineurin in amyotrophic lateral sclerosis. Hum Mol Genet *24*, 1617-1629.

Otomo, A., Kunita, R., Suzuki-Utsunomiya, K., Ikeda, J.E., and Hadano, S. (2011). Defective relocalization of ALS2/alsin missense mutants to Rac1-induced macropinosomes accounts for loss of their cellular function and leads to disturbed amphisome formation. FEBS Letters *585*, 730-736.

Ou, S.H., Wu, F., Harrich, D., García-Martínez, L.F., and Gaynor, R.B. (1995). Cloning and characterization of a novel cellular protein, TDP-43, that binds to human immunodeficiency virus type 1 TAR DNA sequence motifs. Journal of virology *69*, 3584-3596.

Özkan, E., Yu, H., and Deisenhofer, J. (2005). Mechanistic insight into the allosteric activation of a ubiquitin-conjugating enzyme by RING-type ubiquitin ligases. Proceedings of the National Academy of Sciences of the United States of America *102*, 18890-18895.

Pankiv, S., Alemu, E.A., Brech, A., Bruun, J.A., Lamark, T., Overvatn, A., Bjorkoy, G., and Johansen, T. (2010). FYCO1 is a Rab7 effector that binds to LC3 and PI3P to mediate microtubule plus end-directed vesicle transport. J Cell Biol *188*, 253-269.

Pankiv, S., Clausen, T.H., Lamark, T., Brech, A., Bruun, J.A., Outzen, H., Øvervatn, A., Bjørkøy, G., and Johansen, T. (2007). p62/SQSTM1 binds directly to Atg8/LC3 to facilitate degradation of ubiquitinated protein aggregates by autophagy*[S]. Journal of Biological Chemistry *282*, 24131-24145.

Parkinson, N., Ince, P.G., Smith, M.O., Highley, R., Skibinski, G., Andersen, P.M., Morrison, K.E., Pall, H.S., Hardiman, O., Collinge, J.*, et al.* (2006). ALS phenotypes with mutations in CHMP2B (charged multivesicular body protein 2B). Neurology *67*, 1074-1077.

Pasinelli, P., Belford, M.E., Lennon, N., Bacskai, B.J., Hyman, B.T., Trotti, D., and Brown, R.H. (2004). Amyotrophic lateral sclerosis-associated SOD1 mutant proteins bind and aggregate with Bcl-2 in spinal cord mitochondria. Neuron *43*, 19-30.

Patel, S., and Player, M.R. (2008). Small-molecule inhibitors of the p53-HDM2 interaction for the treatment of cancer. Expert Opin Investig Drugs *17*, 1865-1882.

Pérez-Brangulí, F., Mishra, H.K., Prots, I., Havlicek, S., Kohl, Z., Saul, D., Rummel, C., Dorca-Arevalo, J., Regensburger, M., Graef, D.*, et al.* (2014).

Dysfunction of spatacsin leads to axonal pathology in SPG11-linked hereditary spastic paraplegia. Human molecular genetics, 1-16.

Peters, O.M., Cabrera, G.T., Tran, H., Gendron, T.F., McKeon, J.E., Metterville, J., Weiss, A., Wightman, N., Salameh, J., Kim, J.*, et al.* (2015). Human C9ORF72 Hexanucleotide Expansion Reproduces RNA Foci and Dipeptide Repeat Proteins but Not Neurodegeneration in BAC Transgenic Mice. Neuron *88*, 902-909.

Pilli, M., Arko-Mensah, J., Ponpuak, M., Roberts, E., Master, S., Mandell, M.A., Dupont, N., Ornatowski, W., Jiang, S., Bradfute, S.B.*, et al.* (2012). TBK-1 Promotes Autophagy-Mediated Antimicrobial Defense by Controlling Autophagosome Maturation. Immunity *37*, 223-234.

Pind SN, N.C., McCaffery JM, Plutner H, Davidson HW, Farquhar MG, Balch WE (1994). Rab1 and Ca2+ are required for the fusion of carrier vesicles mediating endoplasmic reticulum to Golgi transport. The Journal of Cell Biology *125*, 239-252.

Poole, A.C., Thomas, R.E., Andrews, L.A., McBride, H.M., Whitworth, A.J., and Pallanck, L.J. (2008). The PINK1/Parkin pathway regulates mitochondrial morphology. Proceedings of the National Academy of Sciences of the United States of America *105*, 1638-1643.

Pozuelo-Rubio, M. (2011). Regulation of autophagic activity by 14-3-3zeta proteins associated with class III phosphatidylinositol-3-kinase. Cell Death Differ *18*, 479-492.

Prause, J., Goswami, A., Katona, I., Roos, A., Schnizler, M., Bushuven, E., Dreier, A., Buchkremer, S., Johann, S., Beyer, C.*, et al.* (2013). Altered localization, abnormal modification and loss of function of sigma receptor-1 in amyotrophic lateral sclerosis. Human Molecular Genetics *22*, 1581-1600.

Puls, I., Jonnakuty, C., LaMonte, B.H., Holzbaur, E.L.F., Tokito, M., Mann, E., Floeter, M.K., Bidus, K., Drayna, D., Oh, S.J.*, et al.* (2003). Mutant dynactin in motor neuron disease. Nature genetics *33*, 455-456.

Radivojac, P., Vacic, V., Haynes, C., Cocklin, R.R., Mohan, A., Heyen, J.W., Goebl, M.G., and Iakoucheva, L.M. (2010). Identification, Analysis and Prediction of Protein Ubiquitination Sites. Proteins *78*, 365-380.

Rakhit, R., Crow, J.P., Lepock, J.R., Kondejewski, L.H., Cashman, N.R., and Chakrabartty, A. (2004). Monomeric Cu,Zn-superoxide Dismutase Is a Common Misfolding Intermediate in the Oxidation Models of Sporadic and Familial Amyotrophic Lateral Sclerosis. Journal of Biological Chemistry *279*, 15499-15504.

Rakhit, R., Cunningham, P., Furtos-Matei, A., Dahan, S., Qi, X.-F., Crow, J.P., Cashman, N.R., Kondejewski, L.H., and Chakrabartty, A. (2002). Oxidation-induced Misfolding and Aggregation of Superoxide Dismutase and Its Implications for Amyotrophic Lateral Sclerosis. Journal of Biological Chemistry *277*, 47551-47556.

Rakhit, R., Robertson, J., Vande Velde, C., Horne, P., Ruth, D.M., Griffin, J., Cleveland, D.W., Cashman, N.R., and Chakrabartty, A. (2007). An immunological epitope selective for pathological monomer-misfolded SOD1 in ALS. Nature medicine *13*, 754-759.

Ravikumar, B., Acevedo-Arozena, A., Imarisio, S., Berger, Z., Vacher, C., O'Kane, C.J., Brown, S.D., and Rubinsztein, D.C. (2005). Dynein mutations impair autophagic clearance of aggregate-prone proteins. Nat Genet *37*, 771-776.

Ravikumar, B., Imarisio, S., Sarkar, S., O'Kane, C.J., and Rubinsztein, D.C. (2008). Rab5 modulates aggregation and toxicity of mutant huntingtin through macroautophagy in cell and fly models of Huntington disease. Journal of cell science *121*, 1649-1660.

Ravikumar, B., Moreau, K., Jahreiss, L., Puri, C., and Rubinsztein, D.C. (2010). Plasma membrane contributes to the formation of pre-autophagosomal structures. Nature cell biology *12*, 747-757.

Ravikumar, B., Vacher, C., Berger, Z., Davies, J.E., Luo, S., Oroz, L.G., Scaravilli, F., Easton, D.F., Duden, R., O'Kane, C.J.*, et al.* (2004). Inhibition of

mTOR induces autophagy and reduces toxicity of polyglutamine expansions in fly and mouse models of Huntington disease. Nature genetics *36*, 585-595.

Razi, M., Chan, E.Y.W., and Tooze, S.A. (2009). Early endosomes and endosomal coatomer are required for Autophagy. Journal of Cell Biology *185*, 305-321.

Renna, M., Schaffner, C., Winslow, A.R., Menzies, F.M., Peden, A.A., Floto, R.A., and Rubinsztein, D.C. (2011). Autophagic substrate clearance requires activity of the syntaxin-5 SNARE complex. Journal of cell science *124*, 469-482.

Renton, A.E., Majounie, E., Waite, A., Simón-Sánchez, J., Rollinson, S., Gibbs, J.R., Schymick, J.C., Laaksovirta, H., van Swieten, J.C., Myllykangas, L.*, et al.* (2011). A hexanucleotide repeat expansion in C9ORF72 is the cause of chromosome 9p21-linked ALS-FTD. Neuron *72*, 257-268.

Renvoisé, B., Chang, J., Singh, R., Yonekawa, S., FitzGibbon, E.J., Mankodi, A., Vanderver, A., Schindler, A., Toro, C., Gahl, W.a.*, et al.* (2014). Lysosomal abnormalities in hereditary spastic paraplegia types SPG15 and SPG11. Annals of clinical and translational neurology *1*, 379-389.

Ringholz, G.M., Appel, S.H., Bradshaw, M., Cooke, N.A., Mosnik, D.M., and Schulz, P.E. (2005). Prevalence and patterns of cognitive impairment in sporadic ALS. Neurology *65*, 586-590.

Rippon, G.A., Scarmeas, N., Gordon, P.H., and et al. (2006). AN observational study of cognitive impairment in amyotrophic lateral sclerosis. Archives of Neurology *63*, 345-352.

Ritz, D., Vuk, M., Kirchner, P., Bug, M., Schütz, S., Hayer, A., Bremer, S., Lusk, C., Baloh, R.H., Lee, H.*, et al.* (2011). Endolysosomal sorting of ubiquitylated caveolin-1 is regulated by VCP and UBXD1 and impaired by VCP disease mutations. Nature cell biology *13*, 1116-1123.

Rodriguez, M.S., Desterro, J.M.P., Lain, S., Lane, D.P., and Hay, R.T. (2000). Multiple C-Terminal Lysine Residues Target p53 for Ubiquitin-Proteasome-Mediated Degradation. Molecular and Cellular Biology *20*, 8458-8467.

Rosahl, T.W., Geppert, M., Spillane, D., Herz, J., Hammer, R.E., Malenka, R.C., and Südhof, T.C. (1993). Short-term synaptic plasticity is altered in mice lacking synapsin I. Cell *75*, 661-670.

Rosahl, T.W., Spillane, D., Missler, M., Herz, J., Selig, D.K., Wolff, J.R., Hammer, R.E., Malenka, R.C., and Sudhof, T.C. (1995). Essential functions of synapsins I and II in synaptic vesicle regulation. Nature *375*, 488-493.

Rosen, D.R., Siddique, T., Patterson, D., Figlewicz, D.A., Sapp, P., Hentati, A., Donaldson, D., Goto, J., O'Regan, J.P., and Deng, H.X. (1993). Mutations in Cu/Zn superoxide dismutase gene are associated with familial amyotrophic lateral sclerosis. Nature *362*, 59-62.

Rothenberg, C., Srinivasan, D., Mah, L., Kaushik, S., Peterhoff, C.M., Ugolino, J., Fang, S., Cuervo, A.M., Nixon, R.A., and Monteiro, M.J. (2010). Ubiquilin functions in autophagy and is degraded by chaperone-mediated autophagy. Human Molecular Genetics *19*, 3219-3232.

Rothstein, J.D., Martin, L.J., and Kuncl, R.W. (1992). Decreased glutamate transport by the brain and spinal cord in amyotrophic lateral sclerosis. The New England journal of medicine *326*, 1464-1468.

Rothstein, J.D., Van Kammen, M., Levey, A.I., Martin, L.J., and Kuncl, R.W. (1995). Selective loss of glial glutamate transporter GLT-1 in amyotrophic lateral sclerosis. Ann Neurol *38*, 73-84.

Row, P.E., Liu, H., Hayes, S., Welchman, R., Charalabous, P., Hofmann, K., Clague, M.J., Sanderson, C.M., and Urbé, S. (2007). The MIT Domain of UBPY Constitutes a CHMP Binding and Endosomal Localization Signal Required for Efficient Epidermal Growth Factor Receptor Degradation. Journal of Biological Chemistry *282*, 30929-30937.

Row, P.E., Prior, I.A., McCullough, J., Clague, M.J., and Urbé, S. (2006). The Ubiquitin Isopeptidase UBPY Regulates Endosomal Ubiquitin Dynamics and Is Essential for Receptor Down-regulation. Journal of Biological Chemistry *281*, 12618-12624.

Rubino, E., Rainero, I., Chiò, A., Rogaeva, E., Galimberti, D., Fenoglio, P., Grinberg, Y., Isaia, G., Calvo, A., Gentile, S.*, et al.* (2012). SQSTM1 mutations in frontotemporal lobar degeneration and amyotrophic lateral sclerosis. Neurology *79*, 1556-1562.

Rubino, M., Miaczynska, M., Lippé, R., and Zerial, M. (2000). Selective Membrane Recruitment of EEA1 Suggests a Role in Directional Transport of Clathrin-coated Vesicles to Early Endosomes. Journal of Biological Chemistry *275*, 3745-3748.

Rufini, A., Fortuni, S., Arcuri, G., Condò, I., Serio, D., Incani, O., Malisan, F., Ventura, N., and Testi, R. (2011). Preventing the ubiquitin–proteasome-dependent degradation of frataxin, the protein defective in Friedreich's ataxia. Human Molecular Genetics *20*, 1253-1261.

Russell, R.C., Tian, Y., Yuan, H., Park, H.W., Chang, Y.-Y., Kim, J., Kim, H., Neufeld, T.P., Dillin, A., and Guan, K.-L. (2013). ULK1 induces autophagy by phosphorylating Beclin-1 and activating VPS34 lipid kinase. Nature cell biology *15*, 741-750.

Rusten, T.E., Vaccari, T., Lindmo, K., Rodahl, L.M.W., Nezis, I.P., Sem-Jacobsen, C., Wendler, F., Vincent, J.P., Brech, A., Bilder, D.*, et al.* (2007). ESCRTs and Fab1 Regulate Distinct Steps of Autophagy. Current Biology *17*, 1817-1825.

Ryan, T.A., Li, L., Chin, L.S., Greengard, P., and Smith, S.J. (1996). Synaptic vesicle recycling in synapsin I knock-out mice. The Journal of Cell Biology *134*, 1219-1227.

Saal, L., Briese, M., Kneitz, S., Glinka, M., and Sendtner, M. (2014). Subcellular transcriptome alterations in a cell culture model of spinal muscular atrophy point to widespread defects in axonal growth and presynaptic differentiation. RNA *20*, 1789-1802.

Salton, M., Elkon, R., Borodina, T., Davydov, A., Yaspo, M.L., Halperin, E., and Shiloh, Y. (2011). Matrin 3 binds and stabilizes mRNA. PLoS ONE *6*.

Sapp, P.C., Hosler, B.A., McKenna-Yasek, D., Chin, W., Gann, A., Genise, H., Gorenstein, J., Huang, M., Sailer, W., Scheffler, M.*, et al.* (2003). Identification of two novel loci for dominantly inherited familial amyotrophic lateral sclerosis. Am J Hum Genet *73*, 397-403.

Sareen, D., O'Rourke, J.G., Meera, P., Muhammad, A.K.M.G., Grant, S., Simpkinson, M., Bell, S., Carmona, S., Ornelas, L., Sahabian, A.*, et al.* (2013). Targeting RNA foci in iPSC-derived motor neurons from ALS patients with a C9ORF72 repeat expansion. Science translational medicine *5*, 208ra149.

Sarkar, S., Floto, R.A., Berger, Z., Imarisio, S., Cordenier, A., Pasco, M., Cook, L.J., and Rubinsztein, D.C. (2005). Lithium induces autophagy by inhibiting inositol monophosphatase. J Cell Biol *170*, 1101-1111.

Sarlette, A., Krampfl, K., Grothe, C., Neuhoff, N.v., Dengler, R., and Petri, S. (2008). Nuclear erythroid 2-related factor 2-antioxidative response element signaling pathway in motor cortex and spinal cord in amyotrophic lateral sclerosis. Journal of neuropathology and experimental neurology *67*, 1055-1062.

Sasaki, S., and Iwata, M. (2007). Mitochondrial alterations in the spinal cord of patients with sporadic amyotrophic lateral sclerosis. Journal of neuropathology and experimental neurology *66*, 10-16.

Sathasivam, S., Grierson, a.J., and Shaw, P.J. (2005). Characterization of the caspase cascade in a cell culture model of SOD1-related familial amyotrophic lateral sclerosis: Expression, activation and therapeutic effects of inhibition. Neuropathology and Applied Neurobiology *31*, 467-485.

Sato-Kusubata, K., Yajima, Y., and Kawashima, S. (2000). Persistent activation of Gsalpha through limited proteolysis by calpain. Biochem J *347 Pt 3*, 733-740.

Saxena, S., Cabuy, E., and Caroni, P. (2009). A role for motoneuron subtype-selective ER stress in disease manifestations of FALS mice. Nat Neurosci *12*, 627-636.

Schneider-Poetsch, T., Ju, J., Eyler, D.E., Dang, Y., Bhat, S., Merrick, W.C., Green, R., Shen, B., and Liu, J.O. (2010). Inhibition of Eukaryotic Translation Elongation by Cycloheximide and Lactimidomycin. Nature chemical biology *6*, 209-217.

Schrock, J.M., Spino, C.M., Longen, C.G., Stabler, S.M., Marino, J.C., Pasternak, G.W., and Kim, F.J. (2013). Sequential cytoprotective responses to Sigma1 ligand-induced endoplasmic reticulum stress. Mol Pharmacol *84*, 751-762.

Schwenk, B.M., Lang, C.M., Hogl, S., Tahirovic, S., Orozco, D., Rentzsch, K., Lichtenthaler, S.F., Hoogenraad, C.C., Capell, A., Haass, C*., et al.* (2014). The FTLD risk factor TMEM106B and MAP6 control dendritic trafficking of lysosomes. EMBO Journal *33*, 450-467.

Schwikowski, B., Uetz, P., and Fields, S. (2000). A network of protein-protein interactions in yeast. Nat Biotechnol *18*, 1257-1261.

Schymick, J.C., Talbot, K., and Traynor, B.J. (2007). Genetics of sporadic amyotrophic lateral sclerosis. In Human Molecular Genetics.

Sephton, C.F., Cenik, C., Kucukural, A., Dammer, E.B., Cenik, B., Han, Y., Dewey, C.M., Roth, F.P., Herz, J., Peng, J*., et al.* (2011). Identification of neuronal RNA targets of TDP-43-containing ribonucleoprotein complexes. Journal of Biological Chemistry *286*, 1204-1215.

Shah, S.A., Shen, B.W., and Brünger, A.T. (1997). Human ornithine aminotransferase complexed with L-canaline and gabaculine: structural basis for substrate recognition. Structure *5*, 1067-1075.

Shatunov, A., Mok, K., Newhouse, S., Weale, M.E., Smith, B., Vance, C., Johnson, L., Veldink, J.H., van Es, M.A., van den Berg, L.H*., et al.* (2010). Chromosome 9p21 in sporadic amyotrophic lateral sclerosis in the UK and seven other countries: a genome-wide association study. Lancet Neurol *9*, 986-994.

Shaw, P.J., Ince, P.G., Falkous, G., and Mantle, D. (1995). Oxidative damage to protein in sporadic motor neuron disease spinal cord. Annals of Neurology *38*, 691-695.

Shibata, N., Hirano, A., Kobayashi, M., Sasaki, S., Kato, T., Matsumoto, S., Shiozawa, Z., Komori, T., Ikemoto, A., and Umahara, T. (1994). Cu/Zn superoxide dismutase-like immunoreactivity in Lewy body-like inclusions of sporadic amyotrophic lateral sclerosis. Paper presented at: Neuroscience letters.

Shibata, N., Nagai, R., Uchida, K., Horiuchi, S., Yamada, S., Hirano, A., Kawaguchi, M., Yamamoto, T., Sasaki, S., and Kobayashi, M. (2001). Morphological evidence for lipid peroxidation and protein glycoxidation in spinal cords from sporadic amyotrophic lateral sclerosis patients. Brain research *917*, 97-104.

Shuman, S. (1994). Novel approach to molecular cloning and polynucleotide synthesis using vaccinia DNA topoisomerase. J Biol Chem *269*, 32678-32684.

Siddique, T., Figlewicz, D.A., Pericak-Vance, M.A., Haines, J.L., Rouleau, G., Jeffers, A.J., Sapp, P., Hung, W.Y., Bebout, J., and McKenna-Yasek, D. (1991). Linkage of a gene causing familial amyotrophic lateral sclerosis to chromosome 21 and evidence of genetic-locus heterogeneity. The New England journal of medicine *324*, 1381-1384.

Siddique, T., Pericak-Vance, M.A., Brooks, B.R., Roos, R.P., Hung, W.Y., Antel, J.P., Munsat, T.L., Phillips, K., Warner, K., and Speer, M. (1989). Linkage analysis in familial amyotrophic lateral sclerosis. Neurology *39*, 919-925.

Simon, E., and Kornitzer, D. (2014). Pulse-chase analysis to measure protein degradation. Methods Enzymol *536*, 65-75.

Simpson, E.P., Henry, Y.K., Henkel, J.S., Smith, R.G., and Appel, S.H. (2004). Increased lipid peroxidation in sera of ALS patients: a potential biomarker of disease burden. Neurology *62*, 1758-1765.

Skibinski, G., Parkinson, N.J., Brown, J.M., Chakrabarti, L., Lloyd, S.L., Hummerich, H., Nielsen, J.E., Hodges, J.R., Spillantini, M.G., Thusgaard, T.*, et al.* (2005). Mutations in the endosomal ESCRTIII-complex subunit CHMP2B in frontotemporal dementia. Nature genetics *37*, 806-808.

Smith, R.G., Henry, Y.K., Mattson, M.P., and Appel, S.H. (1998). Presence of 4-hydroxynonenal in cerebrospinal fluid of patients with sporadic amyotrophic lateral sclerosis. Ann Neurol *44*, 696-699.

Soderberg, O., Gullberg, M., Jarvius, M., Ridderstrale, K., Leuchowius, K.-J., Jarvius, J., Wester, K., Hydbring, P., Bahram, F., Larsson, L.-G.*, et al.* (2006). Direct observation of individual endogenous protein complexes in situ by proximity ligation. Nat Meth *3*, 995-1000.

Song, W., Song, Y., Kincaid, B., Bossy, B., and Bossy-Wetzel, E. (2013). Mutant SOD1G93A triggers mitochondrial fragmentation in spinal cord motor neurons: neuroprotection by SIRT3 and PGC-1alpha. Neurobiol Dis *51*, 72-81.

Spreux-Varoquaux, O., Bensimon, G., Lacomblez, L., Salachas, F., Pradat, P.F., Le Forestier, N., Marouan, A., Dib, M., and Meininger, V. (2002). Glutamate levels in cerebrospinal fluid in amyotrophic lateral sclerosis: A reappraisal using a new HPLC method with coulometric detection in a large cohort of patients. Journal of the Neurological Sciences *193*, 73-78.

Sreedharan, J., Blair, I.P., Tripathi, V.B., Hu, X., Vance, C., Rogelj, B., Ackerley, S., Durnall, J.C., Williams, K.L., Buratti, E.*, et al.* (2008). TDP-43 mutations in familial and sporadic amyotrophic lateral sclerosis. Science (New York, NY) *319*, 1668-1672.

Stagi, M., Klein, Z.A., Gould, T.J., Bewersdorf, J., and Strittmatter, S.M. (2014). Lysosome size, motility and stress response regulated by fronto-temporal dementia modifier TMEM106B. Molecular and Cellular Neuroscience *61*, 226-240.

Stenmark, H. (2009). Rab GTPases as coordinators of vesicle traffic. Nature reviews Molecular cell biology *10*, 513-525.

Stenmark, H., and Olkkonen, V.M. (2001). The Rab GTPase family. Genome biology *2*, REVIEWS3007.

Stewart, H., Rutherford, N.J., Briemberg, H., Krieger, C., Cashman, N., Fabros, M., Baker, M., Fok, A., DeJesus-Hernandez, M., Eisen, A.*, et al.* (2012). Clinical and pathological features of amyotrophic lateral sclerosis caused by mutation in the C9ORF72 gene on chromosome 9p. Acta Neuropathol *123*, 409-417.

Stoica, R., De Vos, K.J., Paillusson, S., Mueller, S., Sancho, R.M., Lau, K.-F., Vizcay-Barrena, G., Lin, W.-L., Xu, Y.-F., Lewis, J.*, et al.* (2014). ER-mitochondria associations are regulated by the VAPB-PTPIP51 interaction and are disrupted by ALS/FTD-associated TDP-43. Nature communications *5*, 3996.

Su, W.-C., Chao, T.-C., Huang, Y.-L., Weng, S.-C., Jeng, K.-S., and Lai, M.M.C. (2011). Rab5 and Class III Phosphoinositide 3-Kinase Vps34 Are Involved in Hepatitis C Virus NS4B-Induced Autophagy. Journal of Virology *85*, 10561-10571.

Su, Z., Zhang, Y., Gendron, T.F., Bauer, P.O., Chew, J., Yang, W.Y., Fostvedt, E., Jansen-West, K., Belzil, V.V., Desaro, P.*, et al.* (2014). Discovery of a biomarker and lead small molecules to target r(GGGGCC)-associated defects in c9FTD/ALS. Neuron *83*, 1043-1050.

Sun, Q., Fan, W., Chen, K., Ding, X., Chen, S., and Zhong, Q. (2008). Identification of Barkor as a mammalian autophagy-specific factor for Beclin 1 and class III phosphatidylinositol 3-kinase. Proceedings of the National Academy of Sciences of the United States of America *105*, 19211-19216.

Sun, S., Ling, S.-C., Qiu, J., Albuquerque, C.P., Zhou, Y., Tokunaga, S., Li, H., Qiu, H., Bui, A., Yeo, G.W.*, et al.* (2015). ALS-causative mutations in FUS/TLS confer gain and loss of function by altered association with SMN and U1-snRNP. Nat Commun *6*.

Sutcliffe, J.S., Nelson, D.L., Zhang, F., Pieretti, M., Caskey, C.T., Saxe, D., and Warren, S.T. (1992). DNA methylation represses FMR-1 transcription in fragile X syndrome. Human molecular genetics *1*, 397-400.

Suzuki, H., Kanekura, K., Levine, T.P., Kohno, K., Olkkonen, V.M., Aiso, S., and Matsuoka, M. (2009). ALS-linked P56S-VAPB, an aggregated loss-of-function mutant of VAPB, predisposes motor neurons to ER stress-related death by inducing aggregation of co-expressed wild-type VAPB. J Neurochem *108*, 973-985.

Suzuki, H., Lee, K., and Matsuoka, M. (2011). TDP-43-induced death is associated with altered regulation of BIM and Bcl-xL and attenuated by caspase-mediated TDP-43 cleavage. Journal of Biological Chemistry *286*, 13171-13183.

Suzuki, K., Kirisako, T., Kamada, Y., Mizushima, N., Noda, T., and Ohsumi, Y. (2001). The pre-autophagosomal structure organized by concerted functions of APG genes is essential for autophagosome formation. EMBO Journal *20*, 5971-5981.

Suzuki, N., Maroof, A.M., Merkle, F.T., Koszka, K., Intoh, A., Armstrong, I., Moccia, R., Davis-Dusenbery, B.N., and Eggan, K. (2013). The mouse C9ORF72 ortholog is enriched in neurons known to degenerate in ALS and FTD. Nature neuroscience *16*, 1725-1727.

Swinnen, B., and Robberecht, W. (2014). The phenotypic variability of amyotrophic lateral sclerosis. Nat Rev Neurol *10*, 661-670.

Takahashi, H., Ohama, E., and Ikuta, F. (1991). Are bunina bodies of endoplasmic reticulum origin? An ultrastructural study of subthalamic eosinophilic inclusions in a case of atypical motor neuron disease. Acta Pathol Jpn *41*, 889-894.

Takahashi, Y., Fukuda, Y., Yoshimura, J., Toyoda, A., Kurppa, K., Moritoyo, H., Belzil, V.V., Dion, P.A., Higasa, K., Doi, K.*, et al.* (2013). ERBB4 mutations that disrupt the neuregulin-ErbB4 pathway cause amyotrophic lateral sclerosis type 19. Am J Hum Genet *93*, 900-905.

Takuma, H., Kwak, S., Yoshizawa, T., and Kanazawa, I. (1999). Reduction of GluR2 RNA editing, a molecular change that increases calcium influx through

AMPA receptors, selective in the spinal ventral gray of patients with amyotrophic lateral sclerosis. Ann Neurol *46*, 806-815.

Taneja, K.L., McCurrach, M., Schalling, M., Housman, D., and Singer, R.H. (1995). Foci of trinucleotide repeat transcripts in nuclei of myotonic dystrophy cells and tissues. Journal of Cell Biology *128*, 995-1002.

Tanida, I., Minematsu-Ikeguchi, N., Ueno, T., and Kominami, E. (2005). Lysosomal turnover, but not a cellular level, of endogenous LC3 is a marker for autophagy. Autophagy *1*, 84-91.

Teyssou, E., Takeda, T., Lebon, V., Boillée, S., Doukouré, B., Bataillon, G., Sazdovitch, V., Cazeneuve, C., Meininger, V., Leguern, E.*, et al.* (2013). Mutations in SQSTM1 encoding p62 in amyotrophic lateral sclerosis: Genetics and neuropathology. Acta Neuropathol *125*, 511-522.

Therrien, M., Rouleau, G.A., Dion, P.A., and Parker, J.A. (2013). Deletion of C9ORF72 Results in Motor Neuron Degeneration and Stress Sensitivity in <italic>C. elegans</italic>. PLoS ONE *8*, e83450.

Thrower, J.S., Hoffman, L., Rechsteiner, M., and Pickart, C.M. (2000). Recognition of the polyubiquitin proteolytic signal. The EMBO Journal *19*, 94-102.

Tizon, B., Sahoo, S., Yu, H., Gauthier, S., Kumar, A.R., Mohan, P., Figliola, M., Pawlik, M., Grubb, A., Uchiyama, Y.*, et al.* (2010). Induction of Autophagy by Cystatin C: A Mechanism That Protects Murine Primary Cortical Neurons and Neuronal Cell Lines. PLoS ONE *5*, e9819.

Tollervey, J.R., Curk, T., Rogelj, B., Briese, M., Cereda, M., Kayikci, M., König, J., Hortobágyi, T., Nishimura, A.L., Zupunski, V.*, et al.* (2011). Characterizing the RNA targets and position-dependent splicing regulation by TDP-43. Nature neuroscience *14*, 452-458.

Tooze, S.A., and Yoshimori, T. (2010). The origin of the autophagosomal membrane. Nature cell biology *12*, 831-835.

Topp, J.D., Gray, N.W., Gerard, R.D., and Horazdovsky, B.F. (2004). Alsin is a Rab5 and Rac1 guanine nucleotide exchange factor. Journal of Biological Chemistry *279*, 24612-24623.

Tresse, E., Salomons, F.A., Vesa, J., Bott, L.C., Kimonis, V., Yao, T.P., Dantuma, N.P., and Taylor, J.P. (2010). VCP/p97 is essential for maturation of ubiquitin-containing autophagosomes and this function is impaired by mutations that cause IBMPFD. Autophagy *6*, 217-227.

Tsukihara, T., Aoyama, H., Yamashita, E., Tomizaki, T., Yamaguchi, H., Shinzawa-Itoh, K., Nakashima, R., Yaono, R., and Yoshikawa, S. (1996). The Whole Structure of the 13-Subunit Oxidized Cytochrome c Oxidase at 2.8 Å. Science *272*, 1136-1144.

Udeshi, N.D., Mertins, P., Svinkina, T., and Carr, S.A. (2013). Large-scale identification of ubiquitination sites by mass spectrometry. Nat Protocols *8*, 1950-1960.

Uranishi, H., Tetsuka, T., Yamashita, M., Asamitsu, K., Shimizu, M., Itoh, M., and Okamoto, T. (2001). Involvement of the pro-oncoprotein TLS (translocated in liposarcoma) in nuclear factor-kappa B p65-mediated transcription as a coactivator. J Biol Chem *276*, 13395-13401.

Urwin, H., Authier, A., Nielsen, J.E., Metcalf, D., Powell, C., Froud, K., Malcolm, D.S., Holm, I., Johannsen, P., Brown, J.*, et al.* (2010). Disruption of endocytic trafficking in frontotemporal dementia with CHMP2B mutations. Human Molecular Genetics *19*, 2228-2238.

van Blitterswijk, M., DeJesus-Hernandez, M., Niemantsverdriet, E., Murray, M.E., Heckman, M.G., Diehl, N.N., Brown, P.H., Baker, M.C., Finch, N.A., Bauer, P.O.*, et al.* (2013). Association between repeat sizes and clinical and pathological characteristics in carriers of C9ORF72 repeat expansions (Xpansize-72): A cross-sectional cohort study. The Lancet Neurology *12*, 978-988.

Van Blitterswijk, M., Mullen, B., Nicholson, A.M., Bieniek, K.F., Heckman, M.G., Baker, M.C., Dejesus-Hernandez, M., Finch, N.A., Brown, P.H., Murray, M.E.*, et*

al. (2014). TMEM106B protects C9ORF72 expansion carriers against frontotemporal dementia. Acta Neuropathol *127*, 397-406.

Van Deerlin, V.M., Sleiman, P.M.A., Martinez-Lage, M., Chen-Plotkin, A., Wang, L.-S., Graff-Radford, N.R., Dickson, D.W., Rademakers, R., Boeve, B.F., Grossman, M.*, et al.* (2010). Common variants at 7p21 are associated with frontotemporal lobar degeneration with TDP-43 inclusions. Nature genetics *42*, 234-239.

van Es, M.A., Veldink, J.H., Saris, C.G., Blauw, H.M., van Vught, P.W., Birve, A., Lemmens, R., Schelhaas, H.J., Groen, E.J., Huisman, M.H.*, et al.* (2009). Genome-wide association study identifies 19p13.3 (UNC13A) and 9p21.2 as susceptibility loci for sporadic amyotrophic lateral sclerosis. Nat Genet *41*, 1083-1087.

Vance, C., Al-Chalabi, A., Ruddy, D., Smith, B.N., Hu, X., Sreedharan, J., Siddique, T., Schelhaas, H.J., Kusters, B., Troost, D.*, et al.* (2006). Familial amyotrophic lateral sclerosis with frontotemporal dementia is linked to a locus on chromosome 9p13.2-21.3. Brain *129*, 868-876.

Vance, C., Rogelj, B., Hortobágyi, T., De Vos, K.J., Nishimura, A.L., Sreedharan, J., Hu, X., Smith, B., Ruddy, D., Wright, P.*, et al.* (2009). Mutations in FUS, an RNA processing protein, cause familial amyotrophic lateral sclerosis type 6. Science (New York, NY) *323*, 1208-1211.

Vande Velde, C., Miller, T.M., Cashman, N.R., and Cleveland, D.W. (2008). Selective association of misfolded ALS-linked mutant SOD1 with the cytoplasmic face of mitochondria. Proceedings of the National Academy of Sciences of the United States of America *105*, 4022-4027.

Varoqueaux, F., Sigler, A., Rhee, J.-S., Brose, N., Enk, C., Reim, K., and Rosenmund, C. (2002). Total arrest of spontaneous and evoked synaptic transmission but normal synaptogenesis in the absence of Munc13-mediated vesicle priming. Proceedings of the National Academy of Sciences of the United States of America *99*, 9037-9042.

Vass, R., Ashbridge, E., Geser, F., Hu, W.T., Grossman, M., Clay-Falcone, D., Elman, L., McCluskey, L., Lee, V.M.Y., Van Deerlin, V.M.*, et al.* (2011). Risk genotypes at TMEM106B are associated with cognitive impairment in amyotrophic lateral sclerosis. Acta Neuropathol *121*, 373-380.

Vazquez, A., Flammini, A., Maritan, A., and Vespignani, A. (2003). Global protein function prediction from protein-protein interaction networks. Nat Biotech *21*, 697-700.

Vergne, I., Roberts, E., Elmaoued, R.A., Tosch, V., Delgado, M.A., Proikas-Cezanne, T., Laporte, J., and Deretic, V. (2009). Control of autophagy initiation by phosphoinositide 3-phosphatase Jumpy. The EMBO journal *28*, 2244-2258.

Vielh, E., Touchot, N., Zahraoui, A., and Tavitian, A. (1989). Nucleotide sequence of a rat cDNA: rab1B, encoding a rab1-YPT related protein. Nucleic Acids Research *17*, 1770.

Vilariño-Güell, C., Wider, C., Soto-Ortolaza, A.I., Cobb, S.A., Kachergus, J.M., Keeling, B.H., Dachsel, J.C., Hulihan, M.M., Dickson, D.W., Wszolek, Z.K.*, et al.* (2009). Characterization of DCTN1 genetic variability in neurodegeneration. Neurology *72*, 2024-2028.

Voges, D., Zwickl, P., and Baumeister, W. (1999). The 26S proteasome: a molecular machine designed for controlled proteolysis. Annu Rev Biochem *68*, 1015-1068.

Vollrath, J.T., Sechi, A., Dreser, A., Katona, I., Wiemuth, D., Vervoorts, J., Dohmen, M., Chandrasekar, A., Prause, J., Brauers, E.*, et al.* (2014). Loss of function of the ALS protein SigR1 leads to ER pathology associated with defective autophagy and lipid raft disturbances. Cell death & disease *5*, e1290.

Vucic, S., Nicholson, G.A., and Kiernan, M.C. (2008). Cortical hyperexcitability may precede the onset of familial amyotrophic lateral sclerosis. Brain *131*, 1540-1550.

Wainger, B.J., Kiskinis, E., Mellin, C., Wiskow, O., Han, S.S.W., Sandoe, J., Perez, N.P., Williams, L.A., Lee, S., Boulting, G.*, et al.* (2014). Intrinsic

Membrane Hyperexcitability of ALS Patient-Derived Motor Neurons. Cell reports *7*, 1-11.

Waite, A.J., Bäumer, D., East, S., Neal, J., Morris, H.R., Ansorge, O., and Blake, D.J. (2014). Reduced C9orf72 protein levels in frontal cortex of amyotrophic lateral sclerosis and frontotemporal degeneration brain with the C9ORF72 hexanucleotide repeat expansion. Neurobiology of Aging *35*.

Walker, A.K., Soo, K.Y., Sundaramoorthy, V., Parakh, S., Ma, Y., Farg, M.A., Wallace, R.H., Crouch, P.J., Turner, B.J., Horne, M.K.*, et al.* (2013). ALS-associated TDP-43 induces endoplasmic reticulum stress, which drives cytoplasmic TDP-43 accumulation and stress granule formation. PLoS One *8*, e81170.

Wang, H.-Y., Wang, I.-F., Bose, J., and Shen, C.-K.J. (2004). Structural diversity and functional implications of the eukaryotic TDP gene family. Genomics *83*, 130-139.

Wang, J., Menon, S., Yamasaki, A., Chou, H.-T., Walz, T., Jiang, Y., and Ferro-Novick, S. (2013). Ypt1 recruits the Atg1 kinase to the preautophagosomal structure. Proceedings of the National Academy of Sciences of the United States of America *110*, 9800-9805.

Wang, X., Arai, S., Song, X., Reichart, D., Du, K., Pascual, G., Tempst, P., Rosenfeld, M.G., Glass, C.K., and Kurokawa, R. (2008). Induced ncRNAs allosterically modify RNA-binding proteins in cis to inhibit transcription. Nature *454*, 126-130.

Watanabe, S., Hayakawa, T., Wakasugi, K., and Yamanaka, K. (2014). Cystatin C protects neuronal cells against mutant copper-zinc superoxide dismutase-mediated toxicity. Cell Death and Disease *5*, e1497.

Waterman-Storer, C.M., Karki, S.B., Kuznetsov, S.A., Tabb, J.S., Weiss, D.G., Langford, G.M., and Holzbaur, E.L.F. (1997). The interaction between cytoplasmic dynein and dynactin is required for fast axonal transport. Proceedings of the National Academy of Sciences of the United States of America *94*, 12180-12185.

Waters, S., Marchbank, K., Solomon, E., Whitehouse, C., and Gautel, M. (2009). Interactions with LC3 and polyubiquitin chains link nbr1 to autophagic protein turnover. FEBS Lett *583*, 1846-1852.

Watts, G.D., Wymer, J., Kovach, M.J., Mehta, S.G., Mumm, S., Darvish, D., Pestronk, A., Whyte, M.P., and Kimonis, V.E. (2004). Inclusion body myopathy associated with Paget disease of bone and frontotemporal dementia is caused by mutant valosin-containing protein. Nat Genet *36*, 377-381.

Webb, J.L., Ravikumar, B., Atkins, J., Skepper, J.N., and Rubinsztein, D.C. (2003). ??-synuclein Is Degraded by Both Autophagy and the Proteasome. Journal of Biological Chemistry *278*, 25009-25013.

Wei, H., Wei, S., Gan, B., Peng, X., Zou, W., and Guan, J.-L. (2011). Suppression of autophagy by FIP200 deletion inhibits mammary tumorigenesis. Genes & Development *25*, 1510-1527.

Weidberg, H., and Elazar, Z. (2011). TBK1 Mediates Crosstalk Between the Innate Immune Response and Autophagy. Science signaling *4*, pe39.

Weishaupt, J.H., Waibel, S., Birve, A., Volk, A.E., Mayer, B., Meyer, T., Ludolph, A.C., and Andersen, P.M. (2013). A novel optineurin truncating mutation and three glaucoma-associated missense variants in patients with familial amyotrophic lateral sclerosis in Germany. Neurobiology of Aging *34*.

Whitworth, A.J., and Pallanck, L.J. (2009). The PINK1/Parkin pathway: A mitochondrial quality control system? In J Bioenerg Biomembr, pp. 499-503.

Wiedemann, F.R., Manfredi, G., Mawrin, C., Flint Beal, M., and Schon, E.A. (2002). Mitochondrial DNA and respiratory chain function in spinal cords of ALS patients. Journal of Neurochemistry *80*, 616-625.

Wild, P., Farhan, H., McEwan, D.G., Wagner, S., Rogov, V.V., Brady, N.R., Richter, B., Korac, J., Waidmann, O., Choudhary, C.*, et al.* (2011). Phosphorylation of the autophagy receptor optineurin restricts Salmonella growth. Science (New York, NY) *333*, 228-233.

Williams, A., Sarkar, S., Cuddon, P., Ttofi, E.K., Saiki, S., Siddiqi, F.H., Jahreiss, L., Fleming, A., Pask, D., Goldsmith, P.*, et al.* (2008). Novel targets for Huntington's disease in an mTOR-independent autophagy pathway. Nat Chem Biol *4*, 295-305.

Williamson, T.L., and Cleveland, D.W. (1999). Slowing of axonal transport is a very early event in the toxicity of ALS-linked SOD1 mutants to motor neurons. Nature neuroscience *2*, 50-56.

Winslow, A.R., Chen, C.W., Corrochano, S., Acevedo-Arozena, A., Gordon, D.E., Peden, A.A., Lichtenberg, M., Menzies, F.M., Ravikumar, B., Imarisio, S.*, et al.* (2010). alpha-Synuclein impairs macroautophagy: implications for Parkinson's disease. J Cell Biol *190*, 1023-1037.

Winslow, A.R., and Rubinsztein, D.C. (2011). The Parkinson disease protein α-synuclein inhibits autophagy. In Autophagy, pp. 429-431.

Wong, P.C., Pardo, C.a., Borchelt, D.R., Lee, M.K., Copeland, N.G., Jenkins, N.a., Sisodia, S.S., Cleveland, D.W., and Price, D.L. (1995). An adverse property of a familial ALS-linked SOD1 mutation causes motor neuron disease characterized by vacuolar degeneration of mitochondria. Neuron *14*, 1105-1116.

Wong, Y.C., and Holzbaur, E.L.F. (2014). Optineurin is an autophagy receptor for damaged mitochondria in parkin-mediated mitophagy that is disrupted by an ALS-linked mutation. Proceedings of the National Academy of Sciences *111*, E4439-E4448.

Wood, J.D., Beaujeux, T.P., and Shaw, P.J. (2003). Protein aggregation in motor neurone disorders. In Neuropathology and Applied Neurobiology, pp. 529-545.

Wootz, H., Hansson, I., Korhonen, L., Napankangas, U., and Lindholm, D. (2004). Caspase-12 cleavage and increased oxidative stress during motoneuron degeneration in transgenic mouse model of ALS. Biochem Biophys Res Commun *322*, 281-286.

Wu, C.-H., Fallini, C., Ticozzi, N., Keagle, P.J., Sapp, P.C., Piotrowska, K., Lowe, P., Koppers, M., McKenna-Yasek, D., Baron, D.M.*, et al.* (2012). Mutations in the profilin 1 gene cause familial amyotrophic lateral sclerosis. In Nature, pp. 499-503.

Wu, D.C., Re, D.B., Nagai, M., Ischiropoulos, H., and Przedborski, S. (2006). The inflammatory NADPH oxidase enzyme modulates motor neuron degeneration in amyotrophic lateral sclerosis mice. Proc Natl Acad Sci U S A *103*, 12132-12137.

Wu, X., Yen, L., Irwin, L., Sweeney, C., and Carraway, K.L. (2004). Stabilization of the E3 Ubiquitin Ligase Nrdp1 by the Deubiquitinating Enzyme USP8. Molecular and Cellular Biology *24*, 7748-7757.

Xi, Z., Rainero, I., and Rubino, E. (2014). Hypermethylation of the CpG-island near the C9orf72 G4C2-repeat expansion in FTLD patients. Human Molecular …, 1-20.

Xi, Z., Zinman, L., Moreno, D., Schymick, J., Liang, Y., Sato, C., Zheng, Y., Ghani, M., Dib, S., Keith, J.*, et al.* (2013). Hypermethylation of the CpG island near the G4C2 repeat in ALS with a C9orf72 expansion. American Journal of Human Genetics *92*, 981-989.

Xiao, S., Macnair, L., Mcgoldrick, P., Mckeever, P.M., and Robertson, J. (2015). Isoform Specific Antibodies Reveal Distinct Subcellular Localizations of C9orf72 in Amyotrophic Lateral Sclerosis. Ann Neurol.

Xu, C.-C., Denton, K.R., Wang, Z.-B., Zhang, X., and Li, X.-J. (2016). Abnormal mitochondrial transport and morphology as early pathological changes in human models of spinal muscular atrophy. Disease Models & Mechanisms *9*, 39-49.

Xu, Z., Poidevin, M., Li, X., Li, Y., Shu, L., Nelson, D.L., Li, H., Hales, C.M., Gearing, M., Wingo, T.S.*, et al.* (2013). Expanded GGGGCC repeat RNA associated with amyotrophic lateral sclerosis and frontotemporal dementia causes neurodegeneration. Proc Natl Acad Sci U S A *110*, 7778-7783.

Yamamoto, A., Tagawa, Y., Yoshimori, T., Moriyama, Y., Masaki, R., and Tashiro, Y. (1998). Bafilomycin A₁ Prevents Maturation of Autophagic Vacuoles by Inhibiting Fusion between Autophagosomes and Lysosomes in Rat Hepatoma Cell Line, H-4-II-E Cells. Cell Structure and Function *23*, 33-42.

Yamano, K., Fogel, A.I., Wang, C., van der Bliek, A.M., and Youle, R.J. (2014). Mitochondrial Rab GAPs govern autophagosome biogenesis during mitophagy. Elife *3*, e01612.

Yáñez, M., Galán, L., Matías-Guiu, J., Vela, A., Guerrero, A., and García, A.G. (2011). CSF from amyotrophic lateral sclerosis patients produces glutamate independent death of rat motor brain cortical neurons: Protection by resveratrol but not riluzole. Brain Research *1423*, 77-86.

Yen, W.L., Shintani, T., Nair, U., Cao, Y., Richardson, B.C., Li, Z., Hughson, F.M., Baba, M., and Klionsky, D.J. (2010). The conserved oligomeric Golgi complex is involved in double-membrane vesicle formation during autophagy. Journal of Cell Biology *188*, 101-114.

Ylä-Anttila, P., Vihinen, H., Jokitalo, E., and Eskelinen, E.L. (2009). 3D tomography reveals connections between the phagophore and endoplasmic reticulum. Autophagy *5*, 1180-1185.

Yoshikawa, S., Shinzawa-Itoh, K., and Tsukihara, T. (1998). Crystal Structure of Bovine Heart Cytochrome c Oxidase at 2.8 Å Resolution. J Bioenerg Biomembr *30*, 7-14.

Yoshimura, S.I., Gerondopoulos, A., Linford, A., Rigden, D.J., and Barr, F.A. (2010). Family-wide characterization of the DENN domain Rab GDP-GTP exchange factors. Journal of Cell Biology *191*, 367-381.

Yoshizaki, T., Kusunoki, C., Kondo, M., Yasuda, M., Kume, S., Morino, K., Sekine, O., Ugi, S., Uzu, T., Nishio, Y.*, et al.* (2012). Autophagy regulates inflammation in adipocytes. Biochem Biophys Res Commun *417*, 352-357.

Young, A.R.J., Chan, E.Y.W., Hu, X.W., Köchl, R., Crawshaw, S.G., High, S., Hailey, D.W., Lippincott-Schwartz, J., and Tooze, S.A. (2006). Starvation and ULK1-dependent cycling of mammalian Atg9 between the TGN and endosomes. Journal of cell science *119*, 3888-3900.

Yu, L., McPhee, C.K., Zheng, L., Mardones, G.A., Rong, Y., Peng, J., Mi, N., Zhao, Y., Liu, Z., Wan, F.*, et al.* (2010). Termination of autophagy and reformation of lysosomes regulated by mTOR. Nature *465*, 942-946.

Zerial, M., and McBride, H. (2001). Rab proteins as membrane organizers. Nature reviews Molecular cell biology *2*, 107-117.

Zhang, D., Iyer, L.M., He, F., and Aravind, L. (2012). Discovery of novel DENN proteins: Implications for the evolution of eukaryotic intracellular membrane structures and human disease. Frontiers in Genetics *3*.

Zhang, H., Constantine, R., Vorobiev, S., Chen, Y., Seetharaman, J., Huang, Y.J., Xiao, R., Montelione, G.T., Gerstner, C.D., Davis, M.W.*, et al.* (2011). UNC119 is required for G protein trafficking in sensory neurons. Nature neuroscience *14*, 874-880.

Zhang, K., Donnelly, C.J., Haeusler, A.R., Grima, J.C., Machamer, J.B., Steinwald, P., Daley, E.L., Miller, S.J., Cunningham, K.M., Vidensky, S.*, et al.* (2015). The C9orf72 repeat expansion disrupts nucleocytoplasmic transport. Nature *525*, 56-61.

Zhang, R., Miller, R.G., Gascon, R., Champion, S., Katz, J., Lancero, M., Narvaez, A., Honrada, R., Ruvalcaba, D., and McGrath, M.S. (2009). Circulating endotoxin and systemic immune activation in sporadic amyotrophic lateral sclerosis (sALS). J Neuroimmunol *206*, 121-124.

Zheng, N., Schulman, B.A., Song, L., Miller, J.J., Jeffrey, P.D., Wang, P., Chu, C., Koepp, D.M., Elledge, S.J., Pagano, M.*, et al.* (2002). Structure of the Cul1-Rbx1-Skp1-F boxSkp2 SCF ubiquitin ligase complex. Nature *416*, 703-709.

Zinszner, H., Sok, J., Immanuel, D., Yin, Y., and Ron, D. (1997). TLS (FUS) binds RNA in vivo and engages in nucleo-cytoplasmic shuttling. J Cell Sci *110 (Pt 15)*, 1741-1750.

Zong, M., Wu, X.G., Chan, C.W., Choi, M.Y., Chan, H.C., Tanner, J.A., and Yu, S. (2011). The adaptor function of TRAPPC2 in mammalian TRAPPs explains TRAPPC2-associated SEDT and TRAPPC9-associated congenital intellectual disability. PLoS One *6*, e23350.

Zoppino, F.C.M., Militello, R.D., Slavin, I., Álvarez, C., and Colombo, M.I. (2010). Autophagosome formation depends on the small GTPase rab1 and functional ER exit sites. Traffic *11*, 1246-1261.

Zu, T., Gibbens, B., Doty, N.S., Gomes-Pereira, M., Huguet, A., Stone, M.D., Margolis, J., Peterson, M., Markowski, T.W., Ingram, M.A.C.*, et al.* (2011). Non-ATG-initiated translation directed by microsatellite expansions. Proceedings of the National Academy of Sciences of the United States of America *108*, 260-265.